



UNIVERSIDAD NACIONAL AUTÓNOMA DE MÉXICO
POSGRADO EN CIENCIAS DE LA TIERRA
INSTITUTO DE GEOFÍSICA
PALEOMAGNETISMO Y MAGNETISMO DE ROCAS

**REGISTRO DE VARIACIÓN PALEOSECULAR DEL
CAMPO GEOMAGNÉTICO EN MATERIALES
VOLCÁNICOS Y ARQUEOLÓGICOS EN MEXICO.**

TESIS BASADA EN ARTÍCULOS CIENTÍFICOS QUE PARA OPTAR POR EL
GRADO DE
DOCTOR EN CIENCIAS DE LA TIERRA

PRESENTA:
ALEJANDRO RODRÍGUEZ TREJO

DIRECTOR DE TESIS:
DR. LUIS MANUEL ALVA VALDIVIA INSTITUTO DE GEOFÍSICA

COMITÉ TUTOR:
DRA. MIREILLE PERRIN (AIX MARSEILLE UNIVERSITÉ – CNRS)
DR. EDGARDO CAÑÓN TAPIA (CICESE)

CIUDAD DE MÉXICO DICIEMBRE 2019



UNAM – Dirección General de Bibliotecas

Tesis Digitales
Restricciones de uso

DERECHOS RESERVADOS ©
PROHIBIDA SU REPRODUCCIÓN TOTAL O PARCIAL

Todo el material contenido en esta tesis está protegido por la Ley Federal del Derecho de Autor (LFDA) de los Estados Unidos Mexicanos (México).

El uso de imágenes, fragmentos de videos, y demás material que sea objeto de protección de los derechos de autor, será exclusivamente para fines educativos e informativos y deberá citar la fuente donde la obtuvo mencionando el autor o autores. Cualquier uso distinto como el lucro, reproducción, edición o modificación, será perseguido y sancionado por el respectivo titular de los Derechos de Autor.

*Dedico este trabajo a mis padres,
Magdalena y Alejandro*

*A mis hermanos,
Mariana y Ricardo*

*A mi sobrino,
Rodrigo*

A toda mi hermosa familia, mi abuela, mis tíos, mis tías, mis primos, mis primas, sobrinos, sobrinas, a quienes me ven desde el cielo.

*Gracias a ustedes he llegado hasta aquí,
con ustedes lo tengo todo, sin ustedes no tengo nada.*

*Su apoyo me cobijó durante los momentos duros, sus
consejos me han guiado en los momentos de oscuridad.*

LOS AMO,

A Dios gracias.

Alex



Agradecimientos institucionales

A la Universidad Nacional Autónoma de México, por ser mi casa por tantos años, por brindarme conocimiento, y grandes experiencias. Mi casa para toda la vida.

Al Instituto de Geofísica, por convertirse en mi casa, por darme la oportunidad de convertirme en un hombre de ciencia.

Al Posgrado en Ciencias de la Tierra, por todo el apoyo siempre brindado, por darme la oportunidad de perseguir esta gran meta.

Al CONACyT por haberme otorgado una beca doctoral con la cual pude realizar este sueño, estudiar, crecer, cruzar fronteras y aportar conocimiento a mi país y al mundo.

Al proyecto del PAPIIT IN113117: Paleomagnetismo en rocas volcánicas y materiales arqueológicos del norte de México: variaciones temporales del campo geomagnético e implicaciones geodinámicas, por su apoyo en el trabajo de campo, de laboratorio y para asistencia a congresos nacionales e internacionales.

Al proyecto ANR-CONACyT (Francia-México) 273564: Acrónimo-secular variation and paleointensity in México during the Plio-Quaternary, por su apoyo y financiamiento del trabajo de campo, de laboratorio y para asistencia a congresos nacionales e internacionales.

Au CEREGE, à Aix en Provence, France pour de m'avoir reçu et de m'avoir donné la possibilité d'utiliser leurs installations, merci.

Goya, Goya, cachún cachún ra-ra!!!



Agradecimientos personales

A mi tutor, el Dr. Luis M. Alva Valdivia, “El Doc”, quien me ha apoyado desde el momento en que llegué al Instituto, me ha brindado su apoyo, su conocimiento, sus consejos, su sabiduría, y sobretodo su amistad. Mi gratitud eterna.

Al M. en C. José Antonio González Rangel, por su apoyo en todo momento, su paciencia, y sobretodo por su valiosa amistad.

A la Dra. Beatriz Ortega, por su apoyo y confianza en todo momento, su apoyo y su conocimiento.

A mis compañeros del grupo de paleomagnetismo, M. en C. Bernardo García, M. en C. Arnaldo Hernández, Dra. Miriam Velasco, Dr. Ahmed Mahgoub, M. en C. Manuel Bravo, M. en C. Rubén García, M. en C. Luis Velderrain, y todos los estudiantes de licenciatura y posgrado que han colaborado en el grupo; gracias a todos por su apoyo, por aguantarme, por su paciencia, por los consejos y por las valiosas discusiones en el laboratorio.

A mis amigos y compañeros del posgrado, Diego Quiroz, Félix Rodríguez, Válerie Pompa, Néstor López, Alex Paredes, Alexia Molina, Gonzalo Cid, Balam, Gerardo Mendo, Tania Huerta, Jesús Rojas, Sachenka Quiñones, Víctor Ramón, Diego Aguilar, y muchos mas, gracias por los momentos, por su amistad y por los recuerdos.

A los técnicos Víctor Macías y Martín Espinosa, por su tiempo, paciencia, apoyo y amistad ¡¡Muchas gracias!!

A la señora Aida Sáenz, por el apoyo siempre.

¡¡A Aracely Chamán y Erika Ulloa de la Unidad de Posgrado, mil millones de gracias por su apoyo!!

Au Dre Mireille Perrin pour son temps, ses connaissances, sa sagesse et son soutien. L'expérience en France a été l'une des meilleures de ma vie. Merci beaucoup!!!!

Al Dr. Harald Böhnel, por su apoyo y la confianza que ha depositado en mi, su consejo ha enriquecido mi conocimiento, ¡¡¡gracias por la oportunidad!!!!

Al Dr. Jesús Roberto Vidal Solano, quien ha estado conmigo desde el comienzo de este camino, sus valiosos consejos han enriquecido mi camino, muchas gracias por el apoyo, los momentos y la amistad. ¡¡¡Gracias!!!

A la Dra. Ana María Soler, quien desde el primer momento me ha apoyado, me ha dado confianza y me ha dicho las palabras correctas en el momento correcto, sin duda su consejo ha enriquecido mi camino.

Au Dr. Gwenaël Hervé, pour son temps, sa grande connaissance, son soutien et son amitié. Merci beaucoup.

A TODO el personal del Instituto de Geofísica, gracias por hacer mi estancia la mejor.

A mis amigos, Juan, Luis, Armando, Álvaro, Daniel, y muchos mas, por creer en mi, por su amistad por siempre estar ahí.

Y como dice la canción, gracias a la vida, ¡!!!!que me ha dado tanto!!!!



Resumen

La intensa actividad volcánica y la gran cantidad de materiales arqueológicos disponibles en México han registrado fielmente el campo magnético de la tierra debido a la naturaleza misma de su formación o manufactura, relacionada esencialmente a procesos térmicos. Este registro casi continuo de materiales ha generado la recuperación de datos paleomagnéticos en cuanto su dirección (declinación e inclinación), e intensidad (magnitud) a diferentes escalas temporales. En este trabajo se presentan resultados paleomagnéticos de rocas volcánicas, en su mayoría de la Faja Volcánica Trans Mexicana de los últimos 1.5 Ma. Se presenta un análisis de la variación paleosecular con el aporte de datos nuevos de diferentes unidades volcánicas del campo volcánico de Chichinautzin y Sierra de Santa Catarina (alrededor de la Ciudad de México), así como del volcán El Jorullo (Campo volcánico Michoacán Guanajuato), y del volcán Cerro Colorado (Campo volcánico El Pinacate, NW de Sonora). Los resultados se presentan en conjunto con una compilación y análisis crítico de todos los datos publicados, a partir de la década de los 70's, en la faja volcánica para los últimos 1.5 Ma. Con este análisis se hace énfasis en la selección de: 1) los datos de acuerdo a sus parámetros de calidad en cuanto a los datos direccionales, tomando en cuenta sus parámetros de dispersión (k) y de confiabilidad (α_{95}); y de 2) los polos geomagnéticos virtuales asociados a cada unidad volcánica, dando registro de los cambios de polaridad y valores transicionales. Esto evidenció el registro del comportamiento dipolar del campo magnético de la tierra durante el Pleistoceno tardío en México.

También se presentan resultados de arqueointensidad realizados en cerámicas de los sitios arqueológicos de Chalcatzingo (Morelos) y de Casas Grandes (Chihuahua). Los datos se presentan en conjunto con una compilación de datos de arqueointensidad de los últimos 3,000 años, publicados en México en los últimos años. La compilación se llevó a cabo con la finalidad de hacer un análisis crítico sobre la calidad de los datos reportados de diferentes sitios arqueológicos, de acuerdo a diferentes criterios establecidos (e.g. corrección por anisotropía, corrección por tasa de enfriamiento, entre otros). Entonces, se pudieron identificar los datos de alta calidad, de aquellos que poseen una calidad menor. Esto permitió seleccionar los mejores resultados.

Con ambas compilaciones se logró establecer una estadística de alta confiabilidad para los datos publicados de estudios en México. Los datos direccionales de los últimos 1.5 Ma, cerca del 34%, no cumplen con los criterios de calidad mínimos para ser tomados en cuenta en una compilación y base de datos global. Asimismo, en los datos de arqueointensidad, cerca del 70% tienen problemas con los criterios de selección mínimos para ser aceptados en repositorios de datos, lo que repercute en la confiabilidad de buena parte de los resultados disponibles. Con estos datos de confiabilidad, se establecen y proponen criterios mínimos de aceptación para la publicación de nuevos datos a futuro, lo que repercutirá en un mejor entendimiento de las variaciones seculares del campo magnético de la Tierra y la generación de datos de mayor calidad de acuerdo a los estándares más estrictos.

Abstract

The intense volcanic activity and the big amount of archaeological materials available in Mexico, due to the constant human occupation in the last 3,000 years, it allows to have a good record of the earth's magnetic field in these materials, due to the nature of its formation or manufacturing, related to thermal processes. This almost continuous record on the materials, has generated a great demand for paleomagnetic data regarding its direction (declination and inclination), and intensity (magnitude) at different time scales. This work presents paleomagnetic results of volcanic rocks, mostly from the trans-Mexican volcanic belt of the last 1.5 Ma., Making an analysis of secular paleo variation providing new paleomagnetic data from different volcanic units of the Chichinautzin volcanic field and Sierra de Santa Catarina, located in the surroundings of Mexico City, as well as the El Jorullo volcano located in the Michoacán Guanajuato volcanic field. And from the Cerro Colorado volcano, in the El Pinacate volcanic field, in the State of Sonora in the north of the country. The results are presented together with a compilation and a critical analysis of all data published since the 70's in the volcanic belt for the last 1.5 Ma. With this analysis, emphasis is placed on the selection of data according to its quality parameters in terms of directional data, considering its dispersion (k) and reliability (α_{95}) parameters; of its virtual geomagnetic poles associated with each volcanic unit, giving record of the polarity changes reported and transitional values. Allowing to give evidence of the record of the dipole behavior of the earth's magnetic field during the late Pleistocene in Mexico.

There are also archeointensity results carried out in ceramics of the archaeological sites of Chalcatzingo, in the State of Morelos; and from the Casas Grandes region corresponding to the north of the state of Chihuahua. The data presented in conjunction with a compilation of archaeological data of the last 3,000 years, published in Mexico in recent years. The compilation was carried out with the purpose of making a critical analysis on the quality of the data reported in different archaeological sites, according to different established criteria (e.g. correction for anisotropy, correction for cooling rate, among others), in order to differentiate high quality data from those that have lower reliability. This differentiation allows you to select the best results.

With both compilations, it was possible to establish a parameter of the reliability of the data published in Mexico, where for the directional data of the last 1.5 Ma, about 34% of the available data do not meet the minimum quality criteria to be considered in a compilation and global database. Also, in the archeointensity data, about 70% have problems with the minimum selection criteria to be accepted in data repositories, which affects the reliability of a good part of the available results. With this reliable data, it is possible to establish minimum acceptance criteria for the publication of data in the future, which will result in a better understanding of the secular variations of the earth's magnetic field and the generation of data of a higher quality of agreement to a stricter standard.

Contenido

Resumen

<i>1. Capítulo 1 Principios básicos de Paleomagnetismo</i>	1
<i> 1.1 Introducción</i>	1
<i> 1.2 Definiciones básicas de paleomagnetismo</i>	2
<i> 1.3 Modelos de variación secular del CMT</i>	5
<i> 1.5 Objetivo general del trabajo de tesis</i>	6
<i> 1.6 Objetivos particulares del trabajo de tesis</i>	7
<i> 1.7 Selección del área de Estudio</i>	7
<i> 1.8 Estructura del trabajo de tesis</i>	9
<i> 1.9 Metodología</i>	10
<i> 1.9.1 Instrumentación utilizada</i>	11
<i> 1.9.2 Medición de las propiedades magnéticas</i>	11
<i> 1.9.3 Métodos de desmagnetización y Análisis direccional</i>	13
<i> 1.9.4 Paleointensidad del campo magnético terrestre</i>	14
<i> 1.9.5 Corrección de la paleointensidad por anisotropía</i>	16
<i> 1.9.6 Modelos de variación paleosecular y bases de datos globales</i>	16
<i> 1.9.7 Muestreo paleomagnético</i>	17
<i>Capítulo 2: “Analysis of geomagnetic secular variation for the last 1.5Ma recorded by volcanic rocks of the Trans Mexican Volcanic Belt: new data from Sierra de Chichinautzin, Mexico”</i>	19



<i>Capítulo 3: “Paleomagnetism and rock magnetic properties of Late Pleistocene volcanism from El Pinacate Volcanic Field, northwest Mexico”</i>	35
<i>Capítulo 4: “Emplacement temperature resolution and age determination of Cerro Colorado tuff ring by paleomagnetic analysis, El Pinacate Volcanic Field, Sonora, Mexico”</i>	49
<i>Capítulo 5: “Paleomagnetism and age constraints of historical lava flows from the El Jorullo volcano, Michoacán, Mexico”</i>	60
<i>Capítulo 6: “Critical analysis of the Holocene palaeointensity database in Central America: Impact on geomagnetic modelling”</i>	71
<i>Capítulo 7: “Archeomagnetic dating and magnetic characterization of ceramics from the Casas Grandes region, Chihuahua, Mexico: Paquimé, Galeana, Villa Ahumada and Samalayuca archeological sites”</i>	82
Capítulo 8 Resultados generales	111
Capítulo 9 Discusión y conclusiones	115
Referencias bibliográficas	118



Capítulo 1 Principios básicos de Paleomagnetismo

1.1 Introducción

En México, la intensa actividad volcánica generada en los últimos 100 Ma, así como la constante ocupación humana en los territorios de Mesoamérica y Aridoamérica, ha permitido un amplio registro del campo magnético de la tierra en diversos materiales geológicos y arqueológicos.

El estudio del campo magnético de la tierra (CMT) es de gran importancia en la investigación geofísica por dos razones. Primero, es la única señal de la dinámica del núcleo-manto que puede detectarse en la superficie de la Tierra (Glatzmaier et al., 1999), y segundo, posee potencialmente un registro continuo en diversos materiales. Su registro está basado en la medición directa por instrumentos instalados en satélites desde los años 80's, en observatorios geofísicos, o en barcos en las exploraciones marinas realizadas en los últimos cuatro siglos, además de las mediciones indirectas que portan la magnetización remanente los diversos materiales arqueológicos en los últimos miles de años (registro histórico), o la adquirida por las rocas al momento de su formación, y durante su evolución geológica.

Las variaciones temporales del CMT, desde decenas y hasta miles de años, en dirección e intensidad, dan lugar a un fenómeno denominado *variación paleosecular*. Siendo esta la base para el estudio del paleomagnetismo, el cual se enfoca en el registro del CMT en diferentes materiales al momento de su formación. La PSV permite comprender los cambios en núcleo terrestre, asociados a movimientos convectivos en el núcleo externo, generando un comportamiento similar a la de un dínamo auto-excitado (McElhinny & McFadden, 1998), fenómeno conocido como geodinamo. El estudio de la PSV brinda información que permite comprender los procesos de inversión de polaridad del CMT, siendo el último ocurrido hace ca. 780 ka. Asimismo, es de gran utilidad para realizar estudios de reconstrucción tectónica a una escala de tiempo mayor. La comprensión y desarrollo de modelos de PSV (e.g. Pavón-Carrasco et al., 2014; Constable et al., 2016) a diferentes escalas temporales, permiten llevar a cabo la datación de algunos materiales volcánicos y arqueológicos (e.g. Mahgoub et al., 2017; Alva-Valdivia et al., 2019), mediante el uso de diversas herramientas informáticas, que permiten asociar las variaciones en declinación, inclinación e intensidad del CMT de un modelo de PSV, representado por una curva para una edad determinada.

Actualmente, en México existen numerosos estudios de PSV en materiales volcánicos (e.g. Böhnel y Molina-Garza, 2002; García-Ruiz et al., 2016; Mahgoub et al., 2019; Rodríguez-Trejo et al., 2019a), principalmente flujos de lava, y en diversos materiales arqueológicos (e.g. Alva-Valdivia et al., 2010; Hervé et al., 2019), ambos tipos de material con edad bien definida por datación radiométrica. En el mundo existen diferentes estudios globales de variacion paleosecular (PSV) que emplean datos provenientes de diferentes regiones del mundo (e.g. Opdyke et al., 2015; Panovska et al., 2018; Cromwell et al., 2018; Doubravine et al., 2019). Estos modelos emplean una gran cantidad de datos, lo que permite la creación de modelos robustos de PSV. Sin embargo, en México, a pesar de la gran cantidad de material y de resultados disponibles, existen pocos trabajos publicados que compilen muchos datos a nivel regional, y que propongan un modelo de PSV (e.g. Goguitchaichvili et al., 2018a; Hervé et al., 2019; Mahgoub et al., 2019), para el Pleistoceno tardío en la región. De ahí la necesidad de crear una plataforma que compile todos los datos de paleomagnetismo disponibles en México y otras regiones de Centro y Sud América. Es necesaria la creación de una base de datos que integre datos paleomagnéticos (dirección e intensidad), información sobre los métodos de datación empleados, resultados disponibles sobre sus propiedades magnéticas, ubicación e información geológica, que permita a los paleomagnetistas y geocientíficos a acceder a la información que sea de utilidad para complementar y ampliar cualquier tipo nuevo de estudio. En el mundo existen diferentes plataformas que albergan gran cantidad de datos de diferentes regiones del mundo e.g. MagIC (Tauxe et al., 2016) y GEOMAGIA50.v3.3 (Brown et al., 2015).

1.2 Definiciones básicas de paleomagnetismo

El paleomagnetismo como disciplina científica propia de los estudios geofísicos, se encarga del estudio de las variaciones espaciales y temporales del CMT. Esto es, en diferentes tiempos y en diferentes localidades del globo terrestre. El registro sucede por diversos procesos geológicos debido a procesos térmicos, deposicionales y químicos, entre otros; y en diferentes materiales producto de la actividad humana, como la fabricación de cerámica, la quema de materiales como suelos, etc. El registro de las componentes direccionales y de magnitud del CMT, permite comprender los cambios que ha sufrido. Entonces, estas variaciones pueden ser cambios en la declinación, la inclinación y la intensidad, hasta cambios en la polaridad del CMT. Estos cambios están asociados entre otras cosas a los efectos de las componentes no-dipolares que afectan la configuración del CMT.

El campo geomagnético

El campo geomagnético como lo conocemos, tiene su origen en el interior de la tierra, en la interacción entre el núcleo externo y el núcleo interno por la actividad magneto-hidrodinámica que se asemeja al modelo teórico de un dínamo auto excitado, y que se le conoce como geodinamo (Merril et al., 1996). Para entender este modelo, podemos imaginar un imán de barra, centrado y coincidente con el eje de rotación terrestre (Figura 1). Esta configuración del campo magnético terrestre tiene la forma de un Dipolo Geocéntrico y Axial (GAD). El modelo, por simple que parezca guarda un gran parecido con la configuración actual del CMT.

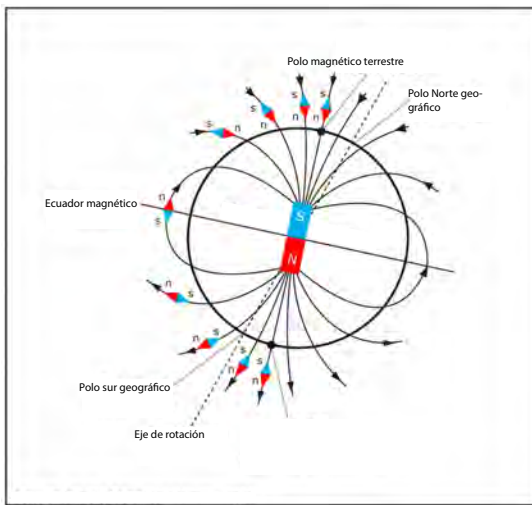


Figura 1. Configuración del modelo de un dipolo geocéntrico y axial.

Un modelo aproximado a la configuración actual del CMT, es el propuesto por Gauss (1838) mediante el uso de armónicos esféricos. El modelo asume que el vector magnético puede describirse como el gradiente espacial de un potencial magnético V_i , el cual se puede representar como:

$$V_i(r, \theta, \phi) = \sum_{n=1}^{\infty} \sum_{m=0}^n R_E \left(\frac{R_E}{r} \right)^{n+1} [g_{i;n}^m \cos m\phi + h_{i;n}^m \sin m\phi] P_n^m(\theta)$$

Donde P_n^m son las funciones ‘Schmidt quasi-normalized’ (Winch et al., 2005) de *Legendre* de grado n y orden m (Whittaker & Watson, 1996). Los coeficientes de Gauss \mathbf{g} & \mathbf{h} , así como la latitud ϕ y longitud θ geográficas. R_E es el radio promedio de la tierra, y r la distancia al centro de la tierra. Con esa representación es posible observar la configuración del CMT desde sus componentes dipolares originadas en el núcleo, y las no dipolares originadas fuera del núcleo terrestre. El modelo demuestra que >90% se debe a la aportación de las componentes dipolares del CMT (Glassmeier et al., 2008).

Componentes del campo magnético de la Tierra

El CMT se puede representar espacialmente como un vector, el cual puede ser descompuesto en diferentes componentes. Las componentes del vector del CMT se muestran en la Figura 2.

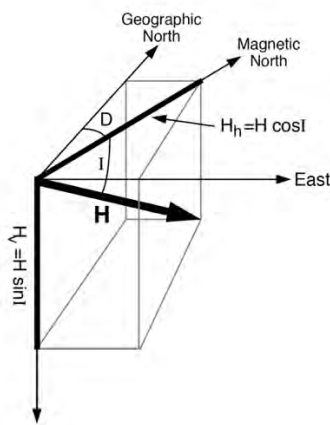


Figura 2. Componentes del vector que conforman el campo magnético terrestre (Butler, 1998).

En paleomagnetismo, como se muestra en la Figura 2, el vector total \mathbf{H} del campo magnético, puede descomponerse en dos componentes:

- La componente vertical \mathbf{H}_v , dada por:

$$\mathbf{H}_v = \mathbf{H} \sin I$$

Donde I representa la inclinación, que es el ángulo vertical formado entre la componente horizontal y \mathbf{H} (Figura 2), y esta en un rango de -90° a 90°.

- La componente horizontal \mathbf{H}_h , dada por:

$$\mathbf{H}_h = \mathbf{H} \cos I$$

La declinación D, es el ángulo azimutal formado entre \mathbf{H}_h y el norte geográfico ($\mathbf{H}_N = \mathbf{H} \cos I \cos D$), y por la componente Este ($\mathbf{H}_E = \mathbf{H} \cos I \sin D$), en un rango que va de 0° a 360°.

La magnitud del campo magnético H está dada por:

$$H = \sqrt{H_N^2 + H_E^2 + H_v^2}$$

Los valores de Declinación e Inclinación determinan la dirección del CMT en cualquier punto del planeta. La dirección en conjunto con el valor de la intensidad permite conocer de manera integral el vector total del CMT. Estos parámetros, son registrados por diferentes materiales geológicos y arqueológicos durante su formación o manufactura, permitiendo conocer el comportamiento secular del CMT en diferentes puntos del tiempo.

Modelo de un dipolo geocéntrico y axial

Un modelo de un dipolo geocéntrico y axial (GAD por sus siglas en inglés) es la base para la comprensión de cualquier estudio paleomagnético. La idea básica del modelo se refiere a un dipolo magnético localizado en el centro de la tierra, y que se encuentra alineado con el eje de rotación terrestre. La Figura 3 muestra gráficamente los componentes de un modelo de un GAD, donde **M** representa el momento magnético del dipolo; λ representa la latitud; r_e el radio promedio de la tierra.

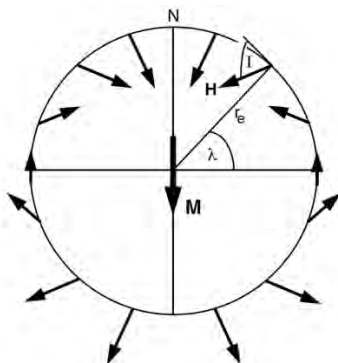


Figura 3. Representación gráfica del modelo de un dipolo geocéntrico y axial.

En la figura puede verse de manera idealizada a las líneas de fuerza del CMT salen del polo sur geográfico para entrar en el polo norte geográfico, y a través del centro de la tierra para completar la configuración, funcionando de manera ideal como se describió anteriormente como un dínamo auto excitado. Las líneas de campo (flechas) muestran de una longitud mayor en los polos con respecto al ecuador geográfico, indicando la magnitud del vector o CMT. Con esta observación, es posible determinar la inclinación del campo de acuerdo a la latitud en la que se encuentre, y está dada por la *ecuación del dipolo*:

$$\tan I = \left(\frac{H_v}{H_h} \right) = \left(\frac{2 \sin \lambda}{\cos \lambda} \right) = 2 \tan \lambda$$

Variación paleosecular del campo magnético

El CMT es muy dinámico, cambiando constantemente a través del tiempo. Estos cambios pueden ir desde fracciones de segundo, siglos, milenios y hasta millones de años. Los cambios del CMT no siguen un patrón determinado, y se ven reflejados tanto en sus componentes direccionales como en su intensidad. Es por ello que la variación paleosecular (PSV) se define como los cambios espaciales y temporales registrados en diferentes escalas temporales, que pueden ir de unos cientos y hasta millones de años. Los registros en materiales históricos del CMT se le conoce como variación secular (SV).

Estos cambios en dirección e intensidad son registrados por diferentes materiales a través del tiempo, tanto rocas volcánicas como en rocas sedimentarias, sedimentos lacustres, etc., así como en materiales arqueológicos diversos. El estudio de estos materiales permite conocer dichas variaciones a través del tiempo. En la actualidad, existen una gran cantidad de trabajos publicados que describen la SV a nivel global y regional, aportando gran cantidad de datos paleomagnéticos. Estos datos conforman la

información disponible a nivel global y regional como el repositorio MagIC (Tauxe et al., 2016) y GEOMAGIA50 (Brown et al., 2015). Asimismo, la existencia de los diversos repositorios de datos ha permitido la creación de modelos de variación paleosecular a nivel global y regional, a diferentes escalas temporales.

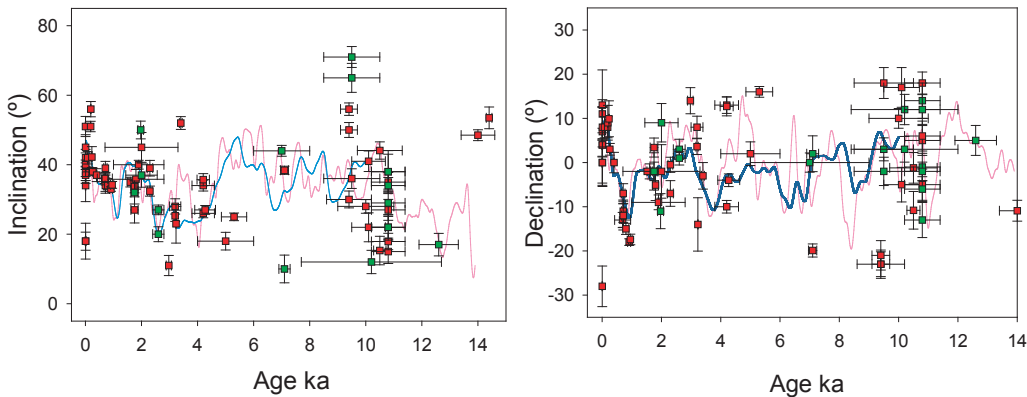


Figura 4. Modelos de variación paleosecular SHA.DIF.14k (línea roja) y CALS10k2 (línea azul) en comparación con datos direccionales de la FVTM. Los símbolos en verde muestran algunos resultados obtenidos en este trabajo; los símbolos en rojo muestran algunos resultados previamente publicados en México.

En la Figura 4 se observa un ejemplo de los modelos globales SHA.DIF.14k y CALS10k2 en perspectiva con datos direccionales de la FVTM. Donde se ve una buena concordancia con los valores esperados. Lo cual no resulta sorpresivo, ya que muchos de los datos mostrados fueron utilizados para la construcción de ambos modelos. Lo anterior demuestra la importancia de reportar datos nuevos de materiales bien datados, y de diferentes localidades.

1. 3 Modelos de variación secular del CMT

Hoy en día existen una gran cantidad de modelos de variación secular, que buscan entender el comportamiento del campo magnético de la tierra a través del tiempo y a diferentes escalas del mismo. Para el Holoceno existen modelos de variación secular como el CALS10k2 (Constable et al., 2016) y el SHA.DIF.14k (Pavón-Carrasco et al., 2014) que describen la actividad del CMT durante los últimos 10 y 14 mil años respectivamente. Existen modelos que describen el comportamiento promedio del CMT en los últimos 5 Ma (e.g. Johnson & Constable, 1995, 1997; Kelly & Gubbins, 1997). En México hay modelos de PSV para los últimos 4000 años (e.g. Hervé et al., 2019; Mahgoub et al., 2019) que describen los cambios en dirección e intensidad del CMT. Así como de manera regional se describe la PSV en la Faja Volcánica Trans Mexicana (FVTM) para los últimos 1.5 Ma (Rodríguez-Trejo et al., 2019). A nivel global y a escalas mayores, que llegan hasta los 10 Ma algunos de ellos (e.g. Johnson et al., 2008; Opdyke et al., 2015; Cromwell et al., 2018; Panovska et al., 2018; Doubrovine et al., 2019).

De manera general, todos los modelos globales buscan describir los cambios que experimenta el CMT a través del tiempo y a diferentes escalas. Se crean tomando como base los datos paleomagnéticos publicados en todo el mundo, y aquellos disponibles en bases de datos globales. De esta manera, la construcción de modelos está basada en registros reales del CMT en diferentes materiales. Posteriormente se hace un pronóstico de variación, con lo cual se construyen curvas de variación secular, empleando diversas herramientas estadísticas (e.g. bootstrap, spline).

Estos modelos, si bien presentan una forma simple de observar las variaciones seculares del CMT a diferentes escalas temporales, estos poseen diversas limitantes que reducen la confiabilidad de los mismos. La principal limitante radica en la baja disponibilidad de datos en diferentes puntos del tiempo, debido a que no es posible obtener muestras asociadas a esa temporalidad, o porque no hay suficientes edades reportadas de diversos materiales. La ausencia de datos en diferentes segmentos incrementa significativamente la incertidumbre de los modelos, reduciendo la confiabilidad.

Otra limitante radica en la confiabilidad de las dataciones asociadas a los materiales, ya que en ocasiones las edades reportadas poseen una incertidumbre alta, o la datación es incorrecta. Estos errores e incertidumbre dificultan el poder asociar un resultado paleomagnético a una unidad de tiempo en una curva, lo cual reduce considerablemente su confiabilidad. Por otro lado, otra limitante que se ve reflejada al momento de comparar diversos modelos de temporalidades similares, es la calidad de los datos paleomagnéticos usados, dado que en ocasiones los datos disponibles en diversas bases de datos globales como GEOMAGIA50, no tienen un proceso de validación o de clasificación de acuerdo a su calidad; o en ocasiones, los datos son publicados sin importar la confiabilidad de los mismos.

Por lo anterior, es posible ver que el alcance de los modelos tanto globales como regionales de variación secular, esta en función de la disponibilidad y de la calidad de los datos paleomagnéticos y de su datación asociada. En este trabajo se busca establecer criterios que permitan una selección mas eficiente de datos que permita mejorar la calidad de los datos que integren un modelo. En la Figura 5 se observa la compatibilidad de algunos resultados obtenidos en México con diversos modelos de variación secular, en función de su latitud.

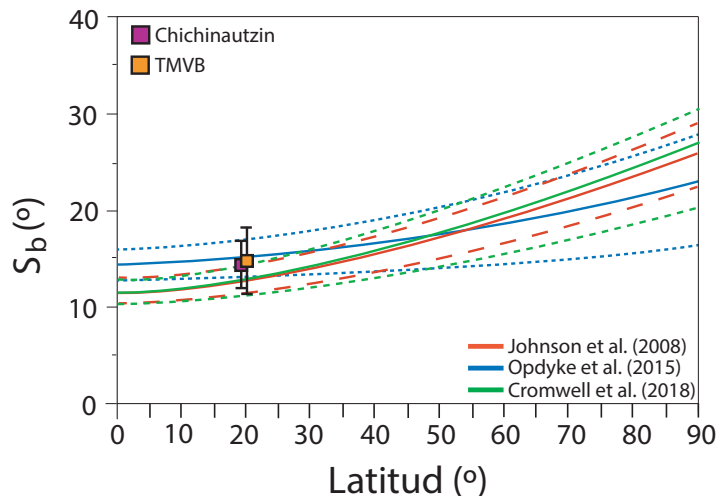


Figura 5. Ejemplos de modelos globales de variación secular y su relación con la latitud.

1.5 Objetivo general del trabajo de tesis

El registro del CMT en diferentes materiales como rocas volcánicas y materiales arqueológicos, permite tener información casi continua de las variaciones que presenta a diferentes escalas de tiempo y espacio. Con ese registro cuasi continuo, los estudios paleomagnéticos de dichos materiales, con edad conocida de su formación o manufactura, permiten la creación de modelos de variación paleosecular del campo geomagnético. Dichos modelos a escalas globales y regionales permiten comprender los cambios sucedidos al CMT en diferentes momentos. Para mejorar dichos modelos es

necesario contar cada vez con mas cantidad de datos, y refinar los ya existentes, realizando un filtrado de acuerdo a su calidad y confiabilidad.

Este trabajo, busca generar nuevos datos que completen los espacios vacíos en dichos modelos, así como hacer un análisis crítico de los datos publicados en las últimas décadas, analizando, evaluando y clasificando la calidad de los mismos, para determinar el impacto que tiene la calidad de los datos publicados en la modelación del CMT a nivel regional. Asimismo, se busca llevar a cabo la datación de algunos de los materiales mediante el uso de los modelos de variación secular mas recientes que se encuentran disponibles.

1.6 Objetivos particulares del trabajo de tesis

El objetivo de este trabajo se puede definir en cinco aspectos principales:

- i. Generar datos nuevos de paleomagnetismo en dirección (declinación e inclinación) e intensidad, a partir de materiales volcánicos y arqueológicos que cuenten con una buena determinación de edad (datación), con la finalidad de aportar datos de alta calidad a las bases de datos globales y regionales, que permitan la construcción de nuevos modelos de variación paleosecular, así como el refinamiento de los modelos ya existentes.
- ii. Hacer un análisis crítico de los datos de paleomagnetismo publicados para México, provenientes de rocas volcánicas de los últimos 1.5 Ma, así como de materiales arqueológicos diversos, a fin de definir una estadística en cuanto a su calidad y confiabilidad.
- iii. Realizar la caracterización de las propiedades magnéticas de muestras volcánicas y materiales arqueológicos, a fin de determinar los minerales portadores de la magnetización; su estabilidad térmica y magnética durante un proceso de calentamiento-enfriamiento progresivo; así como conocer sus parámetros de magnetización de saturación, remanencia y coercitividad.
- iv. Llevar a cabo la datación de materiales por medio de paleomagnetismo y arqueomagnetismo, particularmente de algunos de los materiales que no tengan edad conocida.
- v. Mediante el análisis de las componentes direccionales, estimar la temperatura de emplazamiento de un cuerpo volcánico, por ejemplo, la actividad explosiva freatomagmática, a fin de conocer parte de la historia térmica de la erupción y su posible edad.

1.7 Selección del área de Estudio

Debido a la intensa actividad volcánica preexistente en México, por un lado, en la región de la FVTM, la cual cruza transversalmente el centro del país de Este a Oeste (Ferrari et al., 1994; 1999), se han generado una gran cantidad de datos paleomagnéticos desde la década de los 70's. En el presente se aportan nuevos datos paleomagnéticos de diferentes zonas del país. En el Capítulo 2 se aportan datos direccionales nuevos (declinación e inclinación), en este contexto, es el campo volcánico de la Sierra de Chichinautzin (ChVF) y la Sierra de Santa Catarina (SSC), ubicado en los alrededores de la Ciudad

de México en el Centro del país. Asimismo, se llevó a cabo una compilación y análisis crítico de los datos de paleomagnetismo publicados sobre rocas volcánicas en la FVTM para el Pleistoceno y Holoceno.

Por otro lado, en el capítulo 3 se publican resultados de dirección y paleointensidad del CMT registrados en rocas volcánicas del Pleistoceno tardío del Campo Volcánico de El Pinacate (CVP), así como la datación de dos flujos de lava. El Capítulo 4, describe el procedimiento para el cálculo de temperatura y datación, mediante la obtención de datos paleomagnéticos, del volcán Cerro Colorado, ubicado en el CVP. En el Capítulo 5, se publican datos paleomagnéticos (declinación, inclinación e intensidad) de la erupción histórica (1759–1766 AD) del volcán El Jorullo, ubicado en el campo volcánico Michoacán-Guanajuato (CVMG), en la región SW del estado de Michoacán. El Capítulo 6 describe los datos de arqueointensidad obtenidos a partir de cerámicas del Epiclásico (650 – 900 AD) de la zona arqueológica de Chalcatzingo, ubicada en el estado de Morelos; asimismo en el trabajo se realizó una compilación de datos de arqueomagnetismo publicados sobre materiales arqueológicos en México, haciendo un análisis crítico sobre la confiabilidad y calidad de los mismos.

Asimismo, en el Capítulo 7, se muestran resultados de arqueointensidad y propiedades magnéticas realizados en material cerámico proveniente de la región de Casas Grandes, ubicado en la parte norte del estado de Chihuahua y sur de EEUU. Con los resultados se logró llevar a cabo la diferenciación de dos tipos cerámicos de acuerdo a sus propiedades magnéticas, y la datación de los materiales cerámicos mediante el uso de los resultados de arqueointensidad. En la figura 6 se señalan las localidades de los sitios estudiados en el presente trabajo.

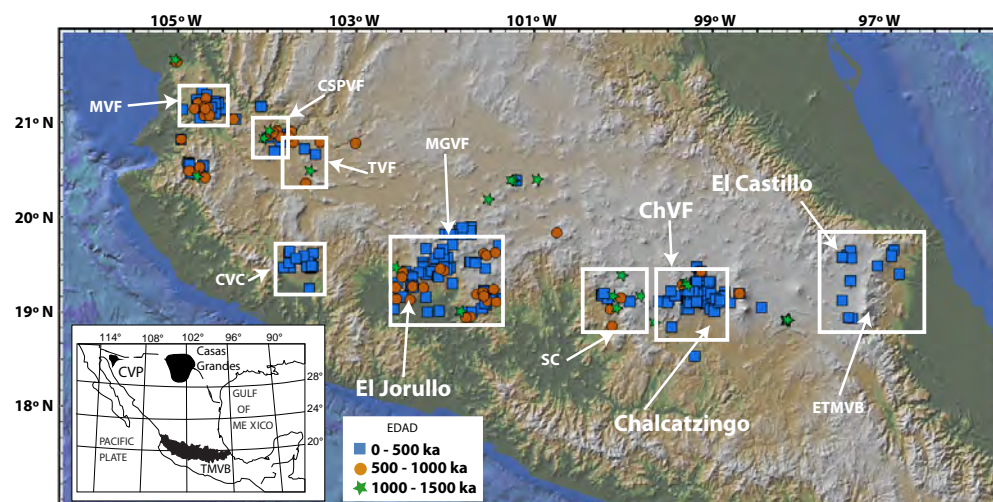


Figura 6. Área de estudio del trabajo de tesis. Unidades volcánicas con datos paleomagnéticos reportados en la faja volcánica transmexicana para los últimos 1.5 Ma. Campo volcánico de Mascota (MVF); Campo volcánico de Ceboruco-San Pedro (CSPVF); Campo volcánico de Tequila (TVF); Complejo volcánico de Colima; Campo Volcánico Michoacán-Guanajuato (MGVF); Sierra de las Cruces (SC); Campo volcánico de Chichinautzin (ChVF); Región Este de la faja volcánica transmexicana (EFVTM). Campo volcánico de El Pinacate (CVP) Imagen modificada de (Rodríguez-Trejo et al., 2019).

1.8 Estructura del trabajo de tesis

Este trabajo compila el proyecto doctoral comprendido por 5 artículos actualmente publicados (Capítulos 2-6) y uno en proceso de arbitraje (Capítulo 7). En los cuales se describe la relación existente entre el registro del campo magnético de la Tierra en rocas volcánicas al momento de su formación, y en algunos materiales arqueológicos en el momento de su manufactura (asociado a procesos térmicos). A continuación, se describen los objetivos particulares de cada uno de los artículos publicados, divididos en dos secciones, de rocas volcánicas y de materiales arqueológicos:

Rocas volcánicas:

Artículo 1: “Analysis of geomagnetic secular variation for the last 1.5Ma recorded by volcanic rocks of the Trans Mexican Volcanic Belt: new data from Sierra de Chichinautzin, Mexico”

El artículo presenta un estudio paleomagnético y de propiedades magnéticas llevado a cabo en diversas estructuras volcánicas del campo volcánico de la Sierra de Chichinautzin y de la Sierra de Santa Catarina de edad Pleistoceno y Holoceno. En el trabajo se detallan los resultados de direcciones medias y polos geomagnéticos virtuales de las unidades volcánicas estudiadas, publicados en alrededor de 50 trabajos. En su conjunto, el artículo describe los nuevos resultados obtenidos junto con los datos previamente publicados en los campos volcánicos mencionados. Asimismo, el trabajo presenta una compilación de los datos paleomagnéticos direccionales publicados sobre la Faja Volcánica Trans-mexicana para el Pleistoceno y Holoceno en México, haciendo una evaluación y análisis crítico de la calidad de los datos publicados, permitiendo diferenciar y clasificar los resultados de acuerdo a su calidad, estableciendo para el futuro, parámetros de calidad que garantizan la publicación de datos de alta confiabilidad.

Artículo 2: “Paleomagnetism and rock magnetic properties of Late Pleistocene volcanism from El Pinacate Volcanic Field, Northwest Mexico”

Se publica un estudio paleomagnético y de propiedades magnéticas realizado en rocas volcánicas del Pleistoceno tardío del Campo volcánico El Pinacate, ubicado en la región Noroeste del estado de Sonora, México. El trabajo presenta resultados direccionales y de intensidad realizados en 16 sitios pertenecientes a 12 unidades volcánicas diferentes. Asimismo, se llevó a cabo la datación de dos unidades volcánicas empleando los resultados direccionales y de intensidad, así como su comparación con modelos de PSV actuales. Los resultados publicados son los primeros en su tipo para el Noroeste de México.

Artículo 3: “Emplacement temperature resolution and age determination of Cerro Colorado tuff ring by paleomagnetic analysis, El Pinacate Volcanic Field, Sonora, Mexico”

El objetivo del artículo es la estimación de la temperatura de emplazamiento, la caracterización de sus propiedades magnéticas, y la datación de la erupción del volcán Cerro Colorado, un anillo de toba localizado dentro del Campo Volcánico El Pinacate, en el desierto de Altar, Estado de Sonora, México. La estimación de la temperatura de emplazamiento y la datación de la erupción se llevaron a cabo luego del análisis direccional de las diferentes componentes de magnetización registradas en los materiales volcánicos; y su posterior comparación con los modelos globales actuales de variación paleosecular.

Artículo 4: “Paleomagnetism and age constraints of historical lava flows from the El Jorullo volcano, Michoacán, Mexico”

El artículo describle un estudio paleomagnético integral llevado a cabo en diversos flujos de lava generados durante la erupción histórica (1759–1766 AD) del volcán El Jorullo, ubicado en región SW de Estado de Michoacán. El Jorullo pertenece al Campo Volcánico Michoacán Guanajuato. El trabajo muestra resultados del análisis direccional y de paleointensidad del campo magnético de la tierra, registrado en diferentes flujos de lava asociados a dicha erupción, así como la caracterización de sus propiedades magnéticas. Con los resultados obtenidos fue posible llevar a cabo la comparación de la edad obtenida con los modelos de variación secular actuales, a fin de demostrar la confiabilidad de los mismos.

Materiales arqueológicos:

Artículo 5: “Critical analysis of the Holocene palaeointensity database in Central America: Impact on geomagnetic modelling”

El artículo muestra los resultados de arqueointensidad obtenidos de varios fragmentos cerámicos encontrados en la zona arqueológica de Chalcatzingo, en el Estado de Morelos. Los cuales están asociados al periodo Epiclásico (650-900 AD). Así mismo, el trabajo presenta una compilación de datos de arqueointensidad y paleointensidad publicados principalmente en México, con la finalidad de llevar a cabo una evaluación y análisis crítico de la calidad y confiabilidad de los mismos. Con ello es posible establecer parámetros de calidad suficientes para producir datos con una confiabilidad y precisión mayores.

Artículo 6: “Archeomagnetic dating and magnetic characterization of ceramics from the Casas Grandes region, Chihuahua, Mexico: Paquimé, Galeana, Villa Ahumada and Samalayuca archeological sites”

El trabajo se encuentra en el apartado de material suplementario, pues esta en arbitraje actualmente. En el se describen los resultados de arqueointensidad obtenidos de diferentes fragmentos cerámicos pertenecientes a diferentes zonas de la región de Casas Grandes, ubicada en el norte del Estado de Chihuahua. Las cerámicas pertenecen a dos grupos cerámicos de la región: Mimbres y Ramos Policromo. El estudio detalla la caracterización de sus propiedades magnéticas, con las cuales fue posible hacer una diferenciación de ambos tipos cerámicos. Y muestra los resultados de arqueointensidad obtenidos, logrando realizar la datación de cada grupo cerámico estudiado. Con estos resultados se da respuesta a diversas preguntas arqueológicas planteadas sobre la cronología de la región. Asimismo, los resultados nuevos aportan datos valiosos a las bases de datos globales.

1.9 Metodología

A continuación se detallan algunos aspectos elementales de los métodos que se emplearon en el proyecto, que abarca la caracterización de las propiedades magnéticas de los materiales, los procesos para la obtención de una dirección paleomagnética y los protocolos de paleointensidad usados hoy día. Así como los parámetros de selección de datos de acuerdo a su calidad para el desarrollo de una base de datos que permita clasificar los resultados de acuerdo a su calidad.

1.9.1 Instrumentación utilizada

Para el trabajo experimental se utilizaron diversos equipos para determinar las propiedades magnéticas de los materiales, así como para medir la dirección e intensidad del CMT registrado en los materiales estudiados. A continuación se mencionan los equipos utilizado en el presente trabajo.

- Para los experimentos de susceptibilidad en función de la temperatura, para curvas a baja (-192°C a 0°C) y alta temperatura (20°C a 680°C) se utilizaron dos equipos: un Bartington MS2 susceptibility meter, y un AGICO MFK2 Kappabridge.
- Para la medición de las curvas de histeresis, magnetización remanente isotermal y curvas de FORC se utilizó un micromagnetómetro Princeton AGM 2900, empleando un campo máximo de 1.2 T
- La medición de la remanencia magnética en las rocas volcánicas se llevó a cabo en magnetómetros de giro AGICO JR-5 y JR-6. Para la medición de material cerámico se utilizó un magnetómetro de giro JR-6 y un magnetómetro criogénico 2G.
- Para la desmagnetización térmica de las muestras se utilizó un horno con blindaje magnético con capacidad para 20 especímenes, y en un rango de temperatura que va de los 100°C a los 600°C.
- La desmagnetización por campos alternos se llevó a cabo empleando un desmagnetizador Molspin, aplicando un campo máximo de 100 mT.
- Los experimentos de paleointensidad se llevaron a cabo empleando un horno con blindaje magnético *MagneticMeasurements*, y aplicando un campo de ca. 40 µT en dos direcciones.

1.9.2 Medición de las propiedades magnéticas

El magnetismo de rocas provee valiosa información sobre los minerales ferromagnéticos contenidos en los diferentes materiales. La adecuada caracterización de dichos materiales permite determinar los minerales portadores de la magnetización.

- Susceptibilidad en función de la temperatura, curvas termomagnéticas:* Este tipo de curvas, permiten identificar la mineralogía magnética y sus posibles transformaciones durante procesos térmicos, en los que es necesario calentar los materiales con incrementos de temperatura hasta temperaturas de 680°C (Figura 7). Esto es posible de acuerdo a la T_c de cada mineral. Con esta información es posible conocer la mineralogía magnética contenida en la muestra. Un método para conocer la T_c puntual de cada fase magnética es la estimación de la primera derivada de las curvas de calentamiento y enfriamiento (Figura 7).

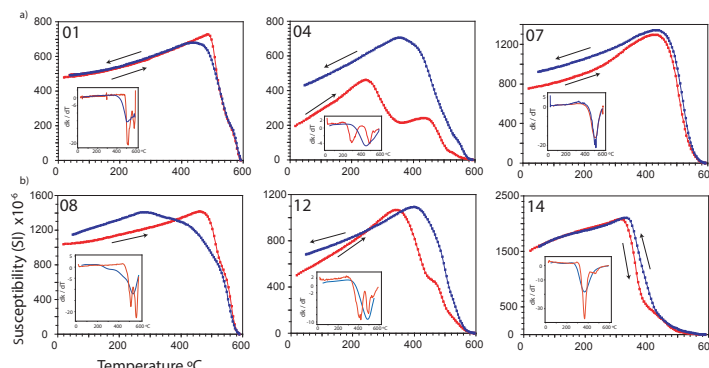


Figura 7. Ejemplos de curvas de susceptibilidad en función de la temperatura y su primera derivada (recuadro interior).

- b) *Curvas de histéresis y de adquisición de una magnetización remanente isotermal (IRM):* permiten determinar diversos parámetros magnéticos que permiten definir la naturaleza misma de los minerales, como lo es la coercitividad (H_c), magnetización de saturación (M_s) y sus respectivos valores de remanencia, que en su conjunto permiten determinar y caracterizar el tipo de dominio magnético, así como el tamaño de partícula magnética y las posibles mezclas de diferentes minerales en la muestra, e.g. Figura 8. Lo cual es de gran utilidad para seleccionar los materiales que potencialmente puedan ser viables para un proceso de paleointensidad. Una adecuada caracterización de estos parámetros permite mejorar la probabilidad de éxito en este tipo de experimentos.

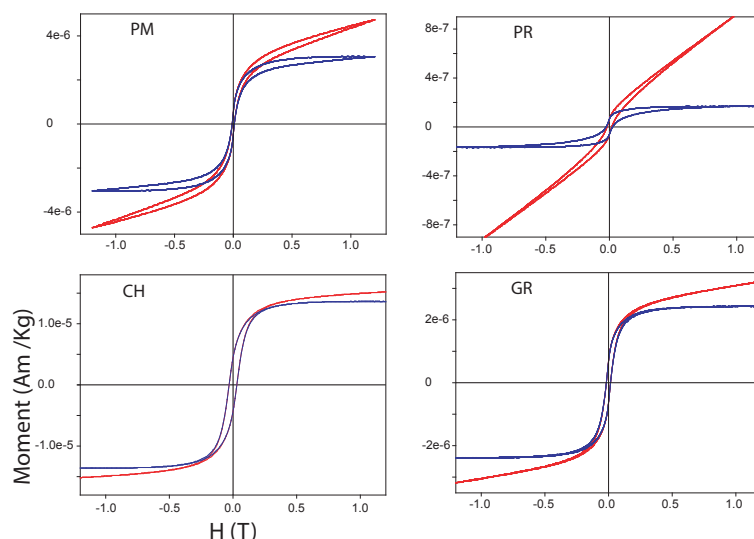


Figura 8. Ejemplos de curvas de histéresis.

- c) *Curvas reversibles de primer orden (FORC, por sus siglas en Inglés):* permiten la caracterización detallada del espectro de coercitividad y la interacción existente entre los diferentes dominios magnéticos contenidos en una muestra (Carvallo et al., 2003; Roberts et al., 2000, 2014; Zhao et al., 2017). Esta técnica es de gran utilidad para definir la relación entre los diferentes dominios magnéticos y el espectro de coercitividad la figura 9 muestra un ejemplo de una curva de FORC.

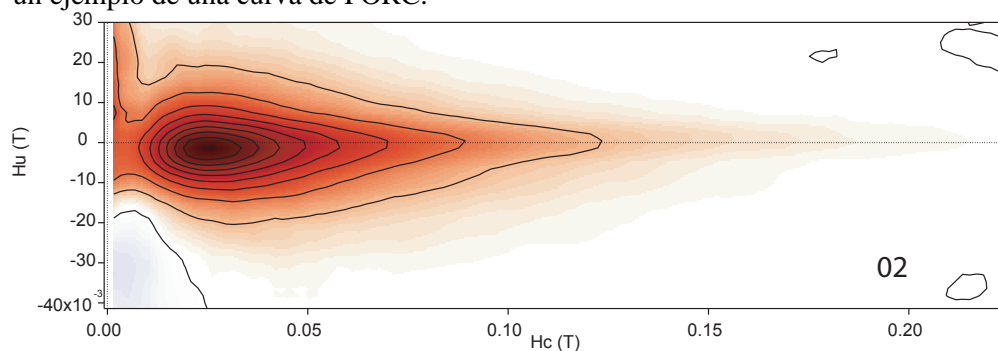


Figura 9. Ejemplo de un pseudo dominio simple representado por un diagrama de FORC.

1.9.3 Métodos de desmagnetización y Análisis direccional

La parte fundamental del paleomagnetismo radica en el análisis de la dirección e intensidad del CMT registrada en distintos tiempos y en diferentes materiales. Para poder conocer la dirección remanente característica (ChRM) es necesario llevar a cabo un proceso de desmagnetización, utilizando principalmente dos métodos, la desmagnetización térmica y la desmagnetización por campos magnéticos alternos. En ambos la función básica es la de identificar (y eliminar) componentes de magnetización en diferentes intervalos de temperatura o campos aplicados en incrementos progresivos (e.g. Figura 10). Esto permite construir un vector resultante que definirá la ChRM, la cual se asume, principalmente, se obtuvo en el momento de formación de la roca. En el caso de las rocas volcánicas, se obtiene durante el enfriamiento y al momento de pasar por debajo de la temperatura de Curie de los minerales magnéticos, en el caso de un mineral como la magnetita, esta se encuentra alrededor de los 580°C.

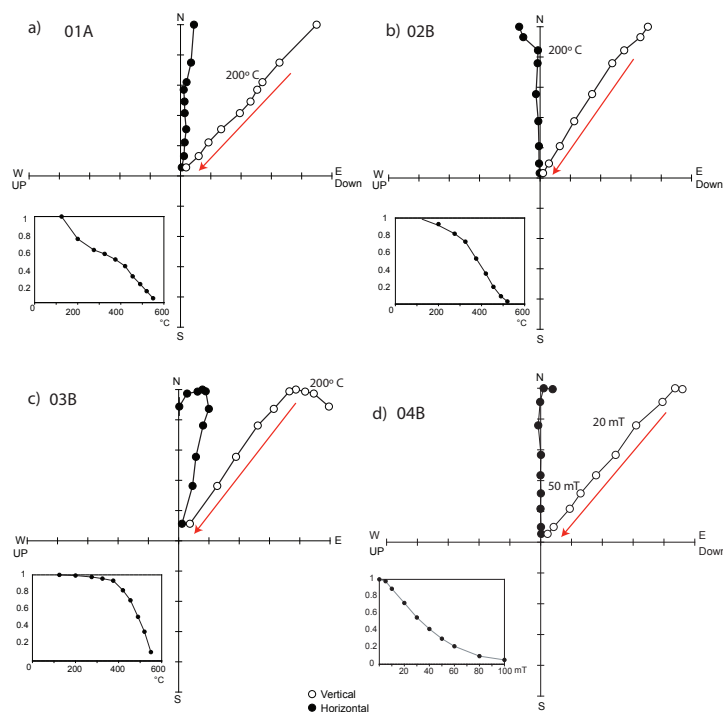


Figura 10. Ejemplos de diagramas de Zijderveld luego de la desmagnetización por temperatura y por campos magnéticos alternos. NO REF...

Posterior al proceso de desmagnetización se lleva a cabo en cada muestra, un análisis de componentes principales (PCA) en el que se estima la linelididad del vector obtenido (Kirschvink, 1980). De esta manera se obtiene una dirección paleomagnética para un grupo de muestras de la misma localidad (sitios) formados en al mismo tiempo. La calidad de los resultados paleomagnéticos se evalúa mediante el análisis estadístico de los datos empleando estadística de Fisher (1953), determinando el nivel de confiabilidad (95%), dispersión (k) y dispersión angular de los vectores estimados. Con estos parámetros estadísticos es posible estimar la calidad de los resultados y hacer una selección de los de mayor confiabilidad.

1.9.4 Paleointensidad del campo magnético terrestre

Para poder tener un estudio integral de paleomagnetismo y por ende de la PSV, es necesario efectuar un análisis detallado del vector completo del CMT, el cual incluye los resultados direccionales y la estimación de la paleointensidad y momento dipolar virtual (VDM). Esto permitirá comprender la variación secular en diferentes ventanas de tiempo, que pueden ir de unas decenas hasta varios miles de años.

Para estimar la paleointensidad del CMT registrada en varios materiales existen diferentes metodologías que permiten calcular con cierta precisión la magnitud del CMT. Esta tarea es considerablemente mas compleja que la obtención de una dirección paleomagnética, y es complementada con el estudio de sus propiedades magnéticas, con la finalidad de seleccionar cuidadosamente las muestras con mayor potencial de éxito. A continuación, se detallan brevemente algunos de los métodos mas usados actualmente, y de los cuales constantemente se publican variaciones en los protocolos, buscando mejorar la calidad y confiabilidad de los resultados.

- a) *Métodos del tipo Thellier-Thellier:* Existe una amplia variedad de métodos basados en el trabajo realizado por Thellier y Thellier (1959), y por los protocolos experimentales sobre la magnetización remanente térmica (TRM) realizados por Koenigsberger (1932). El procedimiento consiste básicamente en el calentamiento progresivo de la muestra en diferentes intervalos de temperatura, en presencia de un campo magnético controlado en el laboratorio, y obteniendo un valor de paleointensidad dada la variación de la adquisición de una pTRM proporcional a la magnetización original. Uno de los procedimientos basado en el trabajo de Thellier mas empleados en la actualidad es el desarrollado por Coe (1967), en el cual propone realizar calentamientos progresivos a diferentes intervalos, calentando la muestra en primera instancia sin la presencia de un campo magnético (Zero-field) y permitiendo el enfriamiento de la misma bajo esa misma condición, posteriormente recalentar la muestra a la misma temperatura pero con la presencia de un campo magnético conocido y controlado en el laboratorio, y permitiendo el enfriamiento bajo la presencia del mismo, obteniendo la magnetización de laboratorio por medio de una diferencia vectorial; a este paso se le conoce como “Zero field in-field” (ZI). Posteriormente propuso llevar a cabo chequeos periódicos en diversos puntos de temperatura inferiores a los medidos, a fin de detectar cualquier alteración térmica de la muestra durante el proceso de calentamiento. De manera análoga Aitken (1981) propuso realizar un procedimiento “In-Field Zero-field” (IZ), en cualquier caso, para estos procedimientos al incrementarse la temperatura la NRM disminuye y la adquisición para cada pTRM se incrementa. Finalmente, el protocolo denominado “In-Field Zero field- Zero field in-field” (IZZI) propuesto por Tauxe y Staudigel (2004), consiste en aplicar los protocolos de Aitken (1988) y Coe (1967) de manera consecutiva, alternando el IZ con el ZI en cada calentamiento. La figura 11 muestra algunos ejemplos de resultados de experimentos de paleointensidad por el método de Thellier-Thellier. Los cambios en los protocolos, buscan mejorar el porcentaje de éxito en los experimentos, reduciendo la alteración durante el proceso de calentamiento; y realizando un mejor seguimiento de la alteración mediante los chequeos.

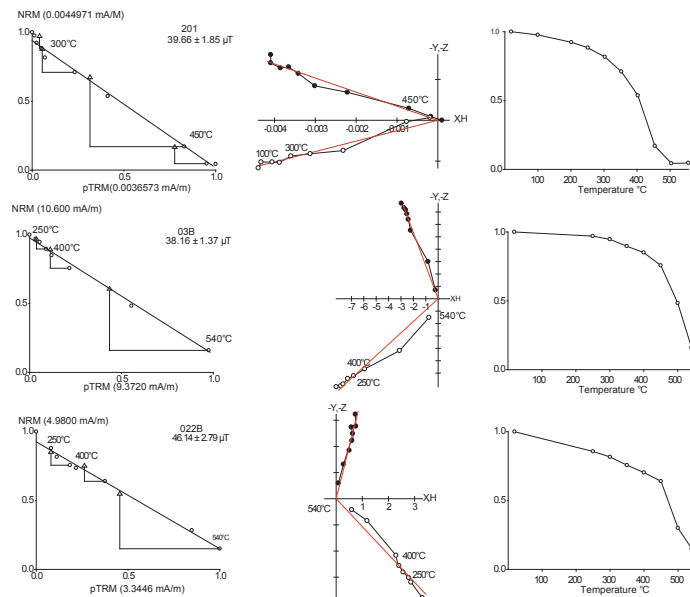


Figura 11. Diagrama de Arai (izquierda), diagrama de Zijderveld (centro) y diagrama de desmagnetización (derecha) luego de aplicar el método de Thellier-Thellier.

- b) *Método de multi-especimen (MSP)*: El método desarrollado por Dekkers y Bohnel (2006), propone una metodología para la obtención de datos de paleointensidad, basado en la linealidad de la magnetización remanente térmica parcial (pTRM) a un campo aplicado, una propiedad que resulta independiente del dominio magnético al que pertenece. Reduciendo los calentamientos de la muestra y por ende la probabilidad de alteración de la misma por ese proceso. Para llevar a cabo el protocolo se deben tomar en cuenta diferentes aspectos, primero, las muestras deben poseer la misma historia magnética, al ser un método que implica varios especímenes que comparten la misma historia durante su formación, de tal manera que cada uno de estos recibirá únicamente un tratamiento, es decir, la adquisición de una pTRM en el laboratorio a un campo magnético determinado, manteniéndose constante dicha temperatura para todos los especímenes, variando de esta manera el campo aplicado a cada uno de estos; induciendo de esta manera un pTRM paralelo al TRM original, y asemejando el campo aplicado al campo original registrado por la muestra, a fin de encontrar la mínima variabilidad entre los mismos.
De esta manera se busca aproximar linealmente la relación de la intensidad del campo magnético original con el inducido en el laboratorio, aplicando a cada espécimen de la muestra un campo magnético diferente y a una temperatura constante. Se obtiene un espectro de pTRM variando en función del campo aplicado, y se normaliza una función de regresión lineal de estos datos, obteniendo el valor de paleointensidad al aproximarse dicha regresión a un valor de cero, lo que implicaría una disminución de la varianza entre el campo aplicado y el valor del campo magnético original.
- c) *Método de microondas (MW)*: El método de microondas (Walton et al., 1996; Hill and Shaw, 1999) se presenta como una alternativa a los métodos tradicionales del tipo Thellier, en la que la muestra se calienta y magnetiza por medio de un campo electromagnético de alta frecuencia. Lo cual permite reducir la alteración producida por los métodos de calentamiento tradicionales. Por su gran complejidad y alto costo, el equipo que permite llevar a cabo este tipo de protocolos solo se encuentra disponible en dos laboratorios: El Laboratorio de

geomagnetismo de la Universidad de Liverpool, en Inglaterra, y en el Laboratorio de Paleomagnetismo de Centro de Geociencias, UNAM.

1.9.5 Corrección de la paleointensidad por anisotropía

La TRM adquirida por un material, depende preferentemente del ángulo en el cual el campo es aplicado, y como regla general la dirección preferente es perpendicular al plano del material, existiendo un plano preferencial en el cual la adquisición de la remanencia se lleva a cabo de mejor manera, independientemente de la forma del material, la cual está en función de la anisotropía misma de la muestra (ATRM).

Los efectos de la ATRM de los materiales al momento de estimar una paleointensidad pueden provocar una sobreestimación del valor real. Primero la dirección de la NRM es diferente a la dirección del campo aplicado durante la adquisición de la pTRM en el laboratorio. Segundo, la componente horizontal del campo magnético original da origen a una magnetización preferente en la misma dirección (Aitken, 1981; 1988). Estos efectos se observan principalmente en materiales arqueológicos.

Para estimar un factor de corrección que permita ajustar la paleointensidad obtenida, se realizan seis calentamientos en presencia de un campo, adicionales al proceso de Thellier. Los calentamientos son en seis posiciones de acuerdo a los tres ejes coordenados (+X, -X, +Y, -Y, +Z, -Z). El cálculo del factor de corrección por ATRM se obtiene resolviendo el tensor construido con los parámetros cartesianos obtenidos de las seis mediciones, en función la dirección de la magnetización de la muestra (Veitch et al., 1984).

1.9.6 Modelos de variación paleosecular y bases de datos globales

En la actualidad, las herramientas informáticas permiten la compilación de una gran cantidad de resultados con diferentes características, localidades, temporalidades, tipos de materiales, entre otros. La tendencia global hoy en día está enfocada a la generación de sistemas de información, que permite procesar toda la información disponible para el desarrollo de modelos analíticos, estadísticos y estocásticos, los cuales sirven para estudiar fenómenos a gran escala. El paleomagnetismo no es la excepción, actualmente existen diferentes herramientas y modelos de PSV (Figura 12) a escala global (e.g. Pavón-Carrasco et al., 2014; Opdyke et al., 2015; Panovska et al., 2018; Cromwell et al., 2018; Doubrovine et al., 2019), y a diversas ventanas temporales. Estas herramientas reúnen en un mismo sitio grandes cantidades de datos paleomagnéticos obtenidos con diferentes metodologías, los cuales son homologados por los diferentes criterios establecidos que verifican la confiabilidad de los resultados. Tal es el caso de los resultados de paleointensidad, para los que existe una gran cantidad de parámetros que determinan su calidad, detallados en el Standard Paleointensity Definitions (SPD) (Paterson et al., 2014).

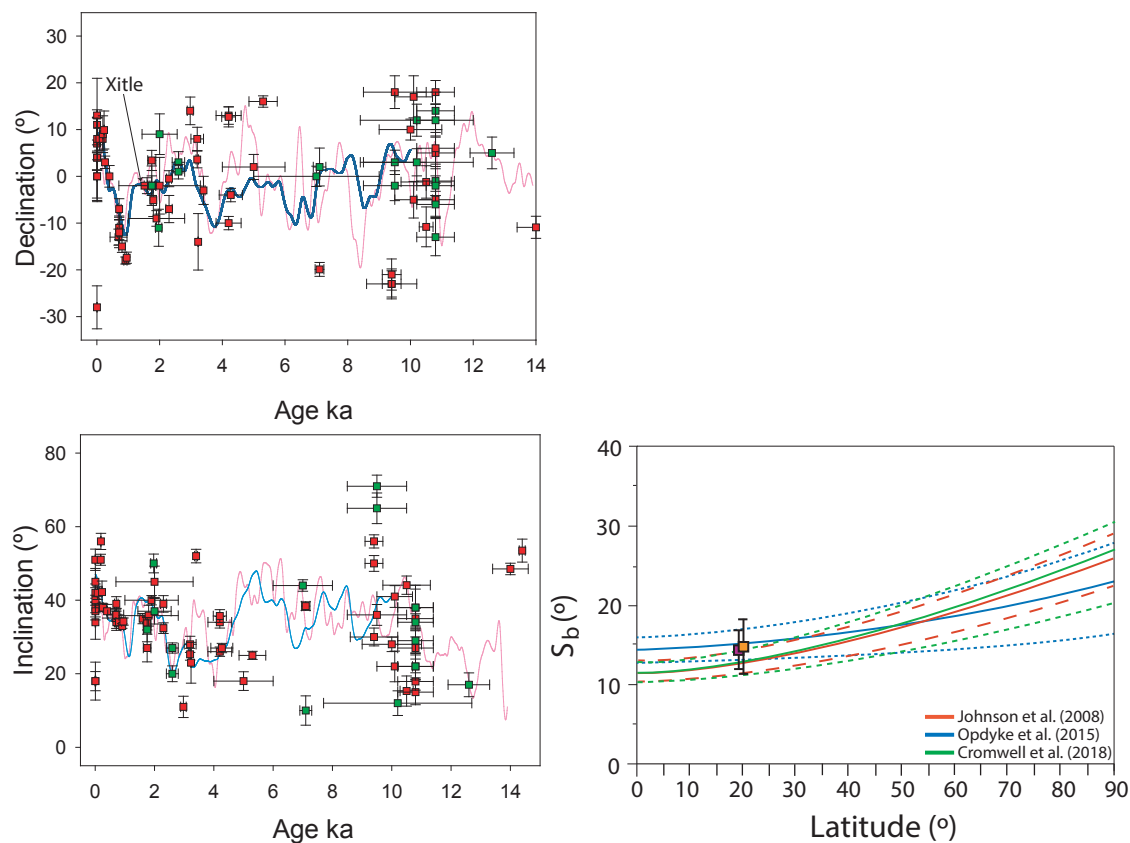


Figura 12. Ejemplos de los modelos de variación secular (izquierda) y paleosecular (derecha) a diferentes escalas, y la comparación de algunos datos de México.

1.9.7 Muestreo paleomagnético

El muestreo paleomagnético para la colección de muestras volcánicas, se llevó a cabo en flujos de lava distribuidos en diferentes localidades de la FVTM y del campo volcánico El Pinate (Figura 6). La selección de los sitios de muestreo se llevó a cabo de acuerdo con dos criterios básicos:

- i) Cada flujo debía contar con una edad radiométrica reportada, o en su defecto con un buen control estratigráfico y de emplazamiento.
- ii) Los sitios de muestreo deben encontrarse *in-situ*, es decir, en el mismo lugar donde fueron formados originalmente.



Figura 13. Trabajo de campo para la obtención de muestras de paleomagnetismo.

Las muestras se obtuvieron mediante el uso de una nucleadora con motor de gasolina con adaptación para barrenar de ca. 25 cm de largo y 2.54 cm de diámetro, con una corona de diamante industrial. Durante el proceso de perforación se utiliza agua para enfriar y lubricar (Figura 13 a, c). Para la orientación espacial de los núcleos se empleó una brújula azimutal y solar de tipo Brunton. Orientando cada núcleo en dirección paralela al sentido de perforación (Δx) (Figura 13 b y d), adquiriendo el azimuth de dicha dirección y el ángulo de inclinación (respecto a la vertical) del núcleo.

Los materiales arqueológicos reportados en el capítulo 6 y en el material suplementario S1, fueron proporcionados por los arqueólogos encargados de cada sitio arqueológico. Los detalles de ubicación y características físicas de cada material se encuentran allí detallado.

Los detalles de ubicación y edad de cada sitio reportado en el presente trabajo se muestran en cada uno de los artículos de los capítulos 2 al 7, y en el material suplementario S1 de este trabajo. La distribución general y ubicación geográfica de todos los sitios reportados se muestran en la Figura 6.

Capítulo 2

Analysis of geomagnetic secular variation for the last 1.5Ma recorded by volcanic rocks of the Trans Mexican Volcanic Belt: new data from Sierra de Chichinautzin, Mexico

A. Rodríguez-Trejo,¹ L. M. Alva-Valdivia,² M. Perrin,³ G. Hervé³ and N. López-Valdés¹

¹Posgrado en Ciencias de la Tierra, Instituto de Geofísica, Universidad Nacional Autónoma de México, Circuito de la Investigación Científica, C.P. 04510 México D. F., México. E-mail: alekz_igf@hotmail.com

²Laboratorio de Paleomagnetismo, Instituto de Geofísica, Universidad Nacional Autónoma de México, Circuito de la Investigación Científica, C.P. 04510 México D. F., México

³Aix Marseille Univ, CNRS, IRD, INRA, Coll France, CEREGE, Aix-en-Provence, France

Accepted 2019 July 5. Received 2019 June 16; in original form 2019 February 7

SUMMARY

The great wealth of volcanism along the Trans Mexican Volcanic Belt (TMVB) and the need to improve the secular variation curve of the Earth magnetic field of the region is the aim of this research. 300 oriented cores from 33 sites and 21 individual cooling units were acquired from Sierra de Chichinautzin volcanic field (ChVF) and Sierra de Santa Catarina (SSC). Directional analysis and rock magnetic experiments were performed (e.g. thermal demagnetization, hysteresis loop, susceptibility vs temperature), achieving 21 new averaged palaeomagnetic directions. New results are consistent with the previous studies on the same cooling unit. We compiled all the palaeomagnetic studies performed on the ChVF, updating age and calculating an average direction per cooling unit and estimating an overall mean direction for the ChVF (Dec = 359.1°, Inc = 35.3°, N = 33, k = 21.6, $\alpha_{95} = 5.5^\circ$, Plat = 87.7° N, Plong = 227.4° E, K = 31.8, A95 = 4.5°).

Afterwards, we compiled all the previous palaeomagnetic studies along the whole TMVB with age ranging from 0 to 1.5 Ma, and constrained the directional analyses by specific quality criteria such as well-defined age, number of samples and quality of kappa) on the cooling unit consistency.

The mean direction and virtual geomagnetic pole (VGP) estimated for the TMVB, during the periods 0–40 ka and 0–1.5 Ma, are close to the geographic pole, supporting the validity of the geocentric axial dipole hypothesis. The directional results of this study also fit well with the predictions at Mexico City of the models SHA.DIF.14k and CALS10k2 calculated for the last 14 ka. The dispersion of the VGP's on the TMVB are also consistent with the expected values proposed by different models of palaeosecular variation. However, large gaps in the temporal record remain that should be filled by further palaeomagnetic studies.



Analysis of geomagnetic secular variation for the last 1.5 Ma recorded by volcanic rocks of the Trans Mexican Volcanic Belt: new data from Sierra de Chichinautzin, Mexico

A. Rodríguez-Trejo,¹ L. M. Alva-Valdivia,² M. Perrin,³ G. Hervé³ and N. López-Valdés¹

¹Posgrado en Ciencias de la Tierra, Instituto de Geofísica, Universidad Nacional Autónoma de México, Circuito de la Investigación Científica, C.P. 04510 México D. F., México. E-mail: alekz.igf@hotmail.com

²Laboratorio de Paleomagnetismo, Instituto de Geofísica, Universidad Nacional Autónoma de México, Circuito de la Investigación Científica, C.P. 04510 México D. F., México

³Aix Marseille Univ, CNRS, IRD, INRA, Coll France, CEREGE, Aix-en-Provence, France

Accepted 2019 July 5. Received 2019 June 16; in original form 2019 February 7

SUMMARY

The great wealth of volcanism along the Trans Mexican Volcanic Belt (TMVB) and the need to improve the secular variation curve of the Earth magnetic field of the region is the aim of this research. 300 oriented cores from 33 sites and 21 individual cooling units were acquired from Sierra de Chichinautzin volcanic field (ChVF) and Sierra de Santa Catarina (SSC). Directional analysis and rock magnetic experiments were performed (e.g. thermal demagnetization, hysteresis loop, susceptibility vs temperature), achieving 21 new averaged palaeomagnetic directions. New results are consistent with the previous studies on the same cooling unit. We compiled all the palaeomagnetic studies performed on the ChVF, updating age and calculating an average direction per cooling unit and estimating an overall mean direction for the ChVF (Dec = 359.1°, Inc = 35.3°, N = 33, k = 21.6, $\alpha_{95} = 5.5^\circ$, Plat = 87.7° N, Plong = 227.4° E, K = 31.8, A95 = 4.5°).

Afterwards, we compiled all the previous palaeomagnetic studies along the whole TMVB with age ranging from 0 to 1.5 Ma, and constrained the directional analyses by specific quality criteria such as well-defined age, number of samples and quality of kappa) on the cooling unit consistency.

The mean direction and virtual geomagnetic pole (VGP) estimated for the TMVB, during the periods 0–40 ka and 0–1.5 Ma, are close to the geographic pole, supporting the validity of the geocentric axial dipole hypothesis. The directional results of this study also fit well with the predictions at Mexico City of the models SHA.DIF14k and CALS10k2 calculated for the last 14 ka. The dispersion of the VGP's on the TMVB are also consistent with the expected values proposed by different models of palaeosecular variation. However, large gaps in the temporal record remain that should be filled by further palaeomagnetic studies.

Key words: Palaeomagnetic secular variation; Rock and mineral magnetism.

1 INTRODUCTION

The Earth's magnetic field, mainly generated in the core of the Earth, has temporal and spatial variations in direction and intensity recorded by diverse geologic materials, as volcanic rocks, archaeological materials or sediments. However, sediments that can give only relative palaeointensity estimates will not be considered here. Global models were developed using data repositories, for example MagIC (<https://www2.earthref.org/MagIC>) or GEOMAGIA50.v3 (Brown *et al.* 2015), to characterize the behaviour and the variation through time of the geodynamo. For the last millennia, models as CALS10k.2 and ARCH10k.1 (Constable *et al.* 2016), SHA.DIF14k

(Pavón-Carrasco *et al.* 2014) were computed by spherical harmonic analysis in space.

An accurate modelling requires a homogeneous spatial distribution of data over the globe. But the present distribution is strongly biased towards mid-latitudes of the northern hemisphere (e.g. Panovska *et al.* 2018), emphasizing the need of data from low latitudes and the Southern hemisphere. Mexico is a key area through its rich archaeological past and its intense and continuous volcanic activity for millions of years. Of particular interest, the TMVB is an active volcanic arc, characterized by thousands of volcanic structures that cross central Mexico from east to west (Fig. 1a). In the TMVB, two important volcanic fields were emplaced from late

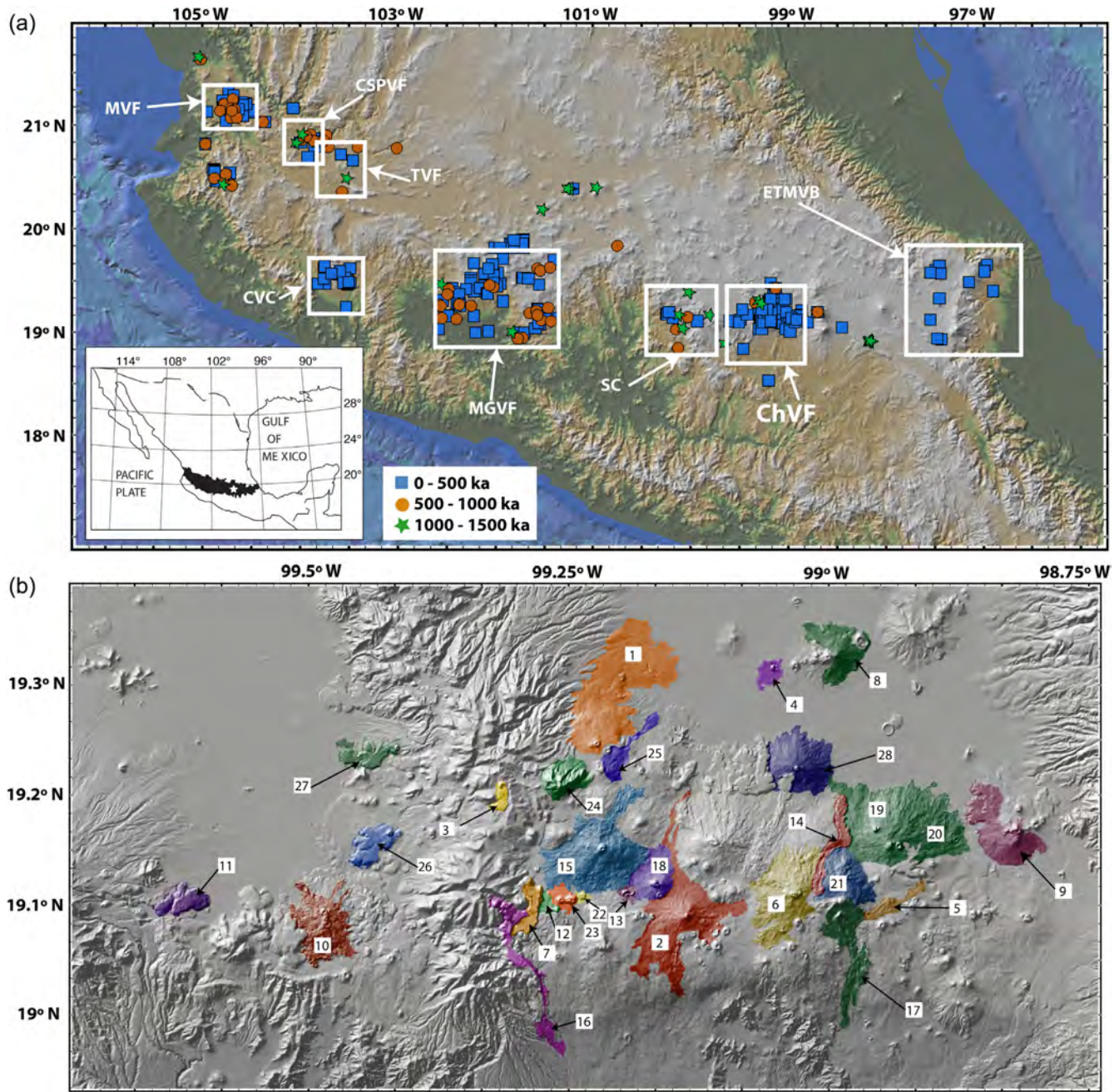


Figure 1. (a) TMVB and location of published palaeomagnetic data for the past 1.5 Ma (Satellite image from Google-earth 2018; ChVF: Sierra de Chichinautzin Volcanic Field; CSPVF: Ceboruco-San Pedro Volcanic Field; CVC: Colima Volcanic Complex; ETMVB: Eastern Trans Mexican Volcanic Belt; MGVF: Michoacán-Guanajuato Volcanic Field; MVF: Mascota Volcanic Field; SC: Sierra de las Cruces; TVF: Tequila Volcanic Field). Age references and site locations are available in Table 1S. (b) Coloured areas represent the sampled cooling units in Sierra de Chichinautzin volcanic field and Sierra de Santa Catarina monogenetic volcanic group (numbers refer to the ID of Table 1, location of the sampling sites and age references are available in Table 2; cooling units 4 and 8 belong to the Sierra de Santa Catarina (SSC) volcanic group).

Pleistocene to Holocene: the Michoacán-Guanajuato Volcanic Field (MGVF, Fig. 1b) in west-central Mexico (e.g. González *et al.* 1997; Michalk *et al.* 2013; Mahgoub *et al.*, 2017, 2019), and the ChVF (Fig. 1b) in central Mexico. There were many palaeomagnetic studies focusing on field directions and intensities, during the last 30 yr (e.g. Herrero-Bervera & Pal 1977; Urrutia-Fucugauchi & Martín Del Pozzo 1993; Böhnel *et al.* 2003; Alva-Valdivia 2005), but new radiocarbon and Argon-Argon ages, obtained in the past 15 yr (e.g.

Siebe *et al.* 2004b; Guilbaud *et al.* 2015; Jaimes-Viera *et al.* 2018) open exciting perspectives for secular variation studies.

In this work, we acquired new palaeomagnetic data from Sierra de Chichinautzin Volcanic Field (ChVF) and Sierra de Santa Catarina (SSC), which were analysed together with previous published data on rocks with well-defined age. Next, a compilation and critical analysis of the available volcanic palaeomagnetic data from

the TMVB improved the understanding of the variation of the geo-magnetic field during the late Pleistocene and Holocene in central Mexico.

2 GEOLOGY, CHRONOLOGY AND SAMPLING

The TMVB is a volcanic arc, 1000-km-long belt extending from the Pacific Ocean to the Gulf of Mexico, formed by subduction along the Acapulco trench, since middle Miocene (*ca.* 16 Ma) to present day (Ferrari *et al.* 1994, 1999). The TMVB is roughly a W–E oriented transverse belt, formed by numerous Mexican geological provinces (Ortega-Gutiérrez *et al.* 1992; Aguirre-Díaz *et al.* 1998). This geometry exposes a configuration of volcanic vents, which include abundant scoria cones grouped in extensive monogenetic volcanic fields, such as the ChVF (Fig. 1). The variations in the subduction angle of the Cocos plate, chemical assemblages, type of volcanism, change in arc width, and the existence of intraplate subduction-related alkaline volcanism, divide the TMVB into three portions: eastern, central and western (Ferrari *et al.* 2000; Gómez-Tuena *et al.* 2007). The scoria cones and related volcanic deposits studied here are part of the central TMVB. During the Pleistocene, more than 8000 volcanic structures, such as stratovolcanoes, scoria and cinder cones, were formed (Demant 1978; Aguirre-Díaz *et al.* 1998).

The ChVF, a still active hazardous volcanic field, consists of more than 220 monogenetic volcanic structures of wide compositional range. The activity started 1.6 Ma and the last eruption, the Xitle volcano, was dated at 1.6 ka BP (e.g. Martin del Pozzo 1982; Siebe *et al.* 2004a; Arce *et al.* 2013). The eruption rate was estimated around $0.016 \text{ km}^3 \text{ ka}^{-1}$ per 100 km^2 for the whole volcanic field (Arce *et al.* 2013) and around $0.6 \text{ km}^3 \text{ ka}^{-1}$ during the Holocene (Siebe *et al.* 2005). Close to the ChVF is located the SSC monogenetic volcanic group (units 4 and 8 in Fig. 1b) with seven volcanoes formed by lava flows and pyroclastic deposits, ranging in age from 132 to 2 ka (Jaimes-Viera *et al.* 2018).

Our palaeomagnetic sampling focused on 21 well-dated volcanic cooling units from the ChVF and SSC (Table 1). A cooling unit is defined here as a volcanic event, during which rocks were emplaced and cooled rapidly, recording almost instantaneously the Earth Magnetic Field. One up to six palaeomagnetic sites have been sampled in a given cooling unit. Ten cooling units were dated using the radiocarbon technique. The uncalibrated ages given in the original papers were carefully analyzed and updated when possible (Table 1). For example, Gonzalez *et al.* (1997) reported a ^{14}C age of 4070 ± 150 uncalibrated BP (Kirianov *et al.* 1990) for the *El Pelado* volcano but we retained only the three ages, 9620 ± 160 , $10\,270 \pm 190$ and $10\,900 \pm 280$ uncalibrated BP, from Siebe *et al.* (2004b). All radiocarbon ages were calibrated using the most recent version of the calibration curve Intcal13 (Reimer *et al.* 2013). The age of seven others cooling units were defined using recent Argon-Argon dates (Arce *et al.* 2013; Jaimes Viera *et al.* 2018). Finally, four cooling units could not be dated more precisely than by their stratigraphic constraints with other cooling units.

The sampling was distributed in three groups: (i) the younger group of age ranging from 2 to 40 ka; (ii) the older group of age from 40 ka to 1.2 Ma, sampling volcanic structures and (iii) Sierra de Santa Catarina monogenetic volcanic group. The samples were collected *in situ*, avoiding fractured and displaced blocks. All samples were drilled directly in the field with a portable gasoline powered drill, and oriented with magnetic and sun compasses. A total of

300 cores, one inch in diameter and 6–15 cm long, were collected from 33 individual sites (8–10 cores per site) belonging to 21 cooling units along the ChVF and SSC (Fig. 1b). Cores were cut into 22-mm-long standard specimens.

3 METHODOLOGY AND LABORATORY PROCEDURES

Rock magnetic experiments were carried out in the Laboratory of Palaeomagnetism at UNAM, Mexico (except when indicated) to identify the magnetic carriers of magnetization, estimate the thermal stability of the ferromagnetic minerals during the heating processes, and characterize the domain state of the magnetic particles.

One sample per cooling unit was selected to measure the k – T curves using MFK-FA and MFK2 susceptibility-meters (Agico, Kappabridge) in UNAM and CEREGE laboratories, respectively. Specimens were heated in air from room temperature up to 620°C .

In order to further investigate the ferromagnetic mineralogy, the hysteresis loops and acquisition of isothermal remanent magnetization (IRM) curves were acquired on small chip rocks from one sample per cooling unit using a Princeton 2900 MicroMag Alternating Gradient Magnetometer, with maximum applied fields up to 1.2 Tesla.

For the determination of the palaeomagnetic directions from the ChVF and SSC, 33 individual sites from 21 different cooling units were studied. Remanent magnetizations were measured using an AGICO JR-6 spinner magnetometer in a magnetically shielded room and analyzed by stepwise alternating field (AF) and/or thermal demagnetization on specimens from all sites. AF demagnetization was carried out on 183 specimens with a Molspin demagnetizer (Molspin Limited, England), using 10 steps up to 100 mT. Thermal demagnetization was performed on 79 specimens in a non-inductive Schönstedt furnace, with 10–12 steps every 40°C from 100 to 600°C .

The directions of the Characteristic Remanent Magnetization (ChRM) were estimated by principal component analysis (Kirschvink 1980), with at least five demagnetization steps and a maximum angular deviation (MAD) below 5° . As there are no report of field evidences for local tectonic movements posterior to the lava emplacement, no tectonic correction was applied.

Mean directions and VGPs were calculated at each site with Fisher statistics (Fisher 1953) and summarized in Table 2 with their α_{95} -confidence circle and Fisher precision parameter (k) parameters. A constant VGP latitude of 45° was used as a cutoff to discriminate the transitional values (Tauxe *et al.* 2003; Johnson *et al.* 2008; Doubrovine *et al.* 2019).

4 ROCK MAGNETISM

4.1 Susceptibility as a function of temperature (k – T)

After the k – T experiments, up to 70 per cent of the curves display two magnetic phases during the heating process and high reversibility (Fig. 2a) or a higher susceptibility for the cooling branch.

The Curie temperature range is between 510 and 540°C for the high-temperature phase corresponding to Ti-poor titanomagnetite. The Curie temperature ranging from 230 to 300°C , the low-temperature phase, is likely Ti-rich titanomagnetite. Two samples show highly reversible curves observed with the unique presence of Ti-poor magnetite (Figs 2c and d). The irreversible curve of El Pelado (Fig. 2b) might be related to the occurrence of Ti-maghemitite

Table 1. Summary of the reported ages for ChVF and SSC, including the estimated calibrated age. The radiocarbon ages were calibrated with IntCal13 curve (Reimer *et al.* 2013) using ChronoModel software (Lanos & Philippe 2017). The average age (given in kyr BP) and its error were defined between the older and younger boundaries of the calibrated date interval at 95 per cent of confidence (2σ).

ID	Cooling unit	Calibrated age (kyrs BP)	Age error (kyrs)	Age method	Uncalibrated ^{14}C (yrs BP)	Reference
1	Xitle	1.61	0.09	^{14}C	1670 \pm 35	Siebe (2000)
2	Chichinautzin	1.75	0.13	^{14}C	1835 \pm 55	Siebe <i>et al.</i> (2004b)
3	Jumento	1.97	0.08	^{14}C	2010 \pm 30	Arce <i>et al.</i> (2015)
4	Guadalupe	2	0.56	Ar-Ar		Jaimes-Viera <i>et al.</i> (2018)
5	Pelagatos	2.6	0.2	^{14}C	2520 \pm 105	Guilbaud <i>et al.</i> (2009)
6	Tláloc	7.1	0.2	^{14}C	6200 \pm 85	Siebe <i>et al.</i> (2005)
7	Tabaquillo	7	9	Ar-Ar		Jaimes-Viera <i>et al.</i> (2018)
8	Mazatepec	23	4	Ar-Ar		Jaimes-Viera <i>et al.</i> (2018)
9	Chinconquiat	>31		Stratigraphy		
10	Tres Cruces	9.4	0.3	^{14}C	8390 \pm 100 8490 \pm 90	Bloomfield (1975)
11	Tenango Basalt	9.5	1.0	^{14}C	8390 \pm 130 8440 \pm 40 8700 \pm 180	Bloomfield (1974)
12	Los Cardos	<10		Stratigraphy		
13	Cima	10.1	0.6	^{14}C	10 160 \pm 210 10 410 \pm 80	Kirianov <i>et al.</i> (1990)
14	Tlacotenco	6.2–14		Stratigraphy		Siebe <i>et al.</i> (2005)
15	El Pelado	10.8	0.6	^{14}C	9620 \pm 160 10 270 \pm 190 10 900 \pm 280	Siebe <i>et al.</i> (2004b)
16	Huiloté	>10		Stratigraphy		
17	Cerro del Agua	12.6	0.7	^{14}C	10 845 \pm 290	Guilbaud <i>et al.</i> (2015)
18	Acopíaxco	>14		Stratigraphy		Lorenzo-Merino (2016)
19	Dos Cerros 1	16.6	0.4	^{14}C	13 695 \pm 110	Guilbaud <i>et al.</i> (2015)
20	Dos Cerros 2	16.6	0.6	^{14}C	13 769 \pm 201	Guilbaud <i>et al.</i> (2015)
21	Cilcuayo	>18.7		Stratigraphy		
22	Raíces-Cajete	18.9	0.3	^{14}C		Mahgoub <i>et al.</i> (2019)
23	Tres Cumbres	21.5	1.8	^{14}C	16 700 \pm 150 19 680 \pm 120	Kirianov <i>et al.</i> (1990)
24	Ajusco 1	390	160	K-Ar		Mora-Alvarez <i>et al.</i> (1991)
25	Ajusco 2	22.6	0.3	^{14}C	18 680 \pm 120	Urrutia-Fucugauchi & Martin del Pozzo (1993)
26	Malinale 1	22.8	1.4	^{14}C	18 900 \pm 600	Kirianov <i>et al.</i> (1990)
27	Cuautl	23.5	0.5	^{14}C	19 530 \pm 160	Bloomfield (1975)
28	Tezontle	26.3	0.8	^{14}C	21 860 \pm 540 21 860 \pm 540	Bloomfield (1975)
29	Teuhatlí	36	1.8	^{14}C	31 790 \pm 755	Guilbaud <i>et al.</i> (2015)
30	Pueblo Viejo	80	20	Ar-Ar		Arce <i>et al.</i> (2013)
31	Palpan	260	20	Ar-Ar		Arce <i>et al.</i> (2013)
32	Atlacholoaya	1020	160	Ar-Ar		Arce <i>et al.</i> (2013)
33	Villa Guerrero	1200	50	Ar-Ar		Arce <i>et al.</i> (2013)

instead of Ti-magnetite, associated to mineral alteration during the heating-cooling process in the laboratory.

4.2 Hysteresis and IRM curves

The determination of saturation magnetization (M_s), saturation remanent magnetization (M_{rs}), coercive force (H_c) and remanent coercive force (H_{cr}) gave information on the domain state of the magnetic grains. With M_{rs}/M_s ratios between 0.1 and 0.6, and H_{cr}/H_c between 1.2 and 4.0. 80 per cent of the samples, fit in the pseudo single domain (PSD) field of the Day plot (Day *et al.* 1977), likely indicating a mixture of single domain (SD) and multidomain (MD) grains (Fig. 3b), also evidenced by the wasp-waisted shape of the 09CH007 sample (Fig. 3a). Hysteresis and IRM curves reach saturation above 800 mT, which is consistent with the presence of magnetite with different contents of titanium and the absence of high-coercivity minerals (Fig. 3).

Samples from *El Pelado* and *Chichinautzin* volcano cooling units are close to SD field and those of *Tenango basalt* and *Palpan* cone to MD field.

5 DIRECTIONAL ANALYSIS

We obtained 33 new site directions from ChVF and SSC monogenetic volcanic group: 32 sites are of normal polarity, and one (*Villa Guerrero*) of reverse polarity (Fig. 5a) with an age at 1200 ± 50 ka (Arce *et al.* 2013), consistent with the Matuyama chron. This is the first reversed polarity reported from the ChVF. After AF and thermal demagnetization, 80 per cent of the samples present a single component of magnetization (Figs 4a and b). The rest of the samples show a secondary component, probably of viscous origin, that could be removed at low field (less than 20 mT; Fig. 4c and d) or low temperature (less than 200 °C; Figs 4e and f). As mentioned before, no structural correction was applied to the samples, as no recent rotation or tectonic displacements were seen in the field or reported in the area in previous published studies (e.g. Herrero-Bervera & Pal 1977; Urrutia-Fucugauchi & Martin del Pozzo 1993).

Values of k and α_{95} from all sites range from 68 to 1495 and 2.7° to 8.5° , respectively, underlying the overall high precision and confidence of our mean directions.

Table 2. Summary of the directional results, where N is the number of specimens used for the calculation of the mean direction at the site level or the number of sites used for the calculation of the mean direction of the cooling unit, when there is more than six sites in a cooling unit. References: TS, This study (1) Herrero-Bervera & Pal 1977, (2) Urrutia-Fucugauchi & Martin Del Pozzo 1993, (3) González *et al.* 1997, (4) Böhnel & Molina-Garza 2002, (5) Morales *et al.* 2001, (6) Alva-Valdivia 2005, (7) Vlag *et al.* 2000, (8) Urrutia-Fucugauchi 1996, (9) Böhnel *et al.* 1997, (10) Mahgoub *et al.* 2019, (11) Mora-Alvarez *et al.* 1991.

ID	Cooling unit	A(ge ka)	Site	Location					VGP					
				Lat ° N	Long ° W	N	Dec	Inc	kappa	α95	Plat ° N	Plong ° E	Ref	
1	Xitle	1.61 ± 0.09	6	19.300	99.200	17	358	34	301	2.1	88	152	1	
			7	19.300	99.200	11	355	34	86	5.0	85	164	1	
			11	19.300	99.200	12	16	36	230	2.9	75	346	1	
			13	19.300	99.200	8	355	39	114	5.2	85	202	1	
			14	19.300	99.200	8	357	52	151	4.5	76	250	1	
			15	19.300	99.200	7	356	34	62	7.7	86	162	1	
			XT-1	19.180	99.100	6	357	32	276	4.0	87	139	2	
			S-9	19.320	99.180	9	350	35	663	2.0	81	172	3	
			Xtitle	19.190	99.110	15	347	36	521	1.7	78	177	9	
			JM	19.320	99.187	13	352	36	269	2.5	82	177	5	
			Flow 1	19.315	99.174	9	4	32	87	5.6	86	18	6	
			Flow 2	19.315	99.174	8	0	35	351	3.0	90	81	6	
			Flow 3	19.315	99.174	10	2	34	131	4.2	88	10	6	
			Flow 4	19.315	99.174	10	3	32	156	3.9	87	25	6	
			Flow 5	19.315	99.174	8	3	35	72	6.6	87	351	6	
			Flow 6	19.315	99.174	9	356	30	309	2.9	85	131	6	
			Flow 7	19.315	99.174	9	5	36	280	3.1	85	342	6	
			Flow 8*	19.315	99.174	8	359	33	57	7.4	88	117	6	
			Xite	19.36	99.17	113	1	34	263	0.8	89	28	4	
			Xtitle CU-1	19.35	99.13	6	357	34.9	477	3.1	86	17	8	
			Xtitle CU-2	19.36	99.15	6	353.6	36.2	151	4.5	84	178	8	
			Xtitle XT-6	19.25	99.26	9	355	37	123	4.7	85	188	8	
			Xtitle P-8	19.33	99.15	8	356	30	67	6.8	85	131	8	
			Average			23	358	35	159	2.4	88	173		
2	Chichinautzin	1.75 ± 0.13	CH-1	19.091	99.080	7	357	30	91	9.7	86	125	TS	
			CH-2	19.119	99.126	8	3	30	214	6.3	86	37	TS	
			CH-IV	19.105	99.161	8	349	32	181	5.7	79	163	TS	
			PL-CH1	19.116	99.147	8	354	34	953	3.0	84	167	TS	
			CH-I	19.107	99.156	7	357	40	153	6.2	85	224	TS	
			1	19.100	99.100	8	358	27	73	6.5	85	103	1	
			GU-PI	19.020	99.140	23	3	34	98	3.1	87	1	10	
			Average			6	357	32	190	4.4	86	147		
			Jumento	19.206	99.315	16	349	50	233	4.4	75	222	TS	
			El Jumento—B*	19.187	99.320	25	354	32	52	4.1	84	156	10	
4	Guadalupe	2 ± 0.56	SC1	19.323	99.023	8	9	37	85	6.0	81	341	TS	
			MMA-23-A	19.117	98.910	8	1	27	1459	2.4	85	72	TS	
5	Pelagatos	2.6 ± 0.2	A2	19.103	98.934	8	3	20	618	3.7	80	61	TS	
			Average			16	2	23	212	3.4	82	66		
			A5	19.140	99.008	7	2	10	180	6.9	76	73	TS	
			Tabaquillo	19.119	99.291	8	360	44	1141	2.7	83	261	TS	
			Mazatepec	23 ± 4	SSC2	19.317	99.036	8	357	34	149	6.3	87	158
			Chinconquiat	>31	A3	19.207	98.859	8	349	21	209	8.5	77	135
			Tres Cruces	9.4 ± 0.3	Site 1 + 2	19.103	99.502	16	339	50	196	3.7	68	206
					S-6	19.12	99.49	7	337	56	463	3.1	63	216
			Tenango	9.5 ± 1	TEO-Alto	19.110	99.596	8	358	65	163	7.2	62	257
					TEO-Bajo	19.110	99.596	7	3	71	315	5.2	53	263
12	Los Cardos	<10	Average			15	1	68	137	4.8	58	262		
			Tenango1	19.0895	99.6258	10	18	36	99	4.9	73	344	10	
			Cardos	19.094	99.260	8	356	39	96	5.6	85	210	TS	
			12*	19.100	99.200	13	6	16	21	9.2	78	52	1	
			Cima 2	19.100	99.190	7	17	22	71	7.2	72	14	2	
			Cima 3	19.100	99.170	7	355	41	139	5.1	84	215	3	
			MMA-25-A	19.153	98.983	8	12	12	253	5.8	72	39	TS	
			MMA-C	19.161	98.991	7	3	4	238	5.0	73	71	TS	
			Average			15	5	7	143	4.3	73	63		
			SITIO D	19.142	99.169	8	14	22	112	6.4	75	19	TS	
13	Cima	10.1 ± 0.6	SITIO A	19.116	99.268	6	358	38	79	8.7	87	213	TS	
			SITIO B	19.120	99.274	8	347	29	124	6.0	77	156	TS	
			SITIO C	19.123	99.277	6	359	38	68	10.5	87	235	TS	
			PL-02	19.120	99.260	8	354	34	954	3.0	85	165	TS	
			PL-01	19.137	99.255	8	12	22	121	5.4	77	23	TS	

Table 2. Continued

ID	Cooling unit	A(ge ka)	Site	Location					VGP				
				Lat ° N	Long ° W	N	Dec	Inc	kappa	α_{95}	Plat ° N	Plong ° E	Ref
			Average			44	0	31	48	6.7	87	81	
			8*	19.200	99.200	9	7	33	51	7.3	83	1	1
			9	19.200	99.200	8	5	27	115	5.2	83	36	1
			10	19.200	99.200	9	6	35	118	4.8	84	349	1
			P-2	19.150	99.210	6	355	15	130	5.9	78	104	2
			S-10	19.140	101.420	7	352	12	60	7.9	75	110	3
			JB	19.186	99.169	8	10	17	198	3.9	76	37	5
			PEL I-II	19.120	99.190	12	18	18	115	4.1	70	18	10
			Average			7	5	23	43	9.3	83	66	
16	Huilote	>10	Huilote 1	19.034	99.270	8	14	11	353	3.0	71	34	5
			Huilote 2	19.034	99.304	8	4	23	277	3.3	82	52	5
17	Cerro del Agua	12.6 ± 0.7	A4	19.008	98.985	8	5	17	187	5.6	79	55	TS
18	Acopioxco	>14	JJ	19.110	99.176	13	353	33	498	1.9	83	162	5
19	Dos Cerros 1	16.6 ± 0.4	MMA-46	19.117	98.910	8	2	50	154	6.2	78	270	TS
20	Dos Cerros 2	16.6 ± 0.6	MMA-44	19.156	98.869	8	10	45	174	5.1	78	311	TS
		16.6 ± 0.6	DCR	19.156	98.868	15	345	48	209	2.7	73	211	10
21	Cilcuayo	>18.7	MMA-79B	19.139	98.971	8	358	20	223	6.2	81	94	TS
22	Raices-Cajete	18.9 ± 0.3	PI3	19.1058	99.2406	6	359	47	194	4.8	81	255	10
23	Tres Cumbres	21.5 ± 1.8	TC-5	19.100	99.260	6	3	22	317	3.8	82	60	2
24	Ajusco*	390 ± 160	JH	19.19	99.25	8	343	22	371	2.9	72	148	5
			C3-B Ajusco	19.43	99.13	14	0	17	18	9.9	79	81	11
			C3-A Ajusco	19.43	99.13	13	124	0	111	3.8	-32	338	11
		22.6 ± 0.3	JL	19.22	99.27	10	359	45	131	4.2	83	254	5
25	Malinale	22.8 ± 1.4	Malinale 1	19.210	99.210	6	6	33	513	3.0	84	2	2
			S-3	19.220	99.210	5	359	34	175	5.8	89	139	3
26	Cuautl	23.5 ± 0.5	S-7	19.170	99.420	6	343	17	255	4.2	71	141	3
27	Tezontle	26.3 ± 0.8	S-5	19.220	99.470	7	353	64	318	3.4	63	250	3
28	Teuhtli	36 ± 1.8	A1	19.162	98.991	8	353	31	119	8.5	83	152	TS
			5	19.200	99.020	11	345	19	118	4.2	73	140	1
			THT	19.244	99.054	8	355.7	26.5	1066.25	1.7	83.3	120	10
29	Pueblo Viejo	80 ± 20	AT-3	18.527	99.197	8	357	57	636	3.6	71	254	TS
30	Palpan	260 ± 20	PA-05	18.843	99.460	8	354	24	387	4.7	82	124	TS
31	Atlacholoaya	1020 ± 160	AT-1	18.689	99.233	8	3	58	227	6.1	70	268	TS
32	Villa Guerrero	1200 ± 50	SH-06	18.894	99.645	7	178	-34	1495	3.2	-88	343	TS

+Mean direction estimated at site level.

*Sites that do not fulfill our selection criteria were discarded for the calculation of mean directions.

The cooling units were divided into two groups according to their ages: (i) the younger group of 17 out of the 21 sampled cooling units with ages ranging from 1.7 to 40 ka and (ii) the older group of 4 out of the 21 cooling units with ages ranging from 80 ka to 1.2 Ma. The mean direction associated to the younger group (Dec = 359.7°, Inc = 33.1°, N = 16, k = 22.8, α_{95} = 7.1°, Plat = 89.6° N, Plong = 205.1° E, K = 37.6, A₉₅ = 6.1), is consistent with the direction of the dipole field (at the average site latitude). The precision interval of K with the 95 per cent confidence (Cox 1969) are ranging from 25 < K < 50. For this estimation, one cooling unit (El Pelado) was discarded for the calculation, because it did not fulfill our selection criteria. The mean direction associated to the older group (Dec = 357.9°, Inc = 49°, N = 4, k = 28.2, α_{95} = 19.2, Plat = 73.1° N, Plong = 253.8° E, K = 38.8, A₉₅ = 23.8) is pretty similar with a scatter likely related to a larger time interval with only four cooling units available. However, the precision interval of K with the 95 per cent confidence (Cox 1969) is ranging from 6 < K < 39, that is statistically indistinguishable with the younger group. The dispersion of the VGP estimated for this study (S_b = 13.4) fits with the expected value for the latitude (ca. 20°) according with the Model G (McFadden *et al.* 1991), and with the projections from different data sets at similar latitudes (e.g. Johnson *et al.* 2008; Opdyke *et al.* 2015; Cromwell *et al.* 2018).

6 COMPARISON WITH PREVIOUS PUBLISHED DATA FROM ChVF

The ChVF has been previously studied reported by twelve palaeomagnetic studies (Herrero-Bervera & Pal 1977; Mora-Alvarez *et al.* 1991; Urrutia-Fucugauchi & Martin del Pozzo 1993; Mooser *et al.* 1974 1994; Urrutia-Fucugauchi 1996; Böhnel *et al.* 1997; Gonzalez *et al.* 1997; Vlag *et al.* 2000; Morales *et al.* 2001; Böhnel & Molina-Garza 2002; Alva-Valdivia 2005; Maghoub *et al.* 2019) for rocks younger than 40 ka. One of these papers (Mooser *et al.* 1974) was not included in the analysis because important information as the sampling location, age and demagnetization protocols were not given in the publication.

A crucial aspect of such a compilation is the quality of the ages attributed to the different data. When possible, the ages given in the original papers were updated (Table 1). Because it was not possible to attribute them a reliable absolute age, the mean results of Ajusco (Morales *et al.* 2001) and the site CH-45 (Urrutia-Fucugauchi & Martin Del Pozzo 1993) had to be discarded. Similar problem occurs with the ages of Acopioxco and Huilote from Morales *et al.* (2001), but a relative age could be estimated by stratigraphy according to recent published data, supported by direct observations in the field. Only updated ages by cooling unit are given in Tables 1 and 2.

According to their location and reported age, the previous pub-

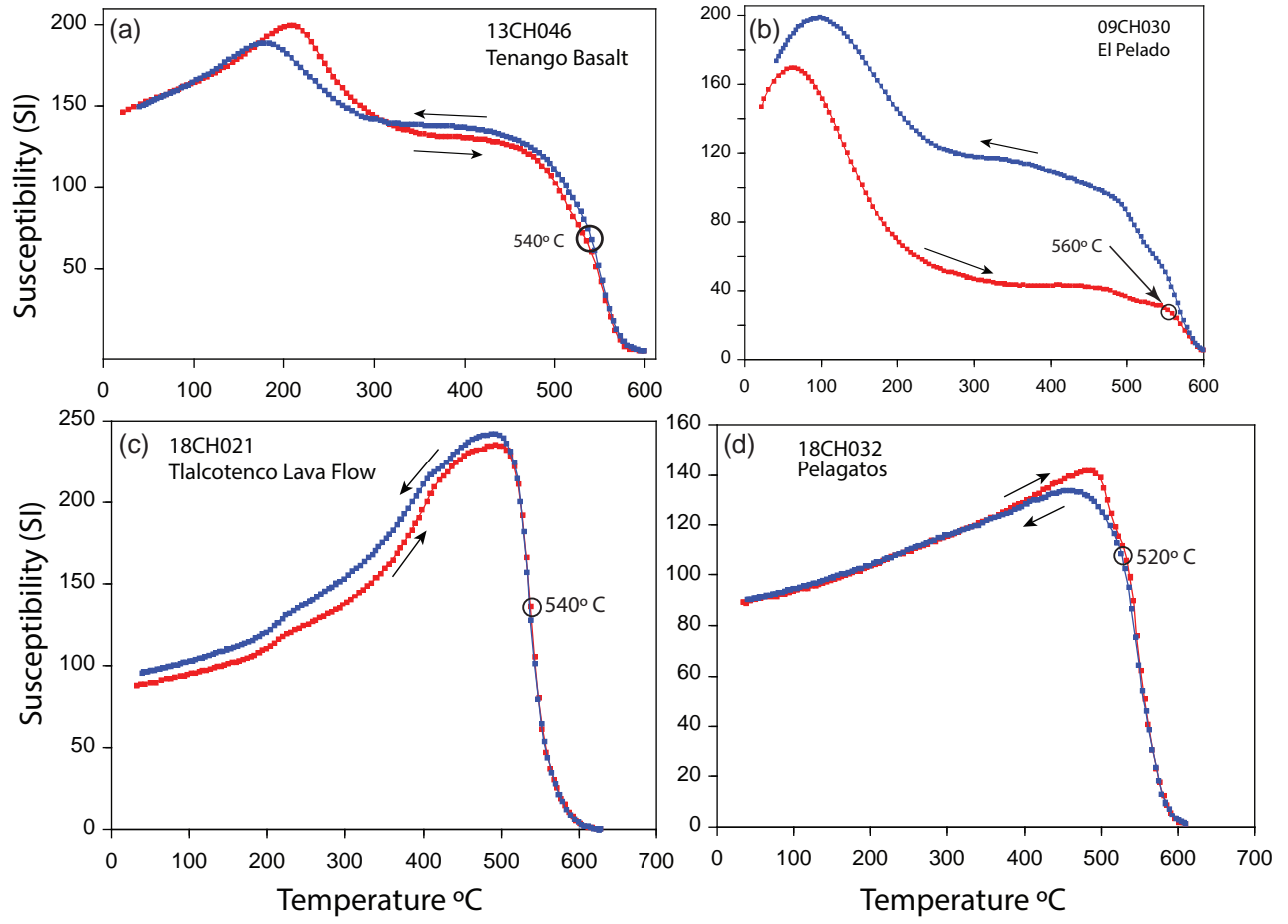


Figure 2. Representative heating (red) and cooling (blue) susceptibility *vs* temperature curves.

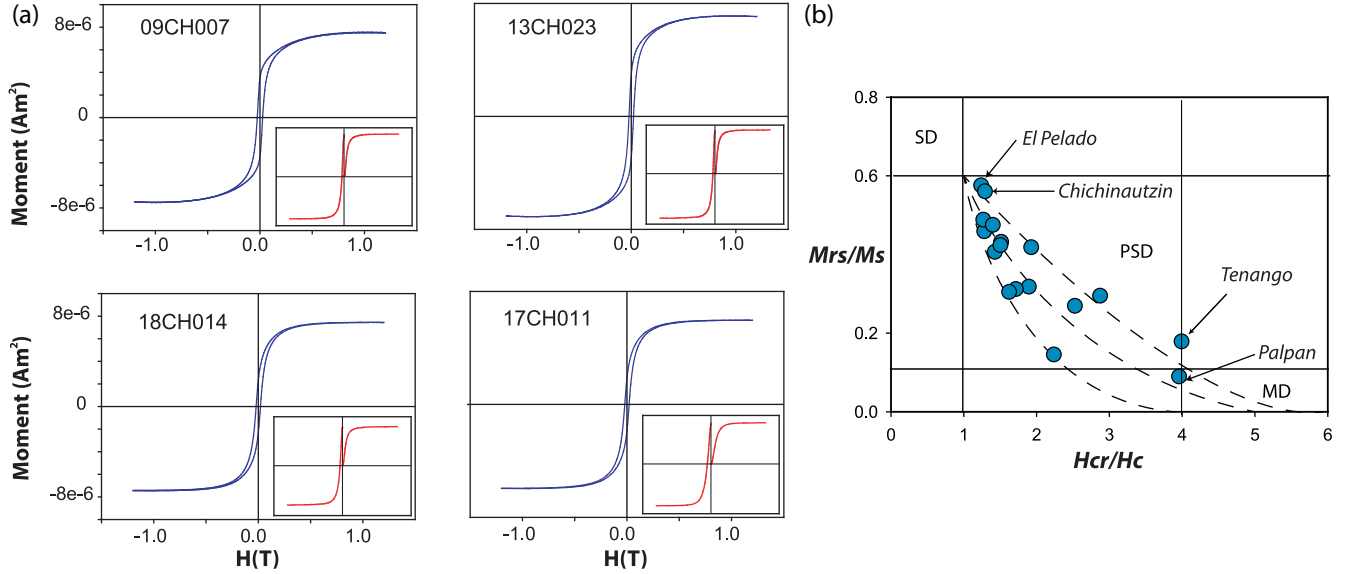


Figure 3. (a) Representative hysteresis plots in blue and IRM acquisition and backfield curves in red. Paramagnetic components are removed. (b) Day plot from ChVF and SSC samples with SD-MD mixing curves of Dunlop (2002).

lished mean directions have been allocated to the different ChVF's cooling units (Fig. 1b, Table 2). When different publications report data from the same cooling unit, as for *Xitle* and *El Pelado* volcanoes, we calculate a mean direction at the cooling unit level

(Table 2). For the special case of *El Pelado* volcano, two means are available: a mean estimated at sample level obtained from 44 samples demagnetized in this study obtained for different locations of the volcano; and a mean calculated at site level from 6 sites reported

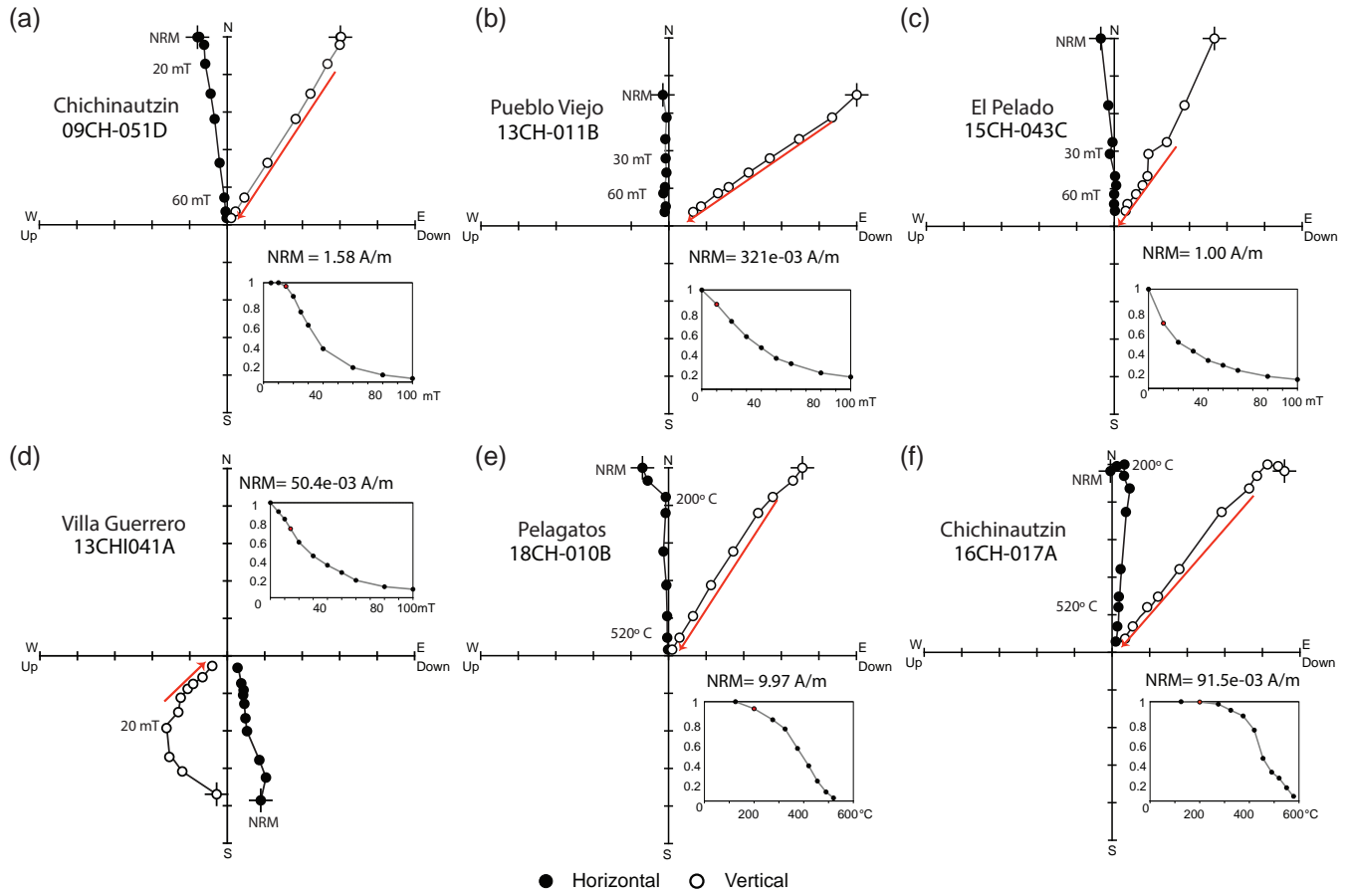


Figure 4. Representative orthogonal plots and demagnetization curves of AF (a–d) and thermal (e–f) demagnetization. Solid (open) circles are the projection on the horizontal (vertical) plane. Red line indicates the number of points selected for the ChRM calculation.

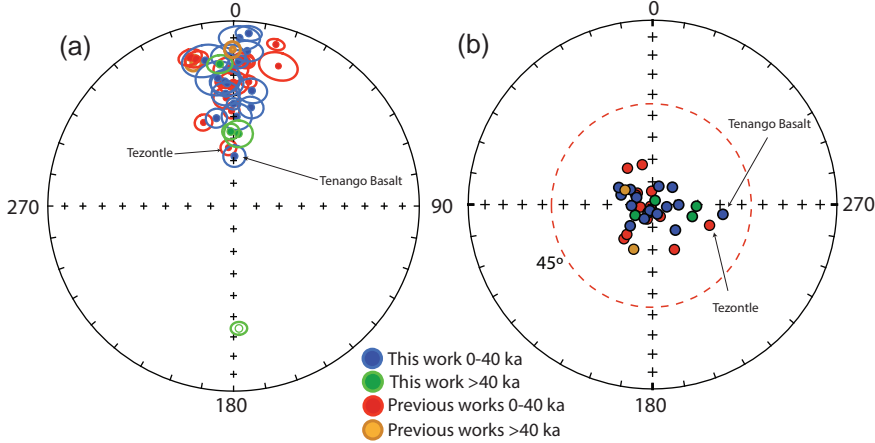


Figure 5. Equal area projection of the mean directions (left) and distribution of the VGP's (right) per cooling unit of the ChVF.

from previous works in El Pelado, details available in Table 2. For the previous published data, when more than two sites were available for a given CU, the mean was calculated at site level. When only two sites were available no average was provided, such as Cima volcano, with three sites available, but one of them were discarded. All the mean directions estimated for a given cooling units in this study were calculated at sample level. In order to assure similar quality between our data and the previously published palaeomagnetic data, we defined some minimum quality criteria: at least four

specimens are required to obtain a mean direction for each cooling unit, and cut off value for k parameter larger than 60 (e.g. Johnson *et al.* 2008; Cromwell *et al.* 2018). This value was determined from the statistical analysis of the directional data compilation from the TMVB on the past 1.5 Ma (Fig. 6) and approaching within 95 per cent confidence of the distribution of the data (ca. 2σ).

A special case is the Tenango basalt, located on the western side of the ChVF, of 8.5 ± 0.16 ka (Bloomfield 1974), that presents high value of inclination (68.2°), atypical for this period and at

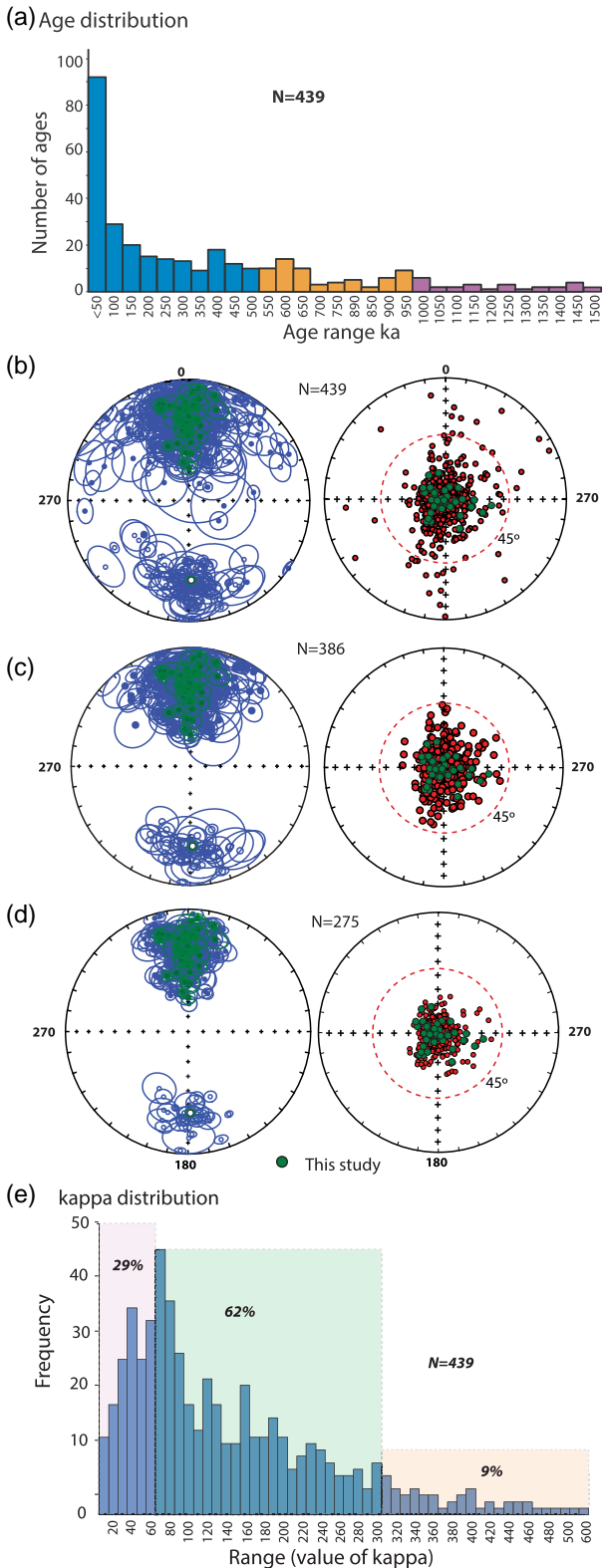


Figure 6. Directional relocated data and VGP. (a) Age distribution; (b) all the data in the compilation; (c) after removing data disturbed, transitional or with age problem; (d) after applying quality criteria; (e) distribution of k for the palaeomagnetic directions of the TMVB for the last 1.5 Ma. Full data set available in Table 1S.

this latitude. Gonzalez *et al.* (1997) report a similar value for the *Tezonite* volcano (21.8 ± 38 Ka, Bloomfield 1975), located at the southwestern part of the ChVF. Finally, other two cooling units present similar high inclination values: *Pueblo Viejo* lava flow and *Atlacholoaya* scoria cone, both cooling units being located at the southwestern boundary of the volcanic field, but belonging to the older group of the ChVF > 40 ka (Arce *et al.* 2013). On the other side, the cooling unit *Tláloc*, 7.1 ± 0.2 ka, and the *Tlalcoitenco* lava flow, $6.4\text{--}14$ ka, (Siebe *et al.* 2005) present atypical low inclination value of 10° and 7° , respectively (Table 2). None of these directions can be considered as transitional because they are inside the 45° cut-off (Johnson *et al.* 2008; Cromwell *et al.* 2018) to differentiate transitional polarities (Fig. 5b). According to the statistical quality of the mean directions, there is no objective reason to discard these sites, and they have been included in the mean calculations.

All selected mean directions per cooling unit are presented with their α_{95} confidence circle in Fig. 5(a), and the associated VGP's in Fig. 5(b). An overall mean was estimated for the last 40 ka (Dec = 359.1° , Inc = 34.1° , N = 30, k = 22.2, $\alpha_{95} = 5.7^\circ$, Plat = 88.6° N, Plong = 208.6° E, K = 32.4, $A_{95} = 4.7^\circ$). This average is similar to the mean direction that was calculated with our samples, and consistent with the expected value of the actual dipole. The 33 available cooling units for the ChVF and SSC were used to calculate the mean for the last 1.5 Ma (Dec = 359.1° , Inc = 35.3° , N = 33, k = 21.6, $\alpha_{95} = 5.5^\circ$, Plat = 87.7° N, Plong = 227.4° E, K = 31.8, $A_{95} = 4.5^\circ$) that remains very close to the geographic pole. The overall dispersion of the VGP's estimated ($S_b = 14.37$) of the previous published data combined with the new data set from this study match (Fig. 8) with the predicted value of the Model G (McFadden *et al.* 1991) and with the curves of latitude dependence of VGP scatter published recently (e.g. Johnson *et al.* 2008; Opdyke *et al.* 2015; Cromwell *et al.* 2018), showing an accurately average secular variation recorded from the ChVF lavas.

7 THE TMVB PALAEOMAGNETIC DATA SET AND THE TIME AVERAGED DIPOLE FIELD FOR THE LAST 1.5 Ma

The Trans Mexican volcanic belt has been active since the last 12 Ma. However, we restricted our compilation to the last 1.5 Ma, the period for which we have most of the palaeomagnetic studies. 48 publications (Table 1S) were retrieved for this period, most of them are fairly recent (72 per cent of the articles were published in the 2000s), and only a few were published in the 1970s. 30 per cent of the data have an age lower than 50 ka, 20 per cent of the data have ages between 50 and 250 ka, and no trend can be seen between the age distribution and the location (Table 1S).

Around 70 per cent of the previous palaeomagnetic data come from the central part of the TMVB: Michoacán-Guanajuato volcanic field (MGVF); Sierra de la Cruces (SC) and ChVF (Fig. 1b). The latitudes of the data are fairly similar (between 18.2° N and 21.7° N), but the longitudes vary a lot more (from 96.5° W to 106° W) covering about 1000 km from east to west. Therefore, to consider these differences in longitude (up to 10°), all compiled directions (Table 1S) were relocated to a common geographic place, arbitrarily chosen at Zócalo downtown in Mexico City (19.4327° N and 99.1332° W).

Altogether 439 individual sites were compiled (Fig. 6b, Table 1S). All data that have been identified by the original authors as remagnetized units, affected by lightning or local tectonics and displaced blocks, or were not considered in the analysis, and are labelled as *disturbed* in Table 1S. Using a 45° cut-off for transitional VGP's,

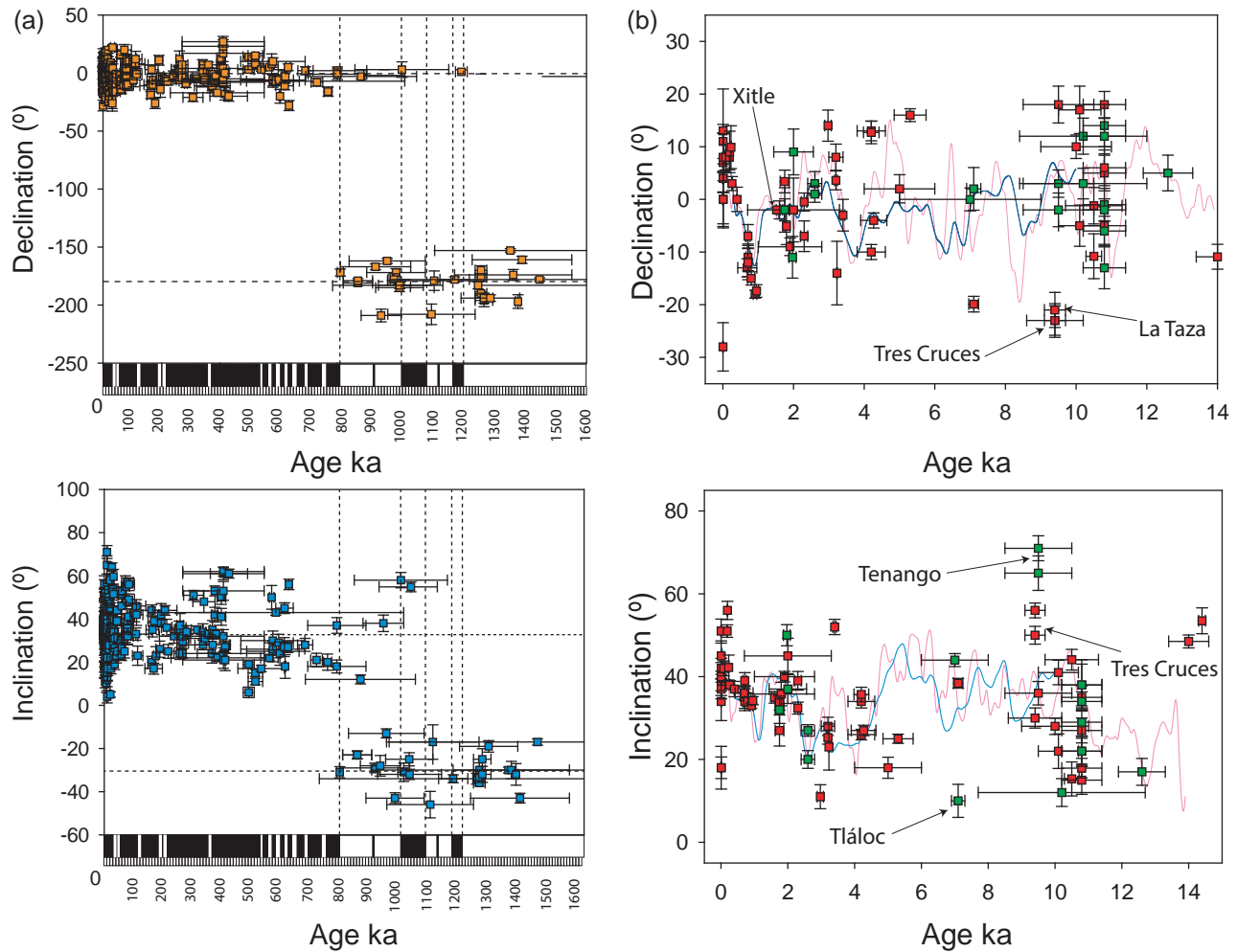


Figure 7. a) Distribution of the declination and inclination parameters on the TMVB for the past 1.5 Ma. b) Data from the past 14 ka from ChVF (green squares) and the TMVB (red squares) with the models SHA.DIF14k (red line) and CALS10k2 (blue line).

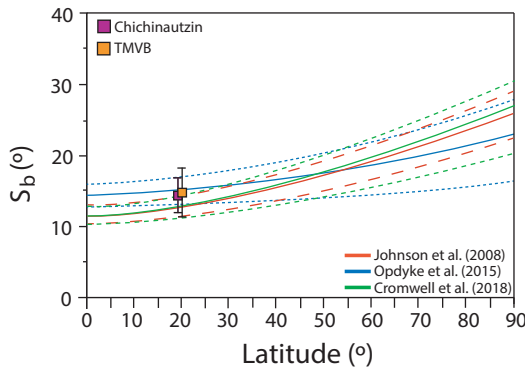


Figure 8. Latitude dependence of the VGP's for the last 5 Ma (Johnson et al. 2008 and Opdyke et al. 2015) and for the last 10 Ma (Cromwell et al. 2018). Modified from, Doubrovine et al. (2019).

some other data (labelled as *transitional* in Table 1S) were also discarded. The same care was paid to the age of the determination and a certain number of the data were discarded because of imprecision or absence of age (labelled as *age* in Table 1S). After applying these three basic criteria, *ca.* 29 per cent of the data (Fig. 6c) were removed. Finally, the quality criteria used to select the ChVF data ($N \geq 4$ and $k > 60$) were applied to the TMVB data (Fig. 6d). The

distribution of k in the published data is summarized in Fig. 6(e), with 29 per cent of the data below the chosen value of 60, 61 per cent of the data having k ranging from 60 to 300, and 9 per cent of the data with very high-quality value over 300.

An overall mean direction and pole were estimated with the selected palaeomagnetic data set, including the new results from ChVF and SSC. Mean directions were estimated for both normal and reverse polarities, ($\text{Dec} = 358.4^\circ$, $\text{Inc} = 35^\circ$, $N = 245$, $k = 31.7$, $\alpha_{95} = 1.5^\circ$) and ($\text{Dec} = 180.6^\circ$, $\text{Inc} = -30.1^\circ$, $N = 25$, $k = 32.5$, $\alpha_{95} = 5.2^\circ$), respectively. The reversal test (McFadden & McElhinny 1990) is positive with a difference of $\sim 3^\circ$ between the reversal and normal polarities, supporting the reliability of the selected data set. The combined mean direction, calculated for the past 1.5 Ma of the TMVB ($\text{Dec} = 358.4^\circ$, $\text{Inc} = 35^\circ$, $N = 275$, $k = 31.7$, $\alpha_{95} = 1.6^\circ$) with its corresponding VGP ($\text{Plat} = 88.3^\circ \text{ N}$, $\text{Plong} = 188.6^\circ \text{ E}$, $K = 40.2$, $A_{95} = 1.4^\circ$), is therefore very robust and strongly support the reliability of the Geocentric Axial Dipole hypothesis.

Mexico is indeed characterized by a very active tectonic setting, especially on the west coast with the subduction of the Cocos Plate beneath the North American Plate along the Acapulco trench. The tectonic activity, considered active in the present days make possible local displacements and vertical axis rotations (e.g. Alva-Valdivia et al. 2017, 2019), with low influence in the general setting

of all the TMVB. However, if this active tectonic was clearly the trigger of the volcanic activity in central México (Gomez-Tuena *et al.* 2007), no large movement that would have disturbed the TMVB directions could be detected, at least for the last 1.5 Ma. The major tectonic movements along the TMVB were reported for the older activity during the Miocene (Alva-Valdivia *et al.* 2000). It is possible that for the younger activity some areas could be affected by regional tectonic activity, generating tilts and/or vertical axis rotations, the data reported from the authors as tectonically disturbed were not considered for this study. The unrecognized tectonic activity in the area that was not reported by the authors is not possible to observe directly, but the accuracy and precision of the date is supported by the statistical parameters published. The palaeosecular variation (PSV) recorded by the volcanic rocks of the TMVB show that latitude dependence of dispersion of the combined polarities of the VGP's estimated for all the data set in this work ($S_b = 14.6$), show that matches with the different models (e.g. Johnson *et al.* 2008; Opdyke *et al.* 2015; Cromwell *et al.* 2018) at the mean latitude of the TMVB (*ca.* 20°). After discarding the disturbed data from the selection criteria, is possible to determine that the TMVB has a reliable record of the PSV for the last 1.5 Ma. The dispersion of the VGP's show that the local tectonic activity doesn't affect considerably to the mean values estimated in this study (Fig. 8). As reported by Opdyke *et al.* (2015), results from lower latitudes show disturbances on the S_b due to the intense activity recorded.

Looking at the evolution of relocated declination and inclination through time, we can see that the Brunhes normal chron (0–781 ka) is well recorded in the TMVB data set (Fig. 7a). It is not the same for the Matuyama reverse chron (781–2581 ka), especially during the first reverse subchron (C1r.1r, 781–988 ka) that presents almost as many normal polarity data as reverse polarity data (Fig. 7a). Part of this dispersion is probably due to age uncertainty, but may also be related to undetected remagnetizations in a recent normal field. While the Jaramillo subchron (988–1072 ka) is accurately recorded, the Cobb subchron (1173–1185 ka) is not represented in the TMVB data set.

8 SECULAR VARIATION RECORDED IN THE TMVB

Considering the limitations of the available data set, we concentrate on a more recent period, for which we have the larger number of studies, *ca.* 34 per cent of the full data set compiled to study the secular variation: the last 14 millennia (Fig. 7b).

For the last 4 millennia, the TMVB results are consistent with the predictions at Mexico City of two recent global models: CALS10k2 (Constable *et al.* 2016) and SHA.DIF.14k (Pavón-Carrasco *et al.* 2014). This result is not surprising as most data considered in this analysis were included in the calculation of these models. During the last four millennia, declination varied between –20° and 20° and inclination varied between 15° and 60°.

For earlier periods, the gaps in the database, especially between 5000 and 8000 BP and beyond 11 000 BP, prevent an accurate recovery of the secular variation. The range of directions between 9000 and 11 000 BP suggests a larger and faster secular variation than predicted by the global models. High inclination values up to 68° and low declination values up to –30° were observed in Tenango, la Taza and Tres Cruces cooling units (Fig. 7b). More data are required to better constrain this large variation and understand its geomagnetic origin.

8.1 Dispersion of the VGP's

During the last years, different compilations of directional data from different latitudes around the world, including Mexico were performed (e.g. Johnson *et al.* 2008; Opdyke *et al.* 2015; Cromwell *et al.* 2018; Doubrovine *et al.* 2019). The objective is to assemble the record of the PSV at different intervals of time at different latitudes, showing the dependence of the dispersion of the VGP scatter with the latitude. In this work the dispersion of the VGP was estimated for the ChVF data, and for the data set compiled for the TMVB, to verify the record of the concordance with the Model G (McFadden *et al.* 1991) and with the compilations proposed for the past 0–5 Ma and 0–10 Ma. For Mexico, with a latitude *ca.* 20°, different works estimate the PSV by the VGP scatter for 0–5 Ma. Mejía *et al.* (2005) estimate the VGP scatter ($S_b = 12.7^\circ$) for the TMVB by selecting 187 sites, and found equivalence with the expected value from Model G ($S_b = 13.5^\circ$). Later, Ruiz-Martínez *et al.* (2000) with 77 selected sites, estimated the dispersion of the VGP ($S_F = 14.8^\circ$) and compared the fit with the Model G and the model that use a data set from Mexico ($S_b = 14.3$) proposed by Johnson *et al.* (2008). In this study, we compare the VGP scatter estimated for ChVF ($S_b = 14.4$) and for the entire compilation of TMVB ($S_b = 14.6$), with the results of three global compilations that uses different results from Mexico from 0 to 5 Ma and from 0 to 10 Ma (Cromwell *et al.* 2018). Fig. 8 shows the correspondence of the results from this study with the expected values according with the three models. In the case of Cromwell *et al.* (2018), is possible to observe a slight lower S_b value, in comparison with the results from the TMVB. This small difference could be associated to a higher average of the model (0–10 Ma). However, in all cases, the results estimated for ChVF and TMVB fit with the expected value of the S_b according to the latitude. This concurrence, supports the hypothesis that the local tectonic activity in the TMVB does not affect significantly the average estimated for the last 1.5 Ma.

9 CONCLUSIONS

The ferromagnetic mineralogy of the ChVF and SSC volcanic groups is dominated by titanomagnetite with different contents in titanium and Curie temperatures ranging from 230 to 540 °C. The magnetic domain state is a mixture of single and multidomain grains.

The directional analysis of the cooling units shows that the mean direction and VGP obtained for the last 40 ka for ChVF are: (Dec = 359.1°, Inc = 34.1°, N = 30, k = 22.2, $\alpha_{95} = 5.7^\circ$); and (Plat = 88.6° N, Plong = 208.6° E, K = 32.4, $A_{95} = 4.7^\circ$), respectively. These values are close to the present GAD value. The directional results of this study also fit well with the predictions in Mexico City of the global models SHA.DIF.14k and CALS10k2 but only a few data are available from 5 to 9 ka, and study of other structures formed in this time range will be necessary to improve the accuracy of the curves. Similarly, the mean direction and corresponding VGP for the past 1.5 Ma are: (Dec = 359.1°, Inc = 35.3°, N = 33, k = 21.6, $\alpha_{95} = 5.5^\circ$); and (Plat = 87.7° N, Plong = 227.4° E, K = 31.8, $A_{95} = 4.5^\circ$), respectively, also consistent with the expected GAD value in this period. A reversed polarity dated at 1020 ± 160 (Arce *et al.* 2013) was found, and this is the first geomagnetic reversal recorded by the ChVF.

The mean directions from ChVF and SSC are consistent with the mean directional data recorded in volcanic rocks for all published data from the TMVB (Dec = 358.4°, Inc = 35°, N = 275, k = 31.7, $\alpha_{95} = 1.4^\circ$) with its corresponding VGP (Plat = 88.3°

N, Plong = 188.6° E, K = 40.2, A₉₅ = 1.4°). The selection criteria allowed identify the highest quality data to describe the evolution of the time average dipole field, and to constrain the results that will give the most reliable mean directions and VGPs. The directional results and the VGP's scatter (Fig. 8) fit with the expected values according with the latitude of the TMVB, proposed by different global compilations (Johnson *et al.* 2008; Opdyke *et al.* 2015; Cromwell *et al.* 2018). The concordance confirms that the TMVB has not been affected considerably by local tectonics in the past 1.5 Ma. However, large gaps remain in the temporal record of the TMVB that should be filled by further palaeomagnetic studies.

ACKNOWLEDGEMENTS

We appreciate the financial support to LMAV from PAPIIT-DGAPA-UNAM IN113117 (Mexico), to LMAV and MP from the ANR-CONACyT (France-Mexico) 273564 research projects. GH was supported by Campus France PRESTIGE program (PRESTIGE-2017-1-0002). Thanks to J. A. González Rangel, M. Espinosa, V. Macias and François Demory for their support in the laboratories. The authors would like to thank Dr. A. Biggin (editor), Dr. P. Doubrovine and an anonymous reviewer for their comments.

REFERENCES

- Aguirre-Díaz, G.J., Ferrari, L., Nelson, S.A., Carrasco-Núñez, G., Lopez-Martínez, M. & Urrutia-Fucugauchi, J., 1998. El cinturón volcánico mexicano: un nuevo proyecto multidisciplinario.
- Alva-Valdivia, L.M., Goguitchaichvili, A., Ferrari, L., Rosas-Elguera, J., Urrutia-Fucugauchi, J. & Zamorano-Orozco, J.J., 2000. Palaeomagnetic data from the Trans-Mexican Volcanic Belt, *Earth, Planets Space*, **52**(7), 467–478.
- Alva-Valdivia, L.M., 2005. Comprehensive paleomagnetic study of a succession of Holocene olivine-basalt flow: Xitle Volcano (Mexico) revisited, *Earth, Planets Space*, **57**(9), 839–853.
- Alva-Valdivia, L.M., Agarwal, A., Caballero-Miranda, C., García-Amador, B.I., Morales-Barrera, W., Rodríguez-Elizarraráz, S. & Rodríguez-Trejo, A., 2017. Paleomagnetic and AMS studies of the El Castillo ignimbrite, central-east Mexico: source and rock magnetic nature, *J. Volc. Geotherm. Res.*, **336**, 140–154.
- Alva-Valdivia, L.M., Agarwal, A., García-Amador, B., Morales-Barrera, W., Agarwal, K.K., Rodríguez, S. & Gonzalez-Rangel, J.A., 2019. Paleomagnetism and tectonics from the late Pliocene to late Pleistocene in the Xalapa monogenetic volcanic field, Veracruz, Mexico, *Bull. geol. Soc. Am.*.
- Arce, J.L., Layer, P.W., Lassiter, J.C., Benowitz, J.A., Macías, J.L. & Ramírez-Espinosa, J., 2013. 40 Ar/39 Ar dating, geochemistry, and isotopic analyses of the quaternary Sierra de Chichinautzin volcanic field, south of Mexico City: implications for timing, eruption rate, and distribution of volcanism, *Bull. Volcanol.*, **75**(12), 774.
- Arce, J.L., Muñoz-Salinas, E., Castillo, M. & Salinas, I., 2015. The ~2000 yr BP Jumento volcano, one of the youngest edifices of the Sierra de Chichinautzin Volcanic Field, Central Mexico, *J. Volc. Geotherm. Res.*, **308**, 30–38.
- Bloomfield, K., 1975. A late-Quaternary monogenetic volcano field in central Mexico, *Geol. Rundsch.*, **64**(1), 476–497.
- Bloomfield, K., 1974. The age and significance of the Tenango Basalt, central Mexico, *Bull. Volcanol.*, **37**(4), 586–595.
- Böhnel, H., Morales, J., Caballero, C., Alva, L., McIntosh, G., Gonzalez, S. & Sherwood, G., 1997. Variation of rock magnetic parameters and paleointensities over a single Holocene lava flow, *J. Geomag. Geoelectr.*, **49**(4), 523–542.
- Böhnel, H. & Molina-Garza, R., 2002. Secular variation in Mexico during the last 40,000 years, *Phys. Earth planet. Inter.*, **133**(1–4), 99–109.
- Böhnel, H., Biggin, A.J., Walton, D., Shaw, J. & Share, J.A., 2003. Microwave palaeointensities from a recent Mexican lava flow, baked sediments and reheated pottery, *Earth planet. Sci. Lett.*, **214**(1), 221–236.
- Brown, M.C., Donadini, F., Korte, M., Nilsson, A., Korhonen, K., Lodge, A., Lengyel, S.N. & Constable, C.G., 2015. GEOMAGIA50.v3: 1. General structure and modifications to the archeological and volcanic database, *Earth Planets Space*, **67**, 83, doi:10.1186/s40623-015-0232-0.
- Constable, C., Korte, M. & Panovska, S., 2016. Persistent high paleosecular variation activity in southern hemisphere for at least 10 000 years, *Earth planet. Sci. Lett.*, **453**, 78–86.
- Cox, A., 1969. Confidence limits for the precision parameter κ , *Geophys. J. Int.*, **17**(5), 545–549.
- Cromwell, G., Johnson, C.L., Tauxe, L., Constable, C.G. & Jarboe, N.A., 2018. PSV10: a global data set for 0–10 Ma time-averaged field and paleosecular variation studies, *Geochem. Geophys. Geosyst.*, **19**(5), 1533–1558.
- Day, R., Fuller, M. & Schmidt, V.A., 1977. Hysteresis properties of titanomagnetites: grain-size and compositional dependence, *Phys. Earth planet. Inter.*, **13**(4), 260–267.
- Del Pozzo, A.M., 1982. Monogenetic vulcanism in sierra Chichinautzin, Mexico, *Bull. Volcanol.*, **45**(1), 9.
- Demant, A., 1978. Características del Eje Neovolcánico Transmexicano y sus problemas de interpretación, *Revista mexicana de ciencias geológicas*, **2**(2), 172–187.
- Doubrovine, P.V., Veikkolainen, T., Pesonen, L.J., Piispa, E., Ots, S., Smirnov, A.V. & Biggin, A.J., 2019. Latitude dependence of geomagnetic paleosecular variation and its relation to the frequency of magnetic reversals: observations from the Cretaceous and Jurassic, *Geochem. Geophys. Geosyst.*, **20**, 1240–1279.
- Dunlop, D.J., 2002. Theory and application of the Day plot (Mrs/Ms versus Hcr/Hc) 2. Application to data for rocks, sediments, and soils, *J. geophys. Res.: Solid Earth*, **107**(B3), EPM 5–1–EPM 5–15.
- Ferrari, L., Garduño, V.H., Pasquare, G. & Tibaldi, A., 1994. Volcanic and tectonic evolution of central Mexico: Oligocene to present, *Geof. Int.*, **33**(1), 91–105.
- Ferrari, L., López-Martínez, M., Aguirre-Díaz, G. & Carrasco-Núñez, G., 1999. Space-time patterns of Cenozoic arc volcanism in central Mexico: From the Sierra Madre Occidental to the Mexican Volcanic Belt, *Geology*, **27**(4), 303–306.
- Ferrari, L., Conticelli, S., Vaggelli, G., Petrone, C.M. & Manetti, P., 2000. Late Miocene volcanism and intra-arc tectonics during the early development of the Trans-Mexican Volcanic Belt, *Tectonophysics*, **318**(1–4), 161–185.
- Fisher, R.A., 1953. Dispersion on a sphere, *Proc. R. Soc. Lond. A*, **217**(1130), 295–305.
- Gómez-Tuena, A., Orozco-Esquivel, M.T. & Ferrari, L., 2007. Igneous petrogenesis of the Trans-Mexican volcanic belt, *Geol. Soc. Am. Spec. Pap.*, **422**, 129–181.
- Gonzalez, S., Sherwood, G., Böhnel, H. & Schnepf, E., 1997. Palaeosecular variation in Central Mexico over the last 30000 years: the record from lavas, *Geophys. J. Int.*, **130**(1), 201–219.
- Guilbaud, M.N., Arana-Salinas, L., Siebe, C., Barba-Pingarrón, L.A. & Ortiz, A., 2015. Volcanic stratigraphy of a high-altitude *mammuthus columbi* (Tlacotenco, sierra Chichinautzin), central México, *Bull. Volcanol.*, **77**(3), 17.
- Guilbaud, M.N., Siebe, C. & Agustín-Flores, J., 2009. Eruptive style of the young high-Mg basaltic-andesite Pelagatos scoria cone, southeast of México City, *Bull. Volcanol.*, **71**(8), 859.
- Herrero-Bervera, E. & Pal, S., 1977. Paleomagnetic study of Sierra de Chichinautzin, Mexico, *Geof. Int.*, **17**(2), 167–180.
- Jaimes-Viera, M.C., MartinDel Pozzo, A.L., Layer, P.W., Benowitz, J.A. & Nieto-Torres, A., 2018. Timing the evolution of a monogenetic volcanic field: Sierra Chichinautzin, Central Mexico, *J. Volc. Geotherm. Res.*, **356**, 225–242.
- Johnson, C.L., Constable, C.G., Tauxe, L., Barendregt, R., Brown, L.L., Coe, R.S. & Staudigel, H., 2008. Recent investigations of the 0–5 Ma geomagnetic field recorded by lava flows, *Geochem. Geophys. Geosyst.*, **9**(4), .

- Kirianov, V.Y., Koloskov, A.B., De la Cruz, S. & Martin, A.L., 1990. The major stages of manifestation of recent volcanism in the Chichinautzin zone, *USSR Acad. Sci. Geol. Ser.*, **311**, 432–434.
- Kirschvink, J.L., 1980. The least-squares line and plane and the analysis of palaeomagnetic data, *Geophys. J. R. astr. Soc.*, **62**(3), 699–718.
- Lanos, P. & Philippe, A., 2017. Hierarchical Bayesian modelling for combining dates in archaeological context, *J. Soc. Fr. Stat.*, **158**(2), 72–88.
- Lorenzo-Merino, A., 2016. M.s. Thesis. Historia eruptiva del volcán Pelado (Sierra de Chichinautzin, México). Posgrado en Ciencias de la Tierra. Universidad Nacional Autónoma de México, México D.F. México, 89 pp.
- Mahgoub, A.N., Böhnel, H., Siebe, C. & Chevrel, M.O., 2017. Paleomagnetic study of El Metate shield volcano (Michoacán, Mexico) confirms its monogenetic nature and young age (\sim 1250 CE), *J. Volc. Geotherm. Res.*, **336**, 209–218.
- Mahgoub, A.N., Juárez-Arriaga, E., Böhnel, H., Siebe, C. & Pavón-Carrasco, F.J., 2019. Late-Quaternary secular variation data from Mexican volcanoes, *Earth planet. Sci. Lett.*, **519**, 28–39.
- McFadden, P.L. & McElhinny, M.W., 1990. Classification of the reversal test in palaeomagnetism, *Geophys. J. Int.*, **103**(3), 725–729.
- McFadden, P.L., Merrill, R.T., McElhinny, M.W. & Lee, S., 1991. Reversals of the Earth's magnetic field and temporal variations of the dynamo families, *J. geophys. Res.: Solid Earth*, **96**(B3), 3923–3933.
- Mejía, V., Böhnel, H., Opdyke, N.D., Ortega-Rivera, M.A., Lee, J.K.W. & Aranda-Gómez, J.J., 2005. Paleosecular variation and time-averaged field recorded in late Pliocene–Holocene lava flows from Mexico, *Geochem. Geophys. Geosyst.*, **6**(7), 2557–2558.
- Michalk, D.M., Böhnel, H.N., Nowaczyk, N.R., Aguírrre-Díaz, G.J., López-Martínez, M., Ownby, S. & Negendank, J.F., 2013. Evidence for geomagnetic excursions recorded in Brunhes and Matuyama Chron lavas from the trans-Mexican volcanic belt, *J. geophys. Res.: Solid Earth*, **118**(6), 2648–2669.
- Mooser, F., Nairn, A.E. & Negendank, J.F., 1974. Palaeomagnetic investigations of the tertiary and quaternary igneous rocks: VIII a palaeomagnetic and petrologic study of volcanics of the valley of Mexico, *Geol. Rundsch.*, **63**(2), 451–483.
- Mora Álvarez, G., Caballero Miranda, C., Urrutia Fucugauchi, J. & Uchiumi, S., 1991. Southward migration of volcanic activity in the Sierra de Las Cruces, basin of Mexico-a preliminary K-Ar dating and palaeomagnetic study, *Geof. Int.*, **30**(2), 61–70.
- Morales, J., Goguitchachvili, A. & Urrutia-Fucugauchi, J., 2001. A rock-magnetic and paleointensity study of some Mexican volcanic lava flows during the Latest Pleistocene to the Holocene, *Earth, Planets Space*, **53**(9), 893–902.
- Opdyke, N.D., Kent, D.V., Foster, D.A. & Huang, K., 2015. Paleomagnetism of Miocene volcanics on São Tomé: Paleosecular variation at the Equator and a comparison to its latitudinal dependence over the last 5 Myr, *Geochem. Geophys. Geosyst.*, **16**(11), 3870–3882.
- Ortega-Gutiérrez, F., Mitre-Salazar, L.M. & Roldan-Quintana, J., 1992. Carta geológica de la República Mexicana. Consejo de Recursos Minerales y en el Instituto de Geología de la UNAM.
- Panovska, S., Constable, C.G. & Brown, M.C., 2018. Global and regional assessments of paleosecular variation activity over the past 100 ka, *Geochem. Geophys. Geosyst.*, **19**, 1559–1580.
- Pavón-Carrasco, F.J., Osete, M.L., Torta, J.M. & De Santis, A., 2014. A geomagnetic field model for the Holocene based on archaeomagnetic and lava flow data, *Earth planet. Sci. Lett.*, **388**, 98–109.
- Reimer, P.J. et al., 2013. IntCal13 and Marine13 Radiocarbon Age Calibration Curves 0–50,000 Years cal BP, *Radiocarbon*, **55**(4), 1869–1887.
- Ruiz-Martínez, V.C., Osete, M.L., Vegas, R., Núñez-Aguilar, J.I., Urrutia-Fucugauchi, J. & Tarling, D.H., 2000. Palaeomagnetism of Late Miocene to Quaternary volcanics from the eastern segment of the Trans-Mexican Volcanic Belt, *Tectonophysics*, **318**(1–4), 217–233.
- Siebe, C., 2000. Age and archaeological implications of Xitle volcano, southwestern Basin of Mexico-City, *J. Volc. Geotherm. Res.*, **104**(1–4), 45–64.
- Siebe, C., Rodríguez-Lara, V., Schaaf, P. & Abrams, M., 2004a. Radiocarbon ages of Holocene Pelado, Guespalapa, and Chichinautzin scoria cones, south of Mexico City: implications for archaeology and future hazards, *Bull. Volcanol.*, **66**(3), 203–225.
- Siebe, C., Rodríguez-Lara, V., Schaaf, P. & Abrams, M., 2004b. Geochemistry, Sr–Nd isotope composition, and tectonic setting of Holocene Pelado, Guespalapa and Chichinautzin scoria cones, south of Mexico City, *J. Volc. Geotherm. Res.*, **130**(3), 197–226.
- Siebe, C., Arana-Salinas, L. & Abrams, M., 2005. Geology and radiocarbon ages of Tláloc, Tlacotenco, Cuauhtzin, Hijo del Cuauhtzin, Teuhatl, and Ocusacayo monogenetic volcanoes in the central part of the Sierra Chichinautzin, México, *J. Volc. Geotherm. Res.*, **141**(3–4), 225–243.
- Tauxe, L., Constable, C., Johnson, C.L., Koppers, A.A., Miller, W.R. & Staudigel, H., 2003. Paleomagnetism of the southwestern USA recorded by 0–5 Ma igneous rocks, *Geochem. Geophys. Geosyst.*, **4**(4), .
- Urrutia-Fucugauchi, J., 1996. Palaeomagnetic study of the Xitle-Pedregal de San Angel lava flow, southern Basin of Mexico, *Phys. Earth planet. Inter.*, **97**(1–4), 177–196.
- Urrutia-Fucugauchi, J. & Martín del Pozzo, A.L., 1993. Implicaciones de los datos paleomagnéticos sobre la edad de la Sierra de Chichinautzin, cuenca de México, *Geof. Int.*, **32**(3), 523–533.
- Vlag, P., Alva-Valdivia, L., De Boer, C.B., Gonzalez, S. & Urrutia-Fucugauchi, J., 2000. A rock-and paleomagnetic study of a Holocene lava flow in Central Mexico, *Phys. Earth planet. Inter.*, **118**(3), 259–272.

SUPPORTING INFORMATION

Supplementary data are available at [GJI](#) online.

Table 1S: Compilation of volcanic data from the TransMexican Volcanic Belt over the last 1.5 Myr

Please note: Oxford University Press is not responsible for the content or functionality of any supporting materials supplied by the authors. Any queries (other than missing material) should be directed to the corresponding author for the paper.

Key words

Authors are requested to choose key words from the list below to describe their work. The key words will be printed underneath the summary and are useful for readers and researchers. Key words should be separated by a semi-colon and listed in the order that they appear in this list. An article should contain no more than six key words.

COMPOSITION and PHYSICAL PROPERTIES	Seismic cycle Space geodetic surveys Tides and planetary waves Time variable gravity Transient deformation	Instability analysis Interferometry Inverse theory Joint inversion Neural networks, fuzzy logic Non-linear differential equations Numerical approximations and analysis Numerical modelling Numerical solutions Persistence, memory, correlations, clustering Probabilistic forecasting Probability distributions Self-organization Spatial analysis Statistical methods Thermobarometry Time-series analysis Tomography Waveform inversion Wavelet transform
Composition and structure of the continental crust		
Composition and structure of the core		
Composition and structure of the mantle		
Composition and structure of the oceanic crust		
Composition of the planets		
Creep and deformation		
Defects		
Elasticity and anelasticity		
Electrical properties		
Equations of state		
Fault zone rheology		
Fracture and flow		
Friction		
High-pressure behaviour		
Magnetic properties		
Microstructure		
Permeability and porosity		
Phase transitions		
Plasticity, diffusion, and creep		
GENERAL SUBJECTS		
Core		
Gas and hydrate systems		
Geomechanics		
Geomorphology		
Glaciology		
Heat flow		
Hydrogeophysics		
Hydrology		
Hydrothermal systems		
Infrasound		
Instrumental noise		
Ionosphere/atmosphere interactions		
Ionosphere/magnetosphere interactions		
Mantle processes		
Ocean drilling		
Structure of the Earth		
Thermochronology		
Tsunamis		
Ultra-high pressure metamorphism		
Ultra-high temperature metamorphism		
GEODESY and GRAVITY		
Acoustic-gravity waves		
Earth rotation variations		
Geodetic instrumentation		
Geopotential theory		
Global change from geodesy		
Gravity anomalies and Earth structure		
Loading of the Earth		
Lunar and planetary geodesy and gravity		
Plate motions		
Radar interferometry		
Reference systems		
Satellite geodesy		
Satellite gravity		
Sea level change		
GEOGRAPHIC LOCATION	Africa Antarctica Arctic region Asia Atlantic Ocean Australia Europe Indian Ocean Japan New Zealand North America Pacific Ocean South America	
GEO MAGNETISM and ELECTROMAGNETISM		
Archaeomagnetism		
Biogenic magnetic minerals		
Controlled source electromagnetics (CSEM)		
Dynamo: theories and simulations		
Electrical anisotropy		
Electrical resistivity tomography (ERT)		
Electromagnetic theory		
Environmental magnetism		
Geomagnetic excursions		
Geomagnetic induction		
Ground penetrating radar		
Magnetic anomalies: modelling and interpretation		
Magnetic fabrics and anisotropy		
Magnetic field variations through time		
Magnetic mineralogy and petrology		
Magnetostratigraphy		
Magnetotellurics		
Marine electromagnetics		
Marine magnetics and palaeomagnetics		
Non-linear electromagnetics		
Palaeointensity		
Palaeomagnetic secular variation		
Palaeomagnetism		
Rapid time variations		
Remagnetization		
Reversals: process, time scale, magnetostratigraphy		
Rock and mineral magnetism		
Satellite magnetics		
GEO PHYSICAL METHODS		
Downhole methods		
Fourier analysis		
Fractals and multifractals		
Image processing		
PLANETS		
Planetary interiors		
Planetary volcanism		
SEISMOLOGY		
Acoustic properties		
Body waves		
Coda waves		
Computational seismology		
Controlled source seismology		
Crustal imaging		
Earthquake dynamics		
Earthquake early warning		
Earthquake ground motions		
Earthquake hazards		
Earthquake interaction, forecasting, and prediction		
Earthquake monitoring and test-ban treaty verification		
Earthquake source observations		
Guided waves		
Induced seismicity		
Interface waves		
Palaeoseismology		
Rheology and friction of fault zones		
Rotational seismology		
Seismic anisotropy		
Seismic attenuation		
Seismic instruments		
Seismic interferometry		
Seismicity and tectonics		
Seismic noise		
Seismic tomography		
Site effects		
Statistical seismology		
Surface waves and free oscillations		
Theoretical seismology		

Tsunami warning	Hotspots	VOLCANOLOGY
Volcano seismology	Impact phenomena	Atmospheric effects (volcano)
Wave propagation	Intra-plate processes	Calderas
Wave scattering and diffraction	Kinematics of crustal and mantle deformation	Effusive volcanism
TECTONOPHYSICS	Large igneous provinces	Eruption mechanisms and flow emplacement
Backarc basin processes	Lithospheric flexure	Experimental volcanism
Continental margins: convergent	Mechanics, theory, and modelling	Explosive volcanism
Continental margins: divergent	Microstructures	Lava rheology and morphology
Continental margins: transform	Mid-ocean ridge processes	Magma chamber processes
Continental neotectonics	Neotectonics	Magma genesis and partial melting
Continental tectonics: compressional	Obduction tectonics	Magma migration and fragmentation
Continental tectonics: extensional	Oceanic hotspots and intraplate volcanism	Mud volcanism
Continental tectonics: strike-slip and transform	Oceanic plateaus and microcontinents	Physics and chemistry of magma bodies
Cratons	Oceanic transform and fracture zone processes	Physics of magma and magma bodies
Crustal structure	Paleoseismology	Planetary volcanism
Diapirism	Planetary tectonics	Pluton emplacement
Dynamics: convection currents, and mantle plumes	Rheology: crust and lithosphere	Remote sensing of volcanoes
Dynamics: gravity and tectonics	Rheology: mantle	Subaqueous volcanism
Dynamics: seismotectonics	Rheology and friction of fault zones	Tephrochronology
Dynamics and mechanics of faulting	Sedimentary basin processes	Volcanic gases
Dynamics of lithosphere and mantle	Subduction zone processes	Volcanic hazards and risks
Folds and folding	Submarine landslides	Volcaniclastic deposits
Fractures, faults, and high strain deformation zones	Submarine tectonics and volcanism	Volcano/climate interactions
Heat generation and transport	Tectonics and climatic interactions	Volcano monitoring
	Tectonics and landscape evolution	Volcano seismology
	Transform faults	
	Volcanic arc processes	

Capítulo 3

Paleomagnetism and rock magnetic properties of Late Pleistocene volcanism from El Pinacate Volcanic Field, northwest Mexico

A. Rodríguez-Trejo^{a,*}, L.M. Alva-Valdivia^b, J.R. Vidal-Solano^c

a Posgrado en Ciencias de la Tierra, Instituto de Geofísica, Universidad Nacional Autónoma de México, Circuito de la Investigación Científica, C.P. 04510, Ciudad de México, Mexico

b Laboratorio de Paleomagnetismo, Instituto de Geofísica, Universidad Nacional Autónoma de México, Circuito de la Investigación Científica, C.P. 04510, Ciudad de México, Mexico

c Departamento de Geología, División de Ciencias Exactas y Naturales, Universidad de Sonora, Mexico

ABSTRACT

The Pinacate Volcanic Field is a Neogene volcanic sequence at the northwestern part of Mexico. This paleomagnetic study (directional and paleointensity) will continue to improve the global paleomagnetic databases. It is the first full vector paleomagnetic analysis within the more than 400 volcanic structures of the Pinacate Volcanic Field, e.g. scoria, cinder cones, large 'pahoehoe' and 'aa' lava flows. A total of 140 oriented standard paleomagnetic cores from 16 sites of lava flows were collected. Rock magnetic experiments such as thermomagnetic analyses show that Ti-poor titanomagnetite is the main magnetic carrier of the remanence. Microscopy of oxide minerals supports this observation. Parameters from hysteresis and FORC diagrams suggest pseudo-single domain grain sizes or a mixture of single and multidomain particles. The directional analysis of 11/12 volcanic structures provide a mean paleomagnetic direction and corresponding mean paleomagnetic pole (calculated from the site VGPs): Dec=0.1°, Inc=54.5°, n=11, α95=6.7°, k=48, Plat=86.5°, Plong=247.8°, A95=7.5°, respectively. The mean paleointensity, obtained by using the Thellier-Coe protocol, and estimated from seven volcanic structures is $42.2 \pm 3.6 \mu\text{T}$, and VDM is $8.1 \pm 1022 \text{ Am}^2$. The obtained directions are compatible with the Late Pleistocene paleodirection as expected from the geocentric axial dipole (GAD) field. The virtual geomagnetic pole scatter (Sb) was calculated at 13.5° which is consistent with the paleosecular variation value expected from El Pinacate latitude.

*Corresponding author.

E-mail address: alekz_igf@hotmail.com (A. Rodríguez-Trejo)

<https://doi.org/10.1016/j.jsames.2019.102368>

Received 19 June 2019; Received in revised form 23 September 2019; Accepted 23 September 2019

Available online xxx



Paleomagnetism and rock magnetic properties of Late Pleistocene volcanism from El Pinacate Volcanic Field, northwest Mexico

A. Rodríguez-Trejo^{a,*}, L.M. Alva-Valdivia^b, J.R. Vidal-Solano^c

^a Posgrado en Ciencias de la Tierra, Instituto de Geofísica, Universidad Nacional Autónoma de México, Circuito de la Investigación Científica, C.P. 04510, Ciudad de México, Mexico

^b Laboratorio de Paleomagnetismo, Instituto de Geofísica, Universidad Nacional Autónoma de México, Circuito de la Investigación Científica, C.P. 04510, Ciudad de México, Mexico

^c Departamento de Geología, División de Ciencias Exactas y Naturales, Universidad de Sonora, Mexico



ARTICLE INFO

Keywords:
Paleointensity
Secular variation
El Pinacate volcanic field
Northwest Mexico

ABSTRACT

The Pinacate Volcanic Field is a Neogene volcanic sequence at the northwestern part of Mexico. This paleomagnetic study (directional and paleointensity) will continue to improve the global paleomagnetic databases. It is the first full vector paleomagnetic analysis within the more than 400 volcanic structures of the Pinacate Volcanic Field, e.g. scoria, cinder cones, large 'pahoehoe' and 'aa' lava flows. A total of 140 oriented standard paleomagnetic cores from 16 sites of lava flows were collected. Rock magnetic experiments such as thermomagnetic analyses show that Ti-poor titanomagnetite is the main magnetic carrier of the remanence. Microscopy of oxide minerals supports this observation. Parameters from hysteresis and FORC diagrams suggest pseudo-single domain grain sizes or a mixture of single and multidomain particles. The directional analysis of 11/12 volcanic structures provides a mean paleomagnetic direction and corresponding mean paleomagnetic pole (calculated from the site VGPs): Dec = 0.1°, Inc = 54.5°, n = 11, α₉₅ = 6.7°, k = 48, Plat = 86.5°, Plong = 247.8°, A₉₅ = 7.5°, respectively. The mean paleointensity, obtained by using the Thellier-Coe protocol, and estimated from seven volcanic structures is $42.2 \pm 3.6 \mu\text{T}$, and VDM is $8.1 \times 10^{-22} \text{ Am}^2$. The obtained directions are compatible with the Late Pleistocene paleodirection as expected from the geocentric axial dipole (GAD) field. The virtual geomagnetic pole scatter (S_b) was calculated at 13.5° which is consistent with the paleosecular variation value expected from El Pinacate latitude.

1. Introduction

Volcanism at the northwestern part of Mexico represents changes in the tectonic configuration from the subduction regime to a transtensional plate margin since Miocene time (Lonsdale, 1989; Stock and Hodges, 1989). During the past 5 Ma, volcanism has been pervasive in the Gulf of California (Demant, 1984; Sawlan, 1991; Paz-Moreno et al., 1999; Schmitt et al., 2006), which is in contrast rare inland (Paz-Moreno, 1992; Paz-Moreno et al., 2003a, b; Corella-Santa Cruz, 2017). El Pinacate Volcanic Field (PVF) was built on the western margin of the North American Plate, near to the northern end of Gulf of California and northwest of Sonora State (Fig. 1). The PVF forms part of the Great Altar Desert, and covers an area of ca. 15000 km² between the Southern Basin and Range Province (Henry, 1989; Henry and Aranda-Gómez, 1992; Hawkesworth et al., 1995) and the Gulf Extensional Province (Stock and Hodges, 1989). The PVF comprises a Neogene volcanic sequence that overlies a Pre-Cambrian and Mesozoic crystalline

basement.

The aim of this work is to perform a full vector analysis of the geomagnetic field (GMF) and to provide the characterization of the magnetic properties on 12 Late Pleistocene cooling units of the volcanic event called *El Pinacate* at the northwestern part of Mexico. The paleomagnetic data (direction and intensity), estimated from precisely dated material, are relevant to create a reliable secular variation curve for Northwestern Mexico, that will contribute to a better understanding of the variations in time and space of the Earth's magnetic field. The compilation of local and global paleomagnetic data can be used to build analytical paleo secular variation (PSV) models that describe the long-term and short-term variations of the dipolar behavior of the GMF at different time scales (e.g. Pavón-Carrasco et al., 2014; Panovska et al., 2018; Cromwell et al., 2018). The developing of accurate regional models of PSV, provide valuable tools that can be used as an accurate dating tool (e.g. Alva-Valdivia et al., 2019a; 2019b).

* Corresponding author.

E-mail address: alekz_igf@hotmail.com (A. Rodríguez-Trejo).

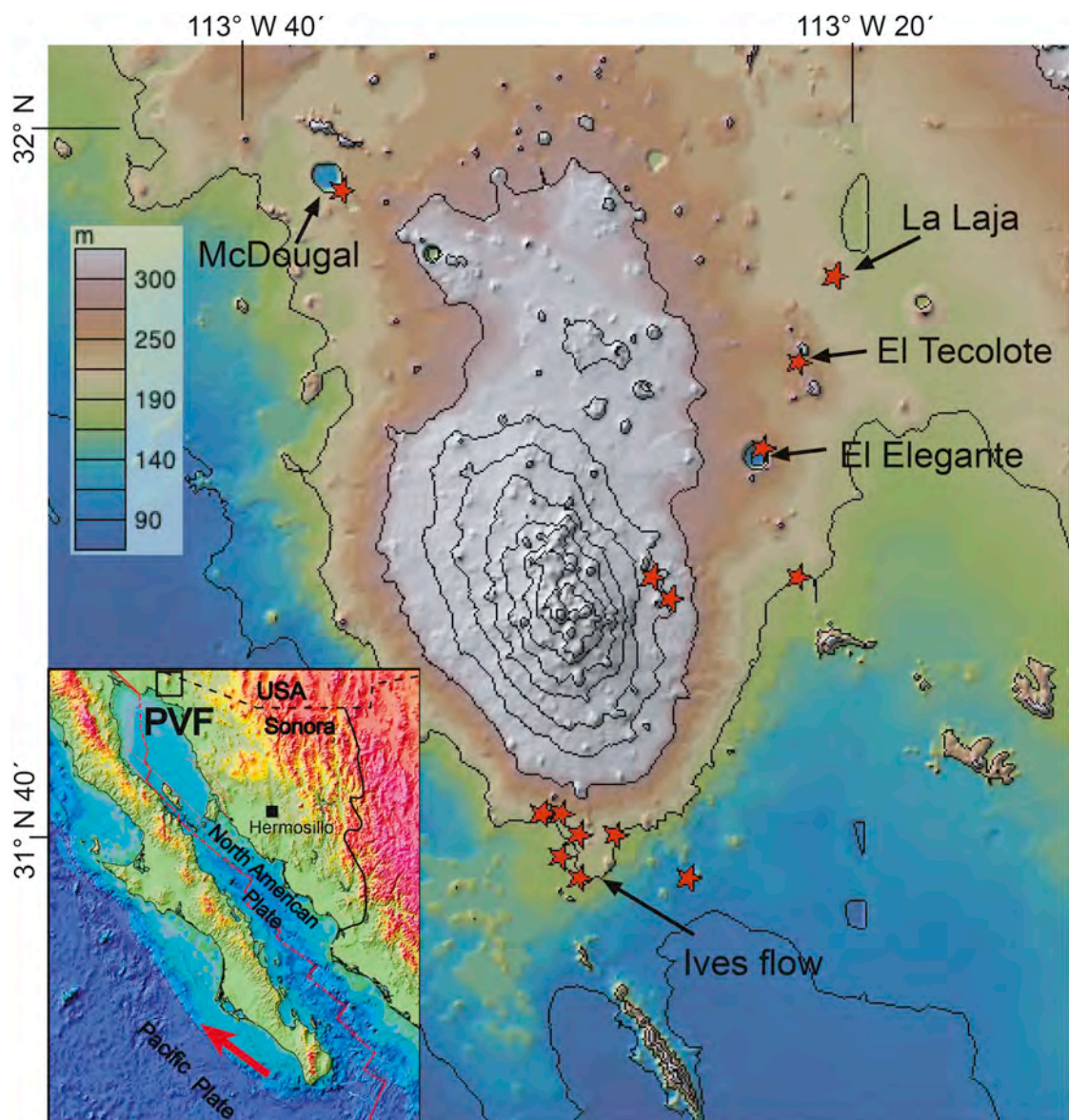


Fig. 1. Elevation map of the El Pinacate Volcanic Field (PVF) and distribution of the paleomagnetic sampling sites (red stars). (For interpretation of the references to color in this figure legend, the reader is referred to the Web version of this article.)

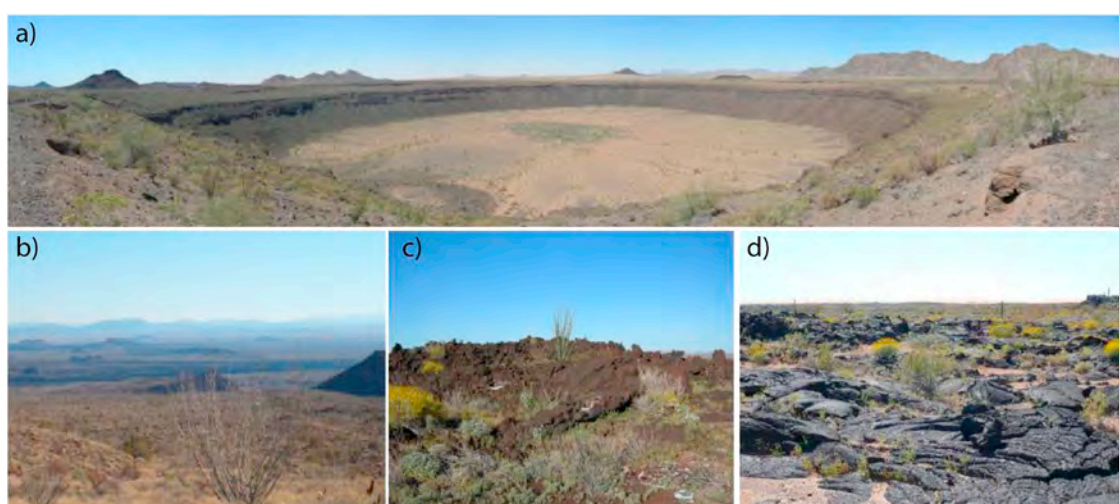


Fig. 2. McDougal crater (a); typical volcanic structures from El Pinacate volcanic field (a, b, c, d); and typical aa (c) and pahoehoe (d) lava flows.

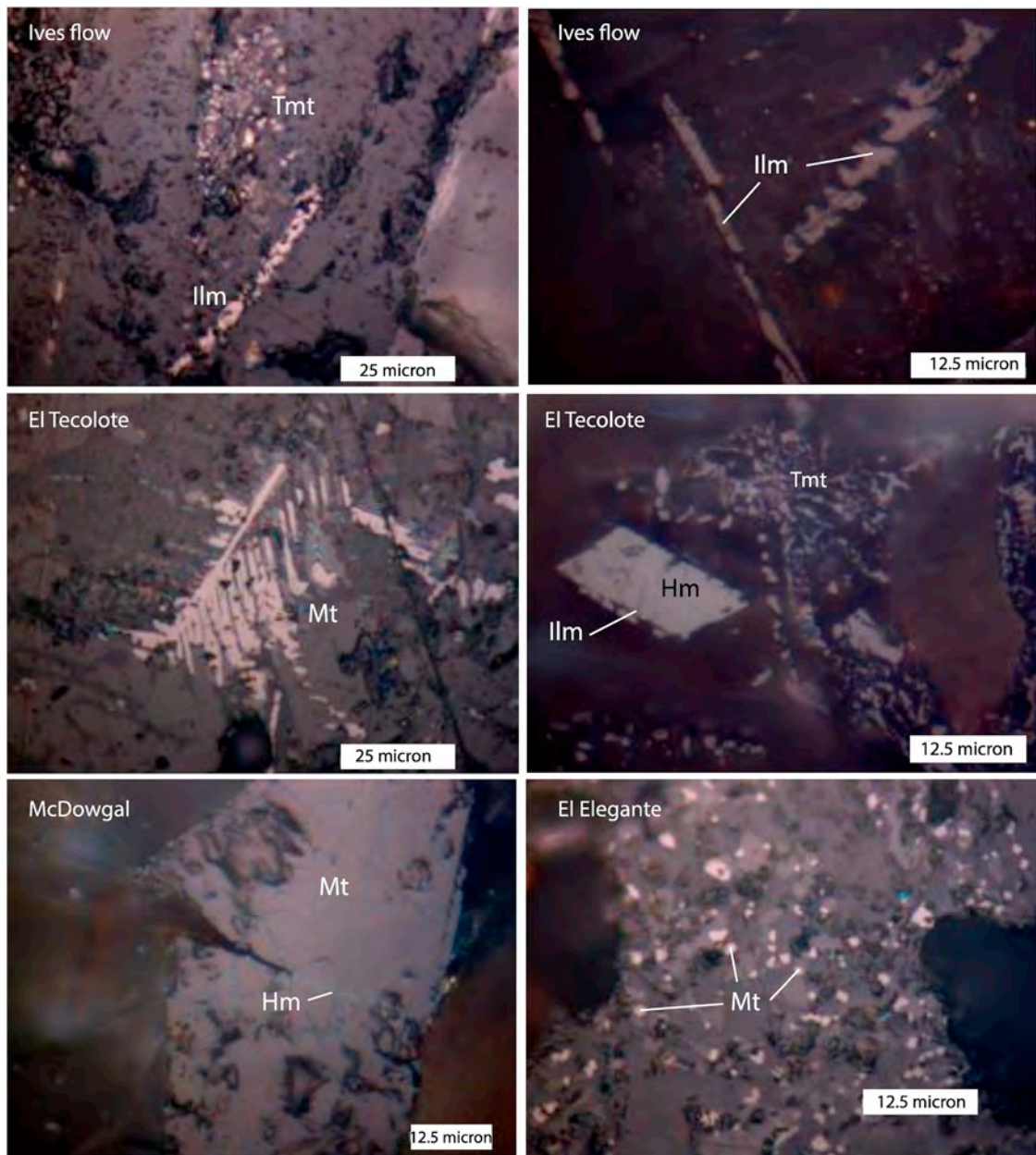


Fig. 3. Microphotographs representative of opaque minerals from the lava flows of the PVF.

2. Geology

The tectonic setting of the PVF is characterized by a change from convergent margin type, essentially controlled by subduction of the Farallon plate under the North America plate, to a trans-tensional plate margin style (Lonsdale, 1989; Stock and Lee, 1994). This tectonic change generated two main volcanic events during the Neogene and Pleistocene (Lynch, 1981): the first is called the *Pre-Pinacate event* that occurred during the Miocene; and the second is called the *Pinacate event* during the Pleistocene. The geology, tectonics, geochemistry and geochronology of both events have been thoroughly described in many scientific papers (Gutmann, 1973, 1976, 1977, 1979, 2002; Lynch, 1981, 1993; Gutmann et al., 2000; Turrin et al., 2008; Paz-Moreno and Demant, 2002, 2004; Vidal-Solano et al., 2005, 2008), and the characterization of the explosive activity in some of the volcanic structures such as in Tecolote volcano (Zawacki et al., 2019). The *Pinacate event* is characterized by intense activity with a large number of lava

emplacements, covering ca. 1500 km² area, and forming a huge volcanic shield over the older Pre-Pinacate lava deposits. It is divided in two eruptive phases: the first phase started with the construction of the Santa Clara shield volcano 1.7–1.1 Ma, which makes up the Sierra Pinacate; the second phase is characterized by intense monogenetic basaltic activity for the last 1 Ma, covering and surrounding almost all of the previous lava flows from the Santa Clara and the *Pre-Pinacate event*. The exhaustive activity produced more than 400 volcanic structures such as scoria and cinder cones, and large ‘pahoehoe’ and ‘aa’ lava emplacements (Fig. 2), such as the Ives flow (Ives, 1942, 1956) with an age of 13 ± 3 ka (Turrin et al., 2008). Many maar type craters, originated by phreatomagmatic activities, were built in this final episode. Wohletz and Sheridan (1983), described the emplacement mechanism of these hydromagmatic volcanoes e.g. El Elegante, with an age of 32–42 ka (Gutmann and Turrin, 2006), Cerro Colorado with an estimated paleomagnetic age ca. 4 ka BP (Alva-Valdivia et al., 2019a, b) and the McDougal crater of 190 ka (Lynch et al., 1993).

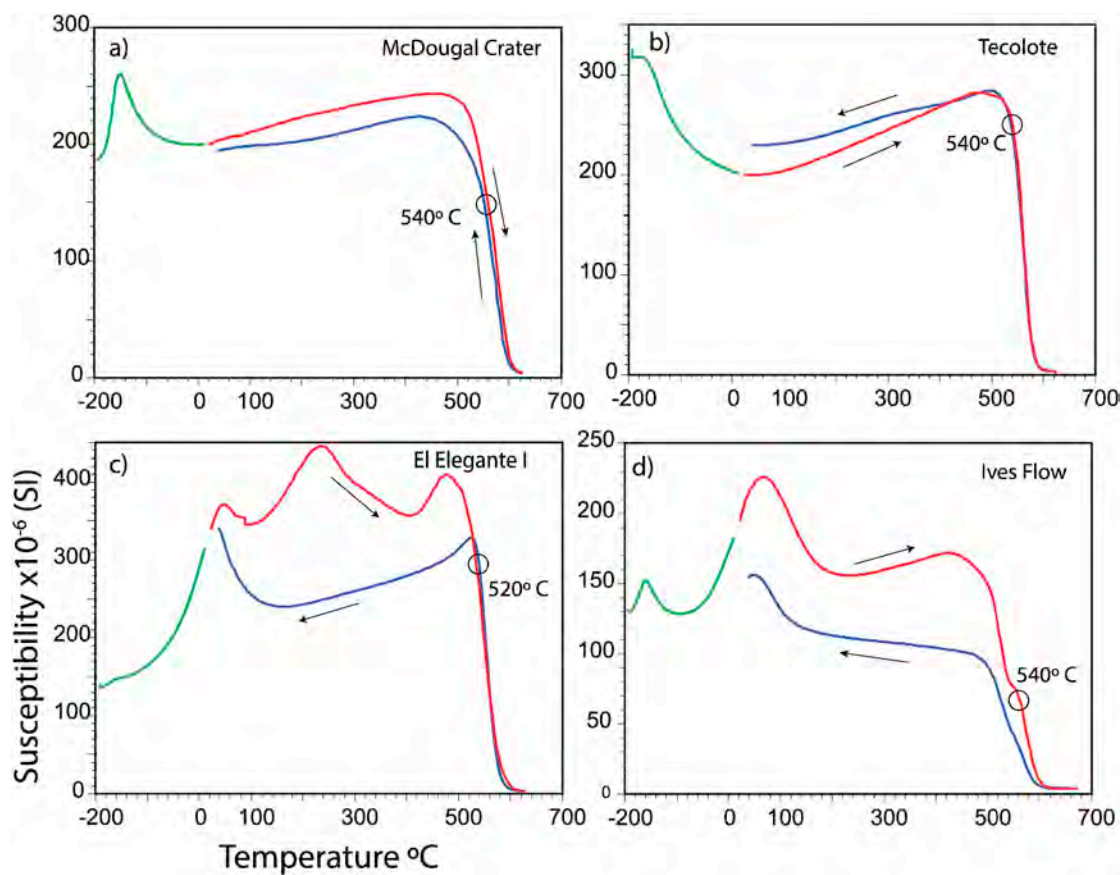


Fig. 4. Typical susceptibility vs. temperature curves. Red line indicates the heating curve. Blue line indicates the cooling curve. Green line indicates low temperature curve (-192°C to room temperature). (For interpretation of the references to color in this figure legend, the reader is referred to the Web version of this article.)

3. Methodology and laboratory procedures

We have obtained 140 standard size cores from 16 sites corresponding to 12 cooling units, using a gasoline-powered drill and oriented directly in the field with both magnetic and sun compass. Site selection was designed according to the already published age data (e.g. Gutmann et al., 2000; Gutmann and Turrin, 2006; Lynch et al., 1993). All sites were selected from the Late Pleistocene volcanic activity.

Susceptibility as a function of temperature curves were measured to identify the mineral magnetic carriers of magnetization and to assess the thermal stability of the samples. Measurements were done using an KLY-3S Kappabridge (AGICO) in the Laboratory of Paleomagnetism, University of Montpellier II (France), in an argon atmosphere. The measurements were done in two consecutive cycles: the first at low temperature, from -192°C to room temperature, followed by heating at high temperature, from room temperature to 700°C and consecutive cooling back to room temperature. Curie temperatures of the samples were estimated by the first derivative method. One small rock chip sample per site was selected for hysteresis, IRM and FORC analyses. The determination of saturation magnetization (M_s), saturation remanent magnetization (M_{rs}), coercive force (H_c) and remanent coercive force (H_{cr}) provided a glimpse on the domain state of the magnetic grains. All the specimens were weighed, and the results normalized by mass. Measurements were performed using a Princeton MicroMag model 2900 alternating gradient magnetometer in fields up to $\pm 1.2\text{ T}$ at room temperature at UNAM.

One specimen from each core was selected for demagnetization. 50% of the selected specimens per site were thermally demagnetized, and the other 50% of the samples were demagnetized using alternating magnetic fields (AF). Stepwise thermal demagnetization procedure was completed using a non-inductive Schonstedt furnace, heating the

sample in step wise intervals from the room temperature up to 600°C , and after cooling, the remanence was measured using a JR-5 (AGICO) spinner magnetometer. AF experiments were performed using a 2G Enterprises cryogenic magnetometer at the University of Montpellier II, in 15–20 demagnetization steps, and up to 160 mT . The demagnetization data defined, for each specimen, the paleomagnetic direction using the Principal Component Analysis (Kirschvink, 1980), with maximum angular deviation (MAD) up to 5° . The characteristic remanent magnetization (ChRM) was estimated for each sample by using 6 to 10 vector points. ChRM was determined by using the software by AGICO-REMASOFT (Chadima and Hrouda, 2006). The mean direction for each site was calculated from at least 6 specimens using Fisher statistics (Fisher, 1953). The 95% confidence level was used to identify outliers.

Paleointensity experiments were carried out in a Magnetic Measurements Thermal Demagnetizer (MMTD) furnace, through step-wise heating at every 50°C from 100°C and up to 500°C , and the last step at 540°C , under an applied field of $40\text{ }\mu\text{T}$, using Thellier-Thellier (1959) paleointensity protocol with the modifications proposed by Coe (1967). The partial thermal remanent magnetization (pTRM) was checked at every 100°C . Acceptance criteria were determined by five quality statistical factors, described in the Standard Paleointensity Definitions (SPD) (Paterson et al., 2014): the f factor is the NRM fraction used for the best-fit on an Arai diagram ($f \geq 0.3$); the gap factor (g) represents the measure of the average NRM lost between successive temperature steps of the segment chosen for the best-fit line on the Arai plot; the quality factor (q) is a measure of the overall quality of the paleointensity estimate and combines the relative scatter of the best-fit line, the NRM fraction and the gap factor ($q \geq 3$); the maximum angular deviation (MAD) of a data point from the best fit line in a vector component diagram (Kirschvink, 1980), defined as the anchored and

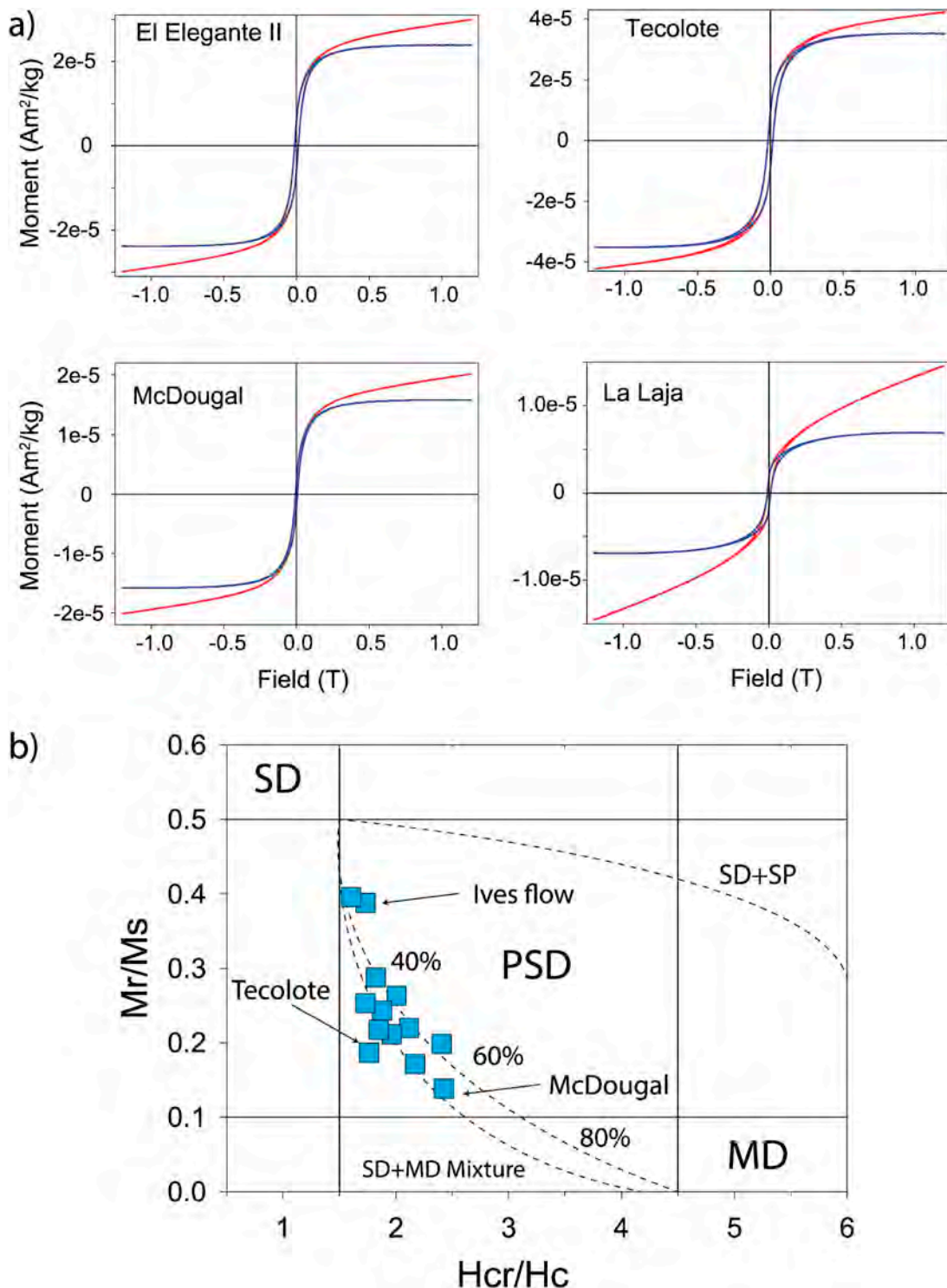


Fig. 5. (a) Representative hysteresis curves. (b) Day-Dunlop plot gives a glimpse on the distribution of the domain state of the samples: single domain (SD); pseudo single domain (PSD); and multidomain (MD).

free-floating, respectively, directional fits to the paleomagnetic vector on a vector component diagram (Kirschvink, 1980); and the $\delta\text{CK} \leq 7\%$, defined as Maximum absolute difference produced by a pTRM check, normalized by the total TRM (Leonhardt et al., 2004a) ($\delta\text{CK} \leq 7$). The results were processed using the Thellier-tool software (Leonhardt et al., 2004b).

Oxide mineral identification were performed under reflected light using polished sections and a DMLP Leica Microscope System.

4. Results

4.1. Opaque magnetic microscopy

We follow the oxidation state and texture classification described in Alva-Valdivia (2005) and references therein. Representative microphotographs are shown in Fig. 3.

In general, the El Pinacate lava flows show small subhedral disseminated titanomagnetites (Fig. 3 d, e). Titanomagnetite is the main

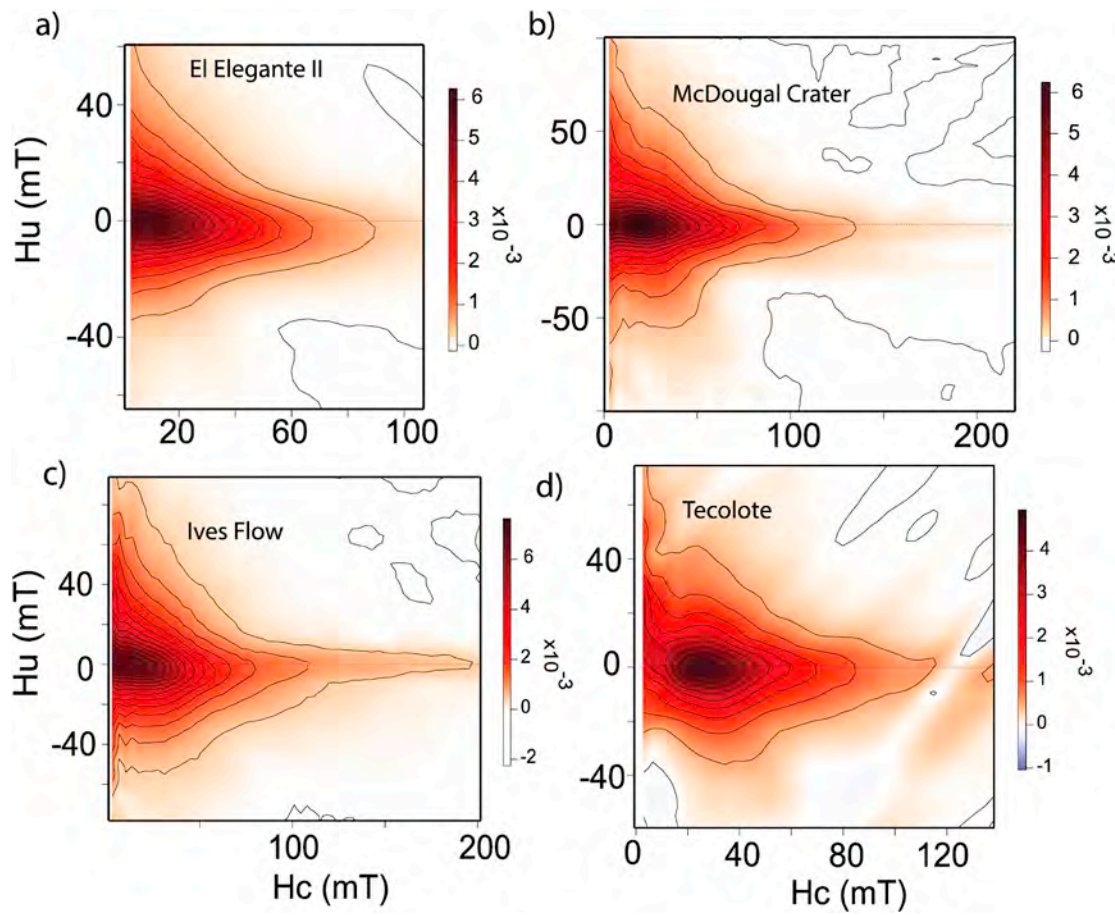


Fig. 6. Representative FORC plots from distinct lava flows.

magnetic carrier and is inhomogeneously distributed with ilmenite intergrowths showing a light gray-brown color, sometimes fractured or with a brecciated texture (Fig. 3 a, c, d). The state of oxidation of titanomagnetites mineral series is C2, for skeletal grains (Fig. 3 c, d), but some subhedral grains with C3–C5 are also present (Fig. 3 a, e). (Titanio)magnetite grain sizes vary from 1 to 45 µm, while titanohematites are > 25 µm with R2–R5 (Fig. 3d) oxidation states (Haggerty, 1976, Fig. 3 a, e, f). The magnetic mineralogy suggests that the natural remanent magnetization carried by these grains is a thermoremanent magnetization, because the described paragenesis typically develops at temperatures higher than 600 °C (O'Reilly, 1984).

4.2. Rock magnetism

The samples show three typical thermomagnetic curves: 1) reversible (Fig. 4a and b), with similarly shaped heating and cooling branches and Curie temperatures between 520° - 540 °C, corresponding to Ti-poor titanomagnetite (e.g., Alva-Valdivia et al., 2019b) and/or magnetite; 2) non-reversible curves with multiple phases (Fig. 4c), revealing 2 or 3 magnetic phases during the heating process, and Curie points from 300 °C to 400 °C and 540 °C. The cooling branch shows a single phase and lower susceptibility, thus indicating a change by oxidation of mineral phases; and 3) non-reversible curves with two Curie points (Fig. 4d) 180 °C and 540 °C, revealing a mixture of Ti-poor and Ti-rich titanomagnetite. The low temperature experiments (−192 °C to room temperature) show the Verwey transition from −160 °C to −140 °C in some samples (Fig. 4a and d), suggesting the presence of titanomagnetite (Vahle and Kontny, 2005). In brief, the main carrier of magnetization is Ti-poor titanomagnetite of high stability up to 450 °C. The reversibility of susceptibility curves during the heating and cooling

processes, suggest no mineral changes (particularly during the 300–500 °C), which help for selection of the samples to get possibly more successful paleointensity determinations (Fig. 4a and b).

Most of the sites show a typical trend, of the hysteresis curves corrected by the mass of the sample, indicating mixtures of single and multidomain or pseudo single domain (PSD) particles (e.g., Dunlop, 2002a, 2002b) with different saturation points, which might suggest the presence of Ti-poor and Ti-rich magnetite. Day plot (Day et al., 1977) shows magnetization ratios $0.13 < \text{Mrs}/\text{Ms} < 0.39$, and coercivity ratios $1.5 < \text{Hcr}/\text{Hc} < 2.4$ (Fig. 5). These ratios again suggest characteristic a single domain + multidomain mixture (SD + MD) resulting from 20% to 80% MD or PSD grain sizes, which is typical of volcanic rocks (e.g., Alva-Valdivia et al., 2019b). Most of the specimens show PSD behavior and small grain sized of magnetite and Ti-poor titanomagnetite.

First order reversal curves (FORC) data processing was performed by using the FORCinel routine (Harrison and Feinberg, 2008) for high-resolution results choosing a smoothing factor between 4 and 5 for all the cases. There are two typical shapes (Fig. 6): e.g. with coercivity elongation (60–120 mT), symmetrical inner contours along the Hc axis, and slightly divergent outer contours spreading over the vertical Hu axis, revealing PSD grains (e.g., Roberts et al., 2000) (Fig. 6d); another type of FORC present symmetrical and highly spread out contours over the vertical axis, with low elongations along the Hc axis (20–60 mT) suggesting interacting MD grain behavior (e.g., Pike et al., 1999) (Fig. 6a, b and 6c). The FORC plots show prevalence of low coercivity components. The FORC configuration curves validate a low interaction between domains and a trend from PSD to MD behavior, which are typical of titanomagnetite dominant mineralogy.

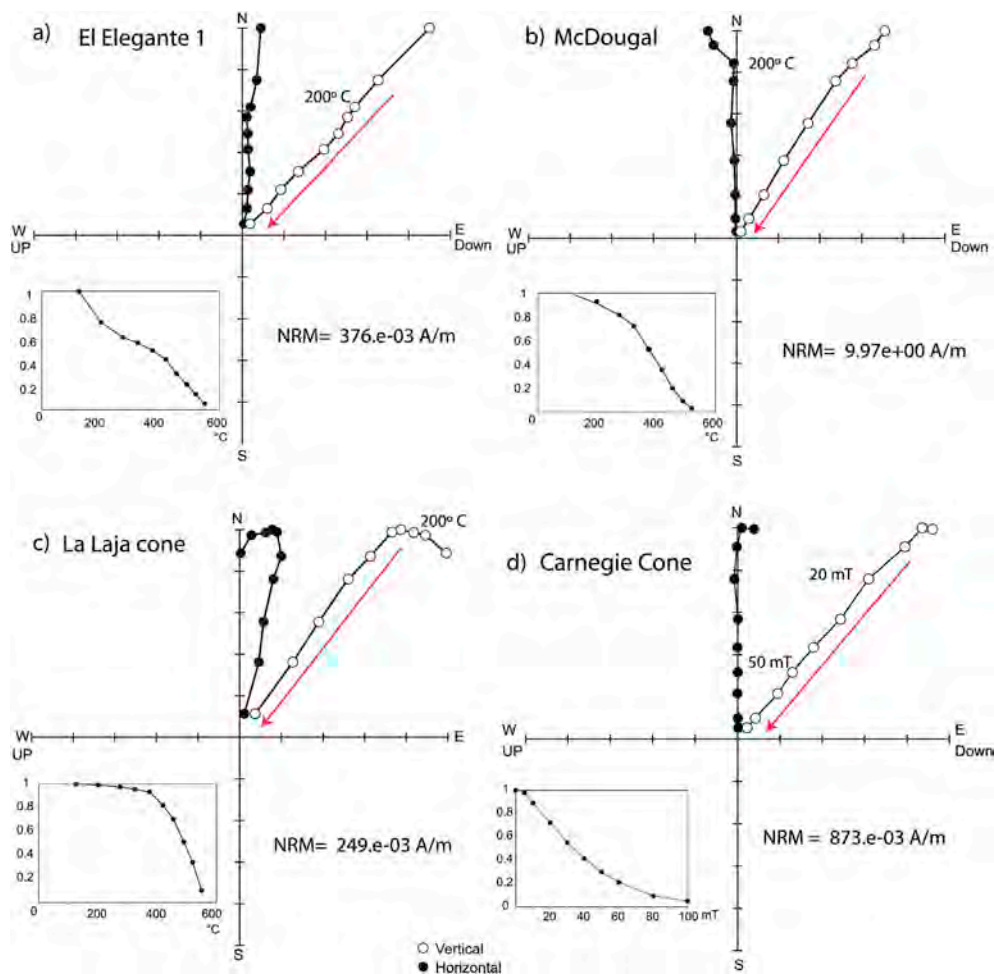


Fig. 7. Representative orthogonal AF and thermal demagnetization plots. The red lines show the vector points used to determine the ChRM direction. (For interpretation of the references to color in this figure legend, the reader is referred to the Web version of this article.)

Table 1

Summary of ChRM directions and VGP. n is the number of specimens used for the calculation of the ChRM; Dec is the declination by site; Inc is the inclination by site; k is the dispersion parameter according with the Fisher statistics; α_{95} is the 95% confidence angle according with the Fisher statistics; Age σ indicates the standard deviation of the age determination. *sites rejected for the calculation of the overall mean.

Cooling Unit	Site	Location		n	Dec (°)	Inc (°)	k	α_{95}	VGP		Age ka	Age σ	Dating method	Age reference
		Lat. °N	Lon. °W						Plat °N	Plong °E				
Ives flow	PVF-061	31.56	113.47	7	339.9	60.2	61.2	5.6	71.3	192.8	13	3	$^{40}\text{Ar}/^{39}\text{Ar}$	Turin et al. (2008)
	PVF-105	31.65	113.49	7	333.7	61.9	60.9	6.6	66.3	192.9				
	PVF-106	31.67	113.49	9	352.6	60.1	144.8	4.3	78.9	216.1				
	PVF-107	31.67	113.47	9	356.5	56.2	64.6	6	84.1	217.9				
	PVF-108*	31.66	113.5	4	31.5	39.1	21.5	20.3	60.5	347.5				
Ivesflow mean direction				32	346.2	59.9	189	5.7	75.6	200.1	13.5	0.5	Paleomagnetism	This study
La Laja cone	PVF-056	31.93	113.35	6	15.2	59.1	120.2	4.4	75.4	299.5	12	4	$^{40}\text{Ar}/^{39}\text{Ar}$	Gutmann et al. (2000)
	PVF-121	31.68	113.51	10	353.9	51.6	266.9	3.2	84.8	164.3	11.14	0.14	Paleomagnetism	This study
	PVF-122	31.68	113.5	9	346.7	58.2	143.8	4.6	77	193.8	11.2	0.23	Paleomagnetism	This study
	PVF-111	31.65	113.43	9	128.5	8.2	74.2	5.1	-26.7	306.7	13-40			Stratigraphy
Cero Tecolote	PVF-019	31.89	113.37	8	1	62.7	68.1	7.2	77.8	250	27	6	$^{40}\text{Ar}/^{39}\text{Ar}$	Gutmann et al. (2000)
	PVF-051	31.79	113.37	8	3.9	58.9	59.9	6.4	81.5	267.4	< 32			Stratigraphy
El Elegante I	PVF-020-I	31.85	113.39	8	356.6	39.7	134.4	5.8	80.2	85.4	32	6	$^{40}\text{Ar}/^{39}\text{Ar}$	Gutmann and Turrin (2006)
El Elegante II	PVF-020-II	31.85	113.39	8	6.5	43.1	857.8	3.1	81.1	24.9	42	13	$^{40}\text{Ar}/^{39}\text{Ar}$	Gutmann and Turrin (2006)
Carnege Cone	PVF-101	31.78	113.44	8	353.4	38.2	41.6	10.5	78.1	97.9	38	8	$^{40}\text{Ar}/^{39}\text{Ar}$	Gutmann et al. (2000)
	PVF-103	31.79	113.45	8	31.6	62	64	8.4	62.7	302.8	> 38			Stratigraphy
McDougal	PVF-054	31.97	113.62	8	354.1	59.6	301.8	5.3	80.3	218.7	190	50	K-Ar	Lynch et al. (1993)
Overall mean direction and paleopole				14	0.1	54.5	48	6.7	86.5	247.8				

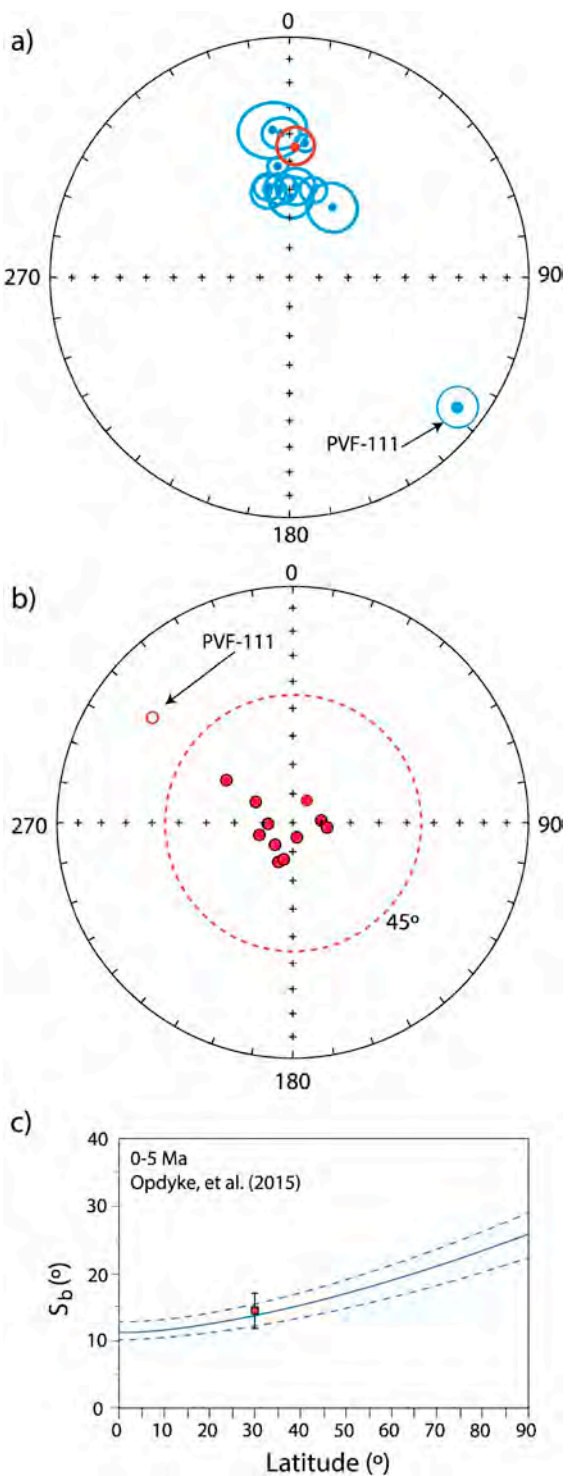


Fig. 8. a) Equal area plot of the mean ChRM by site (blue dots) and mean paleomagnetic direction (red dot) from all sites. b) Distribution of VGP's with a 45° inner circle (dashed line), show the grouping of the directional data with normal polarity (red dots) and the transitional values (empty dot). (c) Comparison of the VGP dispersion in Pinacate volcanic field with the latitude dependence of the VGP dispersion as proposed by Opdyke et al. (2015) for the last 0–5 Ma. (For interpretation of the references to color in this figure legend, the reader is referred to the Web version of this article.)

4.3. Paleomagnetic directions and VGPs

Zijderveld plots (Zijderveld, 2013) of 80% of the samples show a single magnetization component with a well-defined direction (Fig. 7a) and MAD

lower than 3°. Some cases show a small secondary component due to viscous remanent magnetization that was removed at maximum temperature of 200 °C in the thermal demagnetizer (Fig. 7b, c and 7d), or at an AF amplitude between 5 and 10 mT. 16 mean directions (Table 1) were precisely determined, and used to calculate the mean direction and VGP's of the younger volcanic events from the late Pleistocene volcanism.

Site PVF-108 was rejected due to high directional scatter ($k = 21.5$ and $\alpha_{95} = 21.5$) in comparison with the rest of the sites in this study. Site PVF-111 presents a transitional-reversed direction with low inclination value (Inc = 8.2°) and a deflected declination (Dec = 128.5°) and a low latitude VGP that according to its stratigraphically constrained age of 13–40 ka (Table 1) could correspond to the Mono Lake, Laschamp, Rockall, or Hilina Pali/Tianchi excursion (Singer et al., 2014). Such excursions have been reported from different lava flows in Mexico (e.g. García-Ruiz et al., 2016; Mahgoub et al., 2019).

The mean direction and paleopole, estimated from 14/16 sites, from 11 cooling units is: Dec = 0.1, Inc = 54.5, n = 14, $\alpha_{95} = 6.7$, $k = 48$, Plat = 86.5°, Plong = 247.8°, $A_{95} = 7.5$, K = 36.7. However, the absence of radiometric dating for site PVF-111 does not allow establishing a proper relation with any of them. This site was rejected for the calculation of the overall mean. The calculated mean direction is consistent with average secular variation activity of the geomagnetic field reported for the past 50 ka (e.g. Böhnel and Molina-Garza, 2002; Mahgoub et al., 2019; Rodríguez-Trejo et al., 2019) in Mexico, and for the past 100 ka described by global models (e.g. Panovska et al., 2018). The site mean directions vary around the GAD field direction by about ± 20 ° for both declination and inclination (Table 1). With this range of variation, it is possible to discard site PVF as a record of a dipole, and could be associated to an excursion. Also, the estimated paleodirection fits with the GAD setting expected for NW Mexico. Fig. 8a shows the equal area plot of the mean directions for each site within a α_{95} confidence circle and the paleodirection calculated for the PVF. A 45° VGP latitude was established as a minimum value to determine a full record of the PSV and to differentiate the transitional values (Tauxe et al., 2003; Johnson et al., 2008; Doubrovine et al., 2019). Fig. 8b shows the position of the VGPs for the studied sites. All the sites are located within this limit, except site PVF-111, located outside the 45° boundary. The VGP scatter of the dataset was estimated ($S_b = 13.5$) to identify any anomalous dispersion at the latitude of our study region. Fig. 8c shows that the estimated value fits with the model of PSV for the last 0–5 Ma (Opdyke et al., 2015). The VGPs dispersion show that the results have a reliable record of the GAD and thus averaged out secular variation, discarding any local tectonic displacement.

4.4. Paleointensity

After the analysis of magnetic behavior and response during thermal procedures, the samples were selected for the paleointensity process by applying three basic quality criteria: a) the presence of only a single magnetization component as seen in the orthogonal demagnetization diagrams; b) the reversibility of the susceptibility vs. temperature curves, and c) the dominance of PSD magnetic domain state or a SD + MD mixture according with the Day Plot (Day et al., 1977) (Fig. 5). 61 specimens corresponding to 9 from 11 sites accomplished these selection criteria.

High quality paleointensity results were obtained from 23 of 61 specimens from 7 volcanic structures. As shown in the susceptibility vs. temperature curves, Curie temperature ranges from 200 to 540 °C. Some samples were rejected e.g. Fig. 9d, showing thermal alteration above 250 °C in the Arai plot, generating a thermochemical remanent magnetization (TCRM). Alteration between 0 and 350 °C during the heating was observed in 30% of the samples, indicating a mixture of two different unblocking temperature for this segment of the pTRM. This may be due to alteration of the titanomagnetite to a different magnetic carrier, giving lower paleointensity (these samples were rejected for the mean calculation). A summary of the paleointensity results and statistical parameters are listed in Table 2.

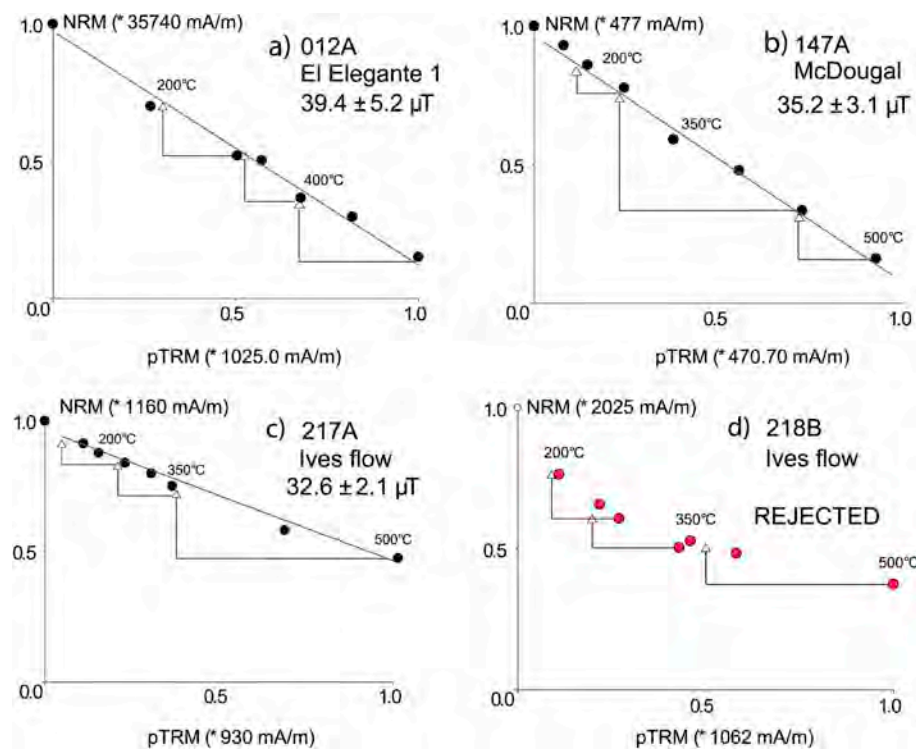


Fig. 9. Representative accepted and rejected paleointensity Arai plots.

Table 2

Summary of paleointensity data: n is the number of steps used in the calculation; statistics for paleointensity determination, f is the best fit NRM fraction used on the Arai plot, g is the gap factor, q is the quality factor; H is the paleointensity and $H\sigma$ the respective standard deviation; VDM is the virtual dipole moment.

Cooling unit	Site	Specimen	n	f	g	q	H (μ T)	H σ	$VDM \times 10^{22} \text{ Am}^2$
Tecolote	PVF-019	035B	6	0.8	0.7	7.7	60.4	2.1	11.6
	PVF-019	036C	7	0.5	0.7	5.6	62.1	2.5	11.9
	PVF-019	038B	7	0.6	0.8	6.4	61.7	1.9	11.8
Site mean							61.4	2.2	11.8
Elegante I	PVF-020-I	008B	8	0.9	0.8	5.5	28.1	3.5	5.4
	PVF-020-I	010A	6	0.5	0.7	5.3	36.2	5.1	6.9
	PVF-020-I	011B	7	0.5	0.6	5.6	31.8	4.1	6.1
	PVF-020-I	012A	7	0.6	0.7	7.5	39.4	5.2	7.6
Site mean							33.9	4.5	6.5
Elegante II	PVF-020-II	014A	7	0.5	0.7	4.7	52.7	6.5	10.1
	PVF-020-II	015B	8	0.5	0.8	6.0	52.5	5.1	10.1
	PVF-020-II	016B	7	0.4	0.7	8.1	57.3	5.4	11
Site mean							54.2	5.7	10.4
PVF-051	PVF-051	112B	7	0.7	0.8	5.8	64.6	6.1	12.4
	PVF-051	117B	8	0.9	0.8	8.0	67.3	6	12.9
McDougal	PVF-054	144B	8	0.8	0.7	14.9	31.7	1.1	6.1
	PVF-054	146B	7	0.8	0.7	8.3	32.4	2.1	6.2
	PVF-054	147A	8	0.8	0.8	7.9	35.2	3.1	6.9
Site mean							33.1	2.1	6.4
La Laja	PVF-056	165C	5	0.5	0.5	5.9	33.8	2.2	6.5
	PVF-056	167A	7	0.7	0.6	6.7	37.3	1.4	7.1
	PVF-056	168A	8	0.4	0.6	7.8	35.3	4.2	6.8
	PVF-056	170B	4	0.7	0.6	4.8	32.2	1.9	6.1

(continued on next page)

Table 2 (continued)

Cooling unit	Site	Specimen	n	f	g	q	H (μ T)	H σ	VDM $\times 10^{22}$ Am 2
Site mean							34.7	2.4	6.6
Ives	PVF-061	217A	5	0.4	0.6	6.2	32.6	2.1	6.3
	PVF-061	220B	8	0.7	0.7	5.7	36.2	3.6	6.9
	PVF-061	221B	7	0.5	0.7	6.3	34.5	2.7	6.6
	PVF-061	224C	8	0.6	0.7	7.1	35.5	3.3	6.8
	PVF-061	227A	8	0.5	0.7	7.4	38.9	3.6	7.5
	PVF-061	228B	8	0.5	0.8	5.1	35.1	3.2	6.7
Site mean							35.5	3.1	6.8

We obtained seven mean paleointensity from the PVF, the results by specimen are ranging from 28.1 to 67.3 μ T, and the mean paleointensity values by site range from 33.1 to 61.4 μ T with a mean of 42.2 μ T. The VDM is ranging from 5.4×10^{22} to 12.9×10^{22} Am 2 with a mean of 8.1×10^{22} Am 2 (Table 2). These results are consistent with the actual settings of the GAD and VDM ca. 8×10^{22} Am 2 for Mexico (Böhnel and Molina Garza, 2002). Secular variation results are in a similar range either in paleointensity or VDM; nevertheless, most of the previous results reported for Mexico are from the TMVB that has a latitude difference of ca. 10° compared with the PVF. However, the difference in latitude preserves the same behavior of the dipole in this period according with numerical and synthetic models for the last 100 ka (Panovska et al., 2018).

5. Paleomagnetic dating

The age of two volcanic units was determined by paleomagnetic dating, using the Matlab tool for archaeomagnetic dating (Pavón-Carrasco et al., 2011) at a 95% confidence level. The age of the Ives Flow was also confirmed by the paleomagnetic method that consists in comparison of the directional results (declination and inclination in this

study) from sites PVF-121 and PVF-122 (Fig. 10), with the global model SHA.DIF.14k (Pavón-Carrasco et al., 2014). Paleointensities were not used for the comparison, due to the unsuccessful results on those sites.

A relative age from sites PVF-121 and PVF-122 was assigned in the field by direct stratigraphic contact, as these lava flows are younger than Ives flows of estimated age 13 ± 3 ka BP (Turrin et al., 2008), and older than Cerro Colorado tuff ring estimated at 3.9 ± 0.6 ka BP (Alva-Valdivia et al., 2019a), the youngest volcanic event registered in the PVF. The age for site PVF-121 (Fig. 10b), with the probability density combined is 11.2 ± 0.3 ka BP. The age for site PVF-122 (Fig. 10c), with the probability density combined is 11.1 ± 0.14 ka BP. Both lava flows have been emplaced in very similar intervals of time. The constrained age by the paleomagnetic method for Ives flow is 13.5 ± 0.5 ka BP determined by the full vector result. Fig. 10a show two possible intervals that are consistent with the reported age of 13 ± 3 ka, Turrin et al. (2008) for Ives Flow.

Pavón-Carrasco et al. (2014) indicate that for ages > 6 ka, the global model loses much resolution and may only represent dipole variations. So, our result is comparatively reasonable, but in spite of the coincidence with the 13.5 ± 0.5 ka BP age, raises hope that the situation is not too incorrect.

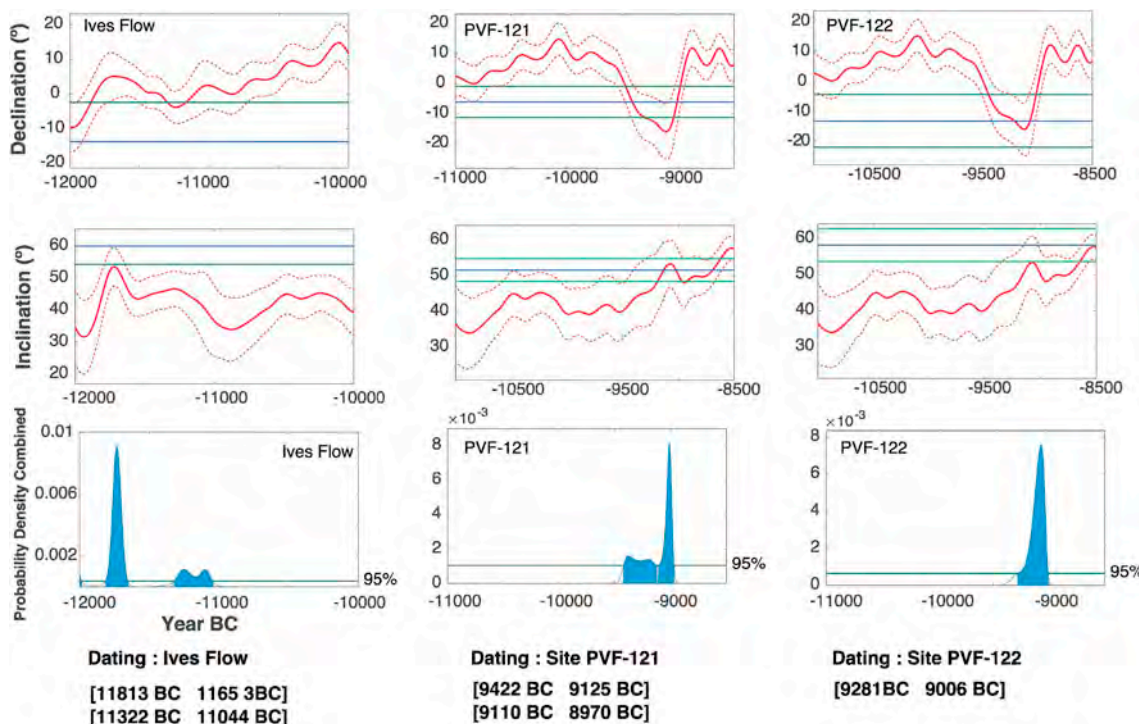


Fig. 10. Summary of the paleomagnetic dating results estimated with the paleomagnetic dating tool (Pavón-Carrasco et al., 2011).

6. Discussion

The PVF has two different volcanic episodes with different lava types and volcanic structures. This study investigates the younger episode, which is characterized mostly by basaltic rocks (Gutmann et al., 2000; Gutmann and Turrin, 2006). Rock magnetic analysis reveals small differences of the magnetic parameters describing the ferromagnetic mineralogy and the magnetic domain state among sites. The carrier of magnetization is defined mainly by Ti-poor titanomagnetite. Oxidation of titanomagnetite is possible by: low temperature below 600 °C, cation-deficient spinel of the metastable titanomaghemitite, which may convert to members of the titanohematite series, and temperature above 600 °C with the direct formation of titanohematites. Conversely, distinct textures of ilmenite intergrowths in titanomagnetite are: trellis lamellae resulting from oxidation-exsolution; sandwich and composite ilmenites can be the product from either oxidation or primary crystallization.

Well-grouped magnetic mean directions and VGP's of normal polarity, and possibly transitional polarity was determined. Mean directions and VGP in general show small within-site dispersion ($\alpha_{95} = 3.2^\circ - 10.5^\circ$) and are of normal polarity. One site (PVF-111) has a transitional direction and was discarded for further calculation, as well as site PVF-108 showing large uncertainty of $\alpha_{95} = 20.3^\circ$. From the remaining 11 sites, an overall mean direction with $\text{Dec} = 0.1^\circ$, $\text{Inc} = 54.5^\circ$, $\alpha_{95} = 6.7^\circ$, $k = 48$, and a paleopole at $\text{Plat} = 86.5^\circ$, $\text{Plong} = 247.8^\circ$, $A_{95} = 7.5^\circ$, $K = 36.7$ was determined. These coincide well with the geocentric axial dipole (GAD) field. The VGP scatter calculated for this work ($S_b = 13.5^\circ$) coincides with the expected value at the latitude of the PVF. However, different direction was observed in the site PVF-111, showing low inclination and southern declination value, much different from the mean value estimated for the Late Pleistocene PVF. This transitional direction was excluded from the mean direction, and further age determination is needed to assign this record to another known excursion. Moreover, the directional results show a reliable record of the GAD of the younger volcanic activity.

We have determined 23 high quality paleointensity values from 61 samples, i.e., with a 32% rate of success. The results of directional and paleointensity analysis agree with previous results (e.g. Gonzalez et al., 1997; Böhnle and Molina Garza, 2002; Conte et al., 2006; Michalk et al., 2010 Coe et al., 1978). Declinations and inclinations of the observed paleomagnetic directions range from -20° to 20° and 20° to 60° , respectively. The paleointensity ranges from $28 \mu\text{T}$ to $67 \mu\text{T}$ (Fig. 9). Results fit with the most recent secular variation model for Mexico on the last 47 ka (Mahgoub et al., 2019). The results vary close to the GAD, that supports that the secular variation recorded in the lava flows correspond to a dipole setting.

The great and continuous activity during the late Pleistocene produced many lava flows and cinder and scoria cones. Many of the flows are not dated or even identified properly. Due to these and other conditions, e.g. adverse climate and insufficient road access to the volcanic shield, have inhibited the sampling of more sites to develop the temporal evolution and origin of the PVF. To create a well-defined regional model up to 50 ka, more studies are needed to cover the empty spaces without paleomagnetic data in the time scale. Thus, at this moment it is not possible to create a reliable high-quality secular variation model because there is not enough data, however, identification of these empty spaces in time are now recognized to be filled. In the PVF there are almost 400 volcanic structures from *El Pinacate* event, and in this work, we present paleomagnetic results of only 16 cooling units for the late Pleistocene. For further studies, it is important to determinate the age of volcanic events to allow that the directional and the paleointensity data contribute to a reliable secular variation model for northwest Mexico.

7. Conclusions

The microscopy of opaque magnetic minerals and rock magnetic analysis show small variation in the magnetic mineralogy of the younger lavas of the PVF. The dominant magnetic carrier of magnetization is Ti-poor titanomagnetite. Thermomagnetic curves revealed different magnetic phases with Curie temperatures ranging from 500 °C to 540 °C. PSD magnetic domain states are most common, probably revealing mixtures of SD and MD particles.

Twelve cooling units of Late Pleistocene volcanic rocks from El Pinacate Volcanic Field in NW Mexico were studied for their rock magnetic properties and paleomagnetic record. Mean paleomagnetic direction and paleopole calculated from 11/12 cooling is: $\text{Dec} = 0.1^\circ$, $\text{Inc} = 54.5^\circ$, $n = 14$, $\alpha_{95} = 6.7^\circ$, $k = 48$, $\text{Plat} = 86.5^\circ$, $\text{Plong} = 247.8^\circ$, $A_{95} = 7.5^\circ$, $K = 36.7$; which agrees with the GAD direction for the Late Pleistocene.

We determined seven high quality mean paleointensity values, from well dated volcanic structures, for the late Pleistocene. The mean results by site ranges in paleointensity from $33.1 \mu\text{T}$ to $61.4 \mu\text{T}$, and VDM from 5.4×10^{22} to $12.9 \times 10^{22} \text{ Am}^2$. The mean paleointensity value is $42.2 \pm 3.5 \mu\text{T}$ and VDM $8.1 \pm 0.7 \times 10^{22} \text{ Am}^2$. These values agree well with the expected values for the same period of time. The results so far contribute to enlarge the Global database of the secular geomagnetic variation in NW Mexico. The paleointensity values are the primary results of the northwestern part of Mexico for this period. More paleointensity studies are required, e.g. including the younger and older volcanic structures and the previous volcanic events such as the Pre-Pinacate event, but are currently limited by scarce geochronology ages.

Two new paleomagnetic ages of 11.1 ± 0.1 ka BP and 11.2 ± 0.3 ka BP were determined for PVF-122 and PVF-121 lava flows respectively. New ages refine the volcanic stratigraphy and provide a better understanding of the chronology and evolution of the younger volcanism in the area. However, there are several volcanic structures in the Pinacate volcanic field without a proper dating that is necessary to analyze.

Acknowledgements

We appreciate the financial support to LAV from PAPIIT-DGAPA-UNAM (Mexico) IN113117 and ANR-CONACyT (France-Mexico) 273564, research projects. This work was also supported by a Research Grant #180784 from CONACyT to JRVS. Thanks to Dr. Pierre Camps, provided facilities to use some instruments of the University of Montpellier II, France. Thanks to Dr. Edgardo Cañón from CICESE, that helped during the field work. T. Calmus helped with infrastructure from ERNO-UNAM. Thanks to R. Peralta for the help with the micro-photographs. Thanks to Dr. E. Cañón Tapia, for the help in the field work. Thanks to J. A. González Rangel, V. Macías and M. Espinoza for their support in the Paleomagnetic laboratory experiments at UNAM. To the editor and reviewers of the Journal for their valuable comments and suggestions.

References

- Alva-Valdivia, L.M., Rodríguez-Trejo, A., Vidal-Solano, J.R., Paz-Moreno, F., Agarwal, A., 2019a. Emplacement temperature resolution and age determination of Cerro Colorado tuff ring by TRM analysis, El Pinacate Volcanic Field, Sonora, Mexico. *J. Volcanol. Geotherm. Res.* 369, 145–154.
- Alva-Valdivia, L.M., Rodríguez-Trejo, A., Morales, J., González-Rangel, J.A., Agarwal, A., 2019b. Paleomagnetism and age constraints of historical lava flows from the El Jurullo volcano, Michoacán, Mexico. *J. South Am. Earth Sci.*
- Alva-Valdivia, L.M., 2005. Comprehensive paleomagnetic study of a succession of Holocene olivine-basalt flow: xitle Volcano (Mexico) revisited. *Earth Planets Space* 57 (9), 839–853.
- Böhnle, H., Molina-Garza, R., 2002. Secular variation in Mexico during the last 40,000 years. *Phys. Earth Planet. Inter.* 133 (1–4), 99–109.
- Chadima, M., Hrouda, F., 2006. Remasoft 3.0 a user-friendly paleomagnetic data browser and analyzer. *Travaux Géophysiques* 27, 20–21.
- Coe, R.S., 1967. The determination of paleo-intensities of the Earth's magnetic field with

- emphasis on mechanisms which could cause non-ideal behavior in Thellier's method. *J. Geomagn. Geoelectr.* 19 (3), 157–179.
- Coe, R.S., Grommé, S., Mankinen, E.A., 1978. Geomagnetic paleointensities from radiocarbon-dated lava flows on Hawaii and the question of the Pacific nondipole low. *J. Geophys. Res.: Solid Earth* 83 (B4), 1740–1756.
- Conte-Fasano, G., Urrutia-Fucugauchi, J., Goguitchaichvili, A., Morales-Contreras, J., 2006. Low-latitude paleosecular variation and the time-averaged field during the late Pliocene and Quaternary—paleomagnetic study of the Michoacan-Guanajuato volcanic field, Central Mexico. *Earth Planets Space* 58 (10), 1359–1371.
- Corella Santa Cruz, C.R., 2017. Petrogenésis del volcanismo alcalino máfico Mioceno tardío-Plioceno del Campo Basáltico San Francisco de Batúc, Sonora Central, México. M.Sc Thesis, Universidad de Sonora, pp. 111p.
- Cromwell, G., Johnson, C.L., Tauxe, L., Constable, C.G., Jarboe, N.A., 2018. PSV10: A global data set for 0–10 Ma time-averaged field and paleosecular variation studies. *Geochem. Geophys. Geosyst.* 19 (5), 1533–1558.
- Day, R., Fuller, M., Schmidt, V.A., 1977. Hysteresis properties of titanomagnetites: grain-size and compositional dependence. *Phys. Earth Planet. Inter.* 13 (4), 260–267.
- Demant, A., 1984. The Reforma caldera, Santa Rosalía area, Baja California. A volcanological, petrographical and mineralogical study. In: Malpica-Cruz, V., Celis-Gutiérrez, S., Guerrero-García, J., Ortílieb, L. (Eds.), Neotectonics and Sea Level Variations in the Gulf of California Area, a Symposium. Univ. Nac. Autón. México, Inst. Geol., pp. 75–96.
- Doubrovine, P.V., Veikkolainen, T., Pesonen, L.J., Piispala, E., Ots, S., Smirnov, A.V., Biggin, A.J., 2019. Latitude dependence of geomagnetic paleosecular variation and its relation to the frequency of magnetic reversals: observations from the Cretaceous and Jurassic. *Geochem. Geophys. Geosyst.*
- Dunlop, D.J., 2002a. Theory and application of the Day plot (Mrs/Ms versus Hcr/Hc) 1. Theoretical curves and tests using titanomagnetite data. *J. Geophys. Res.: Solid Earth* 107 (B3).
- Dunlop, D.J., 2002b. Theory and application of the Day plot (Mrs/Ms versus Hcr/Hc) 2. Application to data for rocks, sediments, and soils. *J. Geophys. Res.: Solid Earth* 107 (B3).
- Fisher, R.A., 1953. Dispersion on a sphere. *Proc. R. Soc. Lond.* 217 (1130), 295–305.
- García-Ruiz, R., Goguitchaichvili, A., Cervantes-Solano, M., Cortés-Cortés, A., Morales-Contreras, J., Maciel-Peña, R., Macías-Vázquez, J.L., 2016. Secular variation and excursions of the Earth magnetic field during the Plio-Quaternary: new paleomagnetic data from radiometrically dated lava flows of the Colima volcanic complex (western Mexico). *Rev. Mex. Ciencias Geol.* 33 (1).
- Gonzalez, S., Sherwood, G., Bühl, H., Schnepf, E., 1997. Palaeosecular variation in Central Mexico over the last 30000 years: the record from lavas. *Geophys. J. Int.* 130 (1), 201–219.
- Gutmann, J.T., 1973. Eruptive History and Petrology of Crater Elegante, Sonora, Mexico. Unpublished Ph.D. Thesis. Stanford University, University Microfilms #72-20704.
- Gutmann, J.T., 1976. Geology of crater Elegante, Sonora, Mexico. *Geol. Soc. Am. Bull.* 87 (12), 1718–1729.
- Gutmann, J.T., 1977. Textures and genesis of phenocrysts and megacrysts in basaltic lavas from the Pinacate volcanic field. *Am. J. Sci.* 277 (7), 833–861.
- Gutmann, J.T., 1979. Structure and eruptive cycle of cinder cones in the Pinacate volcanic field and the controls of Strombolian activity. *J. Geol.* 87 (4), 448–454.
- Gutmann, J.T., Turrin, B.D., Dohrenwend, J.C., 2000. Basaltic rocks from the Pinacate volcanic field yield notably young 40Ar/39Ar ages. *Eos, Trans. Am. Geophys. Union* 81 (4), 33–37.
- Gutmann, J.T., 2002. Strombolian and effusive activity as precursors to phreatomagma-tism: eruptive sequence at maars of the Pinacate volcanic field, Sonora, Mexico. *J. Volcanol. Geotherm. Res.* 113 (1–2), 345–356.
- Guntmann, J., Turrin, B.D., 2006. May). The age of crater Elegante, a maar in the pinacate volcanic field, Sonora, Mexico. In: Geologic Society of America Abstracts with Programs, vol. 38. pp. 32 No. 6.
- Haggerty, S.E., 1976. Opaque mineral oxides in terrestrial igneous rocks. Oxide minerals. Short Course Notes 3.
- Harrison, R.J., Feinberg, J.M., 2008. FORCinel: an improved algorithm for calculating first-order reversal curve distributions using locally weighted regression smoothing. *Geochem. Geophys. Geosyst.* 9 (5).
- Hawkesworth, C.J., Turner, S., Gallagher, K., Hunter, A., Bradshaw, T., Rogers, N., 1995. Calc-alkaline magmatism, lithospheric thinning, and extension in the Basin and Range. *J. Geophys. Res.* 100, 10271–10286.
- Henry, C.D., 1989. Late cenozoic Basin and range structure in western Mexico adjacent to the Gulf of California. *Geol. Soc. Am. Bull.* 101, 1147–1156.
- Henry, C.D., Aranda-Gómez, J.J., 1992. The Southern Basin and range, mid to late cenozoic extension in Mexico. *Geology* 20, 701–704.
- Ives, R.L., 1942. The discovery of Pinacate volcano. *Sci. Mon.* 54 (3), 230–237.
- Ives, R.L., 1956. Age of Cerro Colorado crater, pinacate, Sonora, Mexico. *Eos. Trans. Am. Geophys. Union* 37 (2), 221–223.
- Johnson, C.L., Constable, C.G., Tauxe, L., Barendregt, R., Brown, L.L., Coe, R.S., Staudigel, H., 2008. Recent investigations of the 0–5 Ma geomagnetic field recorded by lava flows. *Geochem. Geophys. Geosyst.* 9 (4).
- Kirschvink, J.L., 1980. The least-squares line and plane and the analysis of palaeomagnetic data. *Geophys. J. Int.* 62 (3), 699–718.
- Leonhardt, R., Krásá, D., Coe, R.S., 2004a. Multidomain behavior during Thellier paleointensity experiments: a phenomenological model. *Phys. Earth Planet. Inter.* 147 (2–3), 127–140.
- Leonhardt, R., Heunemann, C., Krásá, D., 2004b. Analyzing absolute paleointensity determinations: acceptance criteria and the software ThellierTool4. 0. *Geochem. Geophys. Geosyst.* 5 (12).
- Lonsdale, P., 1989. Geology and Tectonic History of the Gulf of California. The Eastern Pacific Ocean and Hawaii: Boulder, Colorado. Geological Society of America, Geology of North America, v. N, pp. 499–521.
- Lynch, D.J., 1981. Genesis and Geochronology of Alkaline Volcanism in the Pinacate Volcanic Field Northwestern Sonora. (Mexico).
- Lynch, D.J., Musselman, T.E., Gutmann, J.T., Patchett, P.J., 1993. Isotopic evidence for the origin of Cenozoic volcanic rocks in the Pinacate volcanic field, northwestern Mexico. *Lithos* 29 (3–4), 295–302.
- Mahgoub, A.N., Juárez-Arriaga, E., Böhnle, H., Siebe, C., Pavón-Carrasco, F.J., 2019. Late-Quaternary secular variation data from Mexican volcanoes. *Earth Planet. Sci. Lett.* 519, 28–39.
- Michalk, D.M., Biggin, A.J., Knudsen, M.F., Böhnle, H.N., Nowaczyk, N.R., Ownby, S., López-Martínez, M., 2010. Application of the multispecimen paleointensity method to Pleistocene lava flows from the Trans-Mexican Volcanic Belt. *Phys. Earth Planet. Inter.* 179 (3–4), 139–156.
- Odyke, N.D., Kent, D.V., Foster, D.A., Huang, K., 2015. Paleomagnetism of Miocene volcanoes on São Tomé: paleosecular variation at the equator and a comparison to its latitudinal dependence over the last 5 myr. *Geochem. Geophys. Geosyst.* 16 (11), 3870–3882.
- O'Reilly, W., 1984. Applications of rock and mineral magnetism. In: Rock and Mineral Magnetism. Springer, Boston, MA, pp. 194–212.
- Panovska, S., Constable, C.G., Brown, M.C., 2018. Global and regional assessments of paleosecular variation activity over the past 100 ka. *Geochem. Geophys. Geosyst.*
- Paterson, G.A., Tauxe, L., Biggin, A.J., Shaar, R., Jonestrask, L.C., 2014. On improving the selection of Thellier-type paleointensity data. *Geochem. Geophys. Geosyst.* 15 (4), 1180–1192.
- Pavón-Carrasco, F.J., Rodríguez-González, J., Osete, M.L., Torta, J.M., 2011. A Matlab tool for archaeomagnetic dating. *J. Archaeol. Sci.* 38 (2), 408–419.
- Pavón-Carrasco, F.J., Osete, M.L., Torta, J.M., De Santis, A., 2014. A geomagnetic field model for the Holocene based on archaeomagnetic and lava flow data. *Earth Planet. Sci. Lett.* 388, 98–109.
- Paz-Moreno, F.A., 1992. Le volcanisme mio-plio-quaternaire de l'Etat du Sonora (nord-ouest du Mexique) : évolution spatiale et chronologique ; implications pétrogénétiques. Thèse. Univ. Aix-Marseille III, pp. 220.
- Paz-Moreno, F.A., Demant, A., 1999. The recent Quaternary Isla San Luis volcanic centre: petrology of a continuous rift-related volcanic suite in the northern Gulf of California, Mexico. *J. Volcanol. Geotherm. Res.* 93, 31–52.
- Paz-Moreno, F.A., Demant, A., 2002. Las rocas máficas: características mineralógicas y geoquímicas del evento volcánico Pinacate, campo volcánico El Pinacate, NW de Sonora, México. III Reunión Nacional de Ciencias de la Tierra, Puerto Vallarta, pp. 238.
- Paz-Moreno, F.A., Demant, A., Cochemé, J.J., Dostal, J., Montigny, R., 2003a. The Quaternary Moctezuma Volcanic Field: A Tholeiitic to Alkali Basaltic Episode in the Central Sonoran Basin and Range Province, Mexico. Special Papers-Geological Society of America, pp. 439–456.
- Paz-Moreno, F.A., Demant, A., 2004. Petrology and geochemistry of a plio-quaternary intracontinental plate volcanic system: the Pinacate volcanic field northwestern Sonora, Mexico. IAVCEI General Assembly, Pucón, Chile, résumés sur CD.
- Paz-Moreno, F.A., Demant, A., Cochemé, J.-J., Dostal, J., Montigny, R., 2003b. The Quaternary Moctezuma volcanic field: a tholeiitic to alkalic volcanic episode in the central Sonoran Basin and Range Province, México. In: Johnson, S.E., Paterson, S.R., Fletcher, J.M., Girty, G.H., Kimbrough, D.L., Martín-Barajas, A. (Eds.), Tectonic Evolution of Northwestern México and Southwestern USA, vol. 374. *Geol. Soc. Am. Spec. Paper*, pp. 439–455.
- Pike, C.R., Roberts, A.P., Veresub, K.L., 1999. Characterizing interactions in fine magnetic particle systems using first order reversal curves. *J. Appl. Phys.* 85 (9), 6660–6667.
- Roberts, A.P., Pike, C.R., Veresub, K.L., 2000. First-order reversal curve diagrams: a new tool for characterizing the magnetic properties of natural samples. *J. Geophys. Res.: Solid Earth* 105 (B12), 28461–28475.
- Rodríguez-Trejo, A., Alva-Valdivia, L.M., Perrin, M., Hervé, G., López-Valdés, N., 2019. Analysis of geomagnetic secular variation for the last 1.5 Ma recorded by volcanic rocks of the Trans Mexican Volcanic Belt: new data from Sierra de Chichinautzin, Mexico. *Geophys. J. Int.* 219 (Issue 1), 594–606. October 2019. <https://doi.org/10.1093/gji/ggz210>.
- Sawlan, M.G., 1991. Magmatic evolution of the Gulf of California rift. In: Dauphin, J.P., Simoneit, B.A. (Eds.), The Gulf and Peninsular Province of the Californias, vol. 47. Amer Assoc Petr Geol Mem, pp. 301–369.
- Schmitt, A.K., Stockli, D.F., Hausback, B.P., 2006. Eruption and magma crystallization ages of Las Tres Virgenes (Baja California) constrained by combined 230Th/238U and (U-Th)/He dating of zircon. *J. Volcanol. Geotherm. Res.* 158, 281–295.
- Singer, B.S., Jicha, B.R., He, H., Zhu, R., 2014. Geomagnetic field excursion recorded 17 ka at Tianchi Volcano, China: new 40Ar/39Ar age and significance. *Geophys. Res. Lett.* 41 (8), 2794–2802.
- Stock, J.M., Hodges, K.V., 1989. Pre-pliocene extension around the Gulf of California and the transfer of Baja California to the pacific plate. *Tectonics* 8 (1), 99–115.
- Stock, J.M., Lee, J., 1994. Do microplates in subduction zones leave a geological record? *Tectonics* 13 (6), 1472–1487.
- Tauxe, L., Constable, C., Johnson, C.L., Koppers, A.A., Miller, W.R., Staudigel, H., 2003. Paleomagnetism of the southwestern USA recorded by 0–5 Ma igneous rocks. *Geochim. Geophys. Geosyst.* 4 (4).
- Thellier, E., 1959. Sur l'intensité du champ magnétique terrestre dans le passé historique et géologique. *Ann. Geophys.* 15, 285–376.
- Turrin, B.D., Gutmann, J.T., Swisher III, C.C., 2008. A 13 ± 3 ka age determination of a tholeiitic Pinacate volcanic field, Mexico, and improved methods for 40Ar/39Ar dating of young basaltic rocks. *J. Volcanol. Geotherm. Res.* 177 (4), 848–856.
- Vahle, C., Kontny, A., 2005. The use of field dependence of AC susceptibility for the interpretation of magnetic mineralogy and magnetic fabrics in the HSDP-2 basalts, Hawaii. *Earth Planet. Sci. Lett.* 238 (1–2), 110–129.

- Vidal-Solano, J.R., Paz-Moreno, F.A., Demant, A., 2005. Caracterización y cronología del evento volcánico terciario Pre-Pinacate, campo El Pinacate, Noroeste de Sonora, México: Boletín del Departamento de Geología. Universidad de Sonora 18, 117–140.
- Vidal-Solano, J.R., Demant, A., Paz Moreno, F.A., Lapierre, H., Ortega-Rivera, M.A., Lee, J.K., 2008. Insights into the tectonomagmatic evolution of NW Mexico: geochronology and geochemistry of the Miocene volcanic rocks from the Pinacate area, Sonora. *Geol. Soc. Am. Bull.* 120 (5–6), 691–708.
- Wohletz, K.H., Sheridan, M.F., 1983. Hydrovolcanic explosions; II, Evolution of basaltic tuff rings and tuff cones. *Am. J. Sci.* 283 (5), 385–413.
- Zawacki, E.E., Clarke, A.B., Arrowsmith, J.R., Bonadonna, C., Lynch, D.J., 2019. Tecolote volcano, Pinacate volcanic field (Sonora, Mexico): a case of highly explosive basaltic volcanism and shifting eruptive styles. *J. Volcanol. Geotherm. Res.* 379, 23–44.
- Zijderveld, J.D.A., 2013. AC demagnetization of rocks: analysis of results. In: *Developments in Solid Earth Geophysics*, vol. 3. Elsevier, pp. 254–286.

Capítulo 4

Emplacement temperature resolution and age determination of Cerro Colorado tuff ring by paleomagnetic analysis, El Pinacate Volcanic Field, Sonora, Mexico

L.M. Alva-Valdivia^{a,*}, A. Rodríguez-Trejo^b, J.R. Vidal-Solano^c, F. Paz-Moreno^c, A. Agarwal^d

^a Laboratorio de Paleomagnetismo, Instituto de Geofísica, Universidad Nacional Autónoma de México, Circuito de la Investigación Científica, C.P. 04510 México D. F., Mexico

^b Posgrado en Ciencias de la Tierra, Instituto de Geofísica, Universidad Nacional Autónoma de México, Circuito de la Investigación Científica, C.P. 04510 México D. F., Mexico

^c Departamento de Geología, División de Ciencias Exactas y Naturales, Universidad de Sonora, Mexico

^d Institute of Earth and Environmental Sciences, Geology, University of Freiburg, Freiburg, Germany

Received 4 September 2018

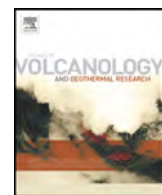
Received in revised form 7 November 2018

Accepted 17 November 2018

Available online 22 November 2018

Abstract

The lithic in the Cerro Colorado tephra deposits is dominated by clasts from shallow country rocks for a diatreme not well mixed, or, by a combination of material that reflects the relative proportions of country rock in a well-mixed diatreme. The clasts in a tephra ring bed might be ideal to use the paleomagnetic study to determine the emplacement temperature. We report emplacement temperature ranges of pyroclastic lithic fragments from the Cerro Colorado Tuff Ring in the El Pinacate Volcanic Field, Sonora, northwestern Mexico. Paleomagnetic analyses, particularly the thermoremanent magnetization procedure was carried out in 38 small cores, drilled from the 10 to 30 cm in size lithic fragments. It estimates the emplacement temperature ranges of the juvenile basaltic cauliflower bombs and not-juvenile diverse blocks produced in the phreatomagmatic eruption. Titanomagnetite and titanohematite are the main magnetic carriers, along with titanomaghemitite. The 22 emplacement temperatures determined in this study are grouped in three temperature ranges, low (310–370 °C), medium (400–460 °C) and high (N500 °C). The low and medium temperature samples show two or more components, while the high temperature samples have, in general, only one component. This wide range of emplacement temperature could be related to the composite thermal history of the pyroclastic material incorporated in the water saturated pyroclastic flow deposit. The comparison of the mean direction of the secondary magnetization component with the secular variation curve of the global model SHA.DIF.14, suggests an age of 3915 ± 59 yr. BP.



Emplacement temperature resolution and age determination of Cerro Colorado tuff ring by paleomagnetic analysis, El Pinacate Volcanic Field, Sonora, Mexico



L.M. Alva-Valdivia ^{a,*}, A. Rodríguez-Trejo ^b, J.R. Vidal-Solano ^c, F. Paz-Moreno ^c, A. Agarwal ^d

^a Laboratorio de Paleomagnetismo, Instituto de Geofísica, Universidad Nacional Autónoma de México, Circuito de la Investigación Científica, C.P. 04510 México D.F., Mexico

^b Posgrado en Ciencias de la Tierra, Instituto de Geofísica, Universidad Nacional Autónoma de México, Circuito de la Investigación Científica, C.P. 04510 México D.F., Mexico

^c Departamento de Geología, División de Ciencias Exactas y Naturales, Universidad de Sonora, Mexico

^d Institute of Earth and Environmental Sciences, Geology, University of Freiburg, Freiburg, Germany

ARTICLE INFO

Article history:

Received 4 September 2018

Received in revised form 7 November 2018

Accepted 17 November 2018

Available online 22 November 2018

Keywords:

Paleomagnetic analysis

Emplacement temperature

Dating determination

Cerro Colorado

El Pinacate Volcanic Field

Sonora

Mexico

ABSTRACT

The lithic in the Cerro Colorado tephra deposits is dominated by clasts from shallow country rocks for a diatreme not well mixed, or, by a combination of material that reflects the relative proportions of country rock in a well-mixed diatreme. The clasts in a tephra ring bed might be ideal to use the paleomagnetic study to determine the emplacement temperature. We report emplacement temperature ranges of pyroclastic lithic fragments from the Cerro Colorado Tuff Ring in the El Pinacate Volcanic Field, Sonora, northwestern Mexico. Paleomagnetic analyses, particularly the thermoremanent magnetization procedure was carried out in 38 small cores, drilled from the 10 to 30 cm in size lithic fragments. It estimates the emplacement temperature ranges of the juvenile basaltic cauliflower bombs and not-juvenile diverse blocks produced in the phreatomagmatic eruption. Titanomagnetite and titanohematite are the main magnetic carriers, along with titanomaghemite. The 22 emplacement temperatures determined in this study are grouped in three temperature ranges, low (310–370 °C), medium (400–460 °C) and high (>500 °C). The low and medium temperature samples show two or more components, while the high temperature samples have, in general, only one component. This wide range of emplacement temperature could be related to the composite thermal history of the pyroclastic material incorporated in the water saturated pyroclastic flow deposit. The comparison of the mean direction of the secondary magnetization component with the secular variation curve of the global model SHA.DIF.14, suggests an age of 3915 ± 59 yr. BP.

© 2018 Elsevier B.V. All rights reserved.

1. Introduction

Cerro Colorado has several remarkable characteristics, which make it very particular: the lack of central floor or rim magnetic anomalies implies that the entire crater, including the feeder vent must be composed of tuff, which implies a tuff pipe with no significant basaltic intrusions (Wood, 1974). The gravity survey of Cerro Colorado revealed a small negative anomaly due to low density playa sediments filling the crater (Sumner, 1972). It could be classified as a tuff ring based in the extensive evidence from many volcanic apparatus showing that subsidence along ring faults began at the end of the eruptive activity when gas pressure is reduced and weight of the cone is greatest (Peterson and Groh, 1963).

Gutmann (2002) suggests absence of basalt flow or eruptive activity preceding the hydrovolcanism that built the Cerro Colorado tuff ring. Accretionary lapilli, mud-armored bombs and many other features indicate that copious amount of water was involved in the Cerro Colorado eruption. Gutmann (2002) remarks that the phreatomagmatic eruptions occurred at many Pinacate vents immediately after emplacement of basal flows and eruptive activity. The like-arc path of craters across the northern part of the Pinacate volcanic field probably reflects an aquifer of high permeability and porosity so that groundwater was supplied in sufficient quantity once hydrovolcanic explosions began. Channel gravels concentrated along a possible former course of the Sonoya River constitute a likely candidate for such an aquifer (arrow at the top-left of Fig. 1). Alternatively, a pause in eruptive activity could be accompanied by convective overturn within the magma column, bringing fresh, gas-charged magma to the surface. These eruptive histories strongly suggest that magmatic withdrawal, rather than just eruptive pyroclastic or effusive activity, was a likely precursor to major phreatomagmatism in the Pinacate volcanic field. Generally, the lithic in the tephra deposits is

* Corresponding author.

E-mail address: lalva@igeofisica.unam.mx (L.M. Alva-Valdivia).

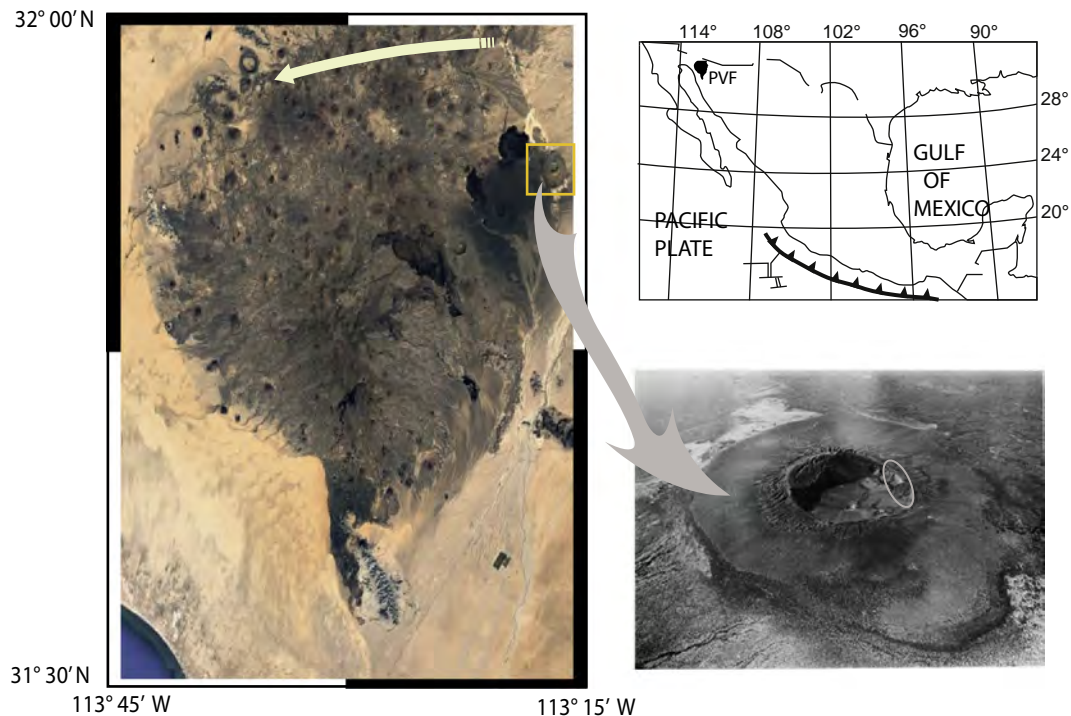


Fig. 1. El Pinacate Volcanic Field study area (PVF, atop left and right). Arrow on the left-top shows the buried paleopath of the Sonoya River. Bottom right: oblique aerial view southward of Cerro Colorado showing the wide outcrop of alluvium from the Playa Díaz on the outer flanks and the high crater rim on the southeast side of the crater; crater rim diameter is about 1 km; ellipse indicate the sampling area.
(Modified from Greeley et al., 1987)

dominated by clasts from shallow country rocks for a diatreme not well mixed, or, by a combination of material that reflects the relative proportions of country rock in a well-mixed diatreme. Valentine and White (2012) and Valentine et al. (2017) determine that the characteristics of juvenile clasts (shape, vesicularity, crystallinity, composition) in a tephra ring bed might have little relation to magma fragmentation processes during the explosion that produced the bed. Then, we expect great variation in the rock magnetic and paleomagnetic properties.

The general position of the lithic rich deposits is sometimes remobilized; so it is difficult to distinguish between primary deposits emplaced at high temperatures and other emplaced at relatively lower temperatures. The pyroclasts forming bomb-sags in the tuff ring deposits of Cerro Colorado are nearly entirely embedded.

Historically, the paleomagnetic emplacement temperature (Te) determination of volcanic deposits have been very successful (Aramaki and Akimoto, 1957; Hoblitt and Kellogg, 1979; McClelland et al., 2004; Kent et al., 1981; Porreca et al., 2008; Paterson et al., 2010; Alva-Valdivia et al., 2012). Determination of the Te from any kind of recent pyroclastic eruption is useful to quantify the regional volcanic risk of danger zones (Zanella et al., 2007).

The Te of pyroclastic flows had been determined since the 80's by the thermoremanent magnetization (TRM) analysis, especially using the lithic fragments embedded within pyroclastic deposits (e.g., McClelland and Druitt, 1989). Lithic fragments can come from the magma chamber, from conduit walls (accessory lithics) or be ripped up along the flow path (accidental lithics). When the rocks are cooled from temperature higher than the Curie temperature of constituting magnetic minerals, the minerals acquire a new magnetization, parallel to the Earth's magnetic field at the time of emplacement. Hence, in fragments embedded in a high-temperature pyroclastic matrix a unique magnetic component will be detected, which would be parallel in all fragments (e.g., Alva-Valdivia et al., 2012, 2017a). In such cases the Te is close to or exceeds the Curie temperature (e.g., Alva-Valdivia et al., 2012).

When rock fragments are incorporated into a pyroclastic flow at an intermediate temperature (400 °C to 500 °C), they lose a portion of their original magnetization, and during the cooling they will acquire a new partial thermoremanence (pTRM). Such lithics are characterized by two components of magnetization: one is the characteristic, ChRM (normally the primary, randomly oriented high-temperature component) and another is a new one (low temperature component homogeneously oriented parallel to the Earth's magnetic field at the time of the deposit emplacement). In the case of two components of magnetization, the intersection of the two components provides an estimate of the Te (McClelland and Druitt, 1989).

It is very important to demagnetize a large number of sampled clasts to produce paleomagnetically reliable, significant statistics. Besides, the paleomagnetic signature can be altered due to secondary chemical changes (chemical remanent magnetization, CRM) (e.g., McClelland-Brown, 1982; McClelland and Druitt, 1989) and by the exposure to the Earth's magnetic field at ambient temperature for a long time (viscous remanent magnetization, VRM). These processes affect samples, producing new magnetic components that may be erroneously interpreted as partial TRM (pTRM) and could lead to false temperature estimations.

The aim of this study is to analyze the paleomagnetic components of the sampled cores from the lithic fragments to determine the Te of the tuff ring. Additionally, the direction of the paleomagnetic component allows us to date their emplacement time. The combination of these new data provides an estimation of the magnitude of the volcanic risk of this type of eruptions.

2. Geological setting and previous studies

2.1. The Pinacate Volcanic Field (PVF)

The PVF belongs to the 'El Pinacate' and 'Gran Desierto de Altar' Biosphere Reserve, protected by the Mexican government CONANP

commission and UNESCO. The PVF is formed by a volcanic shield that covers an area ca. 1500 km², produced by a large eruptive activity which started with the Santa Clara volcano eruption (1.7 My; Lynch, 1981; Vidal-Solano et al., 2008), surrounded by abundant monogenetic volcanoes as cinder and spatter cones, maars, covered by eolic sediments through the whole volcanic field.

Ives (1935, 1964), Gutmann (1979) and Gutmann and Martin (1976) described the PVF as one of the most prominent structures, and sustained detailed studies of the general geology of the whole volcanic field, providing numerous radiometric ages using ⁴⁰Ar/³⁹Ar. Later, Gutmann and Sheridan (1978) described the eruptive activity of the cinder cones and the differentiated strombolian activity.

2.2. The Cerro Colorado

The Cerro Colorado volcano is located at the northeastern margin of the PVF, northwestern Sonora, Mexico (31.915°N, 113.300°W, Fig. 1). It is a tuff ring underlain by a basalt flow (Wohletz and Sheridan, 1983). Cerro Colorado's border is asymmetric and is most prominent on the southeastern side where it rises 110 m above the plains from Playa Díaz. The border is composed of tuff breccia that consist of thinly layered ashes overlain by gravelly tuff with volcanic, granitic and metamorphic rock fragments. Outer border flanks are steep cliffs. The oldest outcrop appears in the western wall and is composed of vesicular basalt overlain by grey tephra deposits. The crater floor consists of alluvium and playa deposits. The outer flank of the crater forms a broad front of alluvium and weathered tuff breccia derived from the rim (Wood, 1974). Gutmann (2002) concludes that no basalt flow or strombolian activity preceded the hydro-volcanism that built Cerro Colorado tuff cone.

The discovered archaeological remains were tentatively dated at 1000–2000 BCE (equivalent to 3000–4000 BP) (Hayden, personal communication, in Wood, 1974), acquired from the Cerro Colorado ash deposits. This makes untenable the Ives (1956) suggestion of the 200–1000 BP age, agreeing with Wood (1974) statement saying that Cerro Colorado may well be much older.

3. Methodology

We collected 38 cores from juvenile basaltic cauliflower bombs and not-juvenile accessory and accidental pyroclastic blocks embedded in palagonized pyroclastic surge deposits on the outer flank (area of ca. 100 m²) at the low crater rim on the NW side (Fig. 2). Rock samples of size ranging from 10 to 30 cm in diameter were drilled with a portable gasoline powered drill. The samples were marked and oriented with an inclinometer, magnetic and solar compass.

10 thermomagnetic curves (k-T) of low-field magnetic susceptibility vs. temperature were measured to identify the remanence magnetic carriers in the samples, using both a Bartington MS2 susceptibility meter and a furnace MS2WFP (4 samples, Fig. 3A) and an MFK-FA

kappabridge (Agico, Brno, Czech Republic) (6 samples, Fig. 3B). During the (k-T) experiments, most of the samples were heated from room temperature up to 700 °C, and then cooled back. The entire processes were carried in an air atmosphere. The bulk magnetic susceptibility was measured during the entire cycle of heating and cooling. Curie temperature (Tc) was determined by the first derivative method (Petrovsky and Kapicka, 2006).

Small rock chip samples (20–30 mg) were used to determine the hysteresis curves, acquisition of isothermal remanent magnetization (IRM) curves, and coercivity of remanence using a Princeton AGFM Micromag 2900 apparatus in fields up to 1.2 Tesla. Hysteresis parameters such as saturation magnetization (Ms), saturation remanence (Mrs), coercive force (Hc) and coercivity of remanence (Hcr), were obtained from these curves. These analyses aided in determining the magnetic domain type distribution of the ferrimagnetic minerals (single domain-SD, multidomain-MD, and pseudo-single domain-PSD components). The First order reversal curves (FORC) were calculated for the same rock chip.

All specimens were demagnetized in a non-inductive thermal demagnetizer (model TSD-1 by the Schonstedt Instrument Co.) and analyzed using a JR-5 spinner magnetometer (AGICO, Brno, Czech Republic) in a magnetically shielded room. Thermal demagnetization (ThD) was performed between 100 °C to 600 °C using 10–12 incremental heating steps. Each step was 25 °C to 30 °C in order to obtain the paleomagnetic components and differentiate the ChRM and secondary directions. Selected specimens were demagnetized by alternating field (AF) performed in ca. 16 steps from 5 mT peak fields up to 100 mT using a Molspin demagnetizer (Molspin Limited, England). The paleomagnetic directions are determined as line or plane data using principal component analysis (Kirschvink, 1980) and in some cases, the sites were treated with the combined analysis on remagnetization circles (planes) and directions (lines) (McFadden and McElhinny, 1988).

The Cerro Colorado minimum 3000 yr BP age (Hayden, personal communication, in Wood, 1974) was used to estimate the potential maximum unblocking temperature for the VRM by the [T_{ub} = 75 + 15 log (3000)], employed for rocks of age between 10² and 10⁶ years. So, remanence that unblocks at temperatures lower than 127 °C is considered as a VRM.

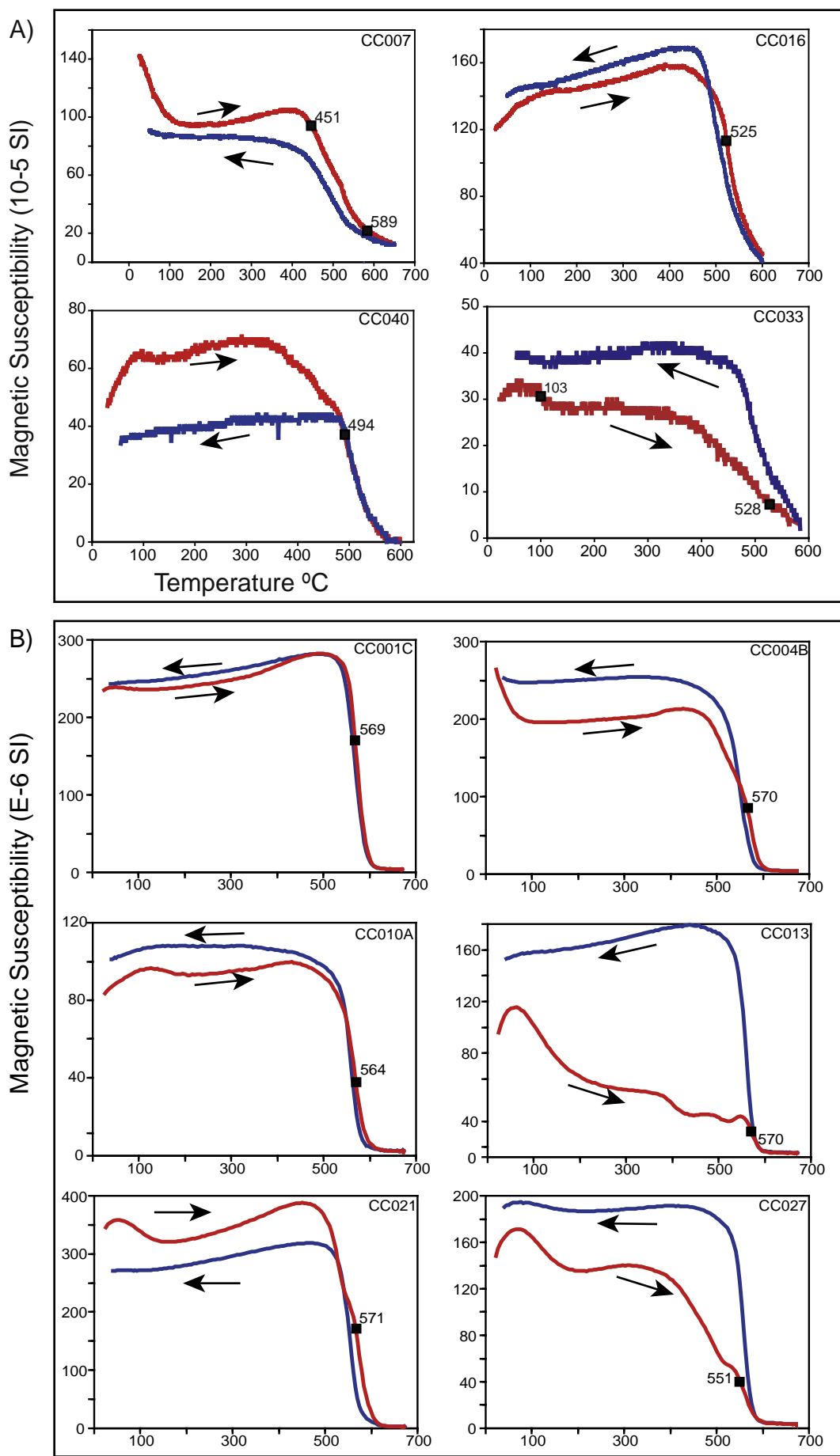
4. Results

4.1. Rock magnetism

Most k-T curves (80%) reveal two magnetic phases during the heating: the first with a Curie temperature ranging from 120 °C to 180 °C, and the second ranging from 480 °C to 520 °C (see for similar examples Alva-Valdivia et al., 2017b). The drop at ~300 °C is due to alteration of the metastable maghemite to the more stable and less magnetic hematite polymorph. In the cooling branch a single magnetic phase is



Fig. 2. Sampled blocks area (bottom part of central photograph). Arrows indicate the position of blocks sampled (right photograph), diameter mean size is 10 cm.



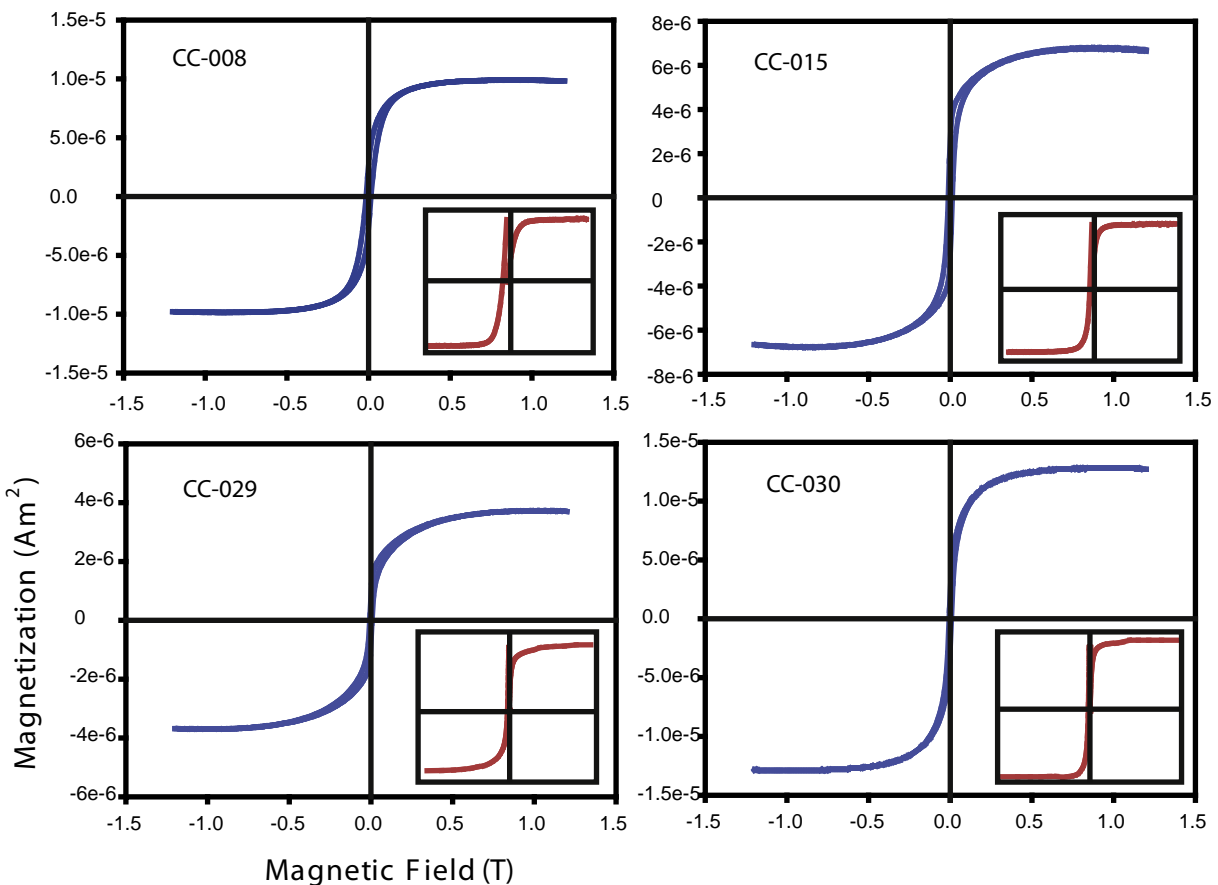


Fig. 4. Typical hysteresis loops from different samples. Inset plots represent the combined IRM and backfield measurements.

observed in most of the cases (90%), showing a transformation from titanomaghemite to magnetite (Fig. 3).

During hysteresis analysis, saturation is achieved in low fields (<750 mT) with a single phase, and coercivity between $2.8 \text{ mT} < H_c < 23.3 \text{ mT}$. 'Wasp-waisted' (Fig. 4c) like shapes were observed in most of the cases (90%), showing different Ti content in titanomagnetite. In one case 'wasp-waisted' like shape was observed, with a saturation value <1 T. We plot the ratios of magnetization and coercivity parameters obtained from the hysteresis, IRM and backfield curves, which ranges are $0.10577 < Mrs/Ms < 0.45120$ and $1.3360 < Hcr/Hc < 3.2467$ (Fig. 5). All samples fall in the pseudo single domain (PSD) region of the Day diagram suggesting a mixture of SD + MD distribution from a 10% to 60% (Day et al., 1977; Dunlop, 2002). As Roberts et al. (2018) highlight, we do not intend to use the Day diagram for any fine-scale description in granulometric terms but just to emphasize relative variations in component mixing to assess this relative granulometric variations and paleomagnetic recording efficiency.

From the FORC plots, low-coercivity elongation (70 to 100 mT) shows a symmetrical inner contour pattern along the H_c axis, and the outer contours show a slight divergent spreading over the vertical H_u axis, that indicates the presence of PSD grains (Roberts et al., 2000). Symmetrical and highly spread out contours over the vertical axis, with low elongations along the H_c axis (10 to 20 mT) suggest an interactive MD grains behavior (Pike et al., 1999). The FORC plots show

prevalence of low coercivity components, which agrees with the hysteresis analysis (Fig. 6). The FORC configuration curves validate a low interaction between domains and a trend to PSD and MD behavior of the samples, which are typical shapes of titanomagnetite dominant mineralogy.

4.2. Characteristic remanent magnetization (ChRM) and secondary paleomagnetic directions

Paleomagnetic procedure reveals that most of the samples show in general stable remanent magnetizations with wide range of intensity of the NRM. Table 1 shows mean direction values of all components (ChRM and secondary) plus the maximum angular deviation (MAD) as well as their Te. The different components of TRM are usually removed at temperatures between 350 °C and 520 °C and show clear vector paths with usually two stable paleomagnetic components (75.6% of samples showing this behavior) and to a minor extent (24.4%), only one stable paleomagnetic component. In addition, 17 samples were discarded due to not well defined paleomagnetic behavior.

Two stable paleomagnetic directions were described in most of the samples, the characteristic component of higher unblocking temperature (>500 °C), and the secondary component, of lower unblocking temperature (from 310 to 370 °C). These components were defined using ThD. Very small temperature steps during the ThD were used to define

Fig. 3. Susceptibility vs. high temperature typical curves of the different behaviors on the samples, arrows indicate heating and cooling branches. A) Curves acquired with the MS2 system; B) Curves acquired with the MFK-FA instrument. Black squares indicate the position and value of the Curie temperature.

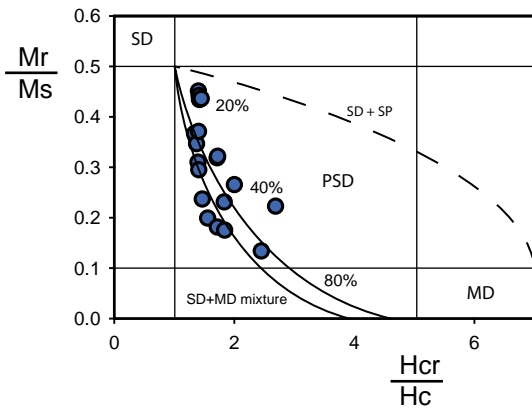


Fig. 5. Day plot of representative samples.

carefully the temperature between ChRM and the secondary components, which gives the Te registered by each sample (Fig. 7). AF demagnetization, vector plots, were used to determine faster the secondary direction, expected parallel or in the same region of the equal area stereoplot, to be used for dating of the volcanic eruption. The ChRM and secondary paleomagnetic components are shown in an equal area plot (Fig. 8) and in Table 1 that summarizes the directional data.

4.3. Paleomagnetic dating

Currently is not available a well constrained regional secular variation curve for Mexico; it was necessary the use of a global model generated by a large compilation of worldwide data, model SHA.DIF.14K

(Pavón-Carrasco et al., 2014). In recent years, the method was successfully used in different studies of volcanic rocks in Mexico (Böhnel et al., 2016; Mahgoub et al., 2018) with reliable results. In this work, using the directional data obtained from Cerro Colorado, a mean direction was determined for the secondary component of magnetization of the samples: Declination = 317.4°, Inclination = 32.4°, α_{95} = 16.1. According with the Bayesian statistics based model and using a 95% confidence, the obtained date is 3915 ± 59 B.P. The declination parameter shows a high deviation from the expected value of the field for the Holocene, possibly related to the movement of the blocks during the emplacement, resulting on a bigger dispersion and scatter on the results, however the inclination is consistent with the expected value, showing smaller dispersion. For the dating the correspondence of the inclination and the α_{95} with the secular variation curve gives a better probability to fit in the estimated age (Fig. 9).

5. Discussion

The low-temperature component orientations were calculated based only on the straight linear segments in the vector diagrams, excluding curved segments with overlapping stability spectra.

The Te determined from the TRM demagnetization process of all the samples is presented in Table 1. The 23 Te determined in the present study range from low to medium temperature (310–370 °C and 400–460 °C showing that we have two or more components) acquired at the same time and the components are defined by orientation deduced with the orthogonal diagram and unblocking temperature. Of course, we could expect to have different unblocking temperatures for the same orientation (component). There is also another component of high temperature (500 °C, samples which have in general only one component). This wide range of Te could be related to the composite thermal history of the rock blocks incorporated in the pyroclastic flow or in the sag layer. There is a small fraction of the randomly-oriented

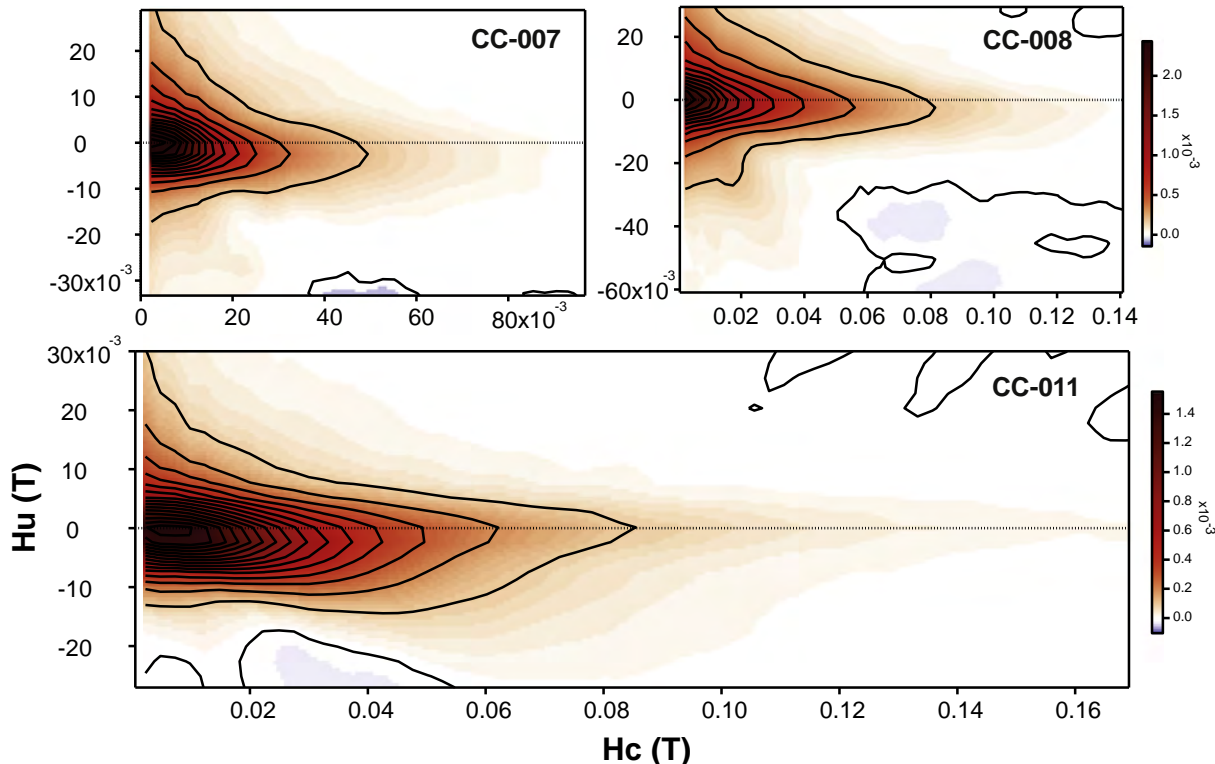


Fig. 6. Typical FORC plots showing the different coercivity intervals in the samples, and the different mixtures on the PSD.

Table 1

Determination of the magnetic components. AFD and ThD, alternating field/thermal demagnetization; D magnetic declination; I magnetic inclination; MAD maximum angular deviation; Te emplacement temperature.

Sample number	Treatment	Component (s)	ChRM		Secondary component		MAD	Te °C
			Dec	Inc	Dec	Inc		
CC-001B	ThD	2	273,3	17,1	305,6	-24,6	2,5	460
CC-001C	ThD	2	276,8	12,8	296,7	-26,3	1,9	460
CC-002A	ThD	2	311,6	45,2	347,5	56,9	15,2	460
CC-002B	AFD	1	325,1	46,3	n.d.	n.d.	8,1	n.d.
CC-003A	ThD	2	129,2	-53,6	277,9	18	11,3	310
CC-003B	AFD	2	242,5	21,7	267,3	27,5	3,2	n.d.
CC-004A	AFD	2	209,5	-79	297,9	29,9	2,3	n.d.
CC-004B	ThD	2	222	-71,7	303,2	21,2	5,5	430
CC-005A	AFD	1	348,6	-22,2	n.d.	n.d.	7,7	n.d.
CC-007A	AFD	2	350,7	77,5	326,1	-14,2	2,5	n.d.
CC-007B	ThD	2	25	71,7	325,1	-16,1	14,5	500
CC-007C	ThD	2	34	62,1	323	-65,6	6,5	500
CC-008A	AFD	2	140,4	-82,2	17,9	25	15,3	n.d.
CC-008B	ThD	2	132,5	-76,3	19,6	-18,5	13,9	460
CC-008C	ThD	2	138,4	75,2	28,5	-20,8	14,4	460
CC-010A	AFD	2	215,7	-14,3	306	-24,2	3,5	n.d.
CC-010B	ThD	1	229,6	-12,7	n.d.	n.d.	13,4	n.d.
CC-020A	ThD	1	291,8	24,1	n.d.	n.d.	1,6	n.d.
CC-020B	ThD	1	301,6	7,5	n.d.	n.d.	7,6	n.d.
CC-011A	AFD	1	313,1	18,1	n.d.	n.d.	2,7	n.d.
CC-011B	ThD	2	308,1	8,1	321	20,9	10,4	370
CC-012A	AFD	2	329,8	4,7	291,5	-7,7	10,8	n.d.
CC-012B	ThD	2	210,5	-27,6	147,9	-61,9	10,6	310
CC-014A	AFD	2	14,2	-0,5	320,3	48,2	12,3	n.d.
CC-016A	ThD	2	225	67	353,8	30	12,6	310
CC-021B	ThD	2	95,3	-41,3	24,2	14,2	6,1	400
CC-021C	ThD	2	97,5	-38,4	25,5	11,2	17,2	430
CC-022A	ThD	2	268,3	-1,5	338	19,6	15,7	370
CC-022B	ThD	2	274,5	-12,4	351	6,3	10,4	370
CC-023A	ThD	2	109,2	76,2	41,6	35,3	4	310
CC-024B	ThD	2	101,9	12,2	339,9	16,8	15,9	n.d.
CC-024C	ThD	1	335,4	15,6	n.d.	n.d.	15,2	n.d.
CC-025A	ThD	2	231,5	-13,7	307,3	11,7	3,9	400
CC-026B	ThD	2	221,5	-17,2	301,1	33	3,4	430
CC-027A	ThD	1	313,7	14,6	n.d.	n.d.	11,2	310
CC-027C	ThD	1	312,7	16,2	n.d.	n.d.	6,8	310
CC-028B	ThD	2	97,4	30	342,1	67	10,9	400
CC-028C	ThD	2	100,3	30,9	336,3	76	11,1	400
CC-029B	ThD	1	179,6	44,7	n.d.	n.d.	5,1	n.d.
CC-030A	ThD	2	27,9	22,6	328	19	8,2 <i>i</i>	370

primary vectors that are aligned by chance with the secondary components, producing apparently single-component magnetizations with high unblocking temperatures, which would suggest erroneously high emplacement temperatures, as showed by the ChRM orientations in Fig. 8. The presence of magnetizations with high unblocking temperatures means clearly that by some physical-chemical processes these blocks could not acquire the secondary component, keeping just the primary one. So, if there are no secondary component, is not possible determine the emplacement temperature.

Certainly, there were many cases (56.1%, 23 samples, were determined by ThD) with no chance to get the Te (n.d., not determined in Table 1), which could suggest that the samples did not reach the temperature of the flow, resulting therefore random directions. However, in many other cases we could determine the Te, as we see as better grouping of the secondary direction in the equal area plot (Fig. 8, left), against the highly dispersed direction of the higher temperature paleomagnetic component (Fig. 8, right). This suggests that the determined Te range (310–460 °C) is the most reliable of the Cerro Colorado tuff ring. The rock magnetism suggests, that the wide range of Te could be due to the thermal history of the pyroclasts in the hydrovolcanic process (Jackson and Bowles, 2014). This Te range could suggest the presence of diverse contribution of distinct fragment size populations inside of the

pyroclastic flow deposit respect to the equilibrium temperature due to heat transfer (McClelland and Druitt, 1989). In the thermal model of McClelland and Druitt (1989), the Te for large fragments could be lower than the equilibrium temperature (Teq) of the whole deposit, so that the Teq is not defined by the lowest value of the Te. This model can explain the large dispersion of Te for our samples, which have an initial maximum temperature of up to 500 °C at the moment of incorporation into the deposit, while the minimum temperature c.a. 300 °C is indicated by the magnetization of the interior of the large fragments. The fragments of higher temperature probably were warm after deposition and their effect could be very important if they were erupted from magma with low interaction with water in conduit system.

We propose that the global Te range is from 310 to 460 °C. The lowest temperature is likely to be found in the smallest bombs, while higher temperatures could be associated with larger bombs with a fast contact with water or an emplacement pyroclastic deposition related to scarce water. The fine grain size indicates an efficient fragmentation mechanism probably related to a deep interaction with the aquifer, and not only to the surficial interaction magma-water (Giordano et al., 2002), which is consistent with the decrease of the measured temperature. We agree with Paterson et al. (2010) about that paleomagnetism is an underestimated tool in volcanology, being the only exception the Te determination.

The thermomagnetic curves suggest that the magnetic mineralogy is made up by distinct minerals with different Curie temperatures (mostly low-Ti titanomagnetite, 500–570 °C and titanomaghemite alteration temperature, at which the metastable maghemite inverts to the more stable and less magnetic hematite polymorph c.a. 300 °C).

The paleomagnetic dating (3915 ± 59 years BP) corresponds with the Middle-Late Holocene Boundary placed at 4.2 ka BP as defined by a mid/low-latitude aridification event (the 4.2 event) by Walker et al. (2012). Nevertheless, due to the nature of the mechanics of the eruption of Cerro Colorado, the dispersion of the directional results increase owing to the movement of the blocks embedded in the matrix of the emplacement of the tuff ring, a rigorous study of the ChRM and the secondary component allowed to determine the precision and dispersion of the declination and inclination. This was a widespread climatic phenomenon that is also reflected in proxy records from North America. More precisely, it agrees in space and time with the establishment of the modern climatic regime in the Sonoran Desert at the beginning of the Late Holocene at 4 ka BP (Van Devender, 1990).

6. Conclusions

We investigate the emplacement temperature of the Cerro Colorado tuff ring. The rock magnetic investigations show that the magnetization carriers are mainly Ti-poor titanomagnetite. However, in some cases reveal distinct mineral phases during the heating and cooling processes through irreversibility of k-T curves showing besides titanomaghemite changing to magnetite.

The emplacement temperature of this deposit range from 310 to 500 °C, which probably is a combined result of the fragment size and water amount, concluding that it is a type of pyroclastic activity of a surtseyan volcanism.

The paleomagnetic classification modified by McClelland and Erwin (2003) suggests that for the rock fragments of the Cerro Colorado deposit, there is a better grouping of the secondary low temperature direction and great directional dispersion for the high -temperature component, indicating therefore that these secondary emplacement temperatures are the most reliable from the paleomagnetic and vulcanological point of view.

The Cerro Colorado age estimation based in the secular variation curve of the global model SHA.DIF. 14 (Pavón-Carrasco et al., 2014) using the mean directional data of the secondary component of magnetization from the analyzed bombs is 3915 ± 59 yr BP that agrees with

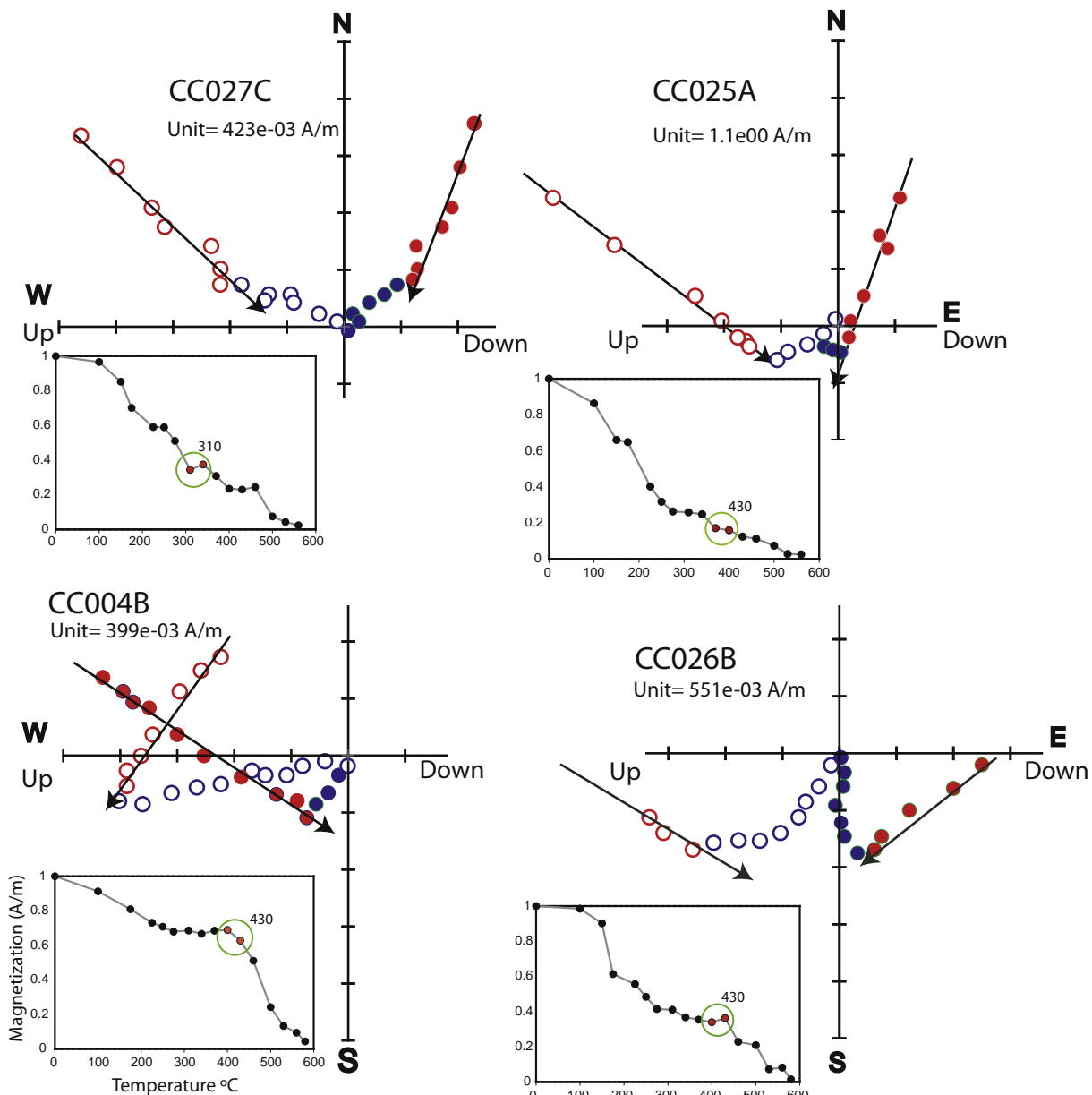


Fig. 7. Typical vector plots showing the secondary magnetic component determination. Arrows indicate the secondary magnetic component direction (filled circles – horizontal, empty circles – vertical). Inset show the intensity demagnetization plot, the T_e is indicated by the green circle. (For interpretation of the references to colour in this figure legend, the reader is referred to the web version of this article.)

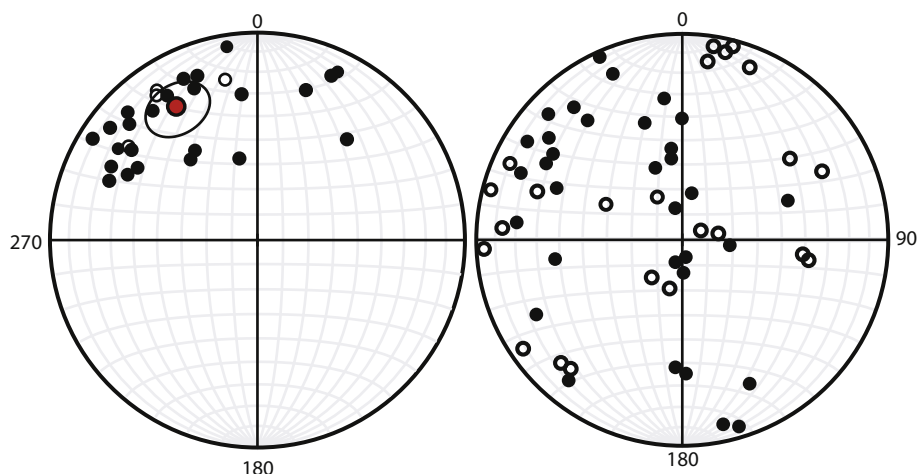


Fig. 8. Equal area plots of secondary (left) and ChRM (right) component directions. Filled/empty circles indicate inclination on the upper/lower hemisphere, respectively.

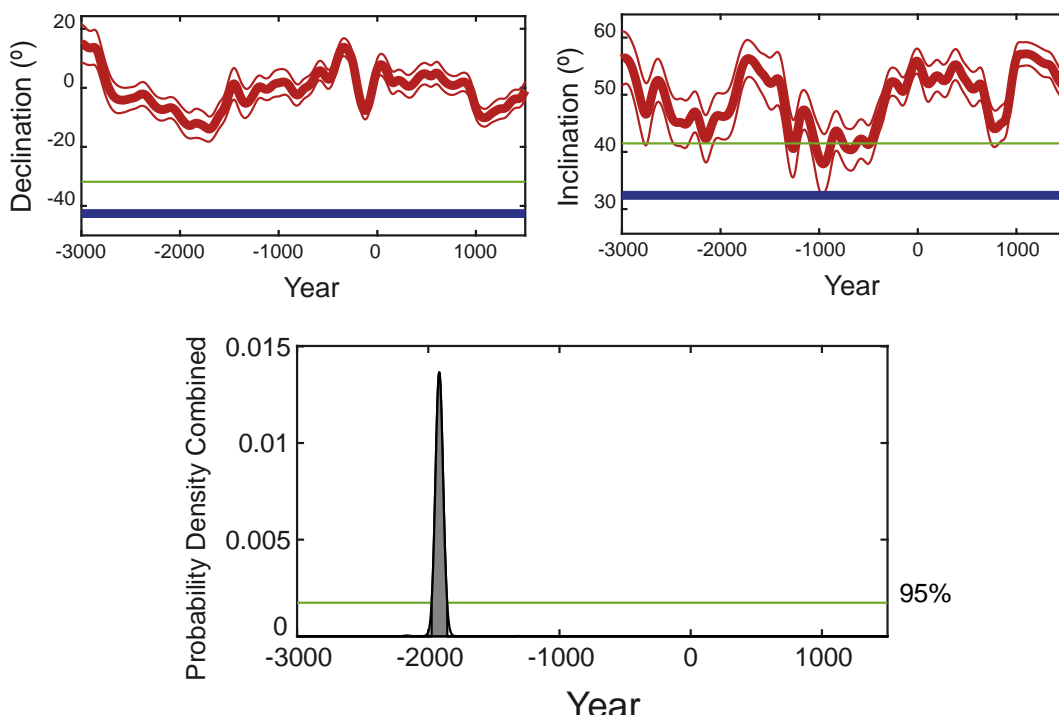


Fig. 9. Cerro Colorado dating, using the secondary magnetization component, by approaching the Declination and Inclination (blue lines, above left and right) data with the SHADIF.14K model (Pavón-Carrasco et al., 2014), and a resulting probability density curve with 95% confidence. Green line is the uncertainty of the process. (For interpretation of the references to colour in this figure legend, the reader is referred to the web version of this article.)

the climatic regime at the beginning of the Late Holocene at 4000 years BP (Van Devender, 1990). The obtained dating agrees with the geological settings in the area. However, as it is the first sight to a dating in Cerro Colorado, is necessary to search for a dating by another method, such as radiocarbon to confirm and constrain the age of the eruptive event.

Acknowledgements

We appreciate the financial support to LMAV from PAPIIT-DGAPA-UNAM IN113117 (Mexico) and ANR-CONACyT (France-Mexico) 273564, research projects. This work was also supported by a Research Grant #180784 from CONACyT (Mexico) to JRVS. We recognize the great contribution to improve this manuscript of two anonymous reviewers. Thanks to C. I. Caballero-Miranda by previous read and suggestions of this manuscript. We thank to J. A. González Rangel for the laboratory support and G. A. Manuel-Viveros for the figure design.

References

- Alva-Valdivia, L.M., Torres-Hernández, J.R., González-Rangel, J.A., Caballero-Miranda, C.I., Rosas-Elguera, J.G., Villalobos-Romero, N., 2012. Paleomagnetismo en la determinación de temperatura de emplazamiento de la Ignimbrita Panalillo, Juárez, San Luis Potosí, México. *Rev. Mex. Cienc. Geol.* 29 (3), 619–638.
- Alva-Valdivia, L.M., Cyphers, A., Rivas-Sánchez, M.L., Agarwal, A., Zurita-Noguera, J., Urrutia-Fucugauchi, J., 2017a. Mineralogical and magnetic characterization of Olmec ilmenite multi-perforated artifacts and inferences on source provenance. *Eur. J. Mineral.* 29, 851–860.
- Alva-Valdivia, L.M., Agarwal, A., Caballero-Miranda, C., García-Amador, B.I., Morales-Barrera, W., Rodríguez-Elizarráz, S., Rodríguez-Trejo, A., 2017b. Paleomagnetic and AMS studies of the El Castillo ignimbrite, central-east Mexico: source and rock magnetic nature. *J. Volcanol. Geotherm. Res.* 336, 140–154.
- Aramaki, S., Akimoto, S., 1957. Temperature estimation of pyroclastic deposits by natural remanent magnetism. *Am. J. Sci.* 255, 619–627.
- Böhnel, H., Pavón-Carrasco, F.J., Sieron, K., Mahgoub, A.N., 2016. Palaeomagnetic dating of two recent lava flows from Ceboruco volcano, western Mexico. *Geophys. Suppl. Monthly Notices Royal Astron. Soc.* 207 (2), 1203–1215.
- Day, R., Fuller, M., Schmidt, V.A., 1977. Hysteresis properties of titanomagnetites: grain size and compositional dependence. *Phys. Earth Planet. Inter.* 13, 260–267.
- Dunlop, D.J., 2002. Theory and application of the Day plot (Mrs/Ms versus Hcr/Hc): 1. Theoretical curves and tests using titanomagnetic data. *J. Geophys. Res.* 107 (B3), 2056. <https://doi.org/10.1029/2001JB000486>.
- Giordano, G., De Rita, D., Cas, R., Rodani, S., 2002. Valley pond and ignimbrite veneer deposits in the small-volume phreatomagmatic 'Peperino-Albano' basic ignimbrite, Lago Albano maar, Colli Albani volcano, Italy: Influence of topography. *J. Volcanol. Geotherm. Res.* 118, 131–144.
- Greeley, R., Christensen, P.R., McHone, J.F., 1987. Radar characteristics of small craters: implications for Venus. *Earth, Moon and Planets* 37, 89–111.
- Gutmann, J.T., 1979. Structure and eruptive cycle of cinder cones in the Pinacate volcanic field and the controls of Strombolian activity. *J. Geol.* 87 (4), 448–454.
- Gutmann, J.T., 2002. Strombolian and effusive activity as precursors to phreatomagmatism: eruptive sequence at maars of the Pinacate volcanic field, Sonora, Mexico. *J. Volcanol. Geotherm. Res.* 113 (1–2), 345–356.
- Gutmann, J.T., Martin, R.F., 1976. Crystal chemistry, unit cell dimensions and structural state of labradorite megacrysts from Sonora, Mexico. *Schweiz. Mineral. Petrogr. Mitt.* 56, 55–64.
- Gutmann, J.T., Sheridan, M.F., 1978. Geology of the Pinacate volcanic field, Sonora, Mexico. *Ariz. B. Geol. Min. Technol. Spec. Pap.*, pp. 47–59.
- Hoblitt, R.P., Kellogg, K.S., 1979. Emplacement temperatures of unsorted and unstratified deposits of volcanic rock debris as determined by paleomagnetic techniques. *Geol. Soc. Am. Bull.* 90, 633–642.
- Ives, R.L., 1935. Recent Vulcanism in Northwestern Mexico. *Geol. Publish. Co.*
- Ives, R.L., 1956. Age of Cerro Colorado crater, Pinacate, Sonora, Mexico. *EOS Trans. Am. Geophys. Union* 37 (2), 221–223.
- Ives, R.L., 1964. The Pinacate region, Sonora, Mexico. *Calif. Acad. Sci., Occasional Papers* 47. San Francisco.
- Jackson, M., Bowles, J.A., 2014. Curie temperatures of titanomagnetite in ignimbrites: effects of emplacement temperatures, cooling rates, exsolution, and cation ordering. *Geochim. Geophys. Geosyst.* 15, 4343–4368. <https://doi.org/10.1002/2014GC005527>.
- Kent, D.V., Ninkovich, D., Pescatore, T., Sparks, R.S.J., 1981. Palaeomagnetic determination of emplacement temperature of Versuvius AD 79 pyroclastic deposits. *Nature* 290, 393–396.
- Kirschvink, J.L., 1980. The least-squares line and plane and the analysis of palaeomagnetic data. *Geophys. J. Int.* 62 (3), 699–718.
- Lynch, D.J., 1981. Genesis and Geochronology of Alkaline Volcanism in the Pinacate Volcanic Field, Northwestern Sonora, Mexico. (PhD diss.). Univ. Arizona, Tucson.
- Mahgoub, A.N., Reyes-Guzmán, N., Böhnel, H., Siebe, C., Pereira, G., Dorison, A., 2018. Palaeomagnetic constraints on the ages of the Holocene Malpaís de Zacapu lava flow eruptions, Michoacán (México): implications for archeology and volcanic hazards. *The Holocene* 28 (2), 229–245.

- McClelland, E.A., Druitt, T.H., 1989. Palaeomagnetic estimates of emplacement temperatures of pyroclastic deposits on Santorini, Greece. *Bull. Volcanol.* 51, 16–27.
- McClelland, E., Erwin, P.S., 2003. Was a dacite dome implicated in the 9,500 B.P. collapse of Mt Ruapehu? A palaeomagnetic investigation. *Bull. Volcanol.* 65, 294–305.
- McClelland, E., Wilson, C.J., Bardot, L., 2004. Paleotemperature determinations for the 1.8-Ka Taupo Ignimbrite, New Zealand, and implications for the emplacement history of a high-velocity pyroclastic flow. *Bull. Volcanol.* 66, 492–513.
- McClelland-Brown, E., 1982. Discrimination of TRM and CRM by blocking-temperature spectrum analysis. *Phys. Earth Planet. Inter.* 30, 405–414.
- McFadden, P.L., McElhinny, M.W., 1988. The combined analysis of remagnetization circles and direct observations in palaeomagnetism. *Earth Planet. Sci. Lett.* 87 (1–2), 161–172.
- Paterson, G.A., Roberts, A.P., Mac Niocaill, C., Muxworthy, A.R., Gurioli, L., Viramonté, J.G., Navarro, C., Weider, S., 2010. Paleomagnetic determination of emplacement temperatures of pyroclastic deposits: an under-utilized tool. *Bull. Volcanol.* 72, 309–330. <https://doi.org/10.1007/s00445-009-0324-4>.
- Pavón-Carrasco, F.J., Osepe, M.L., Torta, J.M., De Santis, A., 2014. A geomagnetic field model for the Holocene based on archaeomagnetic and lava flow data. *Earth Planet. Sci. Lett.* 388, 98–109.
- Peterson, N.V., Groh, E.A., 1963. Maars of south-central Oregon. *Ore Bin* 25, 73–89.
- Petrovsky, Kapicka, 2006. On determination of the Curie point from thermomagnetic curves. *J. Geophys. Res.* 111, B12S27. <https://doi.org/10.1029/2006JB004507>.
- Pike, C.P., Roberts, A.P., Veresub, K.L., 1999. Characterizing interactions in fine magnetic particle systems using first order reversal curves. *J. Appl. Phys.* 85, 6660. <https://doi.org/10.1063/1.370176>.
- Porreca, M., Mattei, M., MacNiocaill, C., Giordano, G., McClelland, E., Funicello, R., 2008. Paleomagnetic evidence for the low temperature emplacement of the phreatomagmatic Peperino Albano ignimbrite (Colli Albani Volcano, Central Italy). *Bull. Volcanol.* 70, 877–893. <https://doi.org/10.1007/s00445-007-0176-8>.
- Roberts, A.P., Pike, C.P., Veresub, K.L., 2000. First-order reversal curve diagrams: a new tool for characterizing the magnetic properties of natural samples. *J. Geophys. Res.* 105 (B12), 28,461–28,475. <https://doi.org/10.1029/2000JB000326>.
- Roberts, A.P., Taupe, L., Heslop, D., Zhao, X., Jiang, Z., 2018. A critical appraisal of the "Day" diagram. *J. Geophys. Res.* 123, 2618–2644. <https://doi.org/10.1002/2017JB015247>.
- Sumner, J.R., 1972. Tectonic significance of gravity and aeromagnetic investigations at the head of the Gulf of California. *Geol. Soc. Am. Bull.* 83 (10), 3103–3120.
- Valentine, G.A., White, J.D., 2012. Revised conceptual model for maar-diatremes: subsurface processes, energetics, and eruptive products. *Geology* 40 (12), 1111–1114.
- Valentine, G.A., White, J.D.L., Ross, P.-S., Graettinger, A.H., Sonder, I., 2017. Updates to concepts on phreatomagmatic maar-diatremes and their pyroclastic deposits. *Front. Earth Sci.* 5, 68. <https://doi.org/10.3389/feart.2017.00068>.
- Van Devender, T.R., 1990. Late Quaternary vegetation and climate of the Sonoran Desert, United States and Mexico. In: Betancourt, J.L., Van Devender, T.R., Martin, P.S. (Eds.), *Packrat Middens: The Last 40,000 Years of Biotic Change*. University of Arizona Press, Tucson, pp. 134–165.
- Vidal-Solano, J.R., Demant, A., Paz-Moreno, F.A., Lapierre, H., Ortega-Rivera, M.A., Lee, J.K.W., 2008. Insights into the tectonomagmatic evolution of NW Mexico: geochronology and geochemistry of the Miocene volcanic rocks from the Pinacate area, Sonora. *Geol. Soc. Am. Bull.* 120, 691–708. <https://doi.org/10.1130/B26053.1>.
- Walker, M.J.C., Berkelhammer, M., Björck, S., Cwynar, L.C., Fisher, D.A., Long, A.J., Lowe, J.J., Newnham, R.M., Rasmussen, S.O., Weiss, H., 2012. Formal subdivision of the Holocene Series/Epoch: a Discussion Paper by a Working Group of INTIMATE (Integration of ice-core, marine and terrestrial records) and the Subcommission on Quaternary Stratigraphy (International Commission on Stratigraphy). *J. Quat. Sci.* 27 (7), 649–659.
- Wohletz, K.H., Sheridan, M.F., 1983. Martian rampart crater ejecta: experiments and analysis of melt-water interaction. *Icarus* 56 (1), 15–37.
- Wood, C.A., 1974. Reconnaissance geophysics and geology of the Pinacate craters, Sonora, Mexico. *Bull. Volcanol.* 38 (1), 149–172.
- Zanella, E., Gurioli, L., Pareschi, M.T., Lanza, R., 2007. Influences of urban fabric on pyroclastic density currents at Pompeii (Italy): 2. Temperature of the deposits and hazard implications. *J. Geophys. Res.* 112, B05214. <https://doi.org/10.1029/2006JB004775>.

Capítulo 5

Paleomagnetism and age constraints of historical lava flows from the El Jorullo volcano, Michoacán, Mexico

L.M. Alva-Valdivia^{a,*}, A. Rodríguez-Trejo^b, J. Morales^c, J.A. González-Rangel^a, A. Agarwal^d

^a Universidad Nacional Autónoma de México: Instituto de Geofísica, Laboratorio de Paleomagnetismo, Ciudad Universitaria, 04510, Ciudad de México, Mexico

^b Posgrado en Ciencias de la Tierra: Instituto de Geofísica, Universidad Nacional Autónoma de México, Mexico

^c Instituto de Geofísica, UNAM, Unidad Michoacán, Campus Morelia, Laboratorio Interinstitucional de Magnetismo Natural (LIMNA), Mexico

^d Albert-Ludwigs-Universität Freiburg, Institut für Geo- und Umweltnaturwissenschaften, Geologie, 79104, Freiburg, Germany

ABSTRACT

The present study employs petrology, rock magnetics, and paleointensity on four lava flows (seven sites) of the El Jorullo volcano; a historical (1759–1766 AD) cinder cone in the Michoacán-Guanajuato Volcanic Field. El Jorullo lava flows cover an extensive area of ~10.8 Km², and a volume ~0.35 Km³. Rock-magnetic experiments and microscopic observations reveal pseudo-single domain size Ti-poor titanomagnetite as the main carrier of magnetization in all sampled flows. Notably the calculated mean direction from all the sites show a slight westwards bias when compared against the secular variation global models. The mean paleo-direction for the El Jorullo historical eruption is: Dec=2.5°, Inc=37.5°, kappa=214, α95=1.8, N=31; the Virtual Geomagnetic Pole has Plat=87° N, Plong=307° E, Kappa=260, A95=1.6; paleointensity data: $45.4 \pm 3.6 \mu\text{T}$; and Virtual Dipole Moment: $10.3 \pm 1 \times 10^{22} \text{ Am}^2$. The paleodirections and the paleointensity values from these lava flows are well-constrained and reliable. These results allow to improve the accuracy and reliability of the global and regional secular variation models available for the last centuries.

<https://doi.org/10.1016/j.jsames.2019.05.016>

Received 26 March 2019; Received in revised form 9 May 2019; Accepted 10 May 2019



Paleomagnetism and age constraints of historical lava flows from the El Jorullo volcano, Michoacán, Mexico



L.M. Alva-Valdivia^{a,*}, A. Rodríguez-Trejo^b, J. Morales^c, J.A. González-Rangel^a, A. Agarwal^d

^a Universidad Nacional Autónoma de México: Instituto de Geofísica, Laboratorio de Paleomagnetismo, Ciudad Universitaria, 04510, Ciudad de México, Mexico

^b Posgrado en Ciencias de la Tierra: Instituto de Geofísica, Universidad Nacional Autónoma de México. Mexico

^c Instituto de Geofísica, UNAM, Unidad Michoacán, Campus Morelia, Laboratorio Interinstitucional de Magnetismo Natural (LIMNA). Mexico

^d Albert-Ludwigs-Universität Freiburg, Institut für Geo- und Umweltnaturwissenschaften, Geologie, 79104, Freiburg, Germany

ARTICLE INFO

Keywords:

Paleointensity
Rock magnetism
El Jorullo volcano
Historical eruption
Mexico

ABSTRACT

The present study employs petrology, rock magnetics, and paleointensity on four lava flows (seven sites) of the El Jorullo volcano; a historical (1759–1766 AD) cinder cone in the Michoacán-Guanajuato Volcanic Field. El Jorullo lava flows cover an extensive area of ~10.8 Km², and a volume ~0.35 Km³. Rock-magnetic experiments and microscopic observations reveal pseudo-single domain size Ti-poor titanomagnetite as the main carrier of magnetization in all sampled flows. Notably the calculated mean direction from all the sites show a slight westwards bias when compared against the secular variation global models. The mean paleo-direction for the El Jorullo historical eruption is: Dec = 2.5°, Inc = 37.5°, kappa = 214, α95 = 1.8, N = 31; the Virtual Geomagnetic Pole has Plat = 87° N, Plong = 307° E, Kappa = 260, A95 = 1.6; paleointensity data: 45.4 ± 3.6 μT; and Virtual Dipole Moment: 10.3 ± 1 × 10²² Am². The paleodirections and the paleointensity values from these lava flows are well-constrained and reliable. These results allow to improve the accuracy and reliability of the global and regional secular variation models available for the last centuries.

1. Introduction

In comparison to the paleomagnetic directional studies, there are less studies dealing with the variation in the intensity of the absolute geomagnetic field (Aubert et al., 2010). This is owed two factors: Firstly, the strong alteration of the mineralogy during the stepwise heating in the Thellier-type double heating method for calculating PI (Thellier, 1938; Thellier and Thellier, 1959; Coe et al. (1978)); Secondly, reliable paleointensity data demand strict rock magnetic characteristics, such as single vector component on the orthogonal diagrams, high reversibility during the heating and cooling and single magnetic phase in the susceptibility vs. temperature measurements. However, geological materials suitable for PI investigations are scarce. Only if these criteria are satisfied, the PI results are reliable because of the validation of additivity, independence, and reciprocity of partial thermoremanent magnetizations (pTRMs).

The El Jorullo volcano is one of the younger monogenetic volcanoes in the Michoacán-Guanajuato Volcanic Field (MGVF), with an important historical eruption from 1759 to 1766 AD. Three PI studies were previously published from volcanic deposits of similar age from the study area: Gratton et al. (2005), Conte-Fasano et al. (2006) and

Dekkers and Böhnel (2006). The first and the third studies focus on methodologies for retrieving the intensity of the geomagnetic field by means of three different procedures: *Thellier-Coe method* (Thellier and Thellier, 1959; Coe et al., 1978), *microwave method* (Walton et al., 1996; Hill et al., 2002) and the *multispecimen method* (Dekkers and Böhnel, 2006). No precise location information of the sampling sites is given in both of these studies, for example Conte-Fasano et al. (2006), provide sampling coordinates of 24 sites in the order of 0.01°, which is ~1 km resolution. The location of the sites is therefore not certain, and they may be outside of the area covered by any of El Jorullo lava flows. These results are, therefore, discarded from further discussion.

Well constrained global models of secular variation for the last 14 ka are available to estimate the mean behavior of the geomagnetic field at different times (e.g. Korte and Constable, 2011; Constable et al., 2016; Pavón-Carrasco et al., 2014). Many of these models were developed by using different available datasets, such as GEOMAGIA50. v3 (Brown et al., 2015). Comparison of the results from well dated and historical events fill the blanks in the records and improve the accuracy of these models.

This study aims high-quality directional and paleointensity calculation from the historical volcanic material from El Jorullo volcano,

* Corresponding author.

E-mail address: lalva@igeofisica.unam.mx (L.M. Alva-Valdivia).

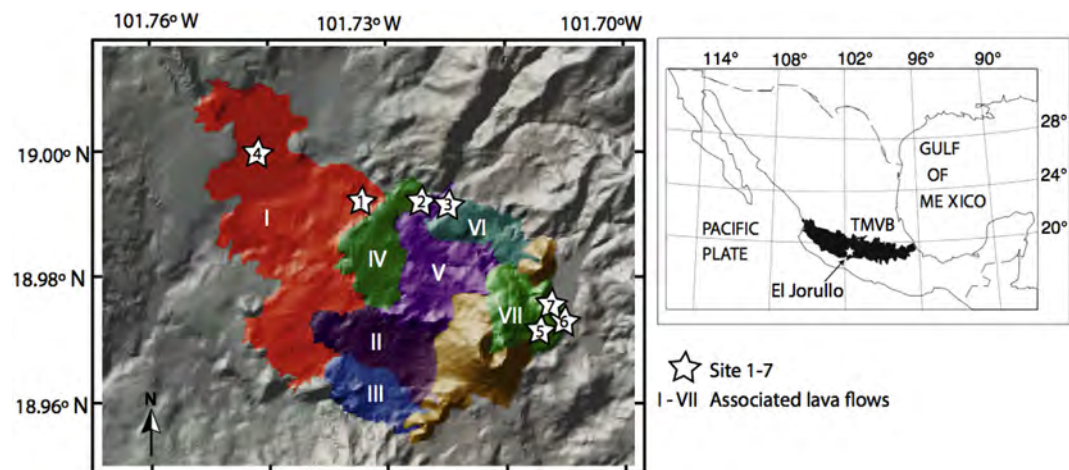


Fig. 1. (Left) Geologic map and location of the paleomagnetic sites (stars). The lava flows (I to VII) of the El Jorullo eruption are also shown (map modified from Guilbaud et al., 2011). (Right) Location of the Trans-Mexican Volcanic Belt (TMVB, black) and study area within it (white star), presented in the Mexico country map.

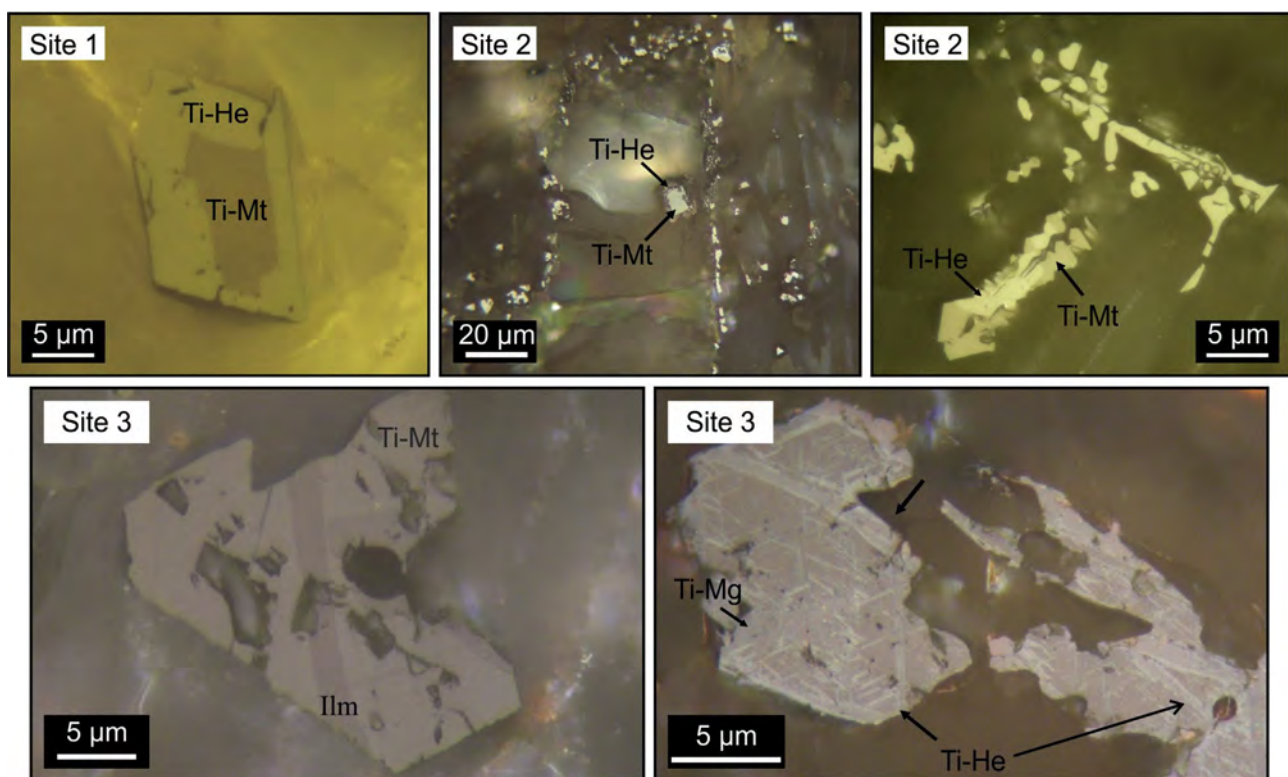


Fig. 2. Reflected light photomicrographs from Site 1: with subhedral titanomagnetite (Ti-Mt) oxidizing to titanohematite (Ti-He) along the circumference; Site 02: half titanomagnetite (Ti-Mt) euhedral crystal oxidized to titanohematite (Ti-He), and a skeletal titanomagnetite (Ti-Mt) grain partially oxidized to titanohematite (Ti-He); Site 03: sandwich type exsolution lamella of ilmenite (Ilm) within a subhedral titanomagnetite (Ti-Mg) grain, and trellis type titanohematite (Ti-He) oxidation lamellae within anhedral titanomagnetite (Ti-Mg).

active from 1759 to 1766 AD. Moreover, the study casts an alert on the reliability of directional data of lava flows. The reported results could be used to compare and calibrate the regional and global synthetic curves and data from direct observation models (Jackson et al., 2000) that estimate the geomagnetic field of the last four centuries.

2. Geology and sampling

El Jorullo volcano ($N18^{\circ}58'25''$, $W101^{\circ}43'03''$; 1230 m. a.s.l.) is a cinder cone (Fig. 1). It is one of the youngest volcanic structures in the Trans-Mexican Volcanic Belt (TMVB), an ca. 1000 km long active volcanic arc that crosses central Mexico from the Pacific Ocean to the

of Mexico. The volcanism is associated to subduction along the Pacific Trench, which is active since Miocene (e.g. Gómez-Tuena et al., 2007; Ferrari et al., 2012). The El Jorullo volcano is located at the southern part of the MGVF, which marks the southern border of the TMVB (Hasenaka and Carmichael, 1985). The El Jorullo volcanic structure formed during a historical eruption from 1759 to 1766 AD creating a main crater (400×500 m in diameter) and four smaller cinder cones along a SSW-NNE fissure (Guilbaud et al., 2011). The high silica contents, makes these lava flows viscous-thicker than the younger volcanic deposits in the region, mainly basalts and basaltic andesites.

In this study, 59 paleomagnetic cores were collected from 7 sites around in the El Jorullo volcano, within the lava flows belonging to the

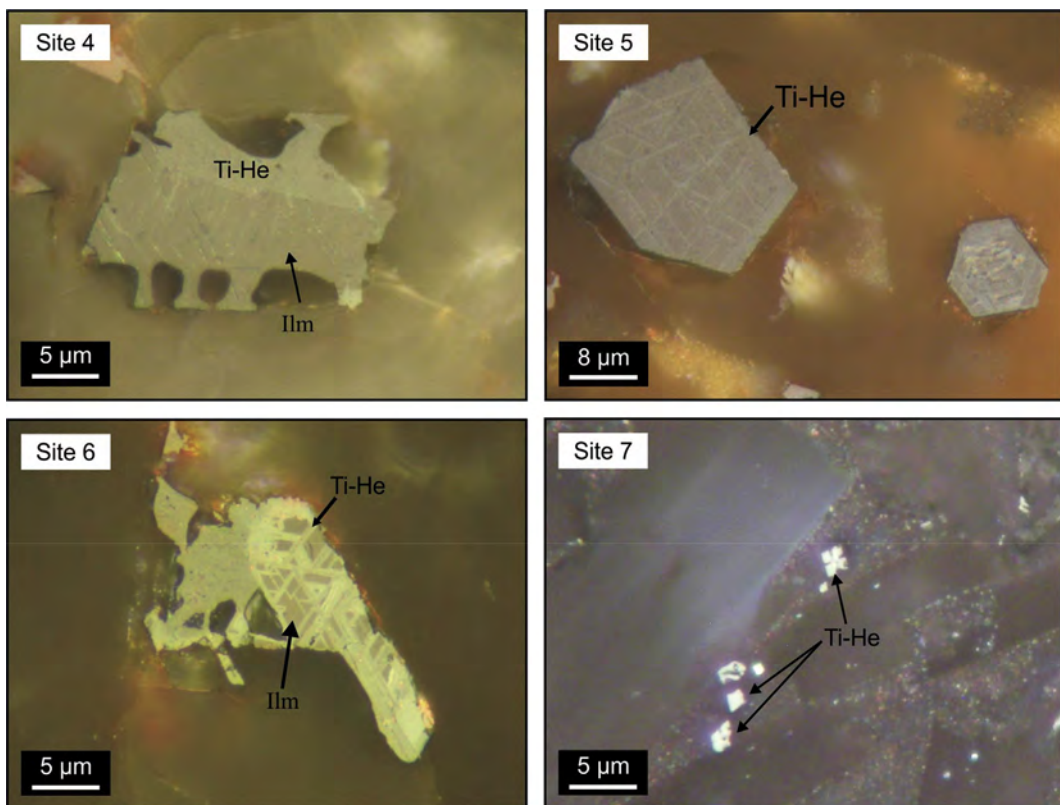


Fig. 3. Reflected light photomicrographs from Site 04: Subhedral ilmenite (Ilm) grain oxide with titanohematite (Ti-He) along the circumference and in fractures; Site 05: Trellis type fine exsolution lamellae of ilmenite within euhedral titanomagnetite grain, which is partly oxidized to titanohematite (Ti-He); Site 06: Anhedral ilmenite grain mostly oxidized to titanohematite (Ti-He) showing trellis type exsolution lamellae; Site 07: Skeletal titanohematite (Ti-He) grains dispersed in the matrix. The grains are oxidation product of skeltal titanomagnetite.

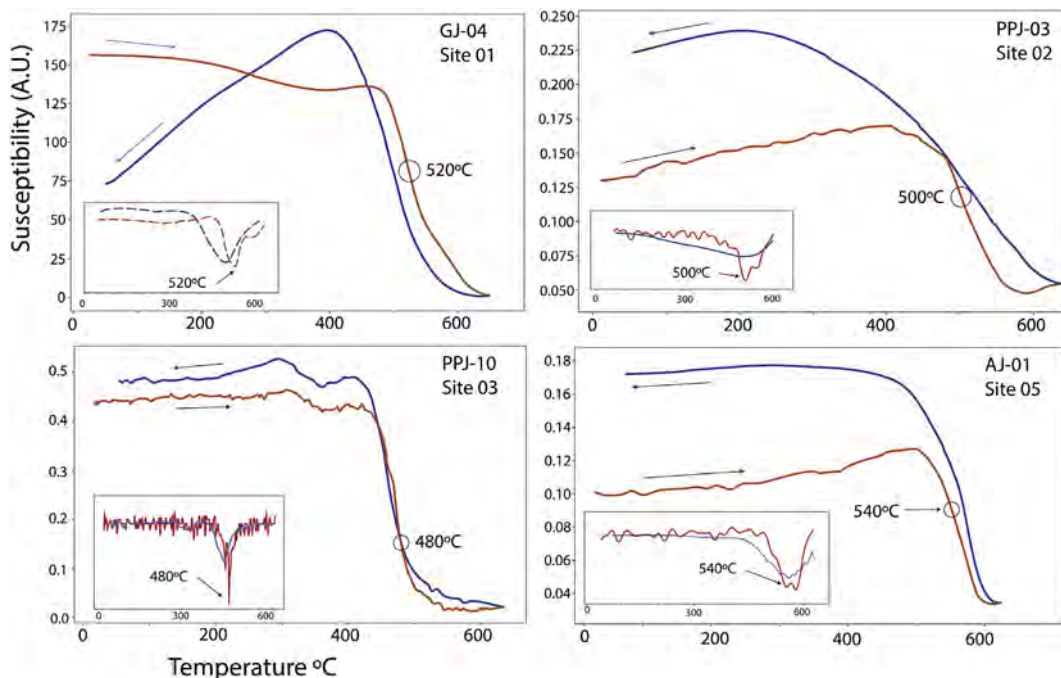


Fig. 4. Typical k-T curves presenting the variation of magnetic susceptibility vs. temperature, the first derivative plot used to determine the Curie temperature (inset).

1759–1766 eruption (Fig. 1). 6 to 12 cores, each < 12 cm long and 1 inch in diameter, were drilled using a portable gasoline-powered drill, oriented *in situ* with both magnetic and sun compasses in most cases. All cores were marked and cut in the laboratory into two to three 2.2 cm

long standard cylindrical specimens.

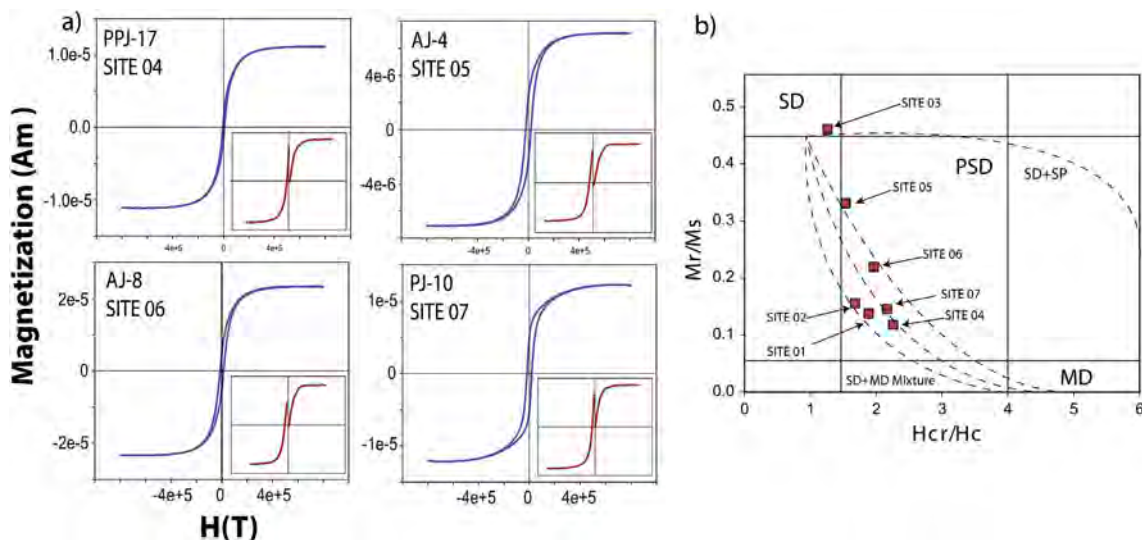


Fig. 5. (a) Typical hysteresis curves and associated IRM and dIRM curves (inset). (b) Hysteresis parameters presented in a Day plot (Day et al., 1977), and curved dashed lines represent the theoretical mixing curves for SD + MD, and SD + Superparamagnetic (SP) mixtures according to Dunlop (2002).

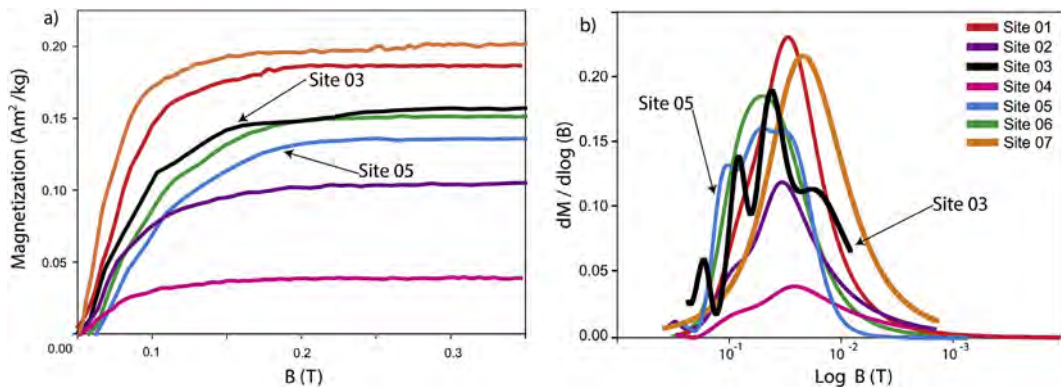


Fig. 6. Acquisition IRM curves from all the sites collected (a), and the coercivity spectra curves from the IRM (b).

3. Methodology and laboratory procedures

The remanence carrying ability and coercivity of ferrimagnetic minerals, such as magnetite, depends vastly on two factors, the exact mineralogy and the domain state (e.g., Tauxe, 2006). To determine the magnetic mineralogy one polished section from each site was studied with reflected light. The magnetic mineralogy was better constrained through the measurement of the variation of magnetic susceptibility with temperature by plotting thermomagnetic curves (k - T) using a Bartington MS2 susceptibility meter and a furnace MS2WFP. During the experiments, samples were heated from room temperature up to 600 °C, and then cooled back to room temperature. The entire process was carried out in air. The bulk susceptibility was measured during the entire cycle of heating and cooling. Curie temperature (T_c) was determined by the first derivative method.

Saturation magnetization (M_s), saturation remanent magnetization (M_{rs}), and coercive force (H_c) was calculated by measuring the hysteresis. Remanent coercive force (H_{rc}) was estimated by measuring the Isothermal Remanent Magnetization (IRM) and by the demagnetization of the IRM (dIRM). These properties were measured using a Princeton AGFM Micromag.

2900 apparatus in fields up to 1.2 T at room temperature. The ratios of these properties provide information on the magnetic domain size distribution (e.g., Day et al., 1977; Dunlop, 2002).

The natural remanent magnetization (NRM) was measured in a Molspin spinner magnetometer. Thermal stepwise demagnetization

from 100 °C to 600 °C was carried out using the Schonstedt TSD-1 thermal demagnetizer. The principal component analysis (PCA), proposed by Kirschvink (1980), was used to estimate the direction of characteristic remanent magnetization (ChRM), using at least 5 demagnetization steps and a maximum angular deviation (MAD) below 5°. Individual magnetization directions were averaged per site and statistical parameters calculated assuming a Fisherian distribution (Fisher, 1953).

For paleointensity experiment, all the samples were heated in an MMTD-model thermal demagnetizer in a 45 µT applied field. The protocol used for determination of the paleointensity was the stepwise heating Thellier and Thellier (1959) with the modifications of Coe et al. (1978) and stability checks of the partial Thermal Remanent Magnetization (pTRM) at every 100 °C. The quality criteria for selection of the results have been according to the Standard Paleointensity Definitions v1.1 (SPD) to select high-quality paleointensity (Paterson et al., 2014). The remanence was measured with a Molspin spinner magnetometer. Paleointensity results were processed by using ThellierTool4.0 software (Leonhardt et al., 2004).

4. Mineralogy and rock magnetism

4.1. Microscopy

The studied samples have abundant feldspar and ferromagnetic phenocrysts. Different sites show large variation in the porphyrocryst

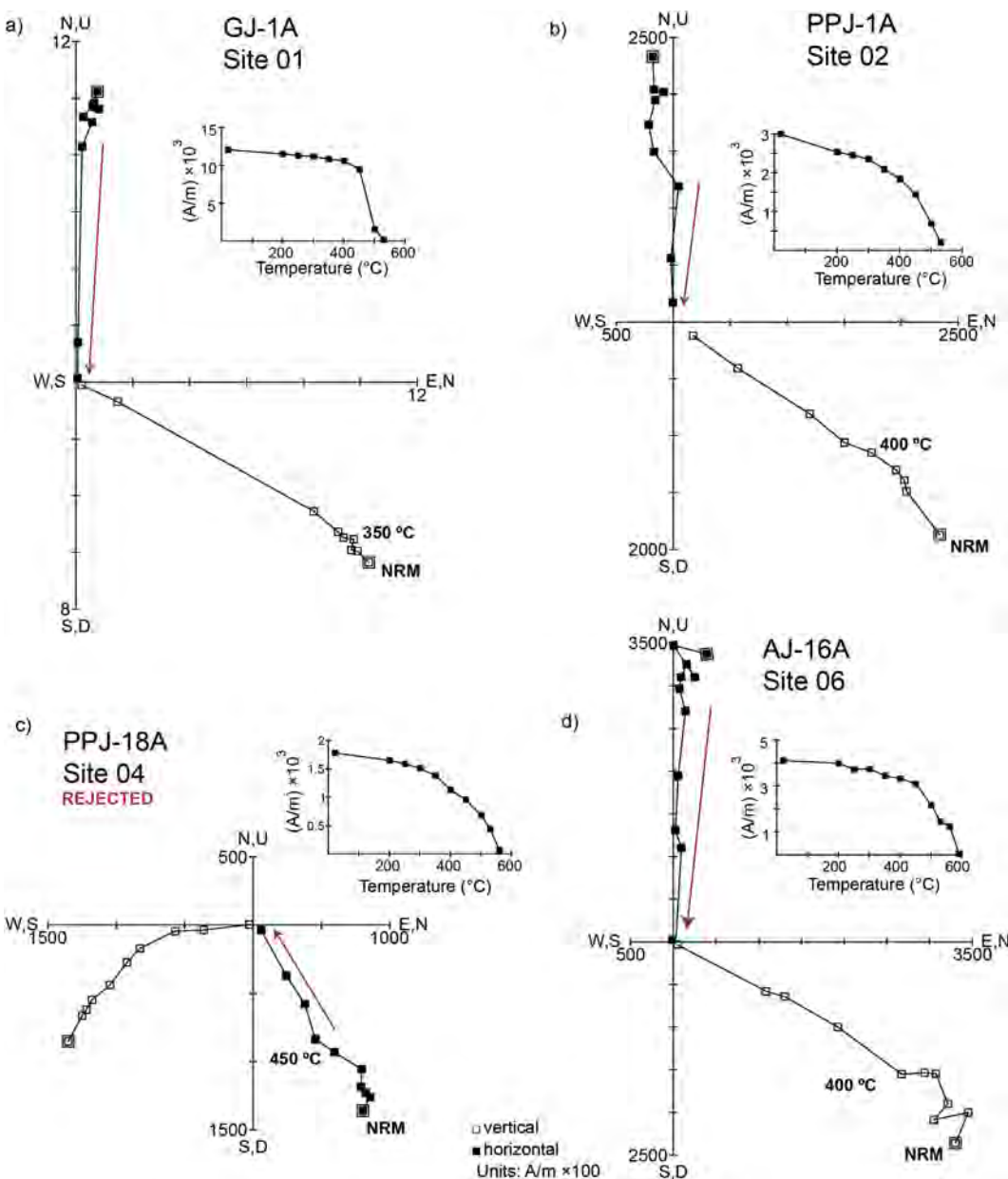


Fig. 7. Orthogonal demagnetization plots from selected lava flows. Close/open circles are the horizontal/vertical component, respectively. Inset shows intensity of thermal demagnetization curves, which highlight a wide distribution of unblocking temperature spectra.

grain size. For example, 100–1000 μm and 200–560 μm at Sites 01 and 02; 20–800 μm at Sites 03 and 07; up to 1800 μm at Sites 04 and 06; and 90–1200 μm at Site 05 (Figs. 2 and 3). Titanomagnetite and ilmenite are the most common Fe-Ti oxides in the studied rocks. The association of titanomagnetite and ilmenite is a consequence of high-temperature exsolution forming trellis type ilmenite lamellae (e.g., Agarwal et al., 2017). Furthermore, titanomagnetite oxidation has commonly led to the formation of titanohematite pseudomorphs. Ilmenite is altered to pseudobrookite and rutile. Typical samples are shown in Fig. 2a, b and 2c. Formation of non-stoichiometric magnetite affects the coercivity and the ability of carrying remanence (Oliva-Urcia and Kontny, 2012).

Sites 01 and 02 show similar black to brownish color. Site 05 presents red color, which is owed to the intense oxidation. All these rocks have micro-porphyritic texture, showing the micro phenocrystals with preferred orientation in Sites 01 and 02, and a well-defined mineral lineation in Site 05. These rocks show abundant irregular fractures and high (Sites 02 and 05) to medium (Site 01) porosity. The microfractures

in rocks of site 5 have random orientation and are filled by titanohematite. Essential and accessory opaque minerals are < 8%. In the Sites 03, 04, 06 and 07 the titanomagnetite is partly oxidized to titanomaghemit and titanohematite, and ilmenite to pseudobrookite and rutile (Fig. 3 a, b, c and d; e.g., Alva-Valdivia et al., 2017b).

Sites 03, 04 and 06 show a light-grey color, while site 07 shows a black color. They present a micro-porphyritic texture, with up to 91% phenocrysts of feldspar and ferromagnetic minerals, which have a preferred orientation. Sites 04, 06 and 07 show irregular fractures, in contrast, Site 03 presents abundant parallel fractures, which follow the preferred orientation of the phenocrysts.

4.2. Rock magnetic properties

4.2.1. Magnetic susceptibility vs. temperature (k - T) curves

During the heating cycle (Fig. 4), the k - T behavior of the samples GJ-4 (Site 01) and PPJ-10 (Site 03) is reversible, but for others it is only partly reversible, e.g., PPJ-3 (Site 03), AJ-1 (Site 05) and PPJ-14 (Site

Table 1

Summary of the paleomagnetic directional results and VGP's from the El Jorullo volcano.

Site	Specimen	Location		Dec (°)	Inc (°)	kappa	α95	VGP		Pol
		Lat °N	Long °W					Plat °N	Plong °E	
1	GJ-1A	18.993	101.725	4	34	752	2.8	86.2	353.1	N
	GJ-5A			3	38	335	3.7	86.3	308.0	N
	GJ-6A			349	30	388	3.9	79.1	154.5	N
2	PPJ-01A	18.993	101.728	356	35	814	1.8	86.2	173.4	N
	PPJ-02A			1	37	411	4.5	88.1	287.8	N
	PPJ-03A			359	29	1230	1.9	86.4	93.6	N
	PPJ-04A			359	28	32	9.2	85.8	91.5	N
	PPJ-05A			1	40	436	4.4	86.1	272.0	N
	PPJ-06			2	37	176	7.2	87.5	306.7	N
3	PPJ-07A	18.993	101.737	357	51	1387	2.1	77.0	246.8	N
	PPJ-08A			4	40	319	5.2	84.7	214.1	N
	PPJ-10A			3	42	275	7.5	84.1	285.7	N
5	AJ-01A	18.977	101.712	359	33	1434	1.6	88.6	121.6	N
	AJ-02A			4	38	820	2.7	86.3	208.5	N
	AJ-03A			5	38	822	2.7	84.8	320.9	N
	AJ-04A			356	37	251	3.1	85.9	192.5	N
	AJ-05A			1	48	2570	1.5	79.9	263.2	N
	AJ-06A			2	37	527	3.3	87.5	306.7	N
	AJ-07A			5	40	426	2.2	84.7	214.1	N
6	AJ-08A	18.978	101.708	4	33	664	3.0	86.1	2.5	N
	AJ-12A			359	35	364	2.9	89.0	185.8	N
	AJ-13A			4	36	1088	2.3	86.1	333.2	N
	AJ-14A			3	33	241	5.9	87.0	7.3	N
	AJ-16A			1	30	1673	1.5	86.9	59.9	N
7	PJ-01A	18.980	101.710	4	35	3020	1.4	86.2	343.1	N
	PJ-02A			351	36	668	2.6	81.5	176.2	N
	PJ-03A			4	35	1282	2.1	86.2	343.1	N
	PJ-04A			1	38	251	3.8	87.5	280.0	N
	PJ-05A			359	39	1224	2.2	86.8	241.3	N
	PJ-09A			1	32	700	2.9	88.1	48.1	N
	PJ-11A			3	36	527	3.3	87.0	328.9	N

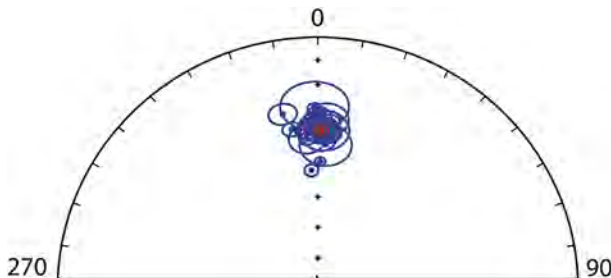


Fig. 8. ChRM by specimen and general mean direction (red circle). (For interpretation of the references to color in this figure legend, the reader is referred to the Web version of this article.)

06). k - T curves show an T_c from 480 °C to 540 °C, with high reversibility and thermal stability above 300 °C, revealing Ti-poor titanomagnetite. The instability below 300 °C is owed to metastable titanomaghemite, which is also observed under the microscope. It decomposes into titanohematite at temperatures over 250 °C (O'Reilly, 2012). Ti-poor titanomagnetite is, therefore, the main carrier of the magnetization in the samples.

4.2.2. Hysteresis and day plot

The hysteresis curves reveal low saturation and coercivity ratios consistent with a typical Ti-poor titanomagnetite. They have pot-bellied or wasp-waisted shapes indicating a dominance of a mixture of single domain (SD) + multi domain grains (MD) (Fig. 5a). The dominance of PSD behavior is evident from characterizing ratios, $0.12 < \text{Mrs} / \text{Ms} < 0.43$ and from $1.26 < \text{Hcr}/\text{Hc} < 2.26$ (Fig. 5b).

Typically, temperature-induced alteration provokes the creation of fine iron-oxide particles, from PSD to SD (e.g., Cottrell and Tarduno, 1999). Such behavior is easily identified in the cooling branch of the k - T

experiments (Fig. 4), and Day plot (site 5 and 3, Fig. 5b). Since, all the specimens exhibit presence of PSD to SD behavior, the PI estimated from them is considered suitable for good pTRM recorders.

In summary, the investigated rocks have pseudo-single domains of Ti poor titanomagnetite, which carry stable magnetization (e.g., Alva-Valdivia et al., 2019). This magnetic mineralogy renders the Jorullo lava deposits a good candidate for PI investigations.

4.2.3. Isothermal remanent magnetization (IRM) and coercivity spectra

Mass normalized IRM acquisition curves reach saturation in different magnetic fields, which indicates difference in their coercivity spectra (Fig. 6a). IRM curves show similar saturation slopes that indicates the predominance of Ti-poor titanomagnetite as the main magnetic carrier of the magnetization. The coercivity spectra obtained from the acquisition IRM curves show that the mean coercivity values vary within a small range in all the sites (Fig. 6b), indicating similar coercivity and comparable mineralogy and domain sizes, which is consistent with the hysteresis and Day plot results. Abrupt change in the slope of the IRM curves at ca. 50 mT and 150 mT from Site 03 and 05, both saturating at ca. 250 mT, indicate a mixture of at least two different coercivities (Fig. 6a). The curves (Fig. 6b) show in more detail the mixture of at least three mean coercivity values, corresponding possibly to differences in the grain size, mineralogy and magnetic domain state. As shown in the IRM curves, coercivity spectra curves show (Fig. 6b) in most of the sites (01, 02 04, 06 and 07) a single mode in the coercivity distribution with similar mean values (peaks) and some differences in the magnetization value. Site 03 and Site 05 show at least three mean peaks. The differences could be related to the presence of a mixture of more than two different magnetic minerals, such as the observed in the optical microscopy and the k - T curves (titanomaghemite and titanohematite), and by the mixture of magnetic domain states showed in the Day plot.

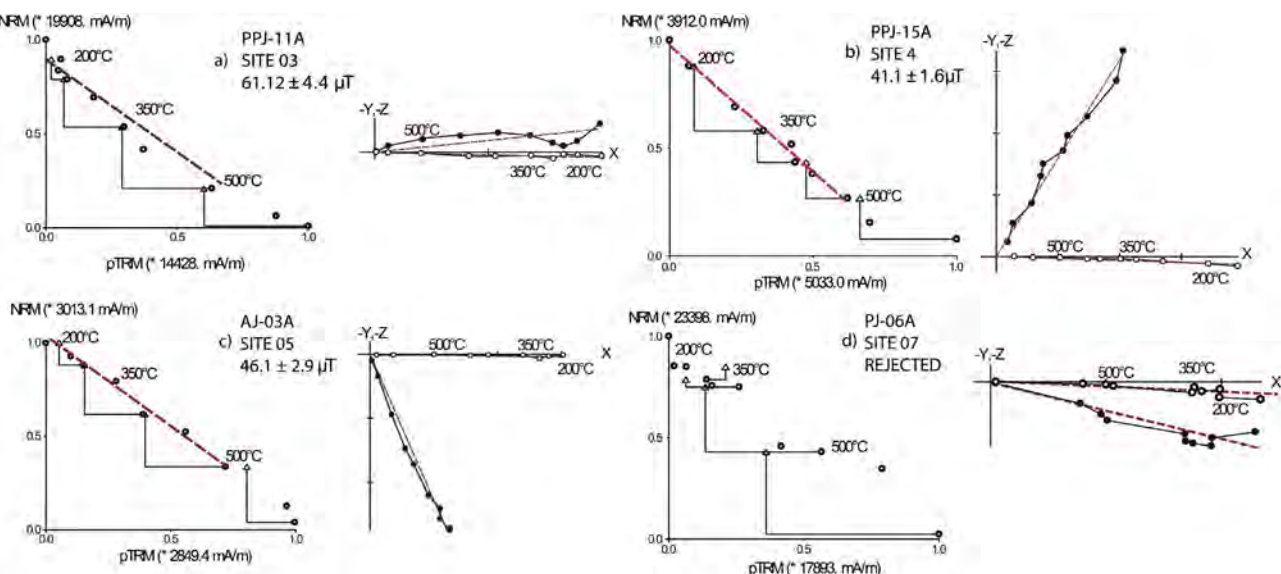


Fig. 9. Arai and Zijderveld diagrams of representative specimens.

Table 2

Summary of paleointensity results obtained in this study, and previous published data. N is the number of specimens used for the calculation of the mean by site; H is the paleointensity and the associated standard deviation; VDM is the Virtual Dipole Moment and the associated standard deviation; PI method, is the paleointensity method used.

Site Name	N	H (μ T)	$H \sigma$	$VDM \times 10^{22}$	$VDM \sigma$
Site 01	3	40.02	1.88	7.53	0.4
Site 02	3	45.52	4.62	8.01	1.0
Site 03	3	47.24	3.20	12.49	0.7
Site 04	6	43.53	3.47	9.81	0.8
Site 04	7	46.84	4.39	11.84	1.0
Site 06	6	45.91	3.68	10.34	2.1
Site 07	5	54.84	4.03	12.40	0.9
Overall mean this study	7	45.4	3.6	10.3	1.0
Previous published results					
Reference	PI Method	H (μ T)	$H \sigma$	$VDM \times 10^{22}$	$VDM \sigma$
Gratton et al., 2005	Thellier-Coe	53.5	9.2	12.1	2.1
	Microwave P	41.3	3.2	9.0	0.7
	Microwave DH	45.0	3.0	10.1	0.7
	Site level mean	46.6	6.3	10.5	1.4
Conte-Fasano et al., 2006	Thellier-Coe	48.0	1.0	8.1	1.1
Dekkers and Böhnel (2006)	Multispecimen	45.0	3.2	10.1	0.7
General mean for El Jorullo		46.3	3.5	9.8	1.0

5. Paleomagnetic directions

After the thermal demagnetization process, the orthogonal Zijderveld vector plots show the ChRM (Fig. 7). In about 90% cases the magnetization shows a single directional component (Fig. 7). There is viscous component in a few samples, removed at temperature around 200 °C.

For determination of reliable ChRM of the El Jorullo historical lava flows, only the high-quality data was used, to ensure high reliability and accuracy. Site 04 of anomalous data was rejected (mean direction: Dec = 140° and Inc = 0°) because the directions do not correspond with other nearby sites. This may be due because the sampling was done in distinct blocks. Nineteen percent of the ChRM data determination by specimen presents low value of kappa (< 60). For 17% of the samples, remagnetization was evident from anomalous NRM results, such as high scatter in the kappa and α_{95} , along with a ChRM

considerably different to the average observed in the related site. All of these samples were discarded. A summary of the accepted specimens is shown in Table 1.

Dec and Inc represent the declination and inclination of the ChRM for each specimen; kappa and α_{95} , are the dispersion parameter and 95% of confidence limit, respectively; Plat and Plong, show the calculated virtual geomagnetic pole (VGP) coordinates for each specimen in degrees; Pol is the determined polarity, R or N denote reverse or normal, respectively.

Reliable mean directions, calculated at core level from 31 specimens are: Dec = 2.5°, Inc = 37.5°, kappa = 214, α_{95} = 1.8, N = 31 and VGP at Plat = 87° N, Plong = 307° E, Kappa = 260, A95 = 1.6 (Fig. 8b). These directions are comparable to the present Geomagnetic Axial Dipole (GAD), according with UNAM magnetic survey and data from the Teoloyucan Magnetic Observatory (<http://132.248.6.186/TEOonline.html>) show an average record for the beginning of 2019: Dec = 5° and Inc = 40.7°.

6. Paleointensity results

Paleointensity experiments were carried out on the seven sampled sites by using the Thellier-Coe et al., 1978 zero-field/in-field protocol with stepwise pTRM check every 100 °C. Arai plots (Fig. 9) show typical behavior occurred during the stepwise heating experiment, e.g. reliable linearity during the acquisition of the pTRM and checks (Fig. 9a, b and 9c); and in some cases, show alteration producing concave curves (Fig. 9d). The acceptable samples present high thermal and magnetic stability from 200 °C to 500 °C according with the pTRM checks (Fig. 9a, b and 9c) and single vector component. At least 55% of samples present the typical concave shape, which is associated to alteration and formation of new minerals during the stepwise heating process, also to the effect of MD grains (Fig. 9d). This thermal alteration can be observed in the k - T curves around 300 °C. These thermal alterations and new minerals may impact artificial pTRM, thus, adversely affecting the final PI calculations. All these cases were not used for paleointensity estimation.

Mean paleointensity and VDM obtained in this study are $45.4 \pm 3.6 \mu$ T and $10.3 \pm 1 \times 10^{22} \text{ Am}^2$, respectively (Table 2). These values agree well with the general mean estimated by Gratton et al. (2005), Dekkers and Böhnel (2006); and Conte-Fasano et al. (2006), $46.3 \pm 3.5 \mu$ T and $9.8 \pm 1 \times 10^{22} \text{ Am}^2$, respectively, and with the estimated model developed from direct observations from 1600 AD,

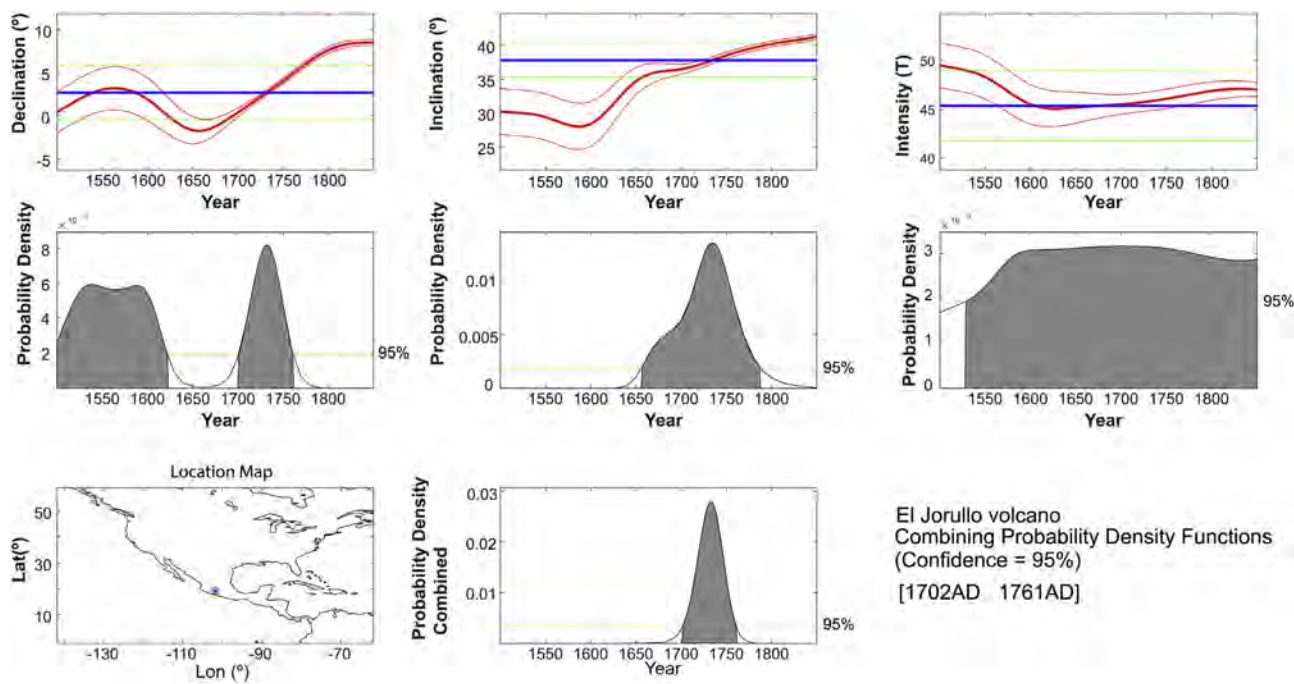


Fig. 10. Global model SHA.DIF.14k and density functions used to determine de age.

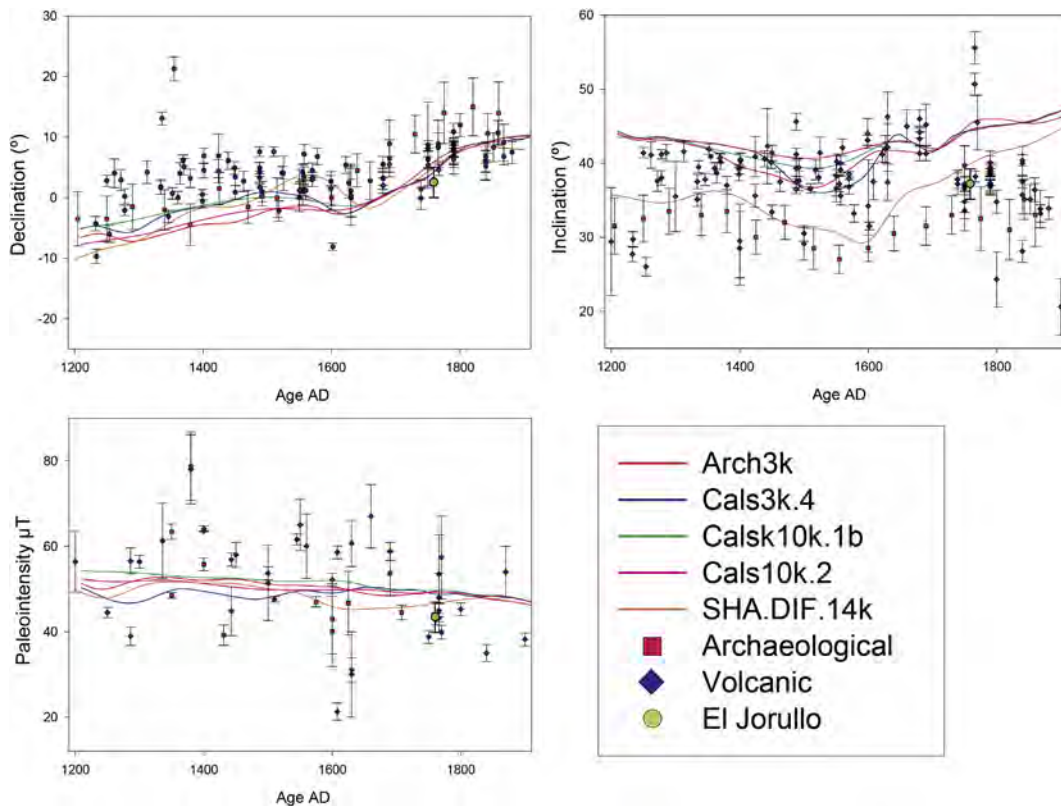


Fig. 11. Comparison of paleodirection and paleointensity of the El Jorullo historical lava flows with previous published secular variation models available in GEOMAGIA50. v3 (Brown et al., 2015). (For interpretation of the references to color in this figure legend, the reader is referred to the Web version of this article.)

43–47 μ T in the middle of the 18th century (Jackson et al., 2000).

7. Age determination

Historical and well registered eruptions provide a good way to test and calibrate the models. The El Jorullo volcano was active from 1759

to 1766, and the paleomagnetic dating was determined by comparing the direction and paleointensity data with the global model SHA.DIF.14k (Pavón-Carrasco et al., 2014, Fig. 10), getting the age of 1720 ± 60 AD. Finally, the probability density combined analysis of magnetic declination, inclination and intensity reveal a refined paleomagnetic age of 1732 ± 30 AD. (Fig. 10). The calculated age is close to

the documented age (1759–1766 AD), with only a few years difference. High scatter, standard deviation > 300 year, is observed when age is determined by using only the intensity (Fig. 10). This high scatter is owed, firstly, to the flat intensity curve during this time, and secondly, to the global model, as no historical intensity data were available for this period of time. The present study, is therefore, important, as it fills the gap by providing new PI data from the El Jorullo volcano. The present study, therefore, improves the accuracy of the global curve models.

8. Comparison with the global models of secular variation

The present results were compared with the secular variation global models such as ARCH3k.1 (Korte et al., 2009), CALS3k.4 (Korte and Constable, 2011), CALS10k.1b (Korte et al., 2011), CALS10k.2 (Constable et al., 2016), SHA. DIF.14k (Pavón-Carrasco et al., 2014), and with published data available in GEOMAGIA50. v3 (Brown et al., 2015). Fig. 11 presents available paleodirection and paleointensity data, for latitudes similar to Mexico, from archeological studies and several volcanic rocks between 1200 and 1900 AD (e.g. the most relevant: Tanaka and Kono, 1991; Hagstrum and Champion, 1995; Böhnel and Molina-Garza, 2002; Sherrod et al., 2006). For this region and period of time, most of the data are from volcanic rocks and less from the archeological sources. In the global databases, paleodirection data are more abundant than paleointensity. In general, the present results are well comparable to the models. More specifically, the inclination calculated here, 37.5°, is closer to the SHA. DIF.14k model from archeological samples instead of volcanic rocks. Nevertheless, from 1600 AD to 1900 AD a slight flatness is observed in all the models, due to few data points. In both directional curves (declination and inclination) is clear that from 1700 AD to 1800 AD the number of data available are few in comparison with the rest of the period. For intensity, as the datasets has lower density of data in comparison with the directional, the curves for all the models from 1200 AD to 1900 AD show a long flatness, making necessary to increase the volume of observations particularly in that period.

9. Discussion

The El Jorullo volcano represents an important episode of an eruption at 1759 AD, which emplaced ca. 10 km³ of volcanic products, at the southern part of the MGVF and TMVB (Guilbaud et al., 2011).

Rock magnetism and microscopy reveal homogeneous composition of magnetic mineralogy, dominated by Ti-poor titanomagnetite as the main carrier of stable magnetization, with slight alteration phases of titanomaghemitite and titanohematite (Figs. 2 and 3). The secondary viscous component may be carried by titanomaghemitite. The titanomagnetite has a PSD magnetic domain state with different mixtures of SD + MD, evident from slight differences in coercivity and grain size observed in IRM, coercivity spectra and hysteresis curves.

Six out of seven sites present mean ChRM and VGP with high quality on the Fisher statistics. The calculated mean declination (2.5°) and inclination (37.5°) agree well with the values provided for this period by the global models of secular variation, as shown in Fig. 11, and are also consistent with previous studies of the MGVF from young volcanoes and with the secular variation range estimated for the TMVB for the last 40 ka (e.g., Böhnel and Molina-Garza, 2002; Mahgoub et al., 2017). Disregarding the errors, the paleodirections from flow I to VII are comparable, thus implying that, the Earth's magnetic field was constant for ca. 7 years between 1759 and 1766, at the time of El Jorullo eruptions.

The present paleointensity results, are slightly different from previous reports, perhaps due to the different methodologies used and inherent heterogeneity in the coercivity and grain size within each lava flow. However, these differences are within the expected range according with the models. Previous paleointensity results published from the El Jorullo volcano (Gratton et al., 2005; Conte-Fasano et al., 2006)

demagnetized the samples using stepwise heating and microwave in alternatively, which is different from the traditional Thellier and Thellier (1959) with Coe et al. (1978) methods for determining the pTRM.

The global models use the available paleomagnetic data to develop curves that approach the behavior of the EMF at different points in time. The low density of available data generates uncertainties and anomalies in the models, revealed from the flat segment of the curves for the last 400 years (Jackson et al., 2000). This, in turn complicates the estimation of precise age. However, recorded volcanic events, such as the El Jorullo eruption, facilitates to update these flat segments in the curves with fresh reliable data, thus, improving the accuracy of the models. The direct real-time observations of the EMF's declination and inclination started around 1600 AD. Our results are consistent with the estimated model of secular variation developed from these historical dataset observations of the EMF from 1600 AD (Malin and Bullard, 1981; Jackson et al., 2000).

10. Conclusions

The intense volcanic activity along the TMVB, and the human occupation of ancient cultures established in central Mexico since the last 2000 years, allows to obtain a high volume of records from the EMF. The historical eruption of the El Jorullo volcano provides a valuable example of monogenetic volcanism in the MGVF, and the direct and precise record of the EMF with accurate age. It, thus, allows to improve the accuracy of the available secular variation curves. The high-quality paleodirections determined (Dec = 2.5, Inc = 37.5°, kappa = 214, α95 = 1.8, N = 31; VGP Plat = 87° N, Plong = 307° E, Kappa = 260, A95 = 1.6), as well as the new paleointensity value (45.4 ± 3.6 μT; VDM = 10.3 ± 1 × 1022 Am²), are important contributions for regional models of secular variation in central Mexico.

Acknowledgements

This research was undertaken during the course of a CONACyT (Mexico)-ANR (France)-273564 and PAPIIT-DGAPA (UNAM-Mexico) IN113117 research Projects. AA thanks the UNAM postdoctoral position. A. Nasser Mahgoub and B. García-Amador read a previous version giving many comments and suggestions that improve greatly this manuscript. The Alexander von Humboldt Foundation is thanked for the postdoctoral fellowship to AA.

Appendix A. Supplementary data

Supplementary data to this article can be found online at <https://doi.org/10.1016/j.jsames.2019.05.016>.

References

- Aubert, J., Tarduno, J.A., Johnson, C.L., 2010. Observations and models of the long-term evolution of Earth's magnetic field. *Space Sci. Rev.* 155 (1–4), 337–370.
- Agarwal, A., Alva-Valdivia, L.M., Rivas-Sánchez, M.L., Herrero-Bervera, E., Urrutia-Fucuguchi, J., Espejel-García, V., 2017. Emplacement dynamics and hydrothermal alteration of the Atengo ignimbrite, southern Sierra Madre Occidental, northwestern Mexico. *J. South Am. Earth Sci.* 80, 559–568.
- Alva-Valdivia, L.M., Agarwal, A., Caballero-Miranda, C., García-Amador, B.I., Morales-Barrera, W., Rodríguez-Elizarrarás, S., Rodríguez-Trejo, A., 2017. Paleomagnetic and AMS studies of the El Castillo ignimbrite, central-east Mexico: Source and rock magnetic nature. *J. Volcanol. Geotherm. Res.* 336, 140–154.
- Alva-Valdivia, L.M., Rodríguez-Trejo, A., Vidal-Solano, J.R., Paz-Moreno, F., Agarwal, A., 2019. Emplacement temperature resolution and age determination of Cerro Colorado tuff ring by paleomagnetic analysis, El Pinacate Volcanic Field, Sonora, Mexico. *J. Volcanol. Geotherm. Res.* 369, 145–154.
- Böhnel, H., Molina-Garza, R., 2002. Secular variation in Mexico during the last 40,000 years. *Phys. Earth Planet. In.* 133 (1–4), 99–109.
- Brown, M.C., Donadini, F., Korte, M., Nilsson, A., Korhonen, K., Lodge, A., ... Constable, C.G., 2015. GEOMAGIA50. v3: 1. General structure and modifications to the archaeological and volcanic database. *Earth Planets Space* 67 (1), 83.
- Coe, R.S., Grommé, S., Mankinen, E.A., 1978. Geomagnetic palaeointensities from

- radiocarbon-dated lava flows on Hawaii and the question of the Pacific nondipole low. *J. Geophys. Res.* 83, 1740–1756.
- Constable, C., Korte, M., Panovska, S., 2016. Persistent high paleosecular variation activity in southern hemisphere for at least 10 000 years. *Earth Planet. Sci. Lett.* 453, 78–86.
- Conte-Fasano, G., Urrutia-Fucugauchi, J., Goguitchaichvili, A., Morales-Contreras, J., 2006. Low-latitude paleosecular variation and the time-averaged field during the late Pliocene and Quaternary—paleomagnetic study of the Michoacan-Guanajuato volcanic field, Central Mexico. *Earth Planets Space* 58 (10), 1359–1371.
- Cottrell, R.D., Tarduno, J.A., 1999. Geomagnetic paleointensity derived from single plagioclase crystals. *Earth Planet. Sci. Lett.* 169 (1–2), 1–5.
- Day, R., Fuller, M., Schmidt, V.A., 1977. Hysteresis properties of titanomagnetites: grain-size and compositional dependence. *Phys. Earth Planet. In.* 13 (4), 260–267.
- Dekkers, M.J., Böhnel, H.N., 2006. Reliable absolute palaeointensities independent of magnetic domain state. *Earth Planet. Sci. Lett.* 248 (1–2), 508–517.
- Dunlop, D.J., 2002. Theory and application of the Day plot (Mrs/Ms versus Hcr/Hc) 2. Application to data for rocks, sediments, and soils. *J. Geophys. Res.: Solid Earth* 107 (B3) EPM-5.
- Ferrari, L., Orozco-Esquivel, T., Manea, V., Manea, M., 2012. The dynamic history of the Trans-Mexican Volcanic Belt and the Mexico subduction zone. *Tectonophysics* 522, 122–149.
- Fisher, R.A., 1953. Dispersion on a sphere. In: Proceedings of the Royal Society of London. Series A. Mathematical and Physical Sciences. vol. 217. pp. 295–305 1130.
- Gómez-Tuena, A., Orozco-Esquivel, M.T., Ferrari, L., 2007. Igneous petrogenesis of the Trans-Mexican volcanic belt. *Geol. Soc. Am. Spec. Pap.* 422, 129–181.
- Gratton, M.N., Goguitchaichvili, A., Conte, G., et al., 2005. Microwave palaeointensity study of the Jorullo volcano (Central Mexico). *Geophys. J. Int.* 161, 627–634.
- Guilbaud, M.N., Siebe, C., Layer, P., Salinas, S., Castro-Govea, R., Garduno-Monroy, V.H., Le Corvec, N., 2011. Geology, geochronology, and tectonic setting of the Jorullo Volcano region, Michoacán, México. *J. Volcanol. Geotherm. Res.* 201 (1–4), 97–112.
- Hagstrum, J.T., Champion, D.E., 1995. Late Quaternary geomagnetic secular variation from historical and 14C-dated lava flows on Hawaii. *J. Geophys. Res.: Solid Earth* 100 (B12), 24393–24403.
- Hasenaka, T., Carmichael, I.S., 1985. The cinder cones of Michoacán—Guanajuato, central Mexico: their age, volume and distribution, and magma discharge rate. *J. Volcanol. Geotherm. Res.* 25 (1–2), 105–124.
- Hill, M.J., Gratton, M.N., Shaw, J., 2002. A comparison of thermal and microwave paleomagnetic techniques using lava containing laboratory induced remanence. *Geophys. J. Int.* 151 (1), 157–163.
- Jackson, A., Jonkers, A.R., Walker, M.R., 2000. Four centuries of geomagnetic secular variation from historical records. *Philos. Trans. R. Soc. London, Ser. A: Mathematical, Physical and Engineering Sciences* 358 (1768), 957–990.
- Kirschvink, J.L., 1980. The least-squares line and plane and the analysis of palaeomagnetic data. *Geophys. J. Int.* 62 (3), 699–718.
- Korte, M., Constable, C., 2011. Improving geomagnetic field reconstructions for 0–3 ka. *Phys. Earth Planet. In.* 188 (3–4), 247–259.
- Korte, M., Constable, C., Donadini, F., Holme, R., 2011. Reconstructing the Holocene geomagnetic field. *Earth Planet. Sci. Lett.* 312 (3–4), 497–505.
- Korte, M., Donadini, F., Constable, C.G., 2009. Geomagnetic field for 0–3 ka: 2. A new series of time-varying global models. *Geochem. Geophys. Geosyst.* 10 (6).
- Leonhardt, R., Heunemann, C., Krása, D., 2004. Analyzing absolute paleointensity determinations: Acceptance criteria and the software ThellierTool4. *O. Geochem. Geophys. Geosyst.* 5 (12).
- Mahgoub, A.N., Böhnel, H., Siebe, C., Chevrel, M.O., 2017. Paleomagnetic study of El Metate shield volcano (Michoacán, Mexico) confirms its monogenetic nature and young age (~ 1250 CE). *J. Volcanol. Geotherm. Res.* 336, 209–218.
- Malin, S.C.R., Bullard, E., 1981. The direction of the Earth's magnetic field at London, 1570–1975. *Philosophical Transactions of the Royal Society of London. Series A, Mathematical and Physical Sciences* 299 (1450), 357–423.
- O'Reilly, W., 2012. Rock and Mineral Magnetism. Springer Science & Business Media.
- Oliva-Urcia, B., Kontny, A., 2012. Remanent magnetization of maghemitized basalts from Krafla drill cores, NE-Iceland. *Studia Geophys. Geod.* 56 (3), 641–657.
- Paterson, G.A., Tauxe, L., Biggin, A.J., Shaar, R., Jonestrask, L.C., 2014. On improving the selection of Thellier-type paleointensity data. *Geochem. Geophys. Geosyst.* 15 (4), 1180–1192.
- Pavón-Carrasco, F.J., Osete, M.L., Torta, J.M., De Santis, A., 2014. A geomagnetic field model for the Holocene based on archaeomagnetic and lava flow data. *Earth Planet. Sci. Lett.* 388, 98–109.
- Sherrod, D.R., Hagstrum, J.T., McGeehin, J.P., Champion, D.E., Trusdell, F.A., 2006. Distribution, 14C chronology, and paleomagnetism of latest Pleistocene and Holocene lava flows at Haleakalā volcano, Island of Maui, Hawai'i: a revision of lava flow hazard zones. *J. Geophys. Res.: Solid Earth* 111 (B5).
- Tanaka, H., Kono, M., 1991. Preliminary results and reliability of palaeointensity studies on historical and 14C dated Hawaiian lavas. *J. Geomagn. Geoelectr.* 43 (5), 375–388.
- Tauxe, L., 2006. Paleomagnetic Principles and Practice, vol. 17 Springer Science & Business Media.
- Thellier, E., 1938. Sur l'aimantation des terres cuites et ses applications géophysiques.
- Thellier, E., Thellier, O., 1959. Sur l'intensité du champ magnétique terrestre dans la passé historique et géologique. *Ann. Geophys.* 15, 285–376.
- Walton, D., Snape, S., Rolph, T.C., Shaw, J., Share, J., 1996. Application of ferrimagnetic resonance heating to palaeointensity determinations. *Phys. Earth Planet. In.* 94 (3–4), 183–186.

Capítulo 6

Critical analysis of the Holocene palaeointensity database in Central America: Impact on geomagnetic modelling

Gwenaël Hervé^a, Mireille Perrin^a, Luis Alva-Valdivia^b, Brina Madingou Tchibinda^a, Alejandro Rodriguez-Trejo^b, Arnaldo Hernandez-Cardona^b, Mario Córdova Tello^c, Carolina Meza Rodriguez^c

^a Aix Marseille Univ, CNRS, IRD, INRA, Coll France, CEREGE, Aix-en-Provence, France

^b Universidad Nacional Autónoma de México: Instituto de Geofísica, Laboratorio de Paleomagnetismo, Mexico City, Mexico

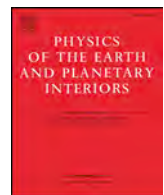
^c Instituto Nacional de Antropología e Historia, Centro Morelos, Mexico

ABSTRACT

Thanks to its rich archaeological heritage, Central America is a key region to recover the past secular variation of the geomagnetic field. This article presents 13 new palaeointensity data on Epiclassic (650 – 900 CE) pottery sherds from Central Mexico. Archaeointensities were determined using the Thellier-Thellier protocol with anisotropy and cooling rate corrections. Average results between 25 and 42 µT reveals a fast secular variation in the second half of the first millennium CE but are not in agreement with global geomagnetic models that predict a higher geomagnetic field strength. To check the reasons of this discrepancy, we compiled all intensity data over the last millennia published in Central America. The Bayesian curve calculated from 194 data covering the last 4 millennia highlights a rapid succession of oscillations of the geomagnetic field strength between 20 and 80 µT. But a critical analysis of the dataset shows a large influence of data quality, 74% of them having a poor cooling unit consistency and experimental quality. The small number of specimens per cooling unit and the anisotropy correction absent or incorrectly made increase the scatter between data, whereas the absence of cooling rate correction biases the dataset towards higher palaeointensity. Discarding these data results in a lower secular variation by removing most extreme values and several intensity oscillations. The weaknesses of the dataset are likely the main reason of the limitations of global models in Central America. Pending the acquisition of new high-quality data, archaeomagnetic dating seems premature in Central America.

<https://doi.org/10.1016/j.pepi.2019.02.004>

Received 19 September 2018; Received in revised form 16 January 2019; Accepted 1 February 2019



Critical analysis of the Holocene palaeointensity database in Central America: Impact on geomagnetic modelling



Gwenaël Hervé^{a,*}, Mireille Perrin^a, Luis Alva-Valdivia^b, Brina Madingou Tchibinda^a, Alejandro Rodriguez-Trejo^b, Arnaldo Hernandez-Cardona^b, Mario Córdova Tello^c, Carolina Meza Rodriguez^c

^a Aix Marseille Univ, CNRS, IRD, INRA, Coll France, CEREGE, Aix-en-Provence, France

^b Universidad Nacional Autónoma de México: Instituto de Geofísica, Laboratorio de Paleomagnetismo, Mexico City, Mexico

^c Instituto Nacional de Antropología e Historia, Centro Morelos, Mexico

ARTICLE INFO

Keywords:

Geomagnetic secular variation
Palaeointensity
Central America
Ceramics

ABSTRACT

Thanks to its rich archaeological heritage, Central America is a key region to recover the past secular variation of the geomagnetic field. This article presents 13 new palaeointensity data on Epiclassic (650 – 900 CE) pottery sherds from Central Mexico. Archaeointensities were determined using the Thellier-Thellier protocol with anisotropy and cooling rate corrections. Average results between 25 and 42 µT reveals a fast secular variation in the second half of the first millennium CE but are not in agreement with global geomagnetic models that predict a higher geomagnetic field strength. To check the reasons of this discrepancy, we compiled all intensity data over the last millennia published in Central America. The Bayesian curve calculated from 194 data covering the last 4 millennia highlights a rapid succession of oscillations of the geomagnetic field strength between 20 and 80 µT. But a critical analysis of the dataset shows a large influence of data quality, 74% of them having a poor cooling unit consistency and experimental quality. The small number of specimens per cooling unit and the anisotropy correction absent or incorrectly made increase the scatter between data, whereas the absence of cooling rate correction biases the dataset towards higher palaeointensity. Discarding these data results in a lower secular variation by removing most extreme values and several intensity oscillations. The weaknesses of the dataset are likely the main reason of the limitations of global models in Central America. Pending the acquisition of new high-quality data, archaeomagnetic dating seems premature in Central America.

1. Introduction

Ground-based and satellite measurements of the geomagnetic field, together with numerical models of the geodynamo, provide a priceless insight of the flux dynamic in the Earth's core. However, this knowledge is limited in time because direct absolute measurements cover a short era, at the most the last four centuries. Beyond, secular variation is recovered from archaeological baked clays, volcanic lava flows and marine or lacustrine sediments. The first two materials acquire a thermoremanent magnetization (TRM) during their last high-temperature heating and give an absolute but discrete estimation of the direction and intensity of the past geomagnetic field. Sediments have the advantage to provide a continuous record of the secular variation but palaeointensity and declination are only relative and require a calibration with absolute data (Panovska et al., 2015).

Several global models of the Holocene secular variation have been

developed by inversion of data using spherical harmonic analysis in space (e.g. Constable et al., 2016; Hellio and Gillet, 2018; Licht et al., 2013; Nilsson et al., 2014; Pavón-Carrasco et al., 2014a). These models are powerful tools to investigate the evolution of the geomagnetic patterns at the core-mantle boundary (e.g. Constable et al., 2016) and to scale cosmogenic nuclides production (Lifton, 2016). The local predictions of the global models are also more and more used for archaeomagnetic dating purposes (e.g. Goguitchaichvili et al., 2016). However, these global models tend to smooth the amplitude of the secular variation observed in regional master curves (e.g. Tema et al., 2017 in Hawaii; Cai et al., 2016 in China; Hervé et al., 2017 in Western Europe), especially for the intensity variations and even more when models include relative sedimentary data. Models built only with absolute data would better fit the data but their spatial and temporal distribution is very uneven, with ~70% of them coming from West Eurasia and North Africa and ~70% dated in the last two millennia. Data are especially

* Corresponding author at: IRAMAT-CRP2A, LabEx LaScArBx, Univ Bordeaux Montaigne, CNRS, Bordeaux, France.

E-mail address: gwenael.herve@u-bordeaux-montaigne.fr (G. Hervé).

lacking in the south hemisphere.

Another limitation is the unequal quality of the data. The impact of this factor on geomagnetic modelling is often underestimated, although it has been demonstrated with the European model SCHA.DIF.3 k (Pavón-Carrasco et al., 2014b). The archaeomagnetic databases, the most complete one being Geomagia50 (Brown et al., 2015), compile all results without *a priori* assessment on the quality of the data point. However, the quality is clearly heterogeneous, as depicted by the number of samples, the experimental and temporal uncertainties and the laboratory protocols. Here, we first present thirteen new intensity data acquired on potteries from Chalcatzingo in Mexico, before to show the influence of a critical analysis on the knowledge of secular variation of the geomagnetic field with the example of the intensity in Central America.

2. New archaeointensity data

2.1. Archaeological context and sampling

Chalcatzingo (Lat: 18.6766°N, Long: 98.7705°W) is located in the Amatzinac valley (Morelos state) at circa 120 km South-East of Mexico City (Fig. 1). The archaeological site has been excavated since the 30 s and presently Mario Córdova Tello and Carolina Meza Rodríguez from the *Instituto Nacional de Antropología e Historia* (INAH) direct the research program. The site was mainly occupied between 800 and 500 BCE during the Preclassic period. The archaeological remains, the most famous being the Olmec style petroglyphs, attest of the importance of the site in the region (e.g. Grove, 1987). The occupation continued later in the Classic (200–650 CE), Epiclassic (650–900 CE) and Postclassic (900–1500 CE) periods of the Central Mexico chronology.

This study focused on the Epiclassic layers from the Terrace 6 “El Cazador”, close to the main square and the pyramid. We sampled 16 sherds of six pottery-types, characteristic of this period in the Amatzinac valley (Martin Arana, 1987): *negro pulido* (2 sherds), *anaranjado rojo estriado* (3), *anaranjado pulido* (2), *anaranjado burdo* (3), *estriado sin engobe* (3) and *Coyotlatelco* (3).

2.2. Rock magnetism

Thermomagnetic curves were measured on powders from six sherds using Agico MFK1 apparatus. The variation of the susceptibility was measured during heating to 450 °C or 620 °C and subsequent cooling. All thermomagnetic curves were reversible, highlighting the suitability

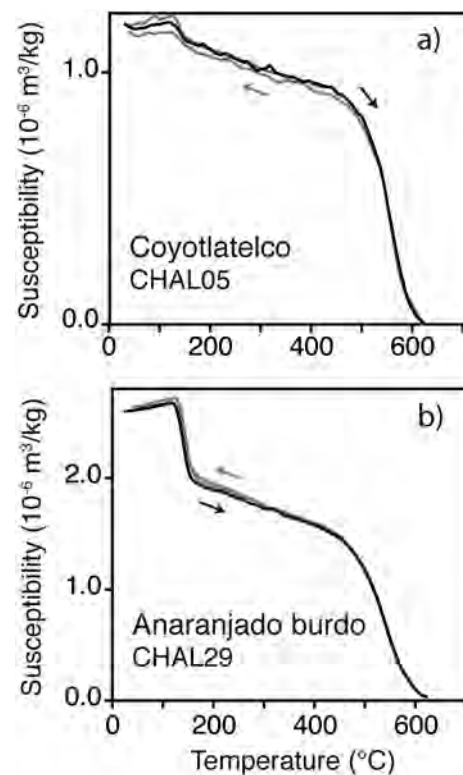


Fig. 2. Representative thermomagnetic curves of Epiclassic sherds from Chalcatzingo.

of Chalcatzingo sherds for archaeointensity experiments. We observed two groups of specimens. The types *anaranjado rojo estriado*, *anaranjado pulido* and *negro pulido* showed a single ferromagnetic carrier, identified as a Ti-poor titanomagnetite by the Curie temperature around 550 °C (Fig. 2a). The *Coyotlatelco*, *estriado sin engobe* and *anaranjado burdo* types presented a second phase with a Curie temperature close to 150 °C (Fig. 2b), which can be a Ti-rich titanomagnetite or an epsilon iron oxide (ϵ -Fe₂O₃) (López-Sánchez et al., 2017).

2.3. Archaeointensity study

Archaeointensity experiments were conducted on 0.6–3.0 g specimens embedded in 2 cm cubes of amagnetic plaster. We used the classical Thellier-Thellier method (Thellier and Thellier, 1959) that consists to heat and cool twice the specimens at each temperature step with a laboratory field applied in both directions of a specimen axis (+z, -z). We performed partial thermoremanent magnetization (pTRM) checks every two steps to monitor the absence of alteration of the ferromagnetic mineralogy. Heating was performed in an ASC TD-48SC furnace with a 30 or 40 µT laboratory field using 9–12 temperature steps up to 620 °C. In total we studied 3 to 5 specimens per sherd for a total of 54 specimens. Measurements were realized on a SQUID cryogenic magnetometer (2G Enterprises, model 755R) at CEREGE.

The archaeointensities were corrected for the effects of TRM anisotropy and cooling rate. The TRM anisotropy tensor was determined at 550 °C using 6 positions (+x, -x, +y, -y, +z and -z axes) followed by a stability check (Chauvin et al., 2000). The cooling rate procedure of Gómez-Paccard et al. (2006) was carried out at the same temperature with a slow cooling over 5 h. This duration, explained by experimental constraints, may underestimate the archaeological cooling but an incorrect estimation of the duration seems to have a low impact on the accuracy of the archaeointensity (Hervé et al., xxxx, accepted). The anisotropy and cooling rate corrections were applied at the specimen level.

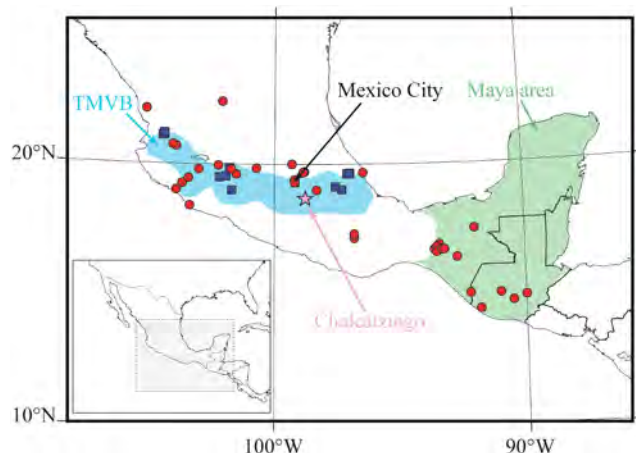


Fig. 1. Spatial distribution of Central America data over the last 4 kyrs. Archaeomagnetic (volcanic) data are plotted in red (blue). The pink star indicates the location of Chalcatzingo. TMVB is the abbreviation of Trans Mexican Volcanic Belt. (For interpretation of the references to colour in this figure legend, the reader is referred to the web version of this article.)

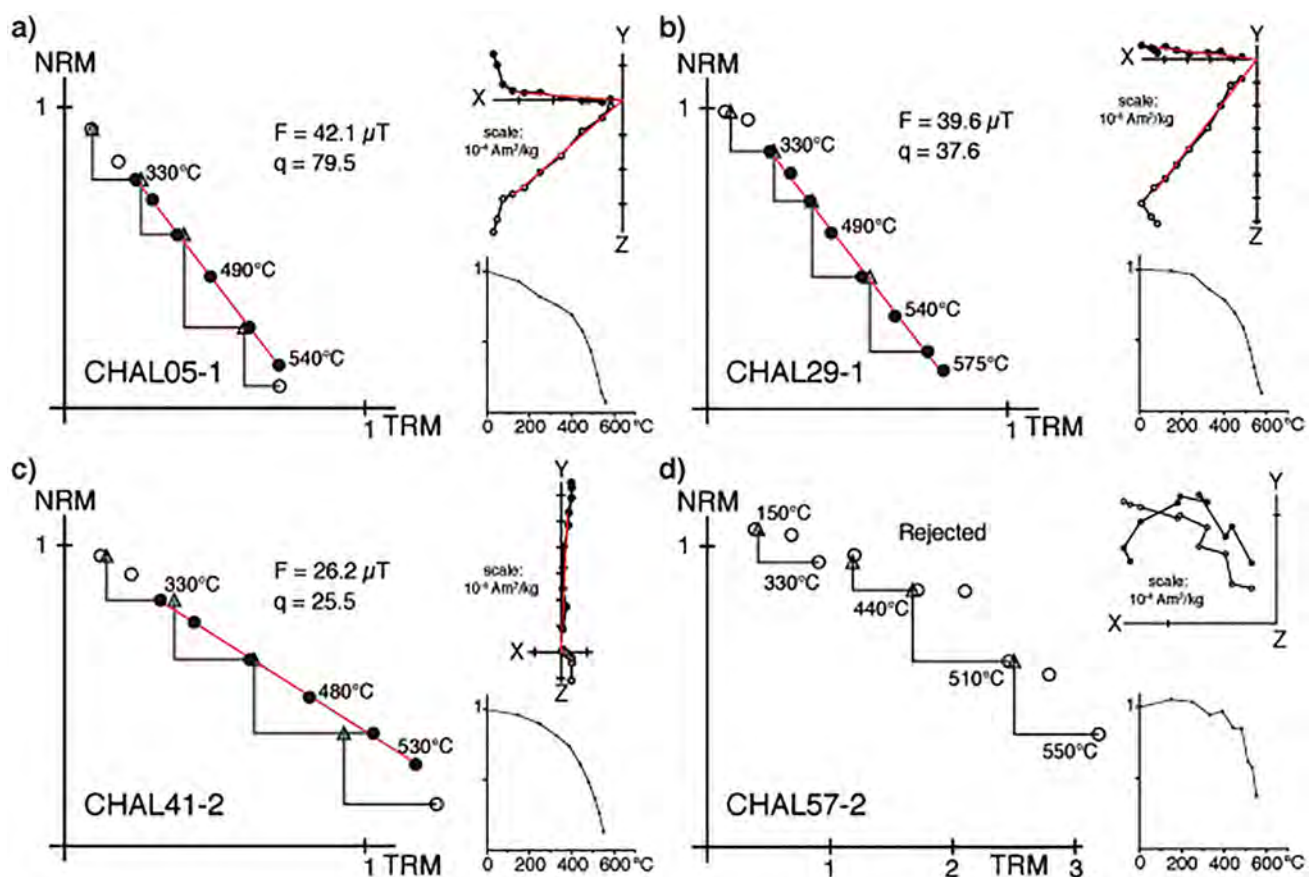


Fig. 3. Representative accepted (a–c) and rejected (d) archaeointensity results with NRM-TRM diagrams, orthogonal plots and demagnetization curves.

Almost all specimens presented a secondary component of magnetization. The characteristic remanent magnetization (ChRM) was isolated above 150–500 °C. The secondary component could be acquired during the cooking use of the pot or since the excavations in the archaeological repository. Except for one sherd, the fraction of the NRM in the ChRM (f factor) was higher than our acceptance value equal to 0.35. Forty-five specimens presented a linear NRM-TRM diagram with positive pTRM-checks on the temperature interval of the ChRM (Fig. 3a–c). The nine other specimens were rejected because of mineralogical changes, as indicated by non-linear NRM-TRM diagram and negative pTRM-checks (Fig. 3d). No results could be obtained for the two sherd of the type *negro pulido* and for one of the type *estriado sin engobe*.

Accepted specimens fulfil up-to-date quality criteria with a quality factor (q) between 5 and 80 (Table 1S, Supplementary Material). Almost all specimens had a ratio of the standard error of the slope to the absolute value of the slope (β) lower than 0.05, a deviation angle (DANG) lower than 5° and a maximum angular deviation (MAD) lower than 5°.

Table 1 listed the 13 new average archaeointensities. All were calculated with three or four specimens and have an experimental uncertainty between 1.5 and 9.5%. The range of the average values between 25 and 42 μT tend to indicate a fast secular variation during the second half of the first millennium CE. No clear relationship is observed between the archaeointensity and the pottery-type. On Fig. 4a, data are

Table 1

Average archaeointensities of Epiclassic sherd from Chalcatzingo. Columns from left to right: type of potteries, name of the sherd, number of accepted over measured specimens, average archaeointensity corrected for the effects of TRM anisotropy and cooling rate with its standard deviation, average archaeointensity relocated to Mexico City, Virtual Axial Dipole Moment.

Type of pottery	Sherd	$N_{\text{acc}}/N_{\text{meas}}$	$F_{\text{ATRM + CR}} \pm \text{SD} (\mu\text{T})$	$F_{\text{Mexico City}} (\mu\text{T})$	$VADM (10^{22} \text{ A.m}^2)$
Anaranjado rojo estriado	CHAL01	4/5	35.1 ± 3.0	35.4	7.9 ± 0.7
	CHAL02	3/5	34.5 ± 2.6	34.8	7.8 ± 0.6
	CHAL03	4/5	34.9 ± 1.0	35.2	7.9 ± 0.2
Coyotlatelco	CHAL04	3/4	31.5 ± 3.0	31.8	7.1 ± 0.7
	CHAL05	4/4	39.5 ± 2.0	39.9	8.9 ± 0.5
	CHAL06	3/4	42.3 ± 0.7	42.7	9.6 ± 0.2
Estriado sin engobe	CHAL22	4/4	36.4 ± 2.9	36.7	8.2 ± 0.7
	CHAL23	3/3	28.3 ± 0.9	28.6	6.4 ± 0.2
Anaranjado burdo	CHAL29	4/4	37.8 ± 0.7	38.1	8.5 ± 0.2
	CHAL30	3/3	39.7 ± 2.4	40.1	9.0 ± 0.5
	CHAL31	4/4	36.9 ± 1.8	37.2	8.3 ± 0.4
Anaranjado pulido	CHAL40	3/3	41.1 ± 2.0	41.5	9.3 ± 0.5
	CHAL41	3/3	24.7 ± 1.4	24.9	5.6 ± 0.3

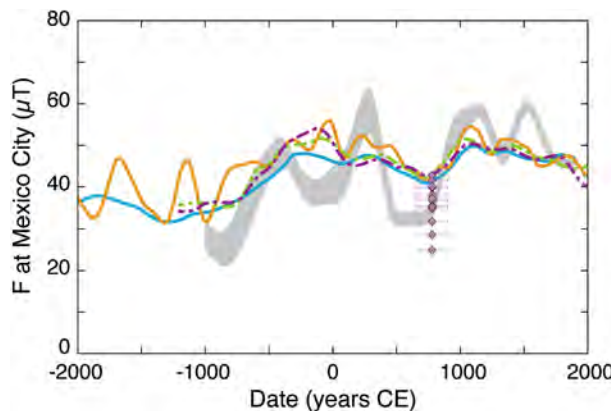


Fig. 4. Comparison of Chalcatzingo data relocated to Mexico City (in pink) with the bootstrap regional curve of Goguitchaichvili et al. (2018a) (in grey) and with the predictions of global models CALS10k.2 (Constable et al., 2016, blue curve), SHA.DIF.14 k (Pavón-Carrasco et al., 2014a, orange curve), COV-ARCH and COV-LAKE (Hellio and Gillet, 2018, green and purple dotted curves). (For interpretation of the references to colour in this figure legend, the reader is referred to the web version of this article.)

relocated to Mexico City using the Virtual Axial Dipole Moment (VADM) correction and compared to the regional curve of Goguitchaichvili et al. (2018a). The curve was computed using a bootstrap approach from 67 data from Mesoamerica and 17 from southwest United States. Our data matches the curve, except CHAL23 and CHAL41 that are below the curve.

Global models CALS10k.2 (Constable et al., 2016), SHA.DIF.14 k (Pavón-Carrasco et al., 2014a) and COV-ARCH/COV-LAKE (Hellio and Gillet, 2018) give consistent predictions at Mexico City. SHA.DIF.14 k and COV-ARCH were calculated using archaeomagnetic and volcanic data, whereas CALS10k.2 and COV-LAKE also include lacustrine and marine sedimentary data. Models also differ by the inverse method. CALS10k.2 and SHA.DIF.14 k imposed regularizations in space and time. The stochastic approach of COV-ARCH and COV-LAKE used the temporal statistics from satellites, ground-based and palaeomagnetic data as prior information through cross-covariance functions. The four models fit only the highest Chalcatzingo values. Their predictions are usually above the regional master curve of Goguitchaichvili et al. (2018a) and predict a slower secular variation.

3. Compilation of Central America intensity data

In order to check the reason of these discrepancies, we compiled all intensity data from Central America from the original articles (Fig. 5a). We carried out the critical analysis only on the last four millennia because data are much too scarce before (5 data between 5000 and 2000 BCE).

A data point is defined as a cooling unit that acquired TRM at the same time, such as a volcanic lava flow, an archaeological kiln or fireplace and a single pottery. For ceramics, a data point is sometimes defined in the literature as the average of independent pots (e.g. Genevey et al., 2016; Gómez-Paccard et al., 2016; Hervé et al., 2017), because they were discovered in a single homogeneous short-lived archaeological feature. This is not the case in Chalcatzingo and in most studies. Even if ceramics were dated in the same period, the probability of no contemporaneous cooling is high, because sherds came from different archaeological layers or from a single layer associated to a long-lived settlement.

The total number of intensity data in Central America over the last four millennia is 194 (including the 13 new data from Chalcatzingo) out of 40 different papers (Table S8 in Supplementary Material). 86% of these studies have been published after the 2000 s. Data from 16 studies are not yet included in the Geomagia database (this study; Böhnel et al.,

2016; Cifuentes-Nava et al., 2017; Goguitchaichvili et al., 2017, 2018b, c; Herrero-Bervera, 2015; Lopez-Tellez et al., 2008; Mahgoub et al., 2017a,b; Michalk et al., 2010; Morales et al., 2012, 2013, 2015; Rodriguez-Ceja et al., 2012; Terán-Gerrero et al., 2016). With this update, our dataset is almost twice larger than the one used in a recently published compilation of Mesoamerica (Goguitchaichvili et al., 2018a) that contains 106 data with only one study (Böhnel et al., 2016) published in the last five years.

Data are concentrated in Central Mexico around the 20°N parallel and in the Mayan area (Chiapas-Guatemala) (Fig. 1). Archaeological baked artefacts (here bricks, burnt walls, burnt soils and ceramics) constitute 87% of the dataset (168 data), the rest coming from volcanic lava flows of the Trans Mexican Volcanic Belt (TMVB). Only 17 data (9%), all volcanic, are full vector data.

Fifty-four cooling units were dated by radiocarbon. When the uncalibrated age was provided, we updated the date of the archaeomagnetic site using the most recent calibration curve IntCal13 (Reimer et al., 2013). In the case of Xitle lava flow, we used the newest age, 1670 ± 35 uncal. BP, of Siebe (2000). Twelve data come from historical eruptions since the Spaniards conquest, the youngest being the Paricutin in 1943–1952. For the 115 others data (i.e. 58%), the dating was defined by stratigraphy or typology of archaeological artefacts. The temporal density of data is higher in the periods of Late Preclassic (circa 400 BCE – 200 CE), Classic (circa 200 – 650 CE) and the youngest half of Postclassic (circa 1200 – 1500 CE) (Fig. 5a). Two important gaps are observed, the first between 800 and 400 BCE and the youngest around 1000 CE.

The intensity values over the last 4 kyrs range between ~ 15 μ T and ~ 90 μ T (Fig. 5b). The dataset looks cloudy, especially in the third and four centuries CE with values from 15 μ T up to 75 μ T. The spread is visually increased by the fact that many data are dated in the same age interval corresponding to an archaeological period, generally wide of several centuries. This tends to divide the dataset in successive time slices, modelled on the archaeological chronologies. The variability of intensities may reflect the secular variation within each archaeological period.

An intensity secular variation curve was computed using a Bayesian framework (Hervé and Lanos, 2018; Lanos, 2004; Schnepp et al., 2015). The curve is given as a smooth continuous curve obtained by averaging cubic splines and took into account experimental and age uncertainties as prior information. The misfit of each data to the curve is minimised by exploring the multidimensional space of probability densities using Monte Carlo Markov Chains. The curve presents a rapid succession of oscillations of the geomagnetic field strength, especially from 400 BCE to 1500 CE, at the time of the highest data density. The oscillations represent the best fit to the intensity variability within the time slices related to age uncertainties. They can imply a fast secular variation of many dozens of μ T over a few centuries, similar to the rates observed in the Levantine area at the beginning of the first millennium BCE (Shaar et al., 2011). But it can also reflect experimental problems and a critical analysis of the database has to be performed, before to evoke a geomagnetic phenomenon.

4. Critical analysis

4.1. Challenges in palaeointensity determination

The linearity between the intensity of the thermoremanent magnetization and the past geomagnetic field strength is the physical basis of the palaeointensity determination. Acquiring reliable data remains a challenging task because several effects can lead to a departure away from the linearity (see Dunlop, 2011 for a review). The required reciprocity of blocking and unblocking temperatures is only verified for single-domain grains without interactions. Alteration of the magnetic grains when heated at the laboratory is another cause of failed experiments. Moreover, palaeointensities should be determined only on

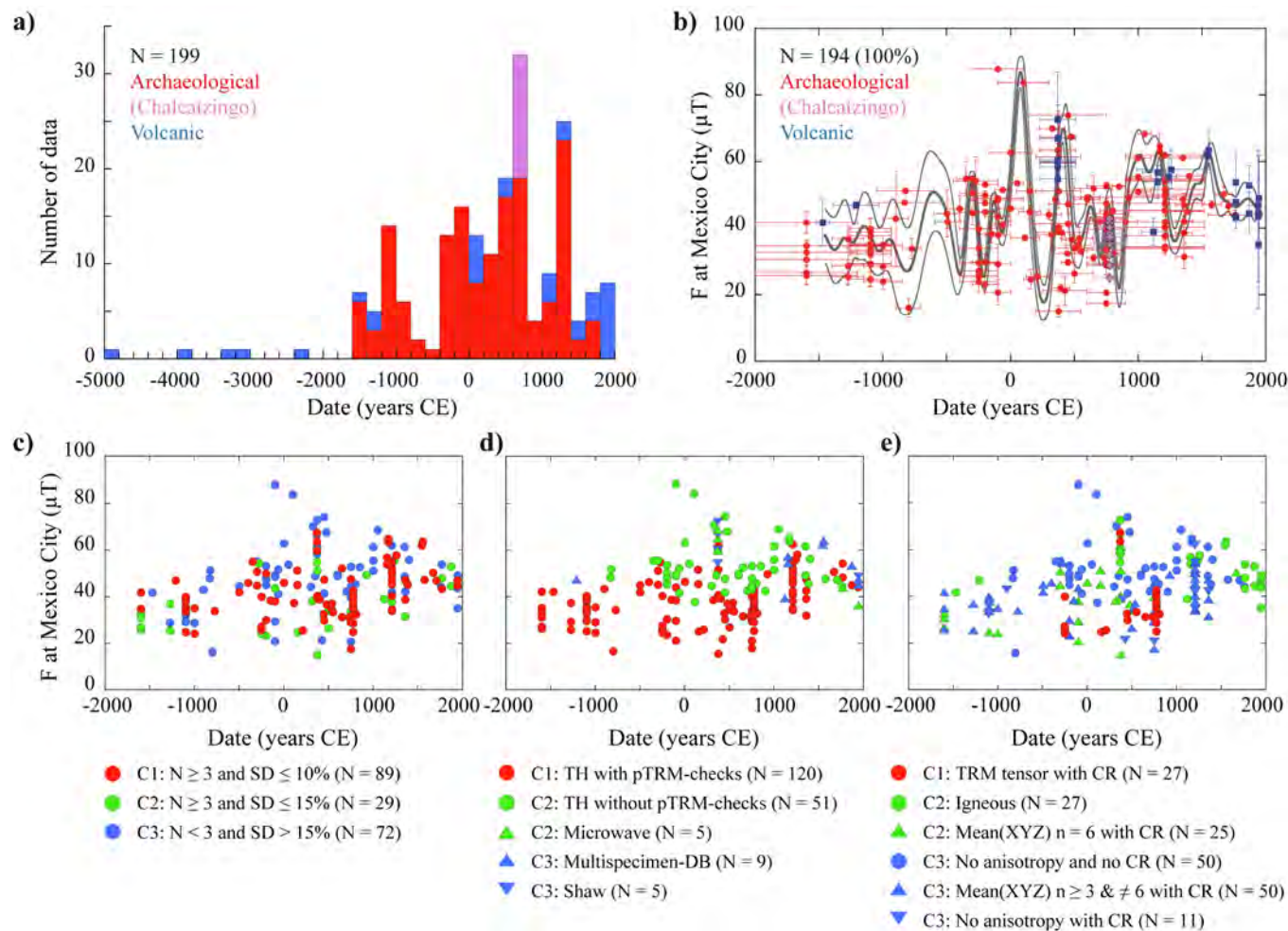


Fig. 5. Critical analysis of the Central American palaeointensity dataset. (a) Temporal distribution of data over the last 7k yrs. (b) Compilation of all archaeomagnetic (in red) and volcanic (in blue) data. The grey curve with its 1σ confidence envelope is computed using a Bayesian method. (c) Ranking of the dataset according to the cooling unit consistency. (d) Ranking according to the quality of the intensity protocol. (e) Ranking according to the consideration of the anisotropy effect. For each criterion, data are ranked in three levels C1, C2 and C3 from the highest to the lowest quality. Plots (c-d-e) excluded four data defined on a secondary component from Rodriguez-Ceja et al. (2009, 2012). TH: Thellier-Thellier protocols; Multispecimen-DB: original multispecimen protocol of Dekkers and Böhnel (2006); N: number of data; For data using Mean (XYZ) anisotropy correction, n: number of specimens used in the average intensity. (For interpretation of the references to colour in this figure legend, the reader is referred to the web version of this article.)

the Characteristic Remanent Magnetization (ChRM) acquired during the last heating above the Curie point. A calculation including a secondary component of magnetization can differ by a few dozens of μT from the intensity calculated on the sole ChRM (Hervé et al., 2013).

The Thellier-Thellier protocol (Thellier and Thellier, 1959) and its derived versions are admitted as the most reliable to control the respect of these conditions thanks to the progressive heating steps and the use of pTRM-checks. But the multiple heatings increase the risk of alteration and alternative protocols were developed.

The microwave (MW) technique (Walton, 1991; Walton and Böhnel, 2008) is based on microwave absorption by magnetic grains using progressive frequency steps, which reduces the heating temperature of the sample. This method does not exactly replicate the acquisition process of the initial TRM, as ferromagnetic grains are excited by magnons instead of phonons in the usual thermal techniques.

The multispecimen (MSP) method is performed on a set of specimens from the same sample. All specimens are heated once at the same temperature (usually in the 300–400 °C temperature range) in different laboratory field values applied parallel to the NRM (Dekkers and Böhnel, 2006). The comparison of the demagnetized NRM intensity with the one of the acquired partial-TRM provides the palaeointensity. The Central American MSP data were obtained with the original

protocol of Dekkers and Böhnel (2006), which do not correct for the NRM fraction and domain state as advised by Fabian and Leonhardt (2010). They are therefore likely overestimated (Schnupp et al., 2016).

Finally, the Shaw method (Shaw, 1974) compares the alternating field (AF) demagnetization of the NRM with the one of a full laboratory TRM. The scaling factor between the two demagnetizing curves is an estimate of the ratio between ancient and laboratory fields. But the linearity between the magnetization and geomagnetic field cannot be checked and the palaeomagnetic community generally considers this method of lower quality.

It is well known that the cooling rate has an important effect on the palaeointensity of archaeological baked clays. The TRM intensity of single-domain grains increases with the cooling rate duration (e.g. Dodson and McClelland-Brown, 1980). As the laboratory cooling is faster than the archaeological cooling, uncorrected palaeointensities are generally overestimated. In the case of the volcanic lava flows, the correction is usually not considered necessary, because the coarser mineralogy makes them less sensitive to the cooling rate effect. For the thick Xitle lava flow, the correction improves the precision of the palaeointensity but does not change significantly the palaeointensity average (Morales et al., 2006) (Table 4S).

The anisotropy correction is also crucial depending on the type of

material. The preferential alignment of the iron oxides during the manufacturing process of baked clays results in distortion of the NRM with respect to the surrounding geomagnetic field (Veitch et al., 1984). Potteries are generally anisotropic and palaeointensity can sometimes be biased up to a factor of two (e.g. Hervé et al., 2017; Ose et al., 2016). The effects can also be high in burnt walls and soils (Palencia-Ortas et al., 2017; Molina Cardin et al., 2018). Conversely, the influence of the TRM anisotropy is assumed negligible in lava flows. But the robustness of this presupposition can be questioned, as the anisotropy of magnetic susceptibility (AMS) is often significant and used as a proxy for flow direction (e.g. Fanjat et al., 2012).

Two different anisotropy corrections were used in the Central American dataset, first the determination of the TRM tensor at the specimen level (Chauvin et al., 2000, see Section 2.3) and secondly a method, peculiar to Mexico, that we called in the following Mean (XYZ) method. Each baked clay fragment is cut in 6 mini-specimens keeping the same orientation. The laboratory field during the Thellier experiments is applied along +x axis for one specimen, -x for another one and +y, -y, +z or -z axis for the four others. Averaging of the six individual intensity estimations is considered to properly correct the TRM anisotropy effect. Poletti et al. (2016) questioned the reliability of this approach. They calculated the TRM tensor at two different temperatures and then roughly determined the intensities from the slope between the two +x TRMs (and -x...) on the NRM-TRM diagram. Their results show that the Mean (XYZ) method results in imprecision and sometimes in inaccuracies up to 10 µT.

4.2. Validity of the Mean (XYZ) anisotropy correction

To further test the reliability of this correction, we performed the Mean (XYZ) and the TRM tensor methods on five samples. The first two, 11369B-1 and 11369B-11, are small bricks baked in an experimental kiln in Sallèles-d'Aude (southern France). The last three, SAQ48, SAQ51 and SAQ54 are pottery sherds discovered in a sedimentary core from Saqqara (Egypt) and supposed to be from the Pharaonic era. Samples were cut in six identical cubic specimens, each positioned in a different position (+x, -x, +y, -y, +z or -z) in the laboratory furnace during the classical Thellier-Thellier protocol and the cooling rate correction. The tensor of TRM anisotropy was then determined with the same protocol as for Chalcatzingo samples. All specimens provided technically reliable intensity results (Fig. 1S and Table 3S in Supplementary Material). The degrees of TRM anisotropy have close values between 1.19 and 1.26 (Table 2).

Table 2 compares the averages intensities of the Mean (XYZ) and TRM anisotropy tensor methods, both being corrected for cooling rate effect. Without the TRM tensor correction, the palaeointensity values at the sample level are distributed over a large range up to 26 µT with systematic differences between axes. The highest palaeointensities values, i.e. the lowest acquired TRMs, are observed for specimens with the laboratory field applied along x axis, perpendicularly to the flattening plane of the brick or the pottery (Veitch et al., 1984). The correction by the TRM tensor groups the palaeointensities, which results in a standard

deviation up to five times lower. The Mean (XYZ) average palaeointensity differ of the TRM tensor value by only -5.6 to 3.8% (IE parameter in Table 2). No relationship seems exist between IE and the anisotropy degree or the standard deviation.

The anisotropy correction depends on the NRM direction within the TRM tensor. In our examples, the Mean(XYZ) palaeointensity is close to the TRM tensor value, because the NRM direction is intermediate between x, y and z axes and because averages are computed from six specimens with an equal contribution of the three axes. Data with two, and of course one, specimens cannot be considered as corrected by the anisotropy.

A balance between the three axes does not mean that one can be fully confident in the average palaeointensity value. If the NRM is parallel to one of the three axes, the two specimens with the laboratory field on this axis will give the true palaeointensity and the inaccuracy can be larger. In the case of SAQ51, if the NRM were close to x-axis, the true palaeointensity would have been around 102–103 µT, whereas the average of the six specimens is $85.5 \pm 11.5 \mu\text{T}$ (Table 3S, Supplementary Material).

For all these reasons, the Mean (X-Y-Z) method enhances noise in a dataset with larger standard deviations and possible high inaccuracies. All Mean (XYZ) palaeointensities can be biased even if the risk is reduced for those calculated with a balanced participation of the three x, y and z axes. Data corrected with the TRM tensor are clearly much more reliable from an experimental point of view.

4.3. Data selection

Estimate a posteriori the quality of a palaeointensity is not straightforward without the raw measurements. Four intensities from Rodriguez-Caja et al. (2009, 2012) have been defined on a secondary component and clearly have to be removed. Another obvious criterion is the expected internal consistency within a given cooling unit. We classified data in three categories according to the number of specimens and the standard deviation (Fig. 5c). Highest quality data (category C1) have at least 3 specimens per cooling unit and a standard deviation (SD) lower than 10%. Those in the second category (C2) have a SD lower than 15%. Other data (C3) represent 38% of the full dataset (i.e. 72 data) in similar proportions for volcanic and archaeomagnetic data (Fig. 5c). One can note that most extreme values are included in this category.

The criterion of the consistency is useful but cannot screen all problems in the palaeointensity protocol (Fig. 5d). For the reasons mentioned above, the most reliable protocol is the Thellier-Thellier protocol with pTRM-checks. This category (C1) is dominant in the dataset (120/190 data). Our mid-quality category (C2) groups microwave data and Thellier-Thellier data without pTRM-checks. We did not assign the latter to the lowest quality category because often it corresponds to the oldest data, as it is the case here (51 data almost all from Bucha et al., 1970; Lee, 1975), when pTRM-checks were not commonly used. Furthermore, the interpretation of pTRM-checks is not straightforward and experience shows that reliable palaeointensity can be obtained with

Table 2

Comparison of intensities determined with the two corrections of anisotropy. For both methods are indicated the minimal and maximal specimen intensity, the mean intensity and its standard deviation in microTeslas and in percentage. All intensities are corrected for the cooling rate effect. IE is the difference in percentage of the Mean (XYZ) intensity with the TRM tensor intensity. k_{\max}/k_{\min} is the average degree of TRM anisotropy.

Sample	Mean (XYZ)					TRM tensor						
	F _{min} (µT)	F _{max} (µT)	F _{mean} (µT)	SD (µT)	SD (%)	F _{min} (µT)	F _{max} (µT)	F _{mean} (µT)	SD (µT)	SD (%)	IE (%)	k_{\max}/k_{\min}
11369B1	45.0	52.3	50.0	2.6	5.2	51.1	54.4	50.9	1.2	2.3	-1.7	1.19
11369B11	45.0	56.6	47.6	4.4	9.2	49.9	53.4	50.5	1.2	2.3	-5.6	1.25
SAQ48	65.8	79.4	71.5	4.7	6.6	76.0	82.7	74.3	2.5	3.4	-3.7	1.20
SAQ51	74.8	100.7	85.5	11.5	13.5	83.2	87.5	82.3	2.5	3.0	3.8	1.25
SAQ54	74.9	99.3	83.8	9.6	11.5	81.1	89.6	83.1	3.4	4.1	0.8	1.26

moderate deviation if the linearity is well maintained over a large NRM proportion. However, the absence of alteration monitoring casts a doubt on the reliability of these data. Finally, the low-quality category (C3) includes the nine multispecimen data without the correction of the NRM fraction (MSP-DB), because they likely overestimate the palaeointensity. The five data acquired with the Shaw protocol also belong to this category.

As archaeological baked clays constitute 86% of the dataset (164/190 data) whose 85% are ceramics (139 data), cooling rate and anisotropy corrections are crucial. For archaeological baked clays, we demonstrated that the anisotropy correction with the TRM tensor is the most reliable (category C1). Two microwave data on potteries associated to the Xitle lava flow are also included in C1 (Böhnel et al., 2003), because the laboratory field was applied parallel to the NRM. Only 27 data are part of this high-quality category (Fig. 5e). Both corrections are assumed not mandatory for igneous material. But this is not fully attested and we preferred to assign these data to the mid-quality C2 category. Regarding the Mean(XYZ) correction, the balanced contribution between x, y, and z axes can be attested only for the 25 average intensities calculated with six specimens. We classified them in the C2 category, bearing in mind that some can be inaccurate especially if the NRM was parallel to a specimen axis. Another number of specimens gives preponderance to one or two axes, which can result in larger inaccuracies and justifies their attachment to the C3 category. Data calculated with three and four specimens are actually more scattered (Fig. 2S, Supplementary Material). The C3 category finally includes the 61 archaeological data without any anisotropy correction, 11 of them being corrected for the cooling rate effect.

The synthesis of this critical analysis ranks the dataset in three groups, C1, C2 and C3. Data of the high quality group (C1) belong to the three C1 categories of the cooling unit consistency, protocol and anisotropy and cooling rate corrections at the same time. They are only 23, i.e. 12% of the initial dataset, (Chalcatzingo data, this study; Fanjat et al., 2013; Rodriguez-Caja et al., 2009, 2012 – only intensities determined on the characteristic magnetization), all dated between 400 BCE and 900 CE (Fig. 6a).

The group C2 gathers data classified at least in the C2 category for the three criteria. The El Jorullo and Xitle lava flows were duplicated in respectively two and four studies and we computed new averages from the same accepted specimens as the authors (Table 4S, Supplementary Material). In the case of the Xitle, the average ($59.8 \pm 5.0 \mu\text{T}$) takes into account only the palaeointensities corrected for the cooling rate effect on the TRM intensity (Fig. 6a).

All other data, those belonging to at least one C3 category, constitute 72% of the dataset (140 data) with almost all the oldest acquired data (Bucha et al., 1970; Lee, 1975). These 50 data on potteries with no anisotropy and cooling rate corrections provide higher palaeointensities than other data (blue circles, Fig. 5e). If the weak cooling consistency influences their scatter, the overestimation very likely results from absence of the cooling rate correction.

5. Discussion

5.1. Impact of the critical analysis on the knowledge of the secular variation

The large number of palaeointensities available for the last kyr in Central America may give the impression that the secular variation curve is well-known, with large and fast variations between 20 and 80 μT . However, the critical analysis shows that many of these oscillations are induced by experimental errors. The main sources of scatter are the absence of cooling unit consistency, the lack or inaccuracy of anisotropy correction and the absence of cooling rate correction on archaeological artefacts. Only 12% of data (23 data) can be considered as high quality (C1 category) that is not enough to compute an intensity secular variation curve. Therefore we also included the 14% of the data (27 data) corresponding to the middle quality (C2 category) (Fig. 6a).

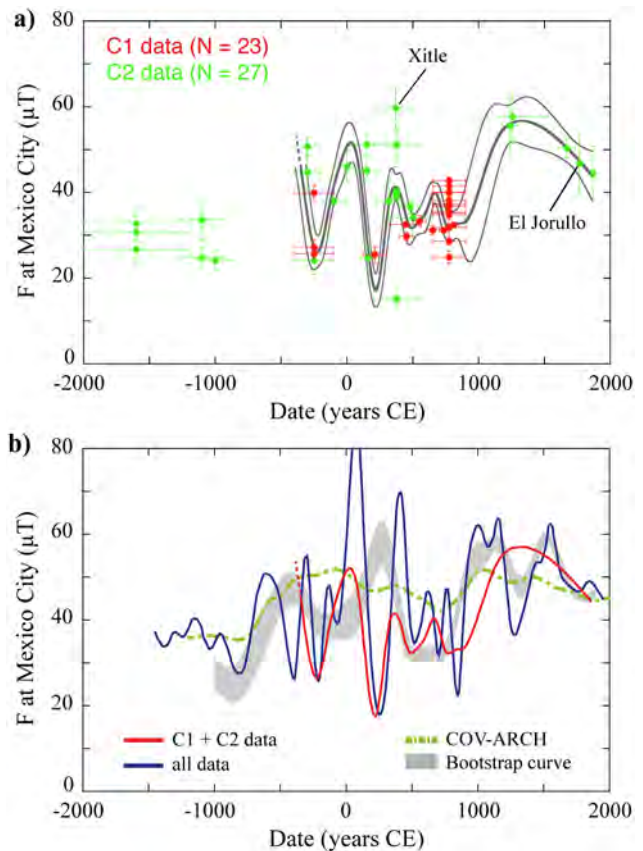


Fig. 6. (a) Secular variation inferred from high-quality data. (b) Comparison of the two Bayesian curves calculated from the total and selected dataset (blue and red curves) with the master curve of Goguitchaichvili et al. (2018a) (grey curve) and with COV-ARCH global model (green dotted curve). (For interpretation of the references to colour in this figure legend, the reader is referred to the web version of this article.)

All data used in the Bayesian curve are plotted per study in Fig. 3S (Supplementary Material).

It is worth pointing out that the selection does not take into account the age uncertainties and inaccuracies in age, perhaps affecting some of the selected data. That could be the case for the Xitle lava flow, whose intensity seems more consistent with an age at the turning point of the Christian era than in the IVth and Vth centuries CE (Fig. 6a). We decided to use the most recently acquired age 1670 ± 35 uncal. BP (Siebe, 2000) on a charcoal included in the lava flow sampled for the palaeomagnetic studies. But other published radiocarbon ages, 1945 ± 55 uncal BP and 2025 ± 55 uncal BP (Delgado et al., 1998; see also Böhnel et al., 1997), dates the eruption of this monogenetic volcano in a more consistent way with other available quality data.

Selecting data has a strong influence on the secular variation reconstruction, as shown by the comparison of the averages Bayesian curves calculated from the entire and selected datasets (blue and red curves, Fig. 6b). After discarding extreme values, the secular variation has smaller amplitude between 20 and 60 μT . The better consistency of the dataset also removes most short-term oscillations of the curve calculated with all data.

The secular variation from ~ 400 BCE to ~ 500 CE is rather well constrained by high/middle quality C1 and C2 data. They highlight a fast variation with a $\sim 45 \mu\text{T}$ maximum in ~ 400 BCE, a $\sim 25 \mu\text{T}$ minimum in ~ 200 BCE, a further $\sim 50 \mu\text{T}$ maximum circa 0 CE and a $\sim 20 \mu\text{T}$ minimum in ~ 200 CE. Next, the field varied more slightly between 30 and 40 μT from ~ 400 to ~ 800 CE that is the period presenting the highest density of quality data.

On the other side, the lack of data and the large age uncertainties

make unclear the secular variation between 2000 and 400 BCE. Address this gap is crucial to better understand the highest secular variation and the largest departure from an axial dipolar field observed at this period in Eurasia (Hervé et al., 2017; Shaar et al., 2011).

Considering only high or middle quality data drastically reduces the available data set and one may wonder if we do not miss some geomagnetic variations. For example, there are only five high-quality data in the second millennium CE and it is not surprising to see that the curves differ during this period. If the high geomagnetic field strength around 50 μT is well constrained, the number of maxima, one or two, is unclear. Unselected data indicates a possible minimum ~ 1300 CE. The timing of the intensity increase is also not clear, either from 1000 CE with C1 and C2 categories or from 800 CE with unselected data.

Finally, the critical analysis of the Central America dataset drastically highlights the need of new high quality data with precise dating for almost all periods. It is clearly a prerequisite to ascertain the secular variation features and to compare the Central American curve to other regional records.

5.2. Comparison with others curves and global models

Our selected curve presents several differences with the bootstrap curve of Goguitchaichvili et al. (2018a), especially between 500 BCE and 500 CE (Fig. 6b). The major discrepancy occurs around 200 CE when they have a maximum and us a minimum. Different reasons could be the source of this inconsistency: (i) their critical analysis (at least 4 specimens, standard deviation lower than 10 μT , corrections of anisotropy and cooling rate) is pretty similar to ours except for the inclusion of all Mean(XYZ) data; (ii) the dataset of Goguitchaichvili et al. (2018a) duplicated data from the same lava flow (e.g. Xitle, El Jorullo, Cebouco, Paricutin) and (iii) included 17 data from southwest USA but not 28 data from Mexico out of the 50 that we classified in the C1 and C2 categories. Some differences between the curves are also related to the computation technique. The variability of intensity data circa 200 BCE is smoothed by the bootstrap method, whereas the Bayesian of Lanos (2004) interprets it by an intensity minimum. Both updated dataset and Bayesian approach likely provides a finer knowledge of the secular variation curve, even though as mentioned before it has to be confirmed by new reliable data.

The global models such as COV-ARCH are built using the Geomagia database without data selection. They are inconsistent with our curve as well as with Goguitchaichvili et al. (2018a) curve (Fig. 6b). First, they predict a smoother secular variation after 500 BCE with intensity varying between 40 and 50 μT , this range corresponding to the average intensity of the total dataset. The model did not succeed to interpret the high data variability and remains blocked in this intensity range. Another inconsistency is the shift to higher intensity values in comparison to our curve. The data of Bucha et al., 1970 and Lee (1975), not corrected for the cooling rate, constitute around 40% of the Central American data in Geomagia. The overestimation emphasizes the need for a selection with the cooling rate correction.

6. Conclusions

The acquisition of 13 new palaeointensities on Epiclassic (650 – 900 CE) sherds from Chalcatzingo completes the Central American database. The up-to-date compilation of 194 available data shows a high variability in palaeointensity during the last 4 millennia. A critical analysis of the database highlights that this variability cannot be only explained by a geomagnetic origin. Selecting data according to the cooling unit consistency and the intensity protocol discards extreme values and predicts less oscillations of the geomagnetic field strength. The results emphasize the importance of the cooling rate correction. Its absence yields to a shift of the geomagnetic reconstructions towards higher intensity values. Another problem, peculiar to the Central American dataset, is the use of an inaccurate anisotropy correction,

here called Mean (XYZ). According to experimental test, this method leads to systematic larger imprecisions and to possible inaccuracies up to 15 μT .

The example of Central America highlights the need of data selection global geomagnetic model. The absence of data selection clearly plays a role in the smoothing and overestimation of the curves inferred from global models compared to our master curve. Considering these problems, the use of current global models for dating purposes in Central America seems inappropriate.

Defining acceptance criteria is not straightforward in global modelling. Our criterion of the cooling unit consistency discards more than 50% of the global dataset and those based on the protocol $\sim 90\%$ (counting on Geomagia50.v3 in October 2018). This low proportion is hardly compatible with the homogeneous data coverage in space and in time that requires the spherical harmonic analysis. Our acceptance limits have to be lowered to better fit with the constraints of global modelling. Priority criteria could focus on parameters biasing the palaeointensity average, such consistency criteria, cooling rate correction for archaeological baked clays and anisotropy correction for potteries.

Acknowledgements

Funding was provided by ANR-CONACYT SVPIntMex project ANR-15-CE31-0011-01 coordinated by M. P. and L. A-V. G.H. also benefited from a support of Campus France PRESTIGE program (PRESTIGE-2017-1-0002). We thank the editor and the reviewer for their careful work. We are grateful to Gabrielle Hellio (Univ. Nantes) for transmitting the COV-ARCH and COV-LAKE predictions at Mexico City and to Philippe Lanos for providing the software to calculate Bayesian local secular variation curves. We acknowledge Mohamed Hamdan (Giza University) and Ahmed Saleh (NRIAG) for providing the pottery sherds from Saqqara.

Appendix A. Supplementary material

Supplementary data to this article can be found online at <https://doi.org/10.1016/j.pepi.2019.02.004>.

References

- Böhnel, H., Morales, J., Caballero Miranda, C., Alva, L., McIntosh, G., Gonzalez, S., Sherwood, G.J., 1997. Variation of rock magnetic parameters and Palaeointensities over a single Holocene lava flow. *J. Geomag. Geoelectr.* 49, 523–542.
- Böhnel, H., Biggin, A., Walton, D., et al., 2003. Microwave palaeointensities from a recent Mexican lava flow, baked sediments and reheated pottery. *Earth Planet. Sci. Lett.* 214, 221–236. [https://doi.org/10.1016/S0012-821X\(03\)00370-4](https://doi.org/10.1016/S0012-821X(03)00370-4).
- Böhnel, H., Pavón-Carrasco, F.J., Síeron, K., Mahgoub, A.N., 2016. Palaeomagnetic dating of two recent lava flows from Cebouco volcano, western Mexico. *Geophys. J. Int.* 207, 1203–1215. <https://doi.org/10.1093/gji/ggw310>.
- Brown, M.C., Donadini, F., Korte, M., Nilsson, A., Korhonen, K., Lodge, A., Lengyel, S.N., Constable, C.G., 2015. GEOMAGIA50.v3: 1. general structure and modifications to the archeological and volcanic database. *Earth Planets Space* 67, 1–31. <https://doi.org/10.1186/s40623-015-0232-0>.
- Bucha, V., Taylor, R.E., Berger, R., Haury, E.W., 1970. Geomagnetic intensity changes during the past 3000 years in the western hemisphere. *Science* 168, 111–114.
- Cai, S., Jin, G., Tauxe, L., Deng, C., Qin, H., Pan, Y., Zhu, R., 2016. Archaeointensity results spanning the past 6 kiloyears from eastern China and implications for extreme behaviors of the geomagnetic field. *Proc. Natl. Acad. Sci. USA* 114, 39–44. <https://doi.org/10.1073/pnas.1616976114>.
- Chauvin, A., García, Y., Lanos, P., Laubenheimer, F., 2000. Paleointensity of the geomagnetic field recovered on archaeomagnetic sites from France. *Phys. Earth Planet. Inter.* 120, 111–136.
- Cifuentes-Nava, G., Goguitchaichvili, A., López-Loera, H., Cervantes, M., Cortés, A., Sánchez-Bettucci, L., Macías, J.L., Morales, J., Rosas-Elguera, J., 2017. Full vector magnetic dating of some pyroclastic rocks associated to the Colima volcano, western Mexico. *Bol. Soc. Geol. Mex.* 69 (3), 577–590.
- Constable, C., Korte, M., Panovska, S., 2016. Persistent high paleosecular variation activity in southern hemisphere for at least 10,000 years. *Earth Planet. Sci. Lett.* 453, 78–86. <https://doi.org/10.1016/j.epsl.2016.08.015>.
- Dekkers, M.J., Böhnel, H.N., 2006. Reliable absolute palaeointensities independent of magnetic domain state. *Earth Planet. Sci. Lett.* 248, 508–517. <https://doi.org/10.1016/j.epsl.2006.05.040>.
- Delgado, H., Molinero, R., Cervantes, P., Nieto-Obregon, J., Lozano-Santa Cruz, R.,

- Macias-Gonzalez, H.L., Mendoza-Rosales, C., Silva-Romo, G., 1998. Geology of Xitle volcano in southern Mexico City – a 2000-year-old monogenetic volcano in an urban area. *Rev. Mex. Cien. Geol.* 15 (2), 115–131.
- Dodson, M.H., McClelland-Brown, E., 1980. Magnetic blocking temperatures of single-domain grains during slow-cooling. *J. Geophys. Res.* 85, 2625–2637.
- Dunlop, D.J., 2011. Physical basis of the Thellier-Thellier and related paleointensity methods. *Phys. Earth Planet. Inter.* 187 (3–4), 118–138. <https://doi.org/10.1016/j.pepi.2011.03.006>.
- Fabian, K., Leonhardt, R., 2010. Multiple-specimen absolute paleointensity determination: an optimal protocol including pTRM normalization, domain-state correction, and alteration test. *Earth Planet. Sci. Lett.* 297, 84–94.
- Fanjat, G., Camps, P., Shcherbakov, V., Barou, F., Sougrati, M.T., Perrin, M., 2012. Magnetic interactions at the origin of abnormal magnetic fabrics in lava flows: a case study from Kerguelen flood basalts. *Geophys. J. Int.* 189, 815–832. <https://doi.org/10.1111/j.1365-246X.2012.05421.x>.
- Fanjat, G., Camps, P., Alva Valdivia, L.M., Sougrati, M.T., Cuevas-Garcia, M., Perrin, M., 2013. First archeointensity determinations on Maya incense burners from Palenque temples, Mexico: new data to constrain the Mesoamerica secular variation curve. *Earth Planet. Sci. Lett.* 363, 168–180. <https://doi.org/10.1016/j.epsl.2012.12.035>.
- Genevey, A., Gallet, Y., Jasset, S., Thébault, E., Bouillon, J., Lefèvre, A., Le Goff, M., 2016. New archeointensity data from French Early Medieval pottery production (6th–10th century AD). Tracing 1500 years of geomagnetic field intensity variations in Western Europe. *Phys. Earth Planet. Inter.* 257, 205–219. <https://doi.org/10.1016/j.pepi.2016.06.001>.
- Goguitchaichvili, A., Morales, J., Aguayo Haro, R., Quiroz Castañón, H., Robles Camacho, J., 2016. First evidence of complex dental practice about 1300 BP in Mesoamerica revealed by absolute geomagnetic intensity. *Studia Geophys. Geod.* 61. <https://doi.org/10.1007/s11200-016-0851-3>.
- Goguitchaichvili, A., Ortega, V., Archer, J., Morales, J., Teran, A., 2017. Absolute geomagnetic intensity record from pre-Columbian pottery dates elite Tlailotlacan woman in ancient Teotihuacan. *J. Arch. Sci.: Rep.* 14, 146–151. <https://doi.org/10.1016/j.jasrep.2017.05.030>.
- Goguitchaichvili, A., Cervantes Solano, M., Lazcano Arce, J.C., Serra Puche, M.C., Morales, J., Soler, A.M., Urrutia-Fucugauchi, J., 2018c. Archaeomagnetic evidence of pre-Hispanic origin of Mezcal. *J. Arch. Sci.: Rep.* 21, 504–511. <https://doi.org/10.1016/j.jasrep.2018.08.022>.
- Goguitchaichvili, A., García, R., Pavón-Carrasco, F.J., Morales Contreras, J.J., Soler Arechalde, A.M., Urrutia-Fucugauchi, J., 2018a. Last three millennia Earth's Magnetic field strength in Mesoamerica and southern United States: implications in geomagnetism and archaeology. *Phys. Earth Planet. Inter.* 279, 79–91. <https://doi.org/10.1016/j.pepi.2018.04.003>.
- Goguitchaichvili, A., García-Ruiz, R., Echeverría, S., Morales, J., Ortiz, S., Urrutia-Fucugauchi, J., 2018b. Last two millenia Earth's magnetic field strength: New archeointensity determinations from Ichkaantijo, early to late maya classic period. *J. Arch. Sci.: Rep.* 18, 292–299. <https://doi.org/10.1016/j.jasrep.2018.01.023>.
- Gómez-Páccard, M., Chauvin, A., Lanos, P., Thiriot, J., Jiménez-Castillo, P., 2006. Archeomagnetic study of seven contemporaneous kilns from Murcia (Spain). *Phys. Earth Planet. Inter.* 157 (1–2), 16–32. <https://doi.org/10.1016/j.pepi.2006.03.001>.
- Gómez-Páccard, M., Osete, M.L., Chauvin, A., Pavón-Carrasco, F.J., Pérez-Asensio, M., Jiménez, P., Lanos, P., 2016. New constraints on the most significant paleointensity change in Western Europe over the last two millennia. A non-dipolar origin? *Earth Planet. Sci. Lett.* 454, 55–64. <https://doi.org/10.1016/j.epsl.2016.08.024>.
- Grove, D.C., 1987. *Ancient Chalcatzingo*. Austin University Press.
- Hellio, G., Gillet, N., 2018. Time-correlation based regression of the geomagnetic field from archeological and sediment record. *Geophys. J. Int.* <https://doi.org/10.1093/gji/ggy214>.
- Herrero-Bervera, E., 2015. Spot reading of the absolute paleointensity of the geomagnetic field obtained from potsherds (Age Ca. 500–430 AD) in Teotihuacan Mexico. *Arch. Disc.* 3, 72–84.
- Hervé, G., Chauvin, A., Lanos, P., 2013. Geomagnetic field variations in Western Europe from 1500 BC to 200 AD. Part II: new intensity secular variation curve. *Phys. Earth Planet. Inter.* 218, 51–65. <https://doi.org/10.1016/j.pepi.2013.02.003>.
- Hervé, G., Lanos, P., 2018. Improvements in archaeomagnetic dating in Western Europe from the Late Bronze to the Late Iron ages: an alternative to the problem of the Hallstattian radiocarbon plateau. *Archaeometry* 60 (4), 870–883. <https://doi.org/10.1011/arcm.12344>.
- Hervé, G., Fassbinder, J., Gilder, S.A., Metzner-Nebelsick, C., Gallet, Y., Genevey, A., Schnepp, E., Geisweid, L., Pütz, A., Reuss, S., Wittenborn, F., Flontas, A., Linke, R., Riedel, G., Walter, F., Westhausen, I., 2017. Fast geomagnetic field intensity variations between 1400 and 400 BCE : New archeointensity data from Germany. *Phys. Earth Planet. Inter.* 270, 143–156. <https://doi.org/10.1016/j.pepi.2017.07.002>.
- Hervé, G., Chauvin, A., Lanos, P., Rochette, P., Perrin, M., Perron d'Arc, M., 2019;al., xxxx. Cooling rate effect on thermoremanence magnetization in archaeological baked clays: an experimental study on modern bricks. *Geophys. J. Int.*
- Lanos, P., 2004. Bayesian inference of calibration curves: application to archaeomagnetism (Lecture No In: Buck, C.E., Millard, A.R. (Eds.), Tools for constructing chronologies: Crossing disciplinary boundaries. Springer, London, pp. 43–82.
- Lee, S., 1975. Secular variation of the intensity of the geomagnetic field during the past 3,000 years in North, Central and South America. *University of Oklahoma*.
- Licht, A., Hulot, G., Gallet, Y., Thébault, E., 2013. Ensembles of low degree archaeomagnetic field models for the past three millennia. *Phys. Earth Planet. Inter.* 224, 38–67. <https://doi.org/10.1016/j.pepi.2013.08.007>.
- Lifton, N., 2016. Implications of two Holocene time-dependent geomagnetic models for cosmogenic nuclide production rate scaling. *Earth Planet. Sci. Lett.* 433, 257–268. <https://doi.org/10.1016/j.epsl.2015.11.006>.
- Lopez-Sanchez, J., McIntosh, G., Osete, M.L., del Campo, A., Villalaín, J.J., Perez, L., Kovacheva, M., Rodriguez de la Fuente, O., 2017. Epsilon iron oxide: origin of the high coercivity stable low Curie temperature magnetic phase found in heated archaeological materials. *Geochem. Geophys. Geosyst.* 18 (7), 2646–2656. <https://doi.org/10.1002/2017GC006929>.
- Lopez-Tellez, J.M., Aguilar-Reyes, B., Morales, J., Goguitchaichvili, A., Calvo-Rathert, M., Urrutia-Fucugauchi, J., 2008. Magnetic characteristics and archeointensity determination on Mesoamerican Pre-Columbian Pottery from Quiahuitlan, Veracruz, Mexico. *Geof. Int.* 47 (4), 329–340.
- Mahgoub, A.N., Böhnel, H., Siebe, C., Chevrel, M., 2017b. Paleomagnetic study of El Metate shield volcano (Michoacán, Mexico) confirms its monogenetic nature and young age (~ 1250 CE). *J. Volc. Geoth. Res.* 336, 209–218. <https://doi.org/10.1016/j.jvolgeores.2017.02.024>.
- Mahgoub, A.N., Reyes-Guzmán, N., Böhnel, H., Siebe, C., Pereira, G., Dorison, A., 2017a. Paleomagnetic constraints on the ages of the Holocene Malpais de Zacapu lava flow eruptions, Michoacán (México): Implications for archeology and volcanic hazards. *Holocene*. <https://doi.org/10.1177/0959683617721323>.
- Martin Arana, R., 1987. Classic and postclassic chalcatzingo. In: Grove, D.C. (Ed.), *Ancient Chalcatzingo*. University of Texas Press, Austin, pp. 387–399.
- Michalk, D.M., Biggin, A.J., Knudsen, M.F., Böhnel, H.N., Nowaczyk, N.R., Ownby, S., López-Martínez, M., 2010. Application of the multispecimen paleointensity method to Pleistocene lava flows from the Trans-Mexican Volcanic Belt. *Phys. Earth Planet. Inter.* 179, 139–156. <https://doi.org/10.1016/j.pepi.2010.01.005>.
- Molina Cardin, A., Campuzano, S.A., Osete, M.L., Rivero-Montero, M., Pavón-Cararsco, F.J., Palencia-Ortas, A., et al., 2018. Updated Iberian archaeomagnetic catalogue: new full vector paleosecular variation curve for the last 3 millennia. *Geochem. Geophys. Geosyst.* 19 (10), 3637–3656.
- Morales, J., Alva-Valdivia, L., Goguitchaichvili, A., et al., 2006. Cooling rate corrected paleointensities from the Xitle lava flow: evaluation of within-site scatter for single spot-reading cooling units. *Earth Planets Space* 58, 1341–1347. <https://doi.org/10.1186/BF0352630>.
- Morales, J., Goguitchaichvili, A., Aguilar-Reyes, B.A., Pineda, M., Carvallo, C., Beramendi-Orosco, L., Gonzalez Hernández, G., Oliveros, A., 2012. Rock-Magnetic and archeointensity investigation of pottery and a burned floor at the Tzintzuntzan archaeological site, Western Mexico. *Gearch* 27, 521–537. <https://doi.org/10.1002/geoa.21426>.
- Morales, J., Goguitchaichvili, A., Ángeles Olay Barrientos, M., Carvallo, C., Aguilar Reyes, B., 2013. Archeointensity investigation on pottery vestiges from Puertas de Rolón, Capacha culture: In search for affinity with other Mesoamerican pre-Hispanic cultures. *Studia Geophys. Geod.* 57 (4), 605–626. <https://doi.org/10.1007/s11200-012-0878-z>.
- Morales, J., Fernández, G., Gogichaisvili, A., Cárdenas, E., Sol, M., Bernal, H., 2015. Archeomagnetic dating of some Pre-Columbian pottery fragments from northern Mesoamerica: implications for the chronology of central Mexico during the Epiclassic period. *J. Arch. Sci.: Rep.* 4, 32–43. <https://doi.org/10.1016/j.jasrep.2015.08.027>.
- Nilsson, A., Holme, R., Korte, M., Suttie, N., Hill, M., 2014. Reconstructing Holocene geomagnetic field variation: new methods, models and implications. *Geophys. J. Int.* 198 (1), 229–248. <https://doi.org/10.1093/gji/ggu120>.
- Osete, M.-L., Chauvin, A., Catanzariti, G., Jimeno, A., Campuzano, S.A., Benito-Batanero, J.P., Tabernero-Galan, C., Roperch, P., 2016. New archaeomagnetic data recovered from the study of celtiberic remains from central Spain (Numantia and Ciadueña, 3rd–1st centuries BC). Implications on the fidelity of the Iberian paleointensity database. *Phys. Earth Planet. Inter.* 260, 74–86. <https://doi.org/10.1016/j.pepi.2016.09.006>.
- Palencia-Ortas, A., Osete, M.L., Campuzano, S.A., McIntosh, G., Larrazabal, J., Sastre, J., 2017. New archaeomagnetic directions from Portugal and evolution of the geomagnetic field in Iberia from Late Bronze Age to Roman Times. *Phys. Earth Planet. Inter.* 270, 183–194. <https://doi.org/10.1016/j.pepi.2017.07.004>.
- Panovska, S., Korte, M., Finlay, C.C., Constable, C.G., 2015. Limitations in paleomagnetic data and modelling techniques and their impact on Holocene geomagnetic field models. *Geophys. J. Int.* 202, 402–418. <https://doi.org/10.1093/gji/ggv137>.
- Pavón-Carrasco, F.J., Gomez-Páccard, M., Hervé, G., Osete, M.L., Chauvin, A., 2014b. Intensity of the geomagnetic field in Europe for the last 3 ka: Influence of data quality on geomagnetic field modeling. *Geochem. Geophys. Geosyst.* 1–16. <https://doi.org/10.1002/2014GC005311>.
- Pavón-Carrasco, F.J., Osete, M.L., Torta, J.M., De Santis, A., 2014a. A geomagnetic field model for the Holocene based on archaeomagnetic and lava flow data. *Earth Planet. Sci. Lett.* 388, 98–109. <https://doi.org/10.1016/j.epsl.2013.11.046>.
- Poletti, W., Trindade, R.I.F., Hartmann, G.A., Damiani, N., Rech, R.M., 2016. Archeomagnetism of Jesuit Missions in South Brazil (1657–1706 AD) and assessment of the South American database. *Earth Planet. Sci. Lett.* 445, 36–47. <https://doi.org/10.1016/j.epsl.2016.04.006>.
- Reimer, P.J., Bard, E., Bayliss, A., Beck, J.W., Blackwell, P.G., Bronk, C., Edwards, R.L., 2013. INTCAL13 and MARINE13 radiocarbon age calibration curves 0–50,000 years Cal BP. *Radiocarbon* 55 (4), 1869–1887.
- Rodriguez-Ceja, M., Goguitchaichvili, A., Morales, J., Ostrooumov, M., Manzanilla, L.R., Reyes, B.A., Urrutia-Fucugauchi, J., 2009. Integrated archeomagnetic and micro-Raman spectroscopy study of pre-Columbian ceramics from the Mesoamerican formative village of Cuauhtan, Teotihuacan Valley, Mexico. *J. Geophys. Res.* 114 (B04103). <https://doi.org/10.1029/2008JB006106>.
- Rodriguez-Ceja, M., Soler-Arechalde, A.M., Morales, J., Goguitchaichvili, A., 2012. Estudios de arqueointensidad y propiedades magnéticas de cerámicas teotihuacanas. Una aportación a la cronología de Mesoamérica. In: Manzanilla, L.R. (Ed.), *Estudios arqueométricos del centro de barrio de Teopancazo en Teotihuacan. CICCH UNAM, Mexico City*.
- Schnepp, E., Obenhaus, M., Lanos, P., 2015. Posterior archaeomagnetic dating: an example from the early medieval site Thunau am Kamp Austria. *J. Arch. Sci. Rep.* 2, 688–698. <https://doi.org/10.1016/j.jasrep.2014.12.002>.

- Schnepp, E., Leonhardt, R., Korte, M., Klett-Drechsel, J., 2016. Validity of archaeomagnetic field recording: An experimental pottery kiln at Coppengrave, Germany. *Geophys. J. Int.* 205, 622–635.
- Shaar, R., Ben-Yosef, E., Ron, H., Tauxe, L., Agnon, A., Kessel, R., 2011. Geomagnetic field intensity: How high can it get? How fast can it change? Constraints from Iron age copper slag. *Earth Planet. Sci. Lett.* 301 (1–2), 297–306. <https://doi.org/10.1016/j.epsl.2010.11.013>.
- Shaw, J., 1974. A new method of determining the magnitude of the palaeomagnetic field: application to five historic lavas and five archaeological samples. *Geophys. J. R. Astron. Soc.* 39, 133–141.
- Siebe, C., 2000. Age and archaeological implications of Xitle volcano, southwestern Basin of Mexico-City. *J. Volcanol. Geotherm. Res.* 104, 45–64.
- Tema, E., Herrero-Bervera, E., Lanos, P., 2017. Geomagnetic field secular variation in Pacific Ocean: a Bayesian reference curve based on Holocene Hawaiian lava flows. *Earth Planet. Sci. Lett.* 478, 58–65. <https://doi.org/10.1016/j.epsl.2017.08.023>.
- Terán-Gerrero, A., Goguitchaichvili, A., Esparza, R., Morales, J., Rosas, J., Soler-Arechalde, A.M., Cárdenas, E., Urrutia-Fucugauchi, J., 2016. A detailed rock-magnetic and archaeomagnetic investigation on wattle and daub building (Bajareque) remains from Teuchitlán tradition (nw Mesoamerica). *J. Arch. Sci.: Rep.* 5, 564–573. <https://doi.org/10.1016/j.jasrep.2016.01.010>.
- Thellier, E., Thellier, O., 1959. Sur l'intensité du champ magnétique terrestre dans le passé historique et géologique. *Ann. Géophys.* 15, 285–376.
- Veitch, R.J., Hedley, I.G., Wagner, J.J., 1984. An investigation of the intensity of the geomagnetic field during Roman times using magnetically anisotropic bricks and tiles. *Archaeol. Sci.* 359–373 Geneva.
- Walton, D., 1991. A new technique for determining palaeomagnetic intensities. *J. Geomag. Geoelec.* 43, 333–339.
- Walton, D., Böhnel, H.N., 2008. The microwave frequency method. *Phys. Earth Planet. Inter.* 167, 145–148. <https://doi.org/10.1016/j.pepi.2008.02.012>.

Capítulo 7

1 Archeomagnetic dating and magnetic characterization of ceramics from the Casas
2 Grandes region, Chihuahua, Mexico: Paquimé, Galeana, Villa Ahumada and
3 Samalayuca archeological sites

4

5 Rodríguez-Trejo A.¹, Cruz-Antillón, R.³, Alva-Valdivia, L. M.², Hervé, G.^{4,5,6}, Perrin, M.⁴,
6 Salgado-Saito, M. M.⁷

7

⁸ ¹ Universidad Nacional Autónoma de México : Posgrado en Ciencias de la Tierra, Instituto de
⁹ Geofísica, Ciudad Universitaria 04510, Ciudad de México, MEXICO

¹⁰ ²Universidad Nacional Autónoma de México: Instituto de Geofísica, Laboratorio de
¹¹ Paleomagnetismo, Ciudad Universitaria 04510, Ciudad de México, MEXICO.

¹² ³Instituto Nacional de Antropología e Historia, Sede Chihuahua, MEXICO.

¹³ ⁴Aix Marseille Univ, CNRS, IRD, INRA, Coll France, CEREGE, Aix-en-Provence, France

⁵ Univ Bordeaux Montaigne, CNRS IRAMAT-CRP2A – UMR 5060, LabEx LaScArBx, F-
33607 Pessac, France

¹⁶ ⁶Univ Rennes, CNRS, Géosciences Rennes – UMR 6118, F-35000 Rennes, France

¹⁷ Universidad Nacional Autónoma de México: Facultad de Ciencias, Ciudad Universitaria 04510,
¹⁸ Ciudad de México, MEXICO.

19

²⁰ Corresponding author: alekz igf@gmail.com

21

22

23

24

25 **Abstract**

26 Casas Grandes culture, located at the northwest, Chihuahua, Mexico, and southwest of New
27 Mexico, USA had an intense occupation in the region during the ceramic period in the area
28 from 0 AD to 1450 AD. Developing very particular ceramic types that define the style on
29 manufacturing pottery in the area. We presented archeointensity and magnetic properties
30 results from 24 pottery sherds, from two typical ceramic types found in the area: Mimbres
31 and Ramos polychrome. The samples belong to four archeological sites from Casas Grandes
32 region: Paquimé, Villa Ahumada, Galeana and Samalayuca. With the magnetic properties
33 experiments it was possible to differentiate the manufacturing materials from each ceramic
34 type in different locations and timing. Archeointensity results give a mean intensity value of
35 $55.4 \pm 4.6 \mu\text{T}$, and VADM $10.8 \times 10^{22} \text{ Am}^2$ for Mimbres type, and $42.5 \pm 2.8 \mu\text{T}$ and 8.2×10^{22}
36 Am^2 for Ramos polychrome. Those values agree with the proposed secular variation models
37 for Mexico. With those parameters was possible to obtain two reliable archeomagnetic dates.
38 For Mimbres ceramic type an estimated age of [1105; 1245] AD, and [1315; 1405] AD for
39 Ramos polychrome. The estimated ages are consistent with the expected values by the
40 archeologists, according with the typology and chronology described in the literature for
41 ceramics of Casas Grandes.

42 **Introduction**

43 In spite of the rich archeological heritage in Mexico and the well characterized and described
44 chronology and occupation history, just a few archeomagnetic studies have been performed
45 as dating method, most of them in the Mesoamerican region (e.g. [Morales et al., 2009](#); [Alva-](#)
46 [Valdivia et al., 2010](#); [Fanjat et al., 2013](#); [Goguitchaichvili et al., 2017](#)). This is an
47 archeomagnetic study of pottery from several sites from the north of Chihuahua, occupied
48 by cultures risen during the period estimated from 1000 to 1450 AD.

49 Archeomagnetism is based on the record of the direction and intensity of the Earth's magnetic
50 field on geological and archeological materials during the exposition to high temperatures
51 (ca. > 400 °C). These thermal phenomena can be produced by different events such as
52 burning, use of kilns, firing places for cooking (hearths), baking of a pottery piece, etc.
53 During the heating at high temperatures, the magnetic minerals (e.g. magnetite, hematite,
54 etc.) of the materials acquired the direction and intensity of the geomagnetic field at the
55 moment of cooling. The study of well dated materials, allow the development of regional and
56 global master curves that reconstitute the secular variation of the Earth's magnetic field
57 during a defined period of time. The master curves from different models focused on different
58 time windows, such as ARCH10k.1 ([Constable et al., 2016](#)), ARCH3k.1 ([Korte et al., 2009](#)),
59 CALS3k.4 ([Korte and Constable, 2011](#)), CALS10k.1b ([Korte et al., 2011](#)), CALS10k.2
60 ([Constable et al., 2016](#)), SHA.DIF.14k ([Pavón-Carrasco et al., 2014](#)), and a repository with
61 data from all around the world for the last 50 ka GEOMAGIA50.v3 ([Brown et al., 2015](#)).

62 The archeomagnetic studies in the Aridoamerica region at the southern part of the United
63 States of America (USA) have been served as a successful dating technique for more than 40
64 years. Several studies ([Cox & Blinman, 1999](#); [Eighmy et al., 1986](#); [Lengyel, 1999](#); [Wolfman,
65 1990](#)) pointed out problems affecting the precision of the southwest master curve generating
66 slight differences, which could hold significant implications for archeomagnetic dating.
67 Finally, Lengyel and [Eighmy \(2002 and references therein\)](#) discuss and apply two correction
68 factors, showing the new version of the archeomagnetic master curve for the Southwest of
69 USA, SWCV2000.

70 The aim of this work is to characterize the magnetic properties and to determine the intensity
71 of the geomagnetic field recorded in two pottery types collected from Paquimé, Galeana,
72 Villa Ahumada and Samalayuca archeological sites in the region occupied by the Casas
73 Grandes culture, Chihuahua, northern Mexico. The archeomagnetic study allowed us to
74 establish the age of fabrication of these ceramics. These two pottery types are catalogued by
75 archeologists as the Mimbres black or red on white and Ramos polychrome, for the period
76 from 900 AD to 1450 AD.

78 **Archeological background**

79 The utilized archeological materials come from the Casas Grandes and Mimbres cultures,
80 located at the northwest, Chihuahua, Mexico, and southwest of New Mexico, USA,
81 respectively. These belong to the major cultural region called ‘Mogollon’ that together with
82 ‘Pueblo Ancestral’ (before Anasazi) and ‘Hokoham’, constitute the cultural macro-region
83 ‘Oasisamerica’ or ‘Aridoamerica’ ([Kirchhoff, 1954](#)), also known as ‘La Gran Chichimeca’
84 ([Di Peso, 1974](#)), ‘Noroeste ([Braniff, 1986](#)) and the ‘Southwest’ ([Cordell, 1984](#)).

85 Since many years ago, the Casas Grandes culture (and its capital Paquimé) has called the
86 attention of specialists ([Bandelier 1890; Brand 1943; Di Peso 1974; Kelley & Phillips Jr.,](#)
87 [2017; Lumholtz 1904; Sayles 1936; Whalen & Minnis, 2001, 2009](#)). Between 1959 and 1961
88 Charles Di Peso ([1974; Di Peso et al., 1974](#)) started a very intensive and rigorous
89 archeological study at Paquimé, which recovered large amount of pottery, shells, and organic
90 materials allowing the statement of the first chronology of the region. He identified Four
91 large periods; Plainwere, Viejo, Medio and Tardío, covering since the appearance of the
92 ceramic (AD 0) up to the colonial era. Currently the period Plainwere is considered
93 hypothetical ([Stewart et al. 2004](#)) and, the Tardío is questioned ([Kelley & Phillips Jr. 2017;](#)
94 [Whelan & Minnis 2009](#)).

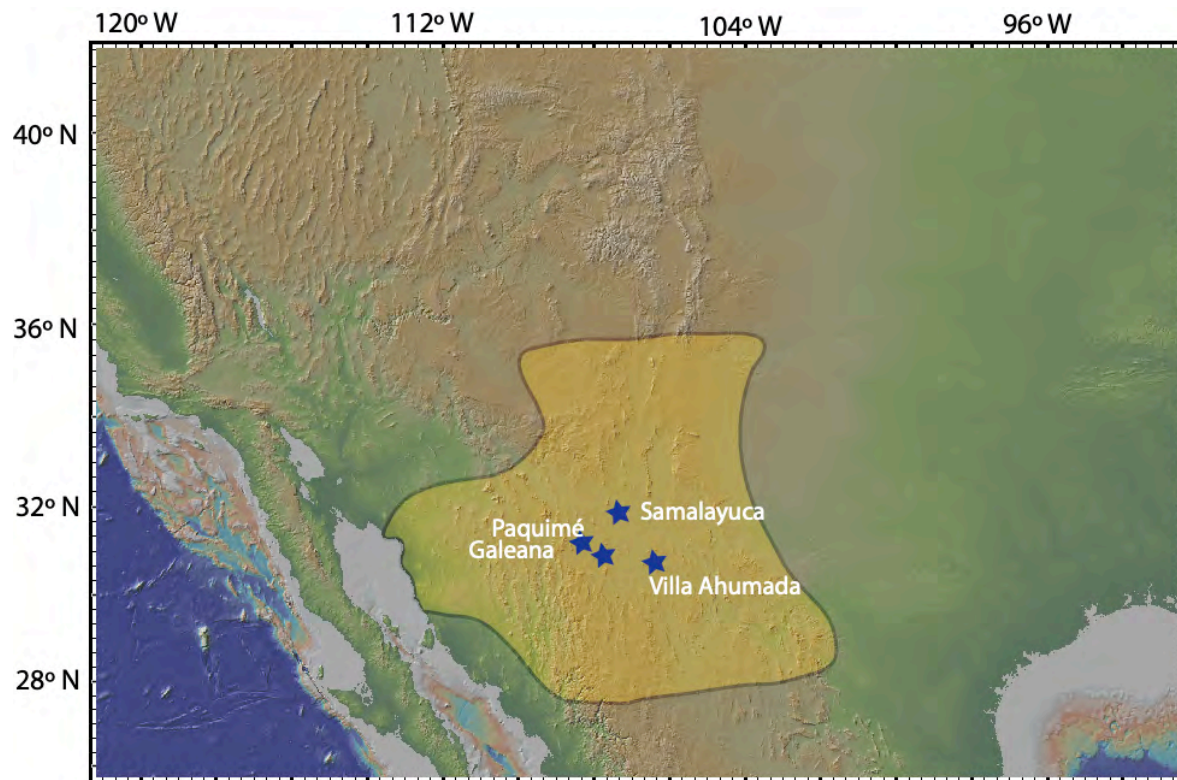
95 The Viejo Period, (700-1200 AD), originally it was dated by Di Peso (1974) between 700
96 ±50 to 1060 AD and consisted of three phases Convento (700 ±50-900 AD), Pilón (900–950
97 AD) and Perros Bravos (950–1060 AD). However, subsequent investigations have been
98 modifying the chronological sequence ([Dean & Ravesloot, 1993; Kelley & Phillips Jr., 2017;](#)
99 [Ravesloot et al., 1995; Stewart et al., 2005; Whelan & Minnis, 2009](#)). Recently, the three
100 phases of Di Peso were adjusted to two: Early Viejo and Late Viejo. The main difference is
101 the presence of the Mimbres Black-on-white ceramic in the Late Viejo sites ([Kelley and](#)
102 [Searcy, 2015](#)).

103 The Medio Period, (1200 to 1450 AD). Originally Charles C. Di Peso (1974) separated it into
104 three phases; Buena Fe (1060-1205 AD), Paquimé (1205-1261 AD) and Diablo (1261-1340
105 AD), however, his proposal has undergone modifications ([Braniff 1986, Dean and Ravesloot](#)

106 1993, LeBlanc 1980, Lakson 1984, Ravesloot *et al.* 1995). Currently the most accepted
107 suggests the start in 1200/50 AD, and the end in 1400/50 AD. (Dean and Ravesloot 1993,
108 Ravesloot *et al.*, 1995). A new perspective headed by Whelan and Minnis (2009: 68),
109 postulates only two phases; Middle early (1200-1300 AD), and Late Middle (1300-1450
110 AD). It was the flourishing of the Casas Grandes culture. Paquimé was built accompanied by
111 great population growth, economic, political, social and cultural development. Architecture
112 reached its maximum development, and polychrome ceramics of different types is the most
113 visible characteristic of this period. Appear a variety of designs, eccentric forms such as
114 human and animal. Manufacturing techniques become more sophisticated, more symmetrical
115 shapes and fine textures.

116 Even though exists several ceramic polychrome types of the Medio period (Di Peso *et al.*
117 1974: 6), the most abundant and characteristic is the Ramos polychrome. In fact, is estimated
118 as a good chronological marker (Di Peso *et al.*, 1974: 6; Kelley & Phillips Jr., 2017) and
119 Whelan & Minnis indicated that appears up to the Late phase of the Medio period, between
120 1300 and 1450 DC ([Whelan & Minnis 2009](#)).

121



122

123 Figure 1. Mogollon cultural region with studied archeological sites (blue stars)
124 and other prominent archeological sites (red diamonds).

125

126 **3. Samples and laboratory procedures**

127 We analyzed 24 pottery sherds of Mimbres and Ramos polychrome types (called PM and PR
128 respectively) from four sites in the Casas Grandes region: Paquimé, Galeana, Villa Ahumada
129 and Samalayuca (Figure 2). Table 1 show the location of the archeological sites.

130



131

132 Figure 2. Representative sample sherds from this study: Ramos polychrome, PR and
 133 Mimbres, PM. Typical decoration, lines and colors from Ramos polychrome pottery, Casas
 134 Grandes region (Parada-Carrillo, 2016).

135

136 A small chip from each sherd was used to measure the susceptibility as a function of the
 137 temperature ($k-T$), in order to determine the thermal stability of the samples during a heating-
 138 cooling process; and to identify the ferromagnetic mineralogy of the samples by determining
 139 the Curie temperature. The experiments were performed on an MFK-FA susceptibility-meter
 140 (Agico, Kappabridge). Specimens were heated in air atmosphere from room temperature up
 141 to 600° C.

142

<i>Archeological site</i>	<i>Location</i>	
	<i>Latitude °N</i>	<i>Longitude °W</i>
Paquimé	30.3674	107.9485
Samalayuca	31.3424	106.4309
Villa Ahumada	30.6165	106.5228
Galeana	30.1079	107.6116

143

Table 1. Location of the archeological sites.

144 Another small rock chip from each sherd was used to investigate the hysteresis properties
145 and the isothermal remanent magnetization (IRM) spectra. We determine, from the hysteresis
146 curves, the saturation magnetization (M_s), the saturation remanent magnetization (M_{rs}), the
147 coercive force (H_c) and the remanent coercive force (H_{cr}). The ratios of these parameters
148 provide rough information on the size distribution of the magnetic domains and the different
149 mixtures of magnetic minerals contained in the samples (e.g., Day et al., 1977; Dunlop,
150 2002). Measurements were done using the Princeton AGFM Micromag 2900 apparatus in
151 fields up to 1.2 Tesla at room temperature.

152 To perform the archeointensity study, three to six samples from each sherd were cut on
153 rectangular shape of approximately 18×5×3 mm. One piece from each sherd was selected to
154 perform a thermal demagnetization to estimate the thermal stability and the number of
155 components of the remanent magnetization of the magnetic vector recorded. Samples were
156 heated in a non-inductive Schönstedt furnace using 10 to 12 steps, from the room temperature
157 up to 580°C. The remanent magnetization was measured with an AGICO JR-6 spinner
158 magnetometer in a magnetically shielded room.

159 Samples were selected for archaeointensity experiments according to three criteria: (1) a
160 single component of thermoremanent magnetization, (2) reversible k-T curves and (3) single
161 (SD) or pseudo single domain (PSD) grains, in order to fulfill the independence and additivity
162 Thellier laws (Thellier and Thellier, 1959).

163 The archeointensity was estimated using the Thellier-Thellier (1959) protocol in a controlled
164 laboratory field of 40 μ T. Methodology consists on a stepwise heating-cooling process of the
165 samples from 150 °C up to 580 °C with steps every 50°C. The process consists in two heating-
166 cooling cycles at the same temperature: the field was applied along one direction (+) at the
167 first step and in the opposite direction (-) at the second step. Partial thermal remanent
168 magnetization (pTRM) checks were performed every 100°C, to verify the thermal stability
169 of the pTRM on the samples at different temperatures. The stepwise heating-cooling process
170 was performed using a MMTD24 oven from Magnetic Measurements. The remanent
171 magnetizations were measured with a JR6 Agico spinner magnetometer.

172 Archeointensity results were processed by using the ThellierTool 4.22 software ([Leonhardt](#)
173 [et al., 2004](#)). Accepted archaeointensity values were selected with the following quality
174 criteria: the intensity was calculated using at least five temperature steps, the quality q factor
175 should be higher than 4, and the f fraction should be greater than 30%. The results were
176 corrected for the effects of TRM anisotropy using [Chauvin et al. \(2000\)](#) protocol, at 540 °C
177 with 6 positions (+x, -x, +y, -y, +z and -z axes) followed by a stability check. The cooling
178 rate effect (e.g. [Veitch et al., 1984](#); [Gomez-Paccard et al., 2006](#); [Hervé et al., 2019a](#)) was
179 estimated by comparing the TRMs acquired during a fast and a slow cooling from 540°C.
180 This protocol fulfills the criteria defined by [Hervé et al., \(2019b\)](#) for the laboratory
181 procedures.

182 After the comparing the average archeointensities of Mimbres and Ramos pottery types with
183 the prediction at Mexico City of SHADIF 14k global model ([Pavón-Carrasco et al., 2014](#)),
184 and with the regional master curves available for Mexico ([Goguitchaichvili et al., 2018](#);
185 [Hervé et al., 2019](#); [Mahgoub et al., 2019](#)) of the last 3,000 years. The archeomagnetic dating
186 was performed by using the Matlab tool ([Pavón-Carrasco et al., 2011](#)) with the master curve
187 from [Mahgoub et al., 2019](#).

188 **4. Results**

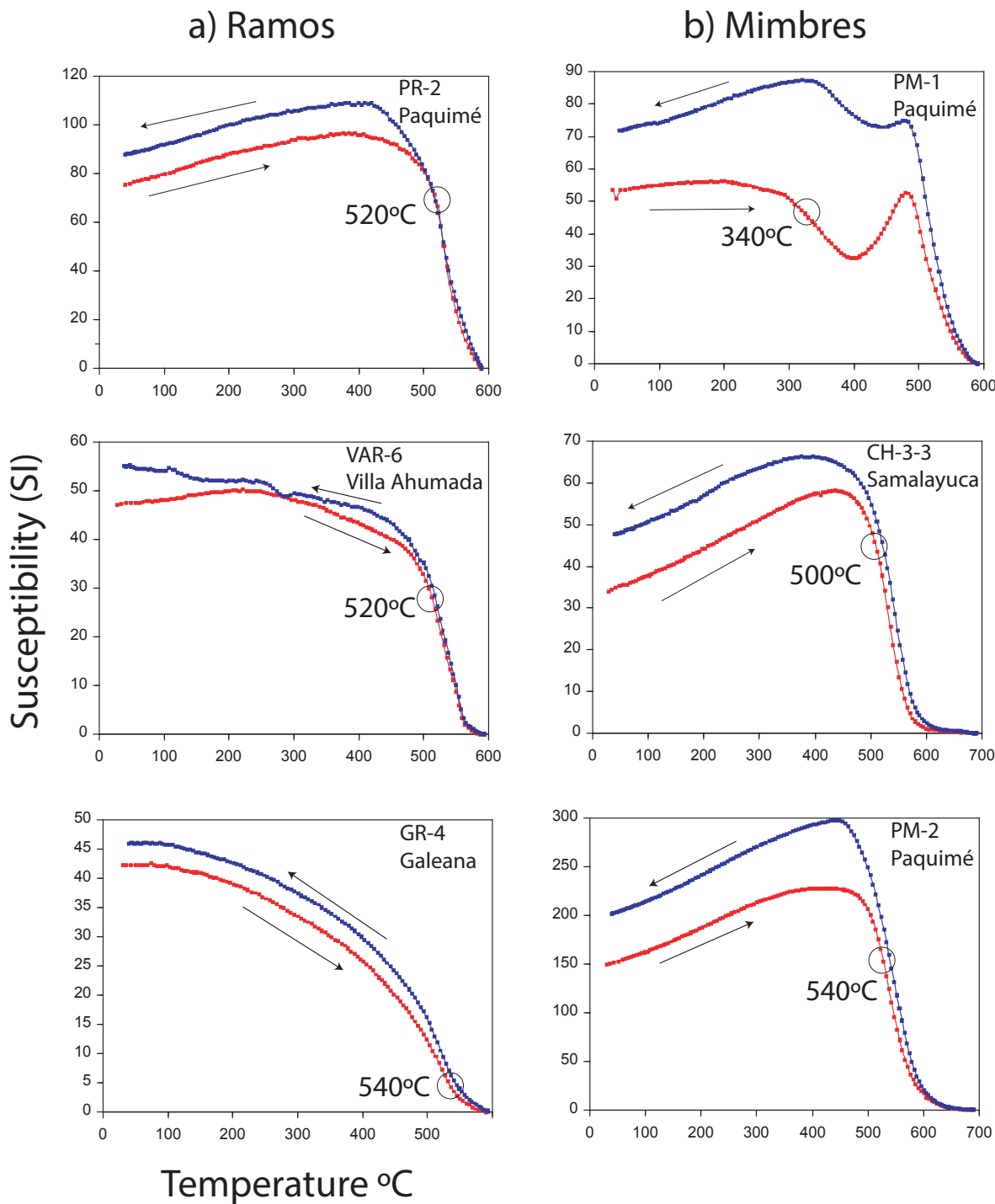
189 **4.1 Magnetic properties**

190 The rock magnetic properties allowed to identify and characterize the carrier of
191 magnetization on the samples. This characterization gives information on the magnetic and
192 thermal stability of the samples, and help to select the best specimens for the archeointensity
193 experiments and to differentiate the two ceramic types.

194 The heating-cooling branches of the k-T curves show high reversibility in most of the
195 cases, suggesting high degree of magnetic stability. They show two representative
196 behaviors: 1) Most of the samples have Curie temperatures of ca. 500-580 °C, revealing a
197 typical behavior of Ti-poor magnetite, with high reversibility of the branches ([Fig. 3, PR-2,](#)

198 GR-4); 2) Heating-cooling branches showing two Curie points: one around 300 °C and
199 another ranging from 480 to 560 °C (Fig. 3 PM-1). The cooling curve is loose reversibility
200 from the 500° C suggesting chemical alteration. This is a typical behavior of a mixture of
201 Ti-poor and Ti-rich titanomagnetite.

202

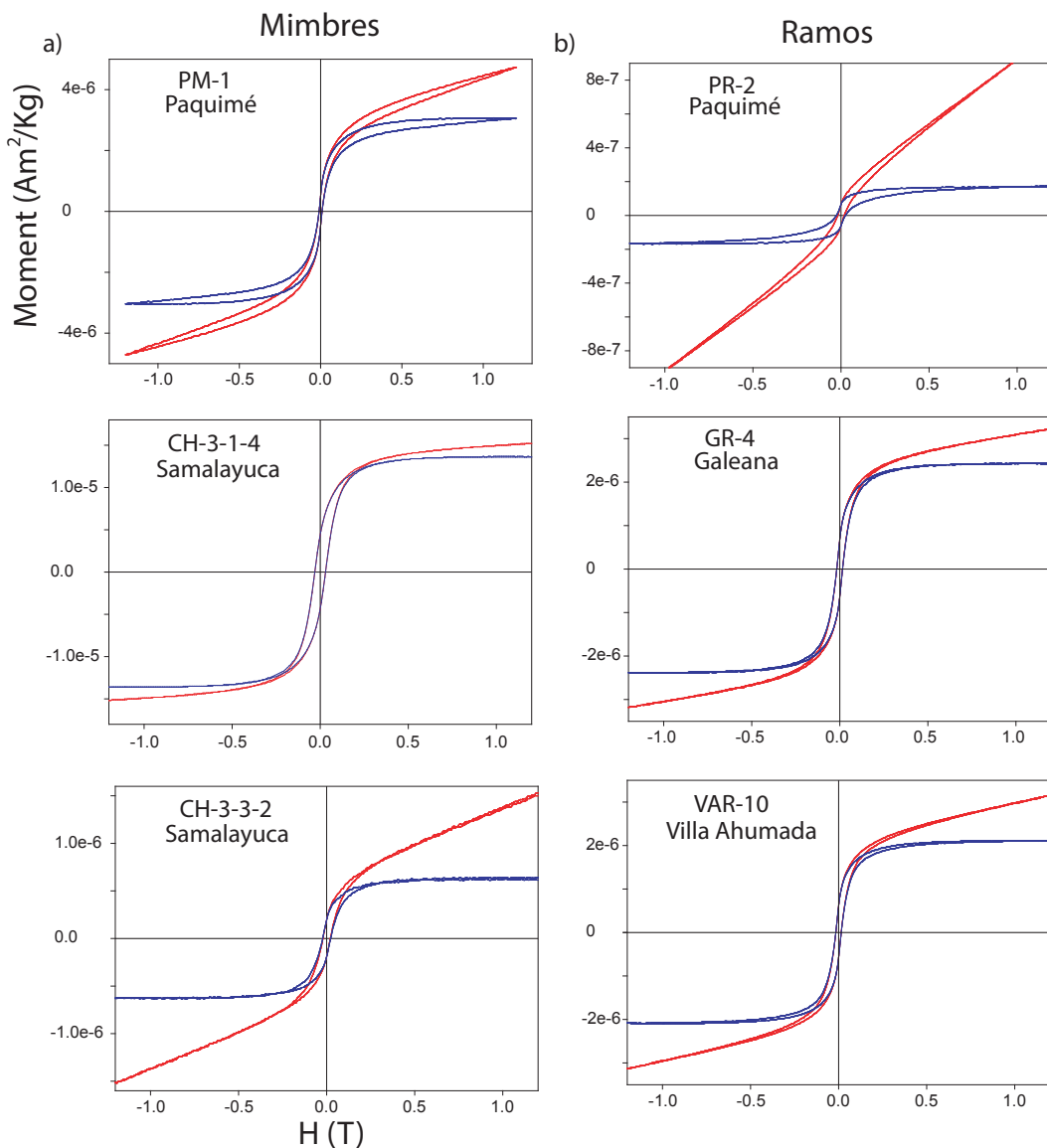


203

204 Figure 3. Representative k-T curves of Ramos polychrome (a) and Mimbres (b) ceramic types
205 from the distinct localities.

206 The hysteresis curves present two different shapes indicating diverse mixtures of magnetic
207 mineralogy. The '*potbellied*' shape, observed in 65% of the samples (e.g. VAR-10 and GR-

208 4 on Figure 4), shows a typical PSD behavior with smaller magnetic grain size (Tauxe, et al.,
 209 1996, 2002). Other specimens (e.g. PM-1 and PR-2) present ‘waspwaisted’ hysteresis curves,
 210 highlighting a mixture of low and high coercivity magnetic minerals, such as titanomagnetite
 211 and minor amount of titanohematite. This mixture shows a trend of superparamagnetic (SP)
 212 (Tauxe et al. 2002) and larger PSD-like to multidomain (MD) grains. Both shapes can be
 213 observed in Mimbres and Ramos polychrome. The larger differences between hysteresis
 214 curves before and after the paramagnetic correction shows that the contribution of
 215 paramagnetic minerals is higher for specimens PR-2 and CH-3-3-2.

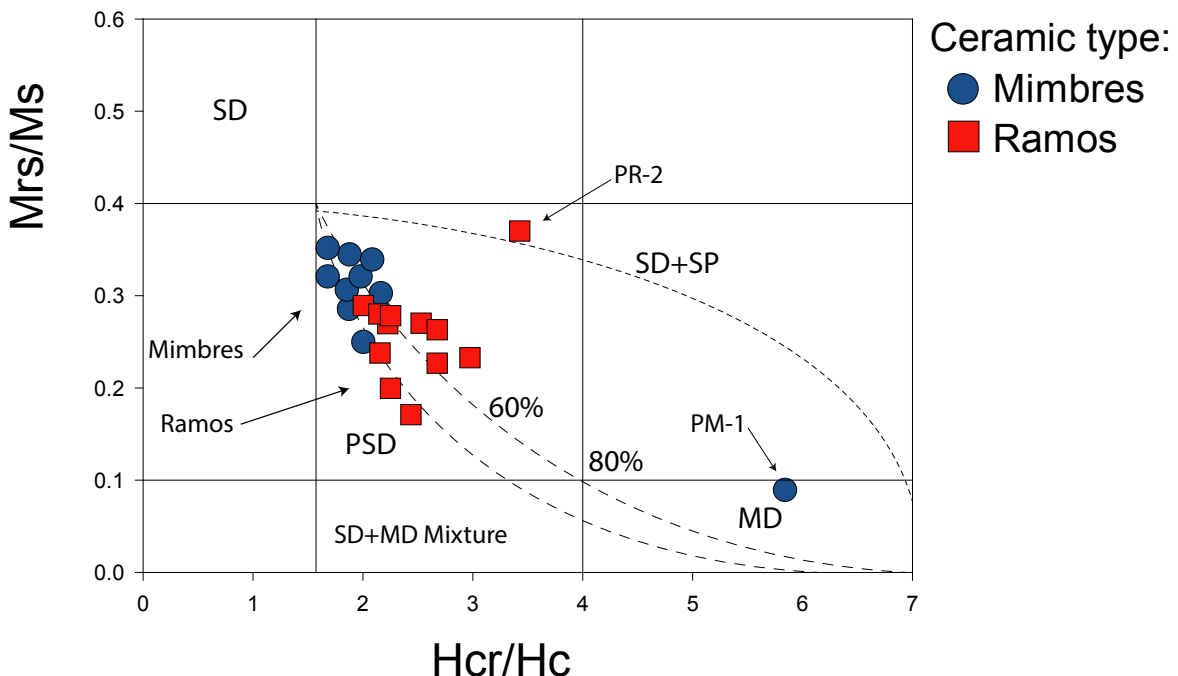


216

217

218 Figure 4. Representative hysteresis curves from the different localities before and after subtraction of
219 the para- and diamagnetic components (in red and blue respectively).

220 The magnetic parameters of hysteresis curves: saturation of magnetization (M_s), saturation
221 remanent magnetization (M_{rs}), coercive force (H_c) and remanent coercive force (H_{cr}), show
222 different ratios in both ceramic types. For Mimbres type, the saturation of magnetization
223 shows a range of $20 < M_s < 686 \text{ mAm}^2/\text{kg}$, and for Ramos polychrome $5 < M_s < 173 \text{ mAm}^2/\text{kg}$.
224 For the saturation of the remanent magnetization, the range for Mimbres is $6 < M_{rs} < 220$, and
225 for Ramos polychrome $2 < M_{rs} < 41$. The results show a considerable difference in the ranges
226 of saturation and remanence of the magnetization in both group of samples. For the
227 coercive force, Mimbres presents a range of $9 < H_c < 31$, and Ramos polychrome $8 < H_c < 26$.
228 Finally, for the remanent coercive force, Mimbres show a range of $47 < H_{cr} < 59$, and Ramos
229 polychrome $18 < H_{cr} < 89$. The results on the coercivity show considerably differences for the
230 H_{cr} parameter, where is considerably higher for Ramos polychrome than Mimbres. The
231 ratios M_{rs}/M_s and H_{cr}/H_c are summarized in the Day plot (Day, 1977; Dunlop, 2002) [Figure 5](#),
232 where is possible to observe two groups, the blue circles representing the Mimbres
233 ceramic type, and the red squares the Ramos polychrome ceramics. According to the
234 magnetic ratios in the Day plot, is possible to distinguish that each ceramic type has
235 particular magnetic properties of coercivity and magnetization. As shown in [Figure 5](#),
236 samples PR-2 and PM-1 appear out of the range of most of the samples. In the case of PR-2
237 fits on the curve for Simple domain + super paramagnetic (SD+SP), showing lower M_s
238 values with higher H_c values, which possibly could be associated to smaller grain size. In
239 the case of PM-1 show a multi domain (MD) behaviour, that possibly can be associated to
240 bigger grain sizes.

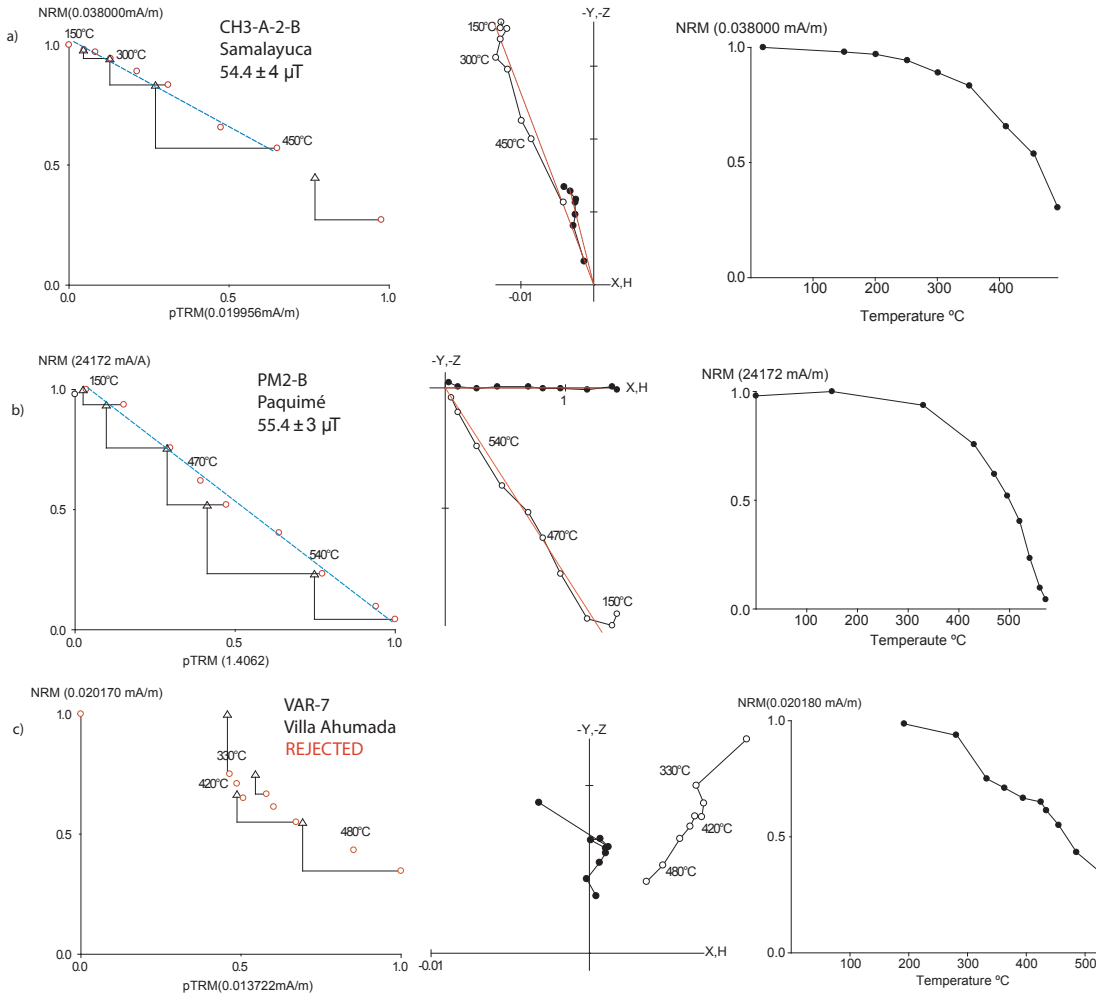


241

242 Figure 5. Day plot of samples from Ramos polychrome (red squares) and Mimbres
243 (blue circles) ceramic types with SD-MD and SD-SP mixing curves of Dunlop (2002).

244 **4.2 Archeointensity**

245 The archaeointensity experiments were performed on 16 selected (according to the
246 aforementioned criteria) pottery sherds from Mimbres and Ramos polychrome ceramic types.
247 The Arai plots in [Figure 6a and 6b](#) are representative of accepted results, with a linear
248 behavior and reproducible pTRM-checks. The proportion of specimens fulfilling our
249 acceptance criteria ($n > 5$, $q > 4$ and $f > 30\%$) is 21%. In most cases, rejected samples show a
250 typical concave-up shape of their Arai plot ([Figure 6c](#)), that is associated to alteration of
251 minerals during the stepwise heating-cooling process or to effect of the MD mixture grains.



252

253 Figure 6. Representative archeointensity plots with accepted (a, b) and rejected (c)
254 experiments.

255

256 Most of the ceramics used to determine the intensity of the geomagnetic field, have strong
257 magnetic anisotropy effect, which could affect the intensity results. The acquisition of an
258 artificial TRM parallel to the original plane is significantly better than that at the
259 perpendicular plane (Aitken et al., 1981). It is important to determine the degree of anisotropy
260 of each sample to recognize the difference between the laboratory and the original field, with
261 respect to its original orientation.

262 Correction of the anisotropy thermoremanent magnetization (ATRM) tensor were obtained

263 for each sample (Veitch et al., 1984) at 540° C, from the acquisition of a TRM in six different
 264 positions along the three-coordinate axis +X, -X, +Y, -Y, +Z and -Z. The intensity results
 265 were corrected for the ATRM factor, by the estimation of a correction factor estimated from
 266 the estimated direction of the ancient field B, and the ATRM tensor. The cooling rate effect
 267 determined in the laboratory was not significant to the estimation of the archeointensity,
 268 avoiding inaccuracies on the estimation of the mean values.

269 A summary of the average archaeointensity results per sherd are given in [Table 2](#). We
 270 calculated the mean archeointensity and virtual axial dipole moment (VADM) values for
 271 both Ramos polychrome and Mimbres ceramic types. Sherds GR1 and PR6 were discarded
 272 for the calculation of the mean values. Those sherds were considered with low quality with
 273 only two specimens for the estimation of a mean value (Hervé et al., 2019). Mimbres pottery
 274 has a mean intensity value of $55.6 \pm 4.2 \mu\text{T}$, and a mean VADM of $10.8 \times 10^{22} \text{ Am}^2$, whereas
 275 the Ramos potteries have a mean intensity value of $40.5 \pm 3 \mu\text{T}$, and mean VADM of 7.3×10^{22}
 276 Am^2 . Results from Casas Grandes are the first high quality data from Northern Mexico.
 277 Archeointensity results with quality factors per specimen are available in [Table S1](#).

Sherd	Locality	Type	N	B (μT)	σ_B (μT)	VADM 10^{22} Am^2
CH3-3	Samalayuca	Mimbres	3	50.7	2.4	9.9
CH3-A-2	Samalayuca	Mimbres	3	55.4	8.9	10.8
GM1	Galeana	Mimbres	3	55.4	4.3	10.7
PM2	Paquimé	Mimbres	4	55.5	3.7	10.8
VAM4	Villa Ahumada	Mimbres	3	60.8	5.5	11.9
VAM1	Villa Ahumada	Mimbres	3	56.7	1.8	11.2
Mimbres mean				55.6	4.2	10.8
GR1*	Galeana	Ramos	2	45.2	2.2	8.8
PR1	Paquimé	Ramos	3	36.5	4.2	7.2
PR4	Paquimé	Ramos	3	33.9	0.7	6.5
PR6*	Paquimé	Ramos	1	48.4	2.1	10.4
VAR5	Villa Ahumada	Ramos	4	45.0	2.9	7.0
VAR6	Villa Ahumada	Ramos	3	44.9	2.6	8.8
Ramos Polychrome mean				40.5	3.0	7.3

279

280 Table 2. Summary of the mean archaeointensity results obtained by sherd, locality and

281 ceramic type in this study. N is the number of sherds used for the calculation of the mean
282 archeointensity B and its standard deviation σ_B ; $VADM$ is the Virtual Axial Dipole Moment.
283 *Results excluded for the calculation of the mean values.

284

285 **5. Discussion**

286

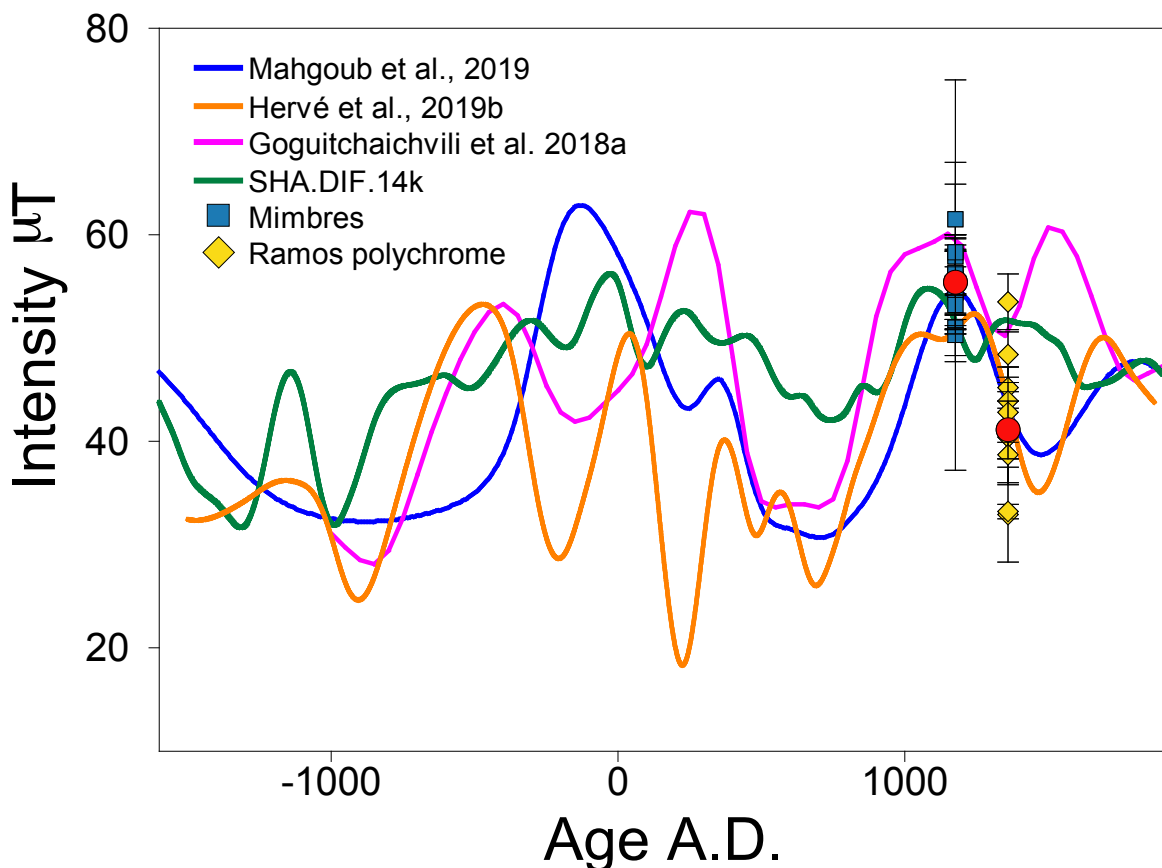
287 **5.1 Comparison with regional and global reference curves**

288 The results were compared with Mexican secular variation curves (Goguitchaichvili et al.,
289 2018a; Mahgoub et al., 2019a, Hervé et al., 2019b) (Figure 7). Hervé et al. (2019b) and
290 Mahgoub et al. (2019a) are calculated after data selection using similar criteria. The latter
291 includes very recently published data (Mahgoub et al., 2019b) that were not included in
292 Hervé et al. (2019b) curve. Goguitchaichvili et al. (2018a) curve is calculated from Mexican
293 and SW USA data selected with less stringent criteria than the two others studies, as data
294 inappropriately corrected for the TRM anisotropy effect are considered. The better fit of our
295 Paquimé data is observed with Mahgoub et al. (2019a) curve, which shows the impact of new
296 Mahgoub et al. (2019b) data for the knowledge of the secular variation in Mexico in
297 comparison to Hervé et al. (2019b) curve. Mimbres and Ramos data confirm the intensity
298 decrease during the first half of the second millennium AD.

299 The Figure 7 also compares our new Paquimé data with the prediction at Mexico City of
300 global model SHA.DIF.14k (Pavón-Carrasco et al., 2014). The model considerably smooths
301 the secular variation, probably because it included low-quality intensity data (see Mahgoub
302 et al. 2019a and Hervé et al., 2019b for discussion) and because of the uneven data
303 distribution at the global scale.

304

305



306

307 I TRANSMIT YOU A WRONG VERSION OF OUR PEPI CURVE. SORRY FOR THAT

308 Figure 7. Comparison of results on Mimbres and Ramos potteries with the average
 309 Mexican master curves of Goguitchaichvili et al. (2018), Hervé et al. (2019b) and Mahgoub
 310 et al. (2019) and the prediction at Mexico City of SHA.DIF.14k global model (Pavon-
 311 Carrasco et al., 2014). Red circles show the archeointensity mean value for the two ceramic
 312 types.

313 **5.2 Archeomagnetic dating**

314 In this section, we discuss the influence of the choice of the reference model in
 315 archaeomagnetic dating. The differences between the three master curves and the models
 316 suggest that this is a very important point. The most reliable reference seems Mahgoub et al
 317 (2019b) curve, because it is based on the most updated high-quality dataset in this region.

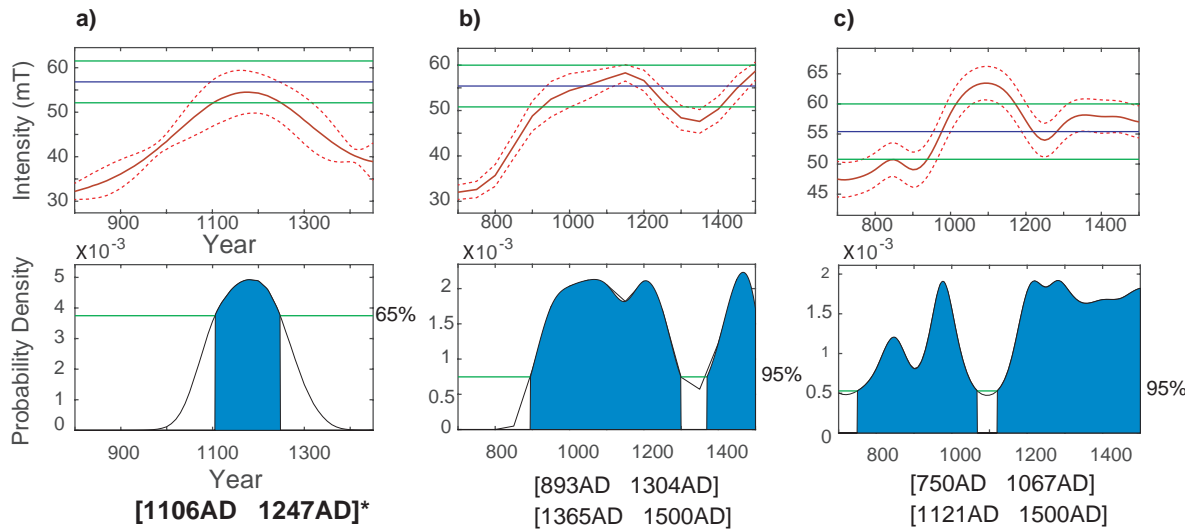
318

319 For this study, we compared the results with the reference master curves from
320 ([Goguitchaichvili et al., 2018a; Mahgoub et al., 2019; Hervé et al., 2019](#)) and with the global
321 model SHA.DIF.14k (Pavón-Carrasco et al., 2014) for the last 3 ka. The average
322 archaeointensity of the Ramos and Mimbres types was relocated to Mexico City using the
323 VADM correction and compared to each reference curve ([Figures 8 and 9](#)). The report
324 provides a probability density function of date, on which intervals of date are calculated at
325 95% of confidence ([Figures 8 and 9](#)).

326
327 The results show that the ages at 95% confidence of Mimbres ceramic type is [1105; 1245]
328 AD ([Figure 8](#)); and for the Ramos polychrome type the age is [1315; 1405] AD ([Figure 9](#)).
329 The results match plenty with the expected value, according with the stratigraphy, timing and
330 typology of the potteries

331

332

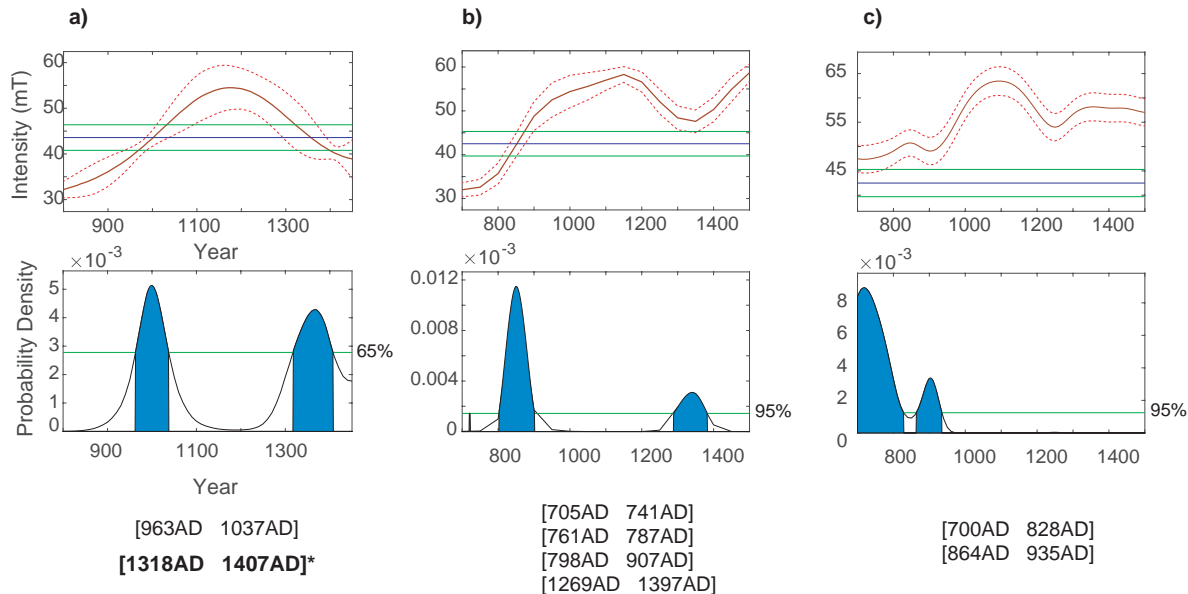


333

334 Figure 8. Archeomagnetic dating results for Mimbres ceramic type using Mexican master
335 curves of a) [Mahgoub et al., 2019](#) and b) [Goguitchaichvili et al., 2018a.](#) and c) the
336 prediction of global model SHA.DIF.14k for Mexico. The comparison of the average
337 archaeointensity relocated to Mexico City with the curves provides the probability density
338 function, on which are defined the intervals of date. * Selected interval according with to

339 the archaeological context.

340



341

342 Figure 9. Archeomagnetic dating results for Ramos polychrome ceramic type using master
343 curves for Mexico proposed by a) [Mahgoub et al., 2019](#) and b) [Goguitchaichvili et al.,](#)
344 2018a. and c) the global model SHA.DIF.14k for Mexico. The comparison of the average
345 archaeointensity relocated to Mexico City with the curves provides the probability density
346 function, on which are defined the intervals of date. * Selected interval according to the
347 archaeological context.

348 *5.2 Archeological implications*

349 The Casas Grandes region was a prominent area with intense human activity in the Northern
350 part of Mexico and Southwest USA, that rises with very particular and representative styles
351 and colors on the manufacturing of ceramic pieces ([Parada-Carrillo, 2016](#)).

352 The results of the magnetic properties carried out on the Ramos polychrome and Mimbres
353 ceramic types, reveal that the magnetic mineralogy is dominated by Ti-poor titanomagnetite
354 as the main carrier of magnetization in both groups. Thermomagnetic curves are
355 characterized by one or two magnetic phases, and Curie temperatures of the samples range
356 from 300 °C to 560 °C, with high reversibility during the heating-cooling process in most of

357 the cases. The hysteresis loop experiments show two dominant mixtures: ‘*potbellied*’ and
358 ‘*wasp-waisted*’ mixtures; revealing the presence of Ti-poor magnetite and a mixture with low
359 contents of titanohematite, and with different magnetic domains ranging from the SD to the
360 PSD in most of the cases. The Day plot (Day, 1977), M_s/M_r vs. H_c/H_{cr} ratios, suggests the
361 presence of magnetic grains from the SD to MD, with the typical behavior of pottery samples
362 (Dunlop, 2002). The ratios and ranges of the magnetic parameters suggest important
363 differences on the composition of the magnetic mineralogy between Mimbres and Ramos
364 polychrome. As shown in Figure 5, two different groups can be delineated, coincident with
365 the two different ceramic types. Nevertheless, the magnetic mineralogy is similar in both
366 types, the magnetic characteristics of grain size, magnetization of saturation and coercive
367 force are different in both ceramics. The magnetic properties results suggest that both ceramic
368 types are well differentiated. Very probably, both the raw material or some of the aggregates
369 for the manufacturing of the pottery could come from different sources, or the technique of
370 manufacture was distinct through time.

371 The archeointensity results show two different ranges for the mean values of these pottery
372 sherds (Table 2). The Ramos polychrome type intensity results range from $33.2 \pm 0.7 \mu\text{T}$ to
373 $45.6 \pm 2.6 \mu\text{T}$, and the Mimbres type range from $50.6 \pm 2.7 \mu\text{T}$ to $61.5 \pm 5.5 \mu\text{T}$. The mean value
374 for each ceramic type is: Mimbres $55.9 \pm 4.5 \mu\text{T}$ and VADM $10.9 \times 10^{22} \text{ Am}^2$, and for Ramos
375 polychrome $42 \pm 2.5 \mu\text{T}$ and VADM $8.1 \times 10^{22} \text{ Am}^2$. The values are consistent with the
376 expected parameters according with the regional reference curves for Mexico (Mahgoub et
377 al., 2019) and the global model SHA.DIF.14k (Pavón-Carrasco et al., 2014). These results
378 follow the trend and evolution of the secular variation of the geomagnetic field recorded at
379 different time scales and locations in Mexico (Mahgoub, et al., 2019; Rodríguez-Trejo et al.,
380 2019) (Figure 8). Our archeointensity results suggest that both ceramic types were
381 manufactured on different periods of time and at different locations in the Casas Grandes
382 region.

383 The archeomagnetic dating confirm the results obtained from the magnetic properties and
384 intensity process, that is, the ceramic types belong to different manufacture periods of time.
385 Mimbres ceramic type reveals an estimated age of [1105; 1245] AD, and Ramos polychrome
386 [1315; 1405] AD. As shown in Figure 7, the results fit with the evolution of the recent

387 proposed curves, and according with the chronology proposed by the archeologists, with an
388 uncertainty from 90 to 140 years. However, is important to include even more well dated
389 values with results of intensity and direction of the geomagnetic field to the reference curves,
390 which will increase the precision and allow to reduce considerably the uncertainty of the
391 dating.

392

393 **6. Conclusions**

394

395 The rock magnetic properties show that the magnetic mineralogy, magnetization and
396 coercive force could be used to differentiate the two different ceramic types studied, possibly
397 manufactured at different time periods at different locations in the Casas Grandes region. The
398 archeointensity results show the mean value for Mimbres: $55.9 \pm 4.5 \text{ } \mu\text{T}$ and VADM of
399 $10.9 \times 10^{22} \text{ Am}^2$; and for Ramos polychrome $42 \pm 2.5 \text{ } \mu\text{T}$ and VADM $8.1 \times 10^{22} \text{ Am}^2$. These
400 values match with the global and regional models available for Mexico. Nevertheless, is
401 necessary to increase the density of data available on the regional models to reduce the
402 uncertainty of the models. Dating of the ceramic types reveals that each was manufactured
403 in different times: Mimbres ceramic type has an estimated age of [1105; 1245] , and Ramos
404 polychrome [1315; 1405] AD. The estimated age fits the expected values of the archeologists,
405 according with the topology and chronology described in the literature for the Casas Grandes
406 ceramics studied. Thus, is essential the use of the archeomagnetic method for dating materials
407 of new regions to improve the chronology and the understanding of how the human activities
408 evolved. Our research concludes the reliability of archeomagnetism as efficient tool for
409 archeological dating, and the analysis of magnetic properties as a suitable alternative tool to
410 characterize and differentiate archeological materials.

411

412 **Acknowledgements**

413 We thank the financial support for the research projects DGAPA-PAPIIT-UNAM IN113117
414 to LA, Mexico and ANR-CONACyT 273564 to MP and LA (France-Mexico).

415

416 **References**

417 Aitken, M. J., Alcock, P. A., Bussell, G. D., & Shaw, C. J. (1981). Archeomagnetic
418 determination of the past geomagnetic intensity using ancient ceramics: allowance for
419 anisotropy. *Archeometry*, 23(1), 53-64.

420 Alva-Valdivia, L. M., Morales, J., Goguitchaichvili, A., de Hatch, M. P., Hernandez-
421 Bernal, M. S., & Mariano-Matías, F. (2010). Absolute geomagnetic intensity data from
422 preclassic Guatemalan pottery. *Physics of the Earth and Planetary Interiors*, 180(1-2), 41-51.

423 Bandelier, A. F. (1890). The Ruins of Casas Grandes. *The Nation*, 51(1313-1314),
424 166-168.

425 Brand, D. D. (1943). The Chihuahua culture area. *New Mexico Anthropologist*, 6(3),
426 115-158.

427 Braniff, C. B. (1986). Ojo de Agua, Sonora, and Casas Grandes, Chihuahua: A
428 Suggested Chronology. *Ripples in the Chichimec Sea*, Southern Illinois University Press,
429 Carbondale, 70-80.

430 Brown, M. C., Donadini, F., Korte, M., Nilsson, A., Korhonen, K., Lodge, A., ... &
431 Constable, C. G. (2015). GEOMAGIA50. v3: 1. General structure and modifications to the
432 archeological and volcanic database. *Earth, Planets and Space*, 67(1), 83.

433 Carl, L. (1904). *El Mexico desconocido: Cinco años de exploración entre las tribus*
434 *de la Sierra Madre Occidental; en la tierra caliente de Tepic y Jalisco, y entre los tarascos de*
435 *Michoacán*. Instituto Nacional Indigenista, México.

436 Constable, C., Korte, M., & Panovska, S. (2016). Persistent high paleosecular

- 437 variation activity in southern hemisphere for at least 10 000 years. *Earth and Planetary*
438 *Science Letters*, 453, 78-86.
- 439 Cordell, L. S. (1984). *Prehistory of the Southwest*. Academic Press.
- 440 Cordell, L. S., & McBrinn, M. (2016). *Archeology of the Southwest*. Routledge.
- 441 Cox, J., & Blinman, E. (1999). Results of archeomagnetic sample analysis. *Pipeline*
442 *Archeology 1990e1993: The El Paso Natural Gas North System Expansion Project, New*
443 *Mexico and Arizona*, 12, 19-1.
- 444 Cruz Antillón, R., & Maxwell, T. D. (1999). The Villa Ahumada Site: Archeological
445 Investigations East of Paquimé. *The Casas Grandes World*, 43-53.
- 446 Cruz Antillón, R., & Maxwell, T. D. (2017). *La Cultura Casas Grandes*. Secretaría de
447 Cultura, Instituto Nacional de Antropología e Historia, Gobierno del Estado de Chihuahua.
- 448 Day, R., Fuller, M., & Schmidt, V. A. (1977). Hysteresis properties of
449 titanomagnetites: grain-size and compositional dependence. *Physics of the Earth and*
450 *planetary interiors*, 13(4), 260-267.
- 451 Dean, J. S., & Ravesloot, J. C. (1993). The chronology of cultural interaction in the
452 Gran Chichimeca. *Culture and Contact: Charles C. Di Peso's Gran Chichimeca*, 83-103.
- 453 Di Peso, C. C. (1965). The Clovis Fluted Point from the Timmy Site, Northwest
454 Chihuahua, Mexico. *Kiva*, 31(2), 83-87.
- 455 Di Peso, C. C. (1974a). *Casas Grandes*, vol. 1–3. Dragoon, Arizona: Amerind
456 Foundation.
- 457 Di Peso, C. C. (1974b). *The Reeve ruin of Southeastern Arizona: A study of a*
458 *prehistoric western pueblo migration into the middle San Pedro valley (No. 8)*. Kraus Reprint
459 Company.
- 460 Di Peso, C. C., Fenner, G. J., & Wesche, A. (1974). *Casas Grandes: a fallen trading*

- 461 center of the Gran Chichimeca (Vol. 8). Dragoon, AZ: Amerind Foundation.
- 462 Dunlop, D. J. (2002). Theory and application of the Day plot (Mrs/Ms versus Hcr/Hc)
463 2. Application to data for rocks, sediments, and soils. *Journal of Geophysical Research: Solid*
464 *Earth*, 107(B3), EPM-5.
- 465 Eighmy, J. L., Hathaway, T. K., & Henderson, T. K. (1986). Secular change in the
466 direction of the geomagnetic field, AD 900 to 1100: new US southwest data. *MASCA*
467 journal, 4(2), 81-85.
- 468 Fanjat, G., Camps, P., Valdivia, L. A., Sougrati, M. T., Cuevas-Garcia, M., & Perrin,
469 M. (2013). First archeointensity determinations on Maya incense burners from Palenque
470 temples, Mexico: New data to constrain the Mesoamerica secular variation curve. *Earth and*
471 *Planetary Science Letters*, 363, 168-180.
- 472 Goguitchaichvili, A., Ortega, V., Archer, J., Morales, J., & Guerrero, A. T. (2017).
473 Absolute geomagnetic intensity record from pre-Columbian pottery dates elite Tlailotlacan
474 Woman in ancient Teotihuacan. *Journal of Archeological Science: Reports*, 14, 146-151.
- 475 Goguitchaichvili, A., Ruiz, R. G., Pavón-Carrasco, F. J., Contreras, J. J. M.,
476 Arechalde, A. M. S., & Urrutia-Fucugauchi, J. (2018). Last three millennia Earth's Magnetic
477 field strength in Mesoamerica and southern United States: Implications in geomagnetism and
478 archeology. *Physics of the Earth and Planetary Interiors*, 279, 79-91.
- 479 Hegmon, M., Nelson, M. C., Anyon, R., Creel, D., LeBlanc, S. A., & Shafer, H. J.
480 (1999). Scale and time-space systematics in the post-AD 1100 Mimbres region of the North
481 American Southwest. *Kiva*, 65(2), 143-166.
- 482 Hervé, G., Chauvin, A., Lanos, P., Rochette, P., Perrin, M., & Perron d'Arc, M.
483 (2019a). Cooling rate effect on thermoremanent magnetization in archaeological baked clays:
484 an experimental study on modern bricks. *Geophysical Journal International*, 217(2), 1413-
485 1424.
- 486

- 487 Hervé, G., Perrin, M., Alva-Valdivia, L., Tchibinda, B. M., Rodriguez-Trejo, A.,
488 Hernandez-Cardona, A., ... & Rodriguez, C. M. (2019b). Critical analysis of the Holocene
489 palaeointensity database in Central America: Impact on geomagnetic modelling. Physics of
490 the Earth and Planetary Interiors, 289, 1-10.
- 491 Kelley, J. H., & Phillips, D. A. (2017). Not so far from Paquimé: essays on the
492 archeology of Chihuahua, Mexico. University of Utah Press.
- 493 Kelley, J. H., & Searcy, M. T. (2015). Beginnings: The Viejo Period. Ancient
494 Paquimé and the Casas Grandes World, 17-40. Eds. Paul E Minnis and Michael E. Whalen,
495 pp. 17-40. Amerind Studies in Anthropology, The University of Arizona Press, Tucson.
- 496 Kelley, J. H., Garvin, R. D., Stewart, J. D., Zborover, D., & Chiykowski, T. (2014).
497 The Viejo Period in West-Central Chihuahua, Part 2: The Calderón site. In Maxwell Museum
498 Technical Series No. 19, Part 2. Maxwell Museum of Anthropology, University of New
499 Mexico Albuquerque.
- 500 Kirchhoff, P. (1954). Gatherers and farmers in the Greater Southwest: a problem in
501 classification. American Anthropologist, 56(4), 529-550.
- 502 Korte, M., Constable, C., Donadini, F., & Holme, R. (2011). Reconstructing the
503 Holocene geomagnetic field. Earth and Planetary Science Letters, 312(3-4), 497-505.
- 504 Korte, M., Donadini, F., & Constable, C. G. (2009). Geomagnetic field for 0–3 ka: 2.
505 A new series of time-varying global models. Geochemistry, Geophysics, Geosystems, 10(6).
- 506 Lengyel, S. N., & Eighmy, J. L. (2002). A revision to the US Southwest
507 archeomagnetic master curve. Journal of archeological science, 29(12), 1423-1433.
- 508 Lengyel, S. N., Eighmy, J. L., & Sullivan, L. P. (1999). On the potential of
509 archeomagnetic dating in the midcontinent region of North America: Toqua site
510 results. Southeastern Archeology, 156-171.
- 511 Leonhardt, R., Heunemann, C., & Krásá, D. (2004). Analyzing absolute

- 512 paleointensity determinations: Acceptance criteria and the software ThellierTool4.
513 0. *Geochemistry, Geophysics, Geosystems*, 5(12).
- 514 Mahgoub, A. N., Juárez-Arriaga, E., Böhnel, H., Siebe, C., & Pavón-Carrasco, F. J.
515 (2019). Late-Quaternary secular variation data from Mexican volcanoes. *Earth and Planetary
516 Science Letters*, 519, 28-39.
- 517 Morales, J., Goguitchaichvili, A., Acosta, G., González-Moran, T., Alva-Valdivia, L.,
518 Robles-Camacho, J., & del Sol Hernández-Bernal, M. (2009). Magnetic properties and
519 archeointensity determination on Pre-Columbian pottery from Chiapas, Mesoamerica. *Earth,
520 planets and space*, 61(1), 83-91.
- 521 Oppelt, N. T. (2002). *List of Southwestern Pottery: Types and Wares: with Dates and
522 References to Descriptions and Illustrations*. Oppelt Publications.
- 523 Parada Carrillo, G. (2016, December). Arquitectura y cerámica de Casas Grandes.
524 Una comparación entre conceptos espaciales arquitectónicos y pictóricos. In *Anales del
525 Instituto de Investigaciones Estéticas* (Vol. 38, No. 109, pp. 171-214). Universidad Nacional
526 Autónoma de México, Instituto de Investigaciones Estéticas.
- 527 Paterson, G. A., Tauxe, L., Biggin, A. J., Shaar, R., & Jonestrask, L. C. (2014). On
528 improving the selection of Thellier-type paleointensity data. *Geochemistry, Geophysics,
529 Geosystems*, 15(4), 1180-1192.
- 530 Pavón-Carrasco, F. J., Osete, M. L., Torta, J. M., & De Santis, A. (2014). A
531 geomagnetic field model for the Holocene based on archeomagnetic and lava flow data. *Earth
532 and Planetary Science Letters*, 388, 98-109.
- 533 Pavón-Carrasco, F. J., Rodríguez-González, J., Osete, M. L., & Torta, J. M. (2011).
534 A Matlab tool for archeomagnetic dating. *Journal of Archaeological Science*, 38(2), 408-419.
- 535 Ravesloot, J. C., Dean, J. S., & Foster, M. S. (1986, October). A new perspective on
536 the Casas Grandes tree-ring dates. In *Fourth Mogollon Conference*, University of Arizona.

537 Ravesloot, J. C., Dean, J. S., & Foster, M. S. (1986, October). A new perspective on
538 the Casas Grandes tree-ring dates. In Fourth Mogollon Conference, University of Arizona.

539 A Rodríguez-Trejo, L M Alva-Valdivia, M Perrin, G Hervé, N López-Valdés,
540 Analysis of geomagnetic secular variation for the last 1.5 Ma recorded by volcanic rocks of
541 the Trans Mexican Volcanic Belt: New data from Sierra de Chichinautzin,
542 Mexico, *Geophysical Journal International*, ggz310, <https://doi.org/10.1093/gji/ggz310>

543

544 Sayles, E. B. (1936). An archeological survey of Chihuahua, Mexico (No. 22). Priv.
545 print. for the Medallion, Gila pueblo.

546 Stewart, J. D., Kelley, J. H., MacWilliams, A. C., & Reimer, P. J. (2005). The Viejo
547 period of Chihuahua culture in northwestern Mexico. Latin American Antiquity, 16(2), 169-
548 192.

549 Stewart, J. D., MacWilliams, A. C., & Kelley, J. H. (2004). Archeological
550 Chronology in West-Central Chihuahua. Surveying the Archeology of Northwest Mexico,
551 edited by Gillian E. Newell and Emiliano Gallaga, 205-245.

552 Tauxe, L., Bertram, H. N., & Seberino, C. (2002). Physical interpretation of hysteresis
553 loops: Micromagnetic modeling of fine particle magnetite. Geochemistry, Geophysics,
554 Geosystems, 3(10), 1-22.

555 Tauxe, L., Mullender, T. A. T., & Pick, T. (1996). Potbellies, wasp-waists, and
556 superparamagnetism in magnetic hysteresis. Journal of Geophysical Research: Solid
557 Earth, 101(B1), 571-583.

558 Thellier, E. (1959). Sur l'intensité du champ magnétique terrestre dans le passé
559 historique et géologique. Ann. Geophys., 15, 285-376.

560 VanPool, C. S., & VanPool, T. L. (2007). Signs of the Casas Grandes shamans.
561 University of Utah Press.

- 562 Veitch, R. J. (1984). An investigation of the intensity of the geomagnetic field during
563 Roman times using magnetically anisotropic bricks and tiles. *Arch. Sci. Geneve.*, 37(3), 359-
564 373.
- 565 Whalen, M. E., & Minnis, P. E. (2001). Casas Grandes and its hinterland: Prehistoric
566 regional organization in northwest Mexico. University of Arizona Press.
- 567 Whalen, M. E., & Minnis, P. E. (2009). The neighbors of Casas Grandes: excavating medio
568 period communities of northwest Chihuahua, Mexico. University of Arizona Press.
- 569 Whalen, M. E., & Minnis, P. E. (2012). Ceramics and polity in the Casas Grandes
570 area, Chihuahua, Mexico. *American Antiquity*, 77(3), 403-423.
- 571 Wolfman, D., Eighmy, J. L., & Sternberg, R. S. (1990). Archeomagnetic
572 dating. *Archeomagnetic Dating*, 237.

8. Resultados generales

En este trabajo reportan los resultados de los cuatro objetivos planteados. En cada artículo se discute de manera particular los resultados de los mismos. A continuación, se describen los resultados generales obtenidos de acuerdo a objetivos particulares:

- i. *Propiedades magnéticas:* La caracterización de las propiedades magnéticas de los materiales trabajados muestra una gran diversidad en cuanto a la respuesta magnética de cada material en cada uno de sus parámetros. Se observa en la mayoría de los casos estudiados y a nivel mineralógico, que la titanomagnetita con bajo contenido de titanio es el principal portador de la remanencia magnética. En cada uno de los artículos se discuten las diferencias existentes en cuanto la mineralogía y propiedades magnéticas de cada grupo de muestras. En el caso reportado en el Capítulo 7, el uso de propiedades magnéticas permitió diferenciar dos grupos cerámicos (Mimbres y Ramos policromo), los cuales fueron manufacturados en diferentes tiempos y en diferentes sitios arqueológicos, pertenecientes a la región de Casas Grandes, Norte del Estado de Chihuahua, y al sur de Estados Unidos, respectivamente. Ambos grupos cerámicos comparten características físicas y decorativas, pero con pequeñas diferencias en su manufactura. Mediante el uso de propiedades magnéticas se logró diferenciar un grupo cerámico de otro, permitiendo al arqueólogo tener un mejor entendimiento de la actividad humana en cuanto a la manufactura y desplazamiento espacial de estos materiales en la región de Casas Grandes.
- ii. *Datación de materiales volcánicos:* El uso de curvas de variación secular en dirección e intensidad como medio para la datación de artefactos arqueológicos y materiales volcánicos se calibró mediante la datación de la erupción histórica del volcán El Jorullo (Capítulo 5) que tuvo lugar en [1759–1766] AD. Mediante el uso del modelo SHA.DIF.14k se obtuvo una edad de [1702–1762] AD, la cual coincide con la edad histórica reportada. En el Capítulo 3 se reportan los resultados de la datación de dos unidades volcánicas del CVP, las unidades PVF-121 y PVF-122 con edades de 11.2 ± 0.3 ka y 11.1 ± 0.14 ka respectivamente, y se logró constreñir la edad de otra unidad volcánica (Flujo Ives) datada previamente por el método de Ar-/Ar. De igual modo se llevó a cabo la datación de la erupción del volcán Cerro Colorado (Capítulo 4), también ubicado en el CVP. Se estimó una edad de 3915 ± 59 años A.P. mediante el análisis de la componente de magnetización secundaria de clastos de roca encajonante que fueron parcialmente remagnetizados, adquirida en el momento de la erupción. La concordancia de los resultados de la datación de los materiales volcánicos con los valores esperados confirma la confiabilidad del uso de datos paleomagnéticos para fines de datación.
- iii. *Datación de materiales arqueológicos:* Para los grupos cerámicos antes mencionados, denominados Mimbres y Ramos policromo (Capítulo 7), se estimaron edades promedio de [1105-1245] AD y [1315-1405] AD respectivamente. La datación se determinó con base en los datos de arqueointensidad estimados mediante el uso del método de Thellier-Thellier, y obteniendo una paleointensidad de 55.4 ± 4.6 μ T y 42.5 ± 2.8 μ T para Mimbres y Ramos policromo, respectivamente. La estimación de la edad se llevó a cabo mediante la comparación de los resultados de intensidad con la curva propuesta por Mahgoub et al., 2019 con datos de los últimos 3000 años. Los resultados obtenidos para ambos grupos cerámicos coinciden con la cronología estimada por los arqueólogos de los diferentes sitios arqueológicos.

- iv. *Estimación de la temperatura de emplazamiento:* El trabajo realizado en Cerro Colorado, y descrito en el Capítulo 3, se llevó a cabo mediante el análisis de la componente secundaria registrada por bloques de roca embebidos en un anillo de toba producido por la erupción freatomagmática que formó la estructura semicircular del cráter. Los bloques conservan en su mayoría, la dirección característica primaria registrada en el momento de su formación, así como la componente secundaria que se registró luego del recalentamiento sufrido en durante el evento explosivo. El análisis de esta segunda componente como indicador térmico del recalentamiento de los materiales, muestra un rango de temperatura de emplazamiento que oscila entre los 310°C y los 460°C en promedio.
- v. *Análisis de datos direccionales:* Los datos paleomagnéticos direccionales reportados en el trabajo de tesis corresponden a cinco regiones volcánicas de México (Figura 6) pertenecientes a >55 sitios de muestreo: Campo volcánico de Sierra de Chichinautzin y Sierra de Santa Catarina (Capítulo 2), campo volcánico El Pinacate (Capítulo 3 y 4), campo volcánico Michoacán-Guanajuato (Capítulo 5). Se reportan datos direccionales de diferentes productos volcánicos con edades que van de los 1.7 ka a los 2.4 Ma. En los artículos se muestran de manera particular los datos direccionales y estadísticos de cada sitio y las medias para cada región de acuerdo a la escala temporal que le corresponde. La dirección media estimada para el ChVF y SSC con edades que van de 1.7 ka a 1.2 Ma (Dec=359.1°, Inc=35.3°, N=33, k=21.6, α₉₅=5.5°, Plat=87.7° N, Plong=227.4° E, K=31.8, A₉₅=4.5°) con 32 unidades volcánicas con polaridades normales y una con una polaridad inversa, concuerdan con el valor actual del GAD. Para el CVP se obtuvo una paleodirección y paleopol polo con 11/12 unidades volcánicas: Dec=0.1, Inc=54.5, n=14, α₉₅=6.7, k=48, Plat=86.5°, Plong=247.8°, A₉₅=7.5, K=36.7, la cual se ajusta a los valores esperados de la PSV de acuerdo a su latitud. Para los datos direccionales estimados para la erupción histórica del volcán El Jorullo, reportada entre 1759–1766 AD (Dec=2.5°, Inc=37.5°, N=7, k=214, α₉₅=1.8°, Plat=87° N, Plong=307° E, K=260, A₉₅=1.6°) pertenecientes a siete sitios de la misma unidad volcánica; los resultados estimados para El Jorullo son consistentes con el valor esperado para ese momento.

Los valores direccionales estimados, a diferentes escalas temporales, que van de 1.7 ka a 2.4 Ma, muestran un comportamiento dipolar, cuyos resultados coinciden con la configuración del GAD en los últimos 5 Ma (Opdyke et al., 2015). La dispersión de los VGP ($S_b=14.4$) coincide con los valores estimados para la latitud de acuerdo a diferentes modelos globales (e.g. Opdyke et al., 2015; Cromwell et al., 2018; Doubrovine et al., 2019). Estos resultados cubren los sectores Oeste, Centro y Oriental de la TMVB. Sin embargo, existe una gran cantidad de unidades volcánicas de las que se pueden obtener datos direccionales, para la gran mayoría es necesario estimar una edad radiométrica confiable.

- vi. *Análisis de paleointensidad de materiales volcánicos:* Los datos reportados corresponden a dos localidades en México:
 - a. El volcán El Jorullo ubicado en el CVMG, del cual se estimó una paleointensidad media de $46.3 \pm 3.5 \mu\text{T}$ y un VDM de $9.9 \pm 1.0 \times 10^{22} \text{ Am}^2$. Esta media se obtuvo utilizando el método de Thellier-Coe (Coe et al., 1978) realizado en 42 especímenes, y existe una buena concordancia con datos publicados previamente por los métodos de multi-espécimen (Dekkers & Böhnel, 2006) y el de microondas (Walton et al., 1996; Hill and Shaw, 1999).
 - b. Para el CVP se obtuvieron datos de paleointensidad de siete unidades volcánicas del Pleistoceno tardío, mediante el uso del método de Thellier-Coe (Coe et al., 1978). Se

obtuvo un rango de paleointensidad que va de los $33.1 \mu\text{T}$ a los $61.4 \mu\text{T}$, y un VDM que va de los $5.4 \times 10^{22} \text{ Am}^2$ a los $12.9 \times 10^{22} \text{ Am}^2$.

vii. *Análisis de paleointensidad de materiales arqueológicos:* Los datos reportados corresponden a dos localidades en México:

- a. La zona arqueológica de Chalcatzingo (Capítulo 6), ubicada en el estado de Morelos. Se reportan datos de arqueointensidad de 54 especímenes, obtenidos mediante el uso del método de Thellier-Thellier (1959), estimando 13 valores de arqueointensidad para fragmentos cerámicos del Epiclásico (650AD -900 AD). Los valores de arqueointensidad oscilan entre los $24.9 \mu\text{T}$ a los $42.7 \mu\text{T}$ y VADM de 5.6 a $9.0 \times 10^{22} \text{ Am}^2$. Estos valores muestran un cambio rápido en cuanto la variación secular en México, contrastando significativamente con algunos de los modelos globales antes mencionados. Con los resultados obtenidos de Chalcatzingo y en conjunto con una compilación y filtrado de datos de intensidad de materiales arqueológicos y volcánicos (194) en México (material suplementario S2). Se propuso una curva Bayesiana de variación secular para los últimos 4 ka, que muestra las diferencias existentes entre los modelos globales y los registros de variación secular en México.
- b. La región de Casas Grandes, ubicada al norte del estado de Chihuahua (Capítulo 7). Se reportan datos de cuatro sitios: Paquimé, Villa Ahumada, Galeana and Samalayuca. La región tuvo una intensa ocupación humana entre 0 AD – 1450 AD. Los datos de arqueointensidad fueron estimados mediante el uso del método de Thellier-Thellier (1959) en 24 especímenes de dos tipos cerámicos diferentes (Mimbres y Ramos policromo), encontrados en toda la región. Ambos tipos cerámicos cuentan con características similares en forma y decoración, pero con temporalidades y estilos de manufactura diferentes. Se obtuvo una arqueointensidad media para cada tipo cerámico: Mimbres [1105 AD – 1245 AD] con una arqueointensidad de $55.4 \pm 4.6 \mu\text{T}$, y VADM $10.8 \times 10^{22} \text{ Am}^2$; y para Ramos policromo [1315 AD – 1406 AD] $42.4 \pm 2.8 \mu\text{T}$, y VADM $8.2 \times 10^{22} \text{ Am}^2$. Estos resultados corresponden a lo esperado en esa temporalidad de acuerdo a las curvas propuestas actuales para México (e.g. Mahgoub et al., 2019; Hervé et al., 2019).

Algunos resultados obtenidos contrastan con los valores esperados para México de acuerdo a algunos de los modelos globales mencionados, mostrando un cambio en paleointensidad y momento dipolar mas rápido en comparación de los propuestos en algunos modelos globales como SHA.DIF14. Casi todos los resultados son coincidentes con los modelos globales, lo cual no es de sorprenderse, ya que muchos de los datos publicados para México han sido usados para la elaboración de dichos modelos. Sin embargo, la cantidad de datos disponibles para intensidad sigue siendo muy pequeña en comparación con la cantidad de datos direccionales, por lo que es necesario la obtención de mas cantidad de datos, que cuenten con datación adecuada. Esto permitirá refinar las curvas existentes y completar los espacios vacíos.

viii. *Análisis de la variación paleosecular del CGM y compilaciones de datos:* La compilación de datos direccionales y de intensidad de materiales volcánicos arqueológicos, publicados en México, muestra las variaciones seculares del CGM. Un análisis crítico sobre la calidad y confiabilidad de estos datos muestra la consistencia y el impacto que tiene en la construcción de modelos regionales y globales de variación secular.

a. *Materiales volcánicos (análisis direccional)*: La Figura 14 muestra la distribución de los sitios analizados. De los datos direccionales se analizaron alrededor de 450 sitios reportados en alrededor de 50 trabajos publicados. La edad reportada va de 1.7 ka a 1.5 Ma, pertenecientes a diferentes flujos de lava de la FVTM. Se obtuvo una paleodirección y un paleopololo para la FVTM en los últimos 1.5 Ma (Dec=358.4°, Inc=35°, N=275, k=31.7, $\alpha_{95}=1.6^\circ$, Plat=88.3° N, Plong=186.6° E, K=40.2, A95=1.4°), la cual coincide con la configuración del GAD. La estimación de la dirección se obtuvo luego de hacer un análisis crítico de los datos publicados anteriormente, en conjunto con los datos publicados en el presente trabajo, donde se toman en cuenta los valores de dispersión (k), la existencia y calidad de una datación adecuada, la cantidad de especímenes empleados en el cálculo entre otros. Del total de datos analizados para la FVTM se uso únicamente ca. 65% de los datos publicados, el resto fue descartado por que no cumplió con alguno de los criterios de calidad establecidos. La falta de una datación adecuada o ausencia completa de edad y una alta dispersión fueron los motivos principales para descartar diversos sitios. Asimismo, se reportan una gran cantidad de datos transicionales, los cuales no se consideraron para el cálculo. La distribución de las dataciones disponibles muestra que ca. del 25% de los datos reportados son de los últimos 50 ka, y ca. El 80% de los datos corresponden a sitios menores a 500 ka. Lo anterior muestra una gran diferencia en la cantidad de datos reportados para edades mayores al medio millón de años, lo cual deja ver la necesidad de generar mas cantidad de datos en periodos de tiempo específicos. Por otro lado, muchos de los datos publicados presentan una dispersión considerable, lo que implica una disminución en la consistencia de los datos, lo que hace deseable la publicación de datos sujetos a un escrutinio mas estricto en cuanto a la estadística propia de cada sitio. Finalmente, los resultados aceptados para la estimación de un paleopololo para la FVTM en los últimos 1.5 Ma muestran que la gran mayoría de los datos existentes cuentan con una alta calidad para poder ser tomados en cuenta para el desarrollo de modelos de PSV regionales y globales. El análisis direccional realizado en la FVTM muestra que el registro de la PSV corresponde a un dipolo que se ajusta al modelo del GAD. Asimismo, la dispersión (S) de los VGP muestra que, de acuerdo a la latitud, se ajusta a los modelos de variación secular existentes a diferentes escalas temporales.

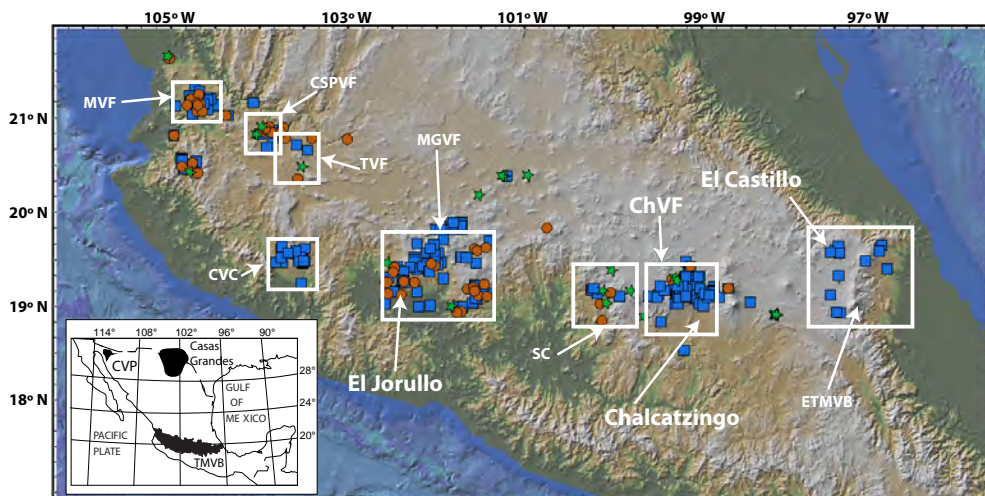


Figura 14. Distribución espacial de los sitios estudiados en este trabajo.

b. *Materiales arqueológicos (arqueointensidad)*: Se analizaron 194 datos de intensidad publicados en cerca de 40 trabajos de México y Centroamérica. Los materiales empleados

son principalmente de origen arqueológico (e.g. cerámica, hornos, pisos quemados, estucos quemados), y algunos datos reportados de diversos flujos de lava. Los datos de paleointensidad observada en los datos analizados fluctúa de 15 μT a 90 μT , un rango considerablemente amplio para un periodo de tiempo de 4 ka. La mayor densidad de datos se concentra en el Preclásico tardío (400 BCE-200 CE) y el Clásico (200-650 AD). Sin embargo, se observan espacios temporales con pocos o ningún dato reportado en 800-400 BCE y alrededor del 1000 AD. Con los datos disponibles se construyó una curva Bayesiana (Hervé and Lanos, 2018; Lanos, 2004; Schnepf et al., 2015) propuesta para los últimos 4 ka. La curva muestra cambios rápidos en la paleointensidad (varias decenas de μT) en periodos de tiempo cortos (e.g. 400 BCE – 1500 CE). Estos cambios rápidos coinciden con el periodo de mayor densidad de datos, lo que podría asociarse a una excursión. Sin embargo, fue necesario llevar a cabo un análisis crítico de los datos existentes, dado que lo observado puede deberse a un artefacto en lugar de un evento geomagnético real. Para ello se clasificaron los resultados (C1, C2 y C3) de acuerdo a diferentes criterios, tales como el método usado para estimar la paleointensidad, si posee correcciones por tensor de anisotropía y por tasa de enfriamiento, entre otros. De este modo se separan los resultados de alta calidad de aquellos con calidades intermedias y bajas, y así es posible observar como una calidad media o baja puede provocar una sobreestimación de los valores de paleointensidad obtenidos. Luego de clasificar los resultados de acuerdo a los criterios establecidos se observa que solo un 12% de los datos publicados poseen la mas alta calidad (C1), cumpliendo con todos los criterios establecidos; un 14% entran en la categoría intermedia (C2) y el resto, alrededor del 74% entra en la categoría con una calidad baja (C3), lo que implica la posible existencia de una sobreestimación de la paleointensidad al no contar con una corrección por tensor de anisotropía y/o enfriamiento.

9. Discusión y conclusiones

9.1 Materiales volcánicos

La distribución espacial (Figura 14) y temporal de los diversos flujos de lava estudiados en el presente trabajo, muestran el registro de dirección e intensidad del CGM en rocas volcánicas de diversos campos volcánicos de México en diferentes latitudes, que van desde el centro del país en la FVTM, y hasta la porción NW de México con el CVP. De acuerdo a la edad de los materiales estudiados, las edades van desde una escala histórica, con la erupción del volcán El Jorullo [1759–1766 AD] y hasta flujos de lava de ChVF con una edad *ca.* 1.2 Ma. Asimismo, la compilación de datos de paleomagnetismo publicados en México en los últimos años, muestra el trabajo realizado por diversos autores en materiales volcánicos de toda la FVTM con edades desde 1.7 ka y hasta 1.5 Ma.

9.1.1 Análisis direccional en rocas volcánicas

Los resultados direccionales muestran una correspondencia con el comportamiento promedio de la configuración de un modelo de un GAD a diferentes escalas de tiempo. Los resultados van de acuerdo a lo esperado en México de acuerdo a diferentes modelos globales de variación secular publicados recientemente (e.g. SHA.DIF.14k, CALS10k2). Lo cual tiene una correspondencia lógica, dado que dichos modelos globales y otros, emplean resultados de México para su desarrollo.

Los resultados de unidades volcánicas menores a 4000 años, se observa una variación en declinación que va desde los -20° a los 20° en promedio, y de los 15° a los 60° en inclinación. Para muestras que van de los 5000 años a los 14 años se observa una variación en declinación que va de los -30° a los

30°, y con inclinaciones que llegan a valores cercanos a los 70°. En este periodo se observan variaciones mayores y en periodos de tiempo mas cortos que en los modelos globales de variación secular. Lo anterior se debe a que los modelos globales emplean una gran cantidad de datos de todo el mundo para definir una variación promedio en todo el globo.

En los resultados de hasta 1.5 Ma, se muestra una variación promedio en la declinación que va desde los -30° y hasta los 35°, de los 15° a los 70° en inclinación. A una escala mayor a los 14 ka, se observa una disminución en la densidad de datos disponibles. La cantidad de unidades volcánicas con fechamientos de alta calidad muestra su mayor densidad en rocas con edades menores a los 100 ka. En unidades volcánicas de edades mayores se observan cada vez en menor cantidad y con incertidumbres mas grandes. Estas diferencias en la disponibilidad de fechamientos, e incertidumbres cada vez mayores, dificultan el manejo de los datos secularmente, haciendo difícil la distribución de los resultados por herramientas estadísticas como histogramas y funciones de distribución de probabilidad.

Sin embargo, la variación del CGM depende en gran medida de la localización. A escalas de tiempo mas pequeñas (menores a 20 ka), es necesario construir no solo modelos de variación secular globales, si no modelos regionales, lo cual permitirá entender de mejor manera las variaciones seculares del CGM a escalas de tiempo cada vez mas pequeñas. En México han sido publicados hasta ahora dos modelos de variación secular (e.g. Mahgoub et al., 2019b) para los últimos 45 ka, y que incluyen datos direccionales de diferentes unidades volcánicas, principalmente de la FVTM. Estos modelos cubren ampliamente el intervalo de tiempo, con una gran cantidad de datos de diferentes localidades. Sin embargo, la gran limitación que presentan dichos modelos es la disponibilidad de datos en segmentos temporales bien definidos, como lo observado en la curva de Mahgoub et al., 2019b, donde entre 15 y 20 ka la densidad de datos es considerablemente menor, en comparación de la curva entre los 0 y los 5 ka.

Las direcciones obtenidas para el CVP muestran un patrón de variación proporcionalmente similar a lo observado en la FVTM. Sin embargo, debido la diferencia en cuanto a la latitud (*ca.* 10°), no es posible discutirlo de manera conjunta. En el CVP, donde el 95% de las unidades volcánicas estudiadas en este trabajo tienen una edad menor a 50 ka. La declinación varía en un rango que va *ca.* de los -25° a los 30°, y la inclinación entre los 40° y 60°. Esta variación es coincidente con lo esperado de acuerdo a su latitud y de acuerdo a diversos modelos globales que estiman la variación paleosecular con datos generados de diferentes latitudes alrededor del mundo (e.g. Opdyke et al., 2015; Cromwell et al., 2018).

La disponibilidad de datos en segmentos temporales determinados, se observa claramente en la compilación de datos realizada en el presente trabajo. La cual disminuye en cuanto se incrementa la edad de las unidades volcánicas. Se observa como cerca del 75% de las edades reportadas en los trabajos de paleomagnetismo publicados de la FVTM, son menos a 200 ka. Y cerca del 60% de las mismas tienen una edad de menos de 50 ka. La ausencia de edades suficientes, que cubran completamente un periodo de tiempo dado, en este caso hasta 1.5 Ma, limita considerablemente el trabajo paleomagnético. Esta circunstancia, crea la necesidad de trabajar mas estrechamente con vulcanólogos, para obtener edades nuevas acompañadas de datos paleomagnéticos nuevos que permitan llenar espacios vacíos en las curvas de variación secular existentes; y de igual manera, realizar dataciones de unidades volcánicas usando datos paleomagnéticos, como las realizadas en el presente trabajo para las unidades volcánicas del CVP y el volcán el Jorullo.

Si bien la distribución de las edades disponibles representa una limitante para la generación de datos paleomagnéticos, la alta incertidumbre de algunas de las edades disponibles crea una limitante para

la generación de modelos de variación secular, ya que dificulta el establecer un rango adecuado para un dato paleomagnético con una edad específica. En la Figura 15 se observa la distribución de los datos direccionales de acuerdo a su edad y valor de declinación e inclinación. Se observa que la incertidumbre de la edad, se incrementa considerablemente conforme aumenta la edad. La necesidad de datación de alta calidad es un parámetro de gran importancia para poder entender los efectos de la variación secular del CGM, y para la construcción de modelos tanto globales como regionales. La baja calidad de las dataciones genera errores y valores de incertidumbre altos, por lo que es necesario seleccionar y filtrar aquellos datos de paleomagnetismo asociados a unidades volcánicas con dataciones de calidad cuestionable, o en su caso buscar una datación mas reciente con un valor de incertidumbre menor.

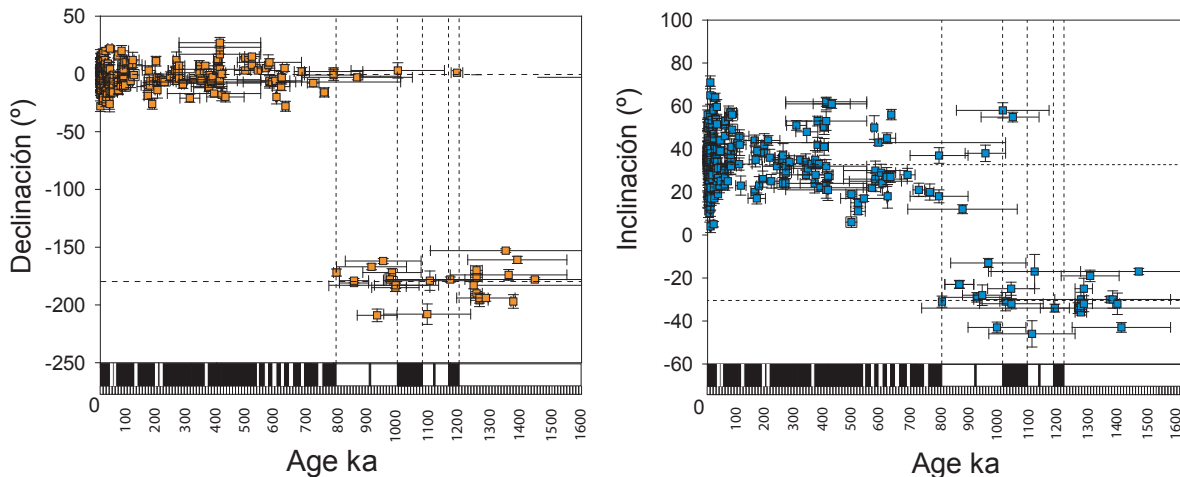


Figura 15. Distribución de datos direccionales disponibles de la FVTM del presente trabajo y publicados previamente. Las barras verticales muestran la variación del α_{95} ; las barras horizontales muestran la incertidumbre de la edad reportada.

9.1.2 Paleointensidad de rocas volcánicas

El estudio de la paleointensidad del CGM registrado en rocas volcánicas, se llevó a cabo en dos localidades de México: la primera en la erupción del volcán El Jorullo, que pertenece al CVMG, en el estado de Michoacán en el centro del país; y a diversas unidades volcánicas del CVP, en el estado de Sonora en el Norte de México. Los resultados las unidades mas jóvenes (menores a 14 ka) muestran una concordancia con los valores esperados por las predicciones de los modelos global SHA.DIF.14k, y mostrando una variación en intensidad que va de los $30 \mu\text{T}$ a los $65 \mu\text{T}$, y un momento dipolar que va de los 5.4 a los $11.8 \times 10^{22} \text{ Am}^2$. Sin embargo, en el período de tiempo en el que están ubicadas la mayoría de las muestras estudiadas, existen aun pocos datos con los cuales sea posible comparar los resultados obtenidos de manera directa. La buena calidad de los resultados permite tener un alto grado de confiabilidad en los mismos, con lo cual es viable la inclusión de estos en bases de datos globales y modelos de variación secular regionales, ya que son los primeros en su tipo para el NW de México.

9.1.3 Compilación de datos direccionales en rocas volcánicas

De los resultados de datos direccionales obtenidos en el presente trabajo y de la compilación de trabajos de paleomagnetismo de rocas volcánicas de la FVTM, se establecieron cuatro criterios básicos para discriminar los datos reportados de aquellos que presentan alguna inconsistencia o baja

confiabilidad en cuanto a su calidad. Los criterios básicos fueron: a) el numero de especímenes reportados por sitio deben ser mayores o iguales a 4, lo que permite verificar que la estadística de Fisher reportada tenga un margen mínimo de calidad; b) que los datos reportados tengan una edad reportada por algún método radiométrico (e.g. ^{14}C , Ar/Ar), lo que permite constreñir de mejor manera los efectos de la variación secular registrada en las muestras; c) los valores del parámetro estadístico k deberán ser mayores a 60, lo que permite seleccionar aquellas muestras que presentan una dispersión óptima y de alta calidad; d) que los datos publicados no estén asociados a efectos de remagnetización (e.g. rayos), bloques movidos que no correspondan a muestras tomadas *in-situ*, o a la presunción de datos correspondientes a direcciones transicionales (excursiones). Los criterios antes mencionados permitieron hacer un filtrado de datos, seleccionando únicamente aquellos que cumplen con los 4 criterios propuestos. De los resultados seleccionados, se observó que cerca del 30% de los datos publicados no cumplen con el requisito de tener un valor de capa mínimo de 60; cerca del 14% de los resultados no cuentan con una edad radiométrica reportada, lo que se ve reflejado en una incertidumbre considerable a la hora de establecer la variación de la dirección con respecto a su edad (Figura 15), haciendo esto mas evidente en los cambios de polaridad registrados. Asimismo, cerca del 7% de los datos fueron reportados con menos de 4 especímenes por sitios, lo que reduce la confiabilidad de los datos publicados. De esta manera, es posible ver que, del total de trabajos analizados en este trabajo, alrededor del 68% cuenta con una calidad suficiente para ser tomados en cuenta en bases de datos globales.

Con los resultados obtenidos, es posible visualizar que la calidad y densidad de datos publicados en México se ha incrementado en tiempos recientes, estableciendo criterios cada vez mas exhaustivos y rigurosos desde la colección de muestras y hasta el procesamiento de datos en el laboratorio. Sin embargo, como ya se ha discutido, es necesario generar nuevos datos en periodos de tiempo con poca cantidad de datos, lo que permitirá cubrir vacíos temporales, que impiden ver el desarrollo progresivo del CGM en los últimos 1.5 Ma registrado en materiales volcánicos.

9.2 Materiales arqueológicos

Los resultados de materiales arqueológicos estudiados en el presente trabajo, abarcan dos sitios arqueológicos del norte y centro de México: Casas Grandes, localizado en la parte Norte del Estado de Chihuahua y SW de EEUU; y el sitio arqueológico de Chalcatzingo, en el Estado de Morelos en el Centro de México. Se obtuvieron datos de arqueointensidad de materiales cerámicos de ambos sitios arqueológicos, con la finalidad de conocer la variación secular del CGM registrada en dichos materiales, y en el caso de la cerámica de Casas Grandes, poder llevar a cabo la datación de dichos materiales mediante el uso de las curvas de variación secular mas recientes publicadas para México.

9.2.1 Arqueointensidad en material cerámico

De las muestras trabajadas en el presente trabajo, se observa una variación en intensidad de va desde los $25 \mu\text{T}$ a los $55 \mu\text{T}$, y una variación en el momento dipolar que va de los 6 a los $11 \times 10^2 \text{ Am}^2$, en un periodo que va de *ca.* 700 AD al 1400 AD.

Los resultados obtenidos son consistentes con los valores esperados de acuerdo al modelo global SHA.DIF.14k, y a los modelos de variación secular publicados para México recientemente (Figura 16). Los resultados promedios para cada grupo cerámico son coincidentes con los cambios propuestos por los diferentes modelos en el periodo antes señalado. En ese mismo periodo se observa una buena concordancia entre los cuatro modelos analizados que se muestran en la Figura 16.

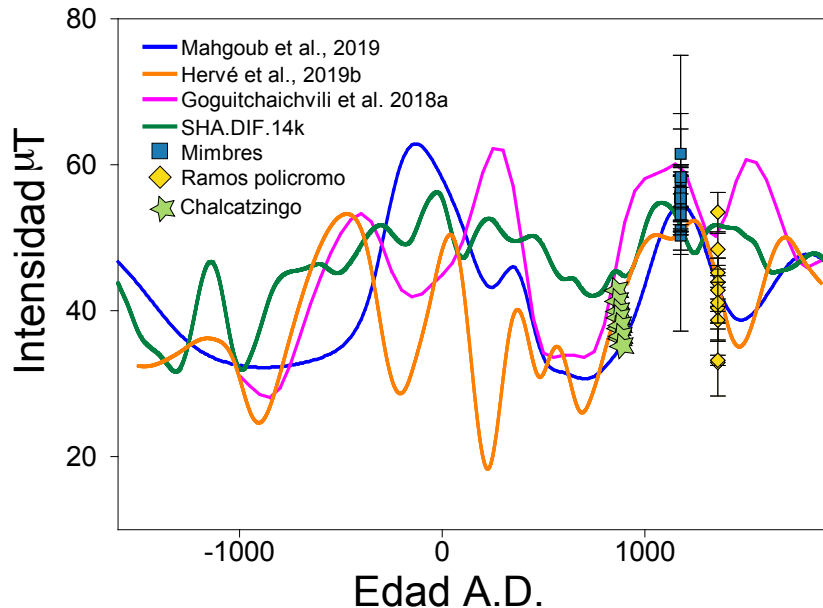


Figura 16. Resultados de arqueointensidad por sitio. Comparación con modelos de variación secular publicados para México.

9.2.2 Compilación y análisis crítico de datos de arqueointensidad de México

De los diversos modelos globales disponibles como son el CALS10k.2 (Constable et al., 2016), SHA.DIF.14 k (Pavón-Carrasco et al., 2014a), COV-ARCH/COV-LAKE (Hellio and Gillet, 2018), entre otros, y modelos regionales (e.g. Goguitchaichvili et al., 2018; Hervé et al., 2019; Mahgoub et al., 2019), existen diferencias significativas en cuanto a la variación secular en períodos de tiempo determinados. Dada esta situación, se llevó a cabo una compilación de datos de arqueointensidad publicados de materiales arqueológicos de México de los últimos 4000 años. Se analizaron 194 resultados de intensidad de cerca de 40 trabajos publicados recientemente. De los cuales, una buena proporción están incluidos en bases de datos globales como GEOMAGIA50. Estos datos han sido utilizados en su mayoría para el desarrollo de diversas curvas de variación secular globales y regionales. Sin embargo, la gran mayoría de estos datos no han sido filtrados de acuerdo a criterios estrictos que garanticen la calidad de los mismos. Como se discutió anteriormente en los datos direccionales de materiales volcánicos, la necesidad de diferenciar los datos de alta calidad de aquellos que no poseen la calidad necesaria para ser incluidos en modelos globales y/o regionales. Para esto, se hizo una clasificación de los datos en tres categorías (C1, C2, C3) de acuerdo a la confiabilidad de los datos, se establecieron los requisitos de acuerdo a los siguientes criterios: número de especímenes empleados, aplicación de correcciones por ATRM y taza de enfriamiento, y una desviación estándar menor al 10%.

Donde C1 representa los datos de mayor calidad, cumpliendo con los tres requisitos antes mencionados. La categoría C2 incluye aquellos que presentan una desviación estandar de alrededor del 15%; y la categoría C3 que representa los valores de calidad mas bajos, los cuales tienen una desviación estandar mayor a 15% y no cumplen con alguna de las correcciones como el ATRM o taza de enfriamiento. Como ya se mencionó anteriormente, solo el 12% de los especímenes se clasificaron como C1; un 14% en la categoría C2; y un 74% en la categoría C3. Estos resultados muestran que una gran proporción de los resultados publicados pueden tener un error asociado, lo cual se refleja en

una estimación errónea de la arqueointensidad estimada. Estas diferencias detectadas generan discrepancias en los diferentes modelos disponibles. En la Figura 16 se observa como en el período del 0 AD – 500 AD, existen diferencias significativas en todos los modelos presentados. Estas diferencias pueden estar asociadas a dos factores principales, el primero a la disponibilidad de muestras de esta temporalidad, que puede ser menor en comparación a otros períodos; y segundo a las estimaciones erróneas de la arqueointensidad. La gran contribución de este trabajo es que se permite visualizar las deficiencias en la selección de datos para su publicación y para su integración en bases de datos y modelos globales y regionales. Haciendo mas exhaustiva la selección de acuerdo a los criterios propuestos.

9.3 Modelos de variación secular del CGM

Los resultados obtenidos de rocas volcánicas y materiales arquelógicos, representan un valioso registro de los cambios en el CGM. Gran parte de estos resultados, direccionales y de paleointensidad, han sido usados para el desarrollo de diversos modelos mencionados en este trabajo. Sin embargo, todos los modelos analizados presentan diferencias en diversos puntos del tiempo. Estas diferencias se pueden asociar, entre otras causas, a la calidad de algunos de los datos paleomagnéticos utilizados, así como a la baja confiabilidad de algunos de los fechamientos asociados a la diferentes unidades. El presente trabajo tiene como uno de sus objetivos el analizar y hacer un análisis crítico de los materiales estudiados y publicados en México, y se ha mostrado que en muchos casos, la calidad y confiabilidad de algunos de los datos usados en los modelos antes mencionados pueden ser cuestionables. Y como ya se ha discutido en los artículos publicados en este trabajo, genera la necesidad de establecer filtros estrictos y selección más rigurosa de datos para la inclusión en estos modelos.

Así, los modelos resultantes serán más consistentes y con menos discrepancias unos con otros. Como ya se mencionó antes, los datos publicados dependen en gran medida de las edades reportadas y de su calidad, así como de la calidad misma de los datos paleomagnéticos obtenidos. Las Figuras 15 y 16 muestran un bosquejo de algunos de los datos paleomagnéticos compilados en este trabajo, en conjunto con los modelos de variación secular disponibles. Es posible observar segmentos con gran concordancia entre los modelos, con una gran densidad de datos e incertidumbres bajas, como es el caso del período entre el 500 AD – 1400 AD. Sin embargo, hay segmentos en los que la baja densidad de datos e incertidumbres altas generan grandes discrepancias entre los modelos.

De manera general, los resultados observados en el presente trabajo, tanto en materiales volcánicos y arqueológicos, dejan ver el crecimiento en cuanto a cantidad de datos publicados en tiempos recientes, así como el mejoramiento de la calidad de los mismos. La publicación cada vez más frecuente de nuevas edades para los materiales trabajados ha permitido abrir el panorama para la colaboración interdisciplinaria y la publicación de nuevos datos de buena calidad. Sin embargo, no se debe dejar de lado el sesgo existente en cuanto los datos disponibles en la actualidad, donde una proporción considerable de los mismos posee una calidad cuestionable. La producción de datos paleomagnéticos debe estar basada en criterios de calidad estrictos, como los mostrados en el presente trabajo. De ahí la necesidad de clasificar, filtrar y seleccionar los datos que se incluirán en modelos variación secular en la actualidad. Con datos de buena calidad y suficientes dataciones disponibles, es posible crear modelos más robustos, con una precisión y definición cada vez mayor. Asimismo, es importante buscar objetivos específicos que permitan llenar los espacios temporales que cuenten con una baja densidad de datos. De este modo, se insta a los paleomagnetistas a seguir trabajando en conjunto para mejorar la comprensión integral del campo magnético de la tierra a través del tiempo.

Referencias

- Aitken, M. J., Alcock, P. A., Bussell, G. D., & Shaw, C. J. (1981). Archeomagnetic determination of the past geomagnetic intensity using ancient ceramics: allowance for anisotropy. *Archeometry*, 23(1), 53-64.
- Aitken, M. J., Allsop, A. L., Bussell, G. D., & Winter, M. B. (1988). Determination of the intensity of the Earth's magnetic field during archaeological times: reliability of the Thellier technique. *Reviews of Geophysics*, 26(1), 3-12.
- Alva-Valdivia, L. M., Rodríguez-Trejo, A., Morales, J., González-Rangel, J. A., & Agarwal, A. (2019). Paleomagnetism and age constraints of historical lava flows from the El Jorullo volcano, Michoacán, Mexico. *Journal of South American Earth Sciences*, 93, 439-448.
- Böhnel, H., & Molina-Garza, R. (2002). Secular variation in Mexico during the last 40,000 years. *Physics of the Earth and Planetary Interiors*, 133(1-4), 99-109.
- Brown, M.C., F. Donadini, M. Korte, A. Nilsson, K. Korhonen, A. Lodge, S.N. Lengyel and C.G. Constable, GEOMAGIA50.v3: 1. General structure and modifications to the archeological and volcanic database, *Earth Planets Space* 67:83, doi:10.1186/s40623-015-0232-0.
- Butler, R. F. (1998). Paleomagnetism: Magnetic domains to geologic terranes. Electronic edition, 23.
- Carvallo, C., Muxworthy, A. R., Dunlop, D. J., & Williams, W. (2003). Micromagnetic modeling of first-order reversal curve (FORC) diagrams for single-domain and pseudo-single-domain magnetite. *Earth and Planetary Science Letters*, 213(3-4), 375-390.
- Coe, R. S. (1967). Paleo-intensities of the Earth's magnetic field determined from Tertiary and Quaternary rocks. *Journal of Geophysical Research*, 72(12), 3247-3262.
- Constable, C., Korte, M., & Panovska, S. (2016). Persistent high paleosecular variation activity in southern hemisphere for at least 10 000 years. *Earth and Planetary Science Letters*, 453, 78-86.
- Constable, C., Korte, M., & Panovska, S. (2016). Persistent high paleosecular variation activity in southern hemisphere for at least 10 000 years. *Earth and Planetary Science Letters*, 453, 78-86.
- Cromwell, G., Johnson, C. L., Tauxe, L., Constable, C. G., & Jarboe, N. A. (2018). PSV10: A global data set for 0–10 Ma time-averaged field and paleosecular variation studies. *Geochemistry, Geophysics, Geosystems*, 19(5), 1533-1558.

Dekkers, M. J., & Böhnel, H. N. (2006). Reliable absolute palaeointensities independent of magnetic domain state. *Earth and Planetary Science Letters*, 248(1-2), 508-517.

Doubrovine, P. V., Veikkolainen, T., Pesonen, L. J., Piispa, E., Ots, S., Smirnov, A. V., ... & Biggin, A. J. (2019). Latitude dependence of geomagnetic paleosecular variation and its relation to the frequency of magnetic reversals: Observations from the Cretaceous and Jurassic. *Geochemistry, Geophysics, Geosystems*.

Ferrari, L., Garduño, V. H., Pasquare, G., & Tibaldi, A. (1994). Volcanic and tectonic evolution of central Mexico: Oligocene to present. *Geofísica Internacional*, 33(1), 91-105.

Ferrari, L., López-Martínez, M., Aguirre-Díaz, G., & Carrasco-Núñez, G. (1999). Space-time patterns of Cenozoic arc volcanism in central Mexico: From the Sierra Madre Occidental to the Mexican Volcanic Belt. *Geology*, 27(4), 303-306.

Fisher, R. A. (1953). Dispersion on a sphere. *Proceedings of the Royal Society of London. Series A. Mathematical and Physical Sciences*, 217(1130), 295-305.

García-Ruiz, R., Goguitchaichvili, A., Cervantes-Solano, M., Cortés-Cortés, A., Morales-Contreras, J., Maciel-Peña, R., ... & Macías-Vázquez, J. L. (2016). Secular variation and excursions of the Earth magnetic field during the Plio-Quaternary: New paleomagnetic data from radiometrically dated lava flows of the Colima volcanic complex (western Mexico). *Revista Mexicana de Ciencias Geológicas*, 33(1), 72-80.

Gauss, C. F. (1841). Allgemeine Theorie des Erdmagnetismus, in Resultate aus den Beobachtungen des magnetischen Vereins im Jahr 1838. *Sci. Mem. Select. Trans. Foreign Acad. Learned Soc. Foreign J.*, 2, 184-251.

Glatzmaier, G. A., Coe, R. S., Hongre, L., & Roberts, P. H. (1999). The role of the Earth's mantle in controlling the frequency of geomagnetic reversals. *Nature*, 401(6756), 885.

Glassmeier, K. H., Soffel, H., & Negendank, J. (Eds.). (2008). *Geomagnetic field variations*. Springer Science & Business Media.

Goguitchaichvili, A., Ruiz, R. G., Pavón-Carrasco, F. J., Contreras, J. J. M., Arechalde, A. M. S., & Urrutia-Fucugauchi, J. (2018). Last three millennia Earth's Magnetic field strength in Mesoamerica and southern United States: Implications in geomagnetism and archeology. *Physics of the Earth and Planetary Interiors*, 279, 79-91.

Hervé, G., & Lanos, P. (2018). Improvements in archaeomagnetic dating in Western Europe from the late Bronze to the Late Iron Ages: an alternative to the problem of the Hallstattian radiocarbon plateau. *Archaeometry*, 60(4), 870-883.

Hervé, G., Perrin, M., Alva-Valdivia, L., Tchibinda, B. M., Rodriguez-Trejo, A., Hernandez-Cardona, A., ... & Rodriguez, C. M. (2019b). Critical analysis of the Holocene

palaeointensity database in Central America: Impact on geomagnetic modelling. Physics of the Earth and Planetary Interiors, 289, 1-10.

Hill, M. J., & Shaw, J. (1999). Palaeointensity results for historic lavas from Mt Etna using microwave demagnetization/remagnetization in a modified Thellier-type experiment. Geophysical Journal International, 139(2), 583-590.

Johnson, C. L., & Constable, C. G. (1995). The time-averaged geomagnetic field as recorded by lava flows over the past 5 Myr. Geophysical Journal International, 122(2), 489-519.

Kelly, P., & Gubbins, D. (1997). The geomagnetic field over the past 5 million years. Geophysical Journal International, 128(2), 315-330.

Koenigsberger, J. G. (1932). Thermoremanenz und spontane Magnetisierung. Phys. Zeits, 33, 468-474.

Lanos, P. (2004). Bayesian inference of calibration curves: application to archaeomagnetism. In Tools for Constructing Chronologies (pp. 43-82). Springer, London.

Mahgoub, A. N., Juárez-Arriaga, E., Böhnel, H., Siebe, C., & Pavón-Carrasco, F. J. (2019). Late-Quaternary secular variation data from Mexican volcanoes. Earth and Planetary Science Letters, 519, 28-39.

McElhinny, M. W., & McFadden, P. L. (1998). The magnetic field of the earth: paleomagnetism, the core, and the deep mantle(Vol. 63). Academic Press.

Néel, L. (1949). Théorie du traînage magnétique des ferromagnétiques en grains fins avec applications aux terres cuites. Ann. géophys., 5, 99-136.

Opdyke, N. D., Kent, D. V., Foster, D. A., & Huang, K. (2015). Paleomagnetism of Miocene volcanics on Sao Tome: Paleosecular variation at the Equator and a comparison to its latitudinal dependence over the last 5 Myr. Geochemistry, Geophysics, Geosystems, 16(11), 3870-3882.

Panovska, S., Constable, C. G., & Brown, M. C. (2018). Global and regional assessments of paleosecular variation activity over the past 100 ka. Geochemistry, Geophysics, Geosystems.

Paterson, G. A., Tauxe, L., Biggin, A. J., Shaar, R., & Jonestrask, L. C. (2014). On improving the selection of Thellier-type paleointensity data. Geochemistry, Geophysics, Geosystems, 15(4), 1180-1192.

Pavón-Carrasco, F. J., Osete, M. L., Torta, J. M., & De Santis, A. (2014). A geomagnetic field model for the Holocene based on archaeomagnetic and lava flow data. Earth and Planetary Science Letters, 388, 98-109.

Roberts, A. P., Heslop, D., Zhao, X., & Pike, C. R. (2014). Understanding fine magnetic particle systems through use of first-order reversal curve diagrams. *Reviews of Geophysics*, 52(4), 557-602.

Roberts, A. P., Pike, C. R., & Verosub, K. L. (2000). First-order reversal curve diagrams: A new tool for characterizing the magnetic properties of natural samples. *Journal of Geophysical Research: Solid Earth*, 105(B12), 28461-28475.

Rodríguez-Trejo, A., Alva-Valdivia, L. M., Perrin, M., Hervé, G., & López-Valdés, N. (2019). Analysis of geomagnetic secular variation for the last 1.5 Ma recorded by volcanic rocks of the Trans Mexican Volcanic Belt: new data from Sierra de Chichinautzin, Mexico. *Geophysical Journal International*, 219(1), 594-606.

Schnepp, E., Leonhardt, R., Korte, M., & Klett-Drechsel, J. (2016). Validity of archaeomagnetic field recording: an experimental pottery kiln at Coppengrave, Germany. *Geophysical Supplements to the Monthly Notices of the Royal Astronomical Society*, 205(1), 622-635.

Tauxe, L., & Staudigel, H. (2004). Strength of the geomagnetic field in the Cretaceous Normal Superchron: New data from submarine basaltic glass of the Troodos Ophiolite. *Geochemistry, Geophysics, Geosystems*, 5(2).

Tauxe, L., Shaar, R., Jonestrask, L., Swanson-Hysell, N. L., Minnett, R., Koppers, A. A. P., ... & Fairchild, L. (2016). PmagPy: Software package for paleomagnetic data analysis and a bridge to the Magnetics Information Consortium (MagIC) Database. *Geochemistry, Geophysics, Geosystems*, 17(6), 2450-2463.

Thellier, E. (1959). Sur l'intensité du champ magnétique terrestre dans le passé historique et géologique. *Ann. Geophys.*, 15, 285-376.

Veitch, R. J. (1984). An investigation of the intensity of the geomagnetic field during Roman times using magnetically anisotropic bricks and tiles. *Arch. Sci. Geneve.*, 37(3), 359-373.

Walton, D., Snape, S., Rolph, T. C., Shaw, J., & Share, J. (1996). Application of ferrimagnetic resonance heating to palaeointensity determinations. *Physics of the earth and planetary interiors*, 94(3-4), 183-186.

Winch, D. E., Ivers, D. J., Turner, J. P. R., & Stening, R. J. (2005). Geomagnetism and Schmidt quasi-normalization. *Geophysical Journal International*, 160(2), 487-504.

Whittaker, E. T., & Watson, G. N. (1996). *A course of modern analysis*. Cambridge university press.

Zhao, X., Roberts, A. P., Heslop, D., Paterson, G. A., Li, Y., & Li, J. (2017). Magnetic domain state diagnosis using hysteresis reversal curves. *Journal of Geophysical Research: Solid Earth*, 122(7), 4767-4789.